
***UV Laser crosslink induction: an
innovative tool for epigenetic
studies***

Rosaria Benedetti

Dottorato in Scienze Biotecnologiche – XIV ciclo
Indirizzo Biotecnologie Vegetali
Università di Napoli Federico II





***UV Laser crosslink induction: an
innovative tool for epigenetic
studies***

Rosaria Benedetti

Dottoranda: Rosaria Benedetti
Relatore: Prof. Gennaro Marino
Coordinatore: Prof. Giovanni Sannia

*The real voyage of
discovery consists not in seeking new landscapes
but in having new eyes.
(Marcel Proust)*

INDEX

RIASSUNTO	pag.	1
SUMMARY	pag.	5
INTRODUCTION	pag.	6
The Epigenetic	pag.	6
Epigenetic regulation of chromatin structure and function	pag.	7
Histone Acetylation and chromatin remodelling	pag.	9
HATs and HDACs	pag.	12
Histone methylation	pag.	16
<i>Lysine methyltransferases</i>	pag.	17
<i>Arginine methyltransferases</i>	pag.	17
<i>Demethylation of Lysines</i>	pag.	18
<i>Removal of Arginine methylation</i>	pag.	19
The Apoptosis program	pag.	19
Ionizing radiation, DNA damage and cellular death	pag.	21
ChIP procedure	pag.	24
The crosslink induction	pag.	27
UV Laser crosslink	pag.	29
Laser theory	pag.	32
Three and four levels laser	pag.	33
Laser components	pag.	34
AIM OF THE THESIS	pag.	36
MATERIALS AND METHODS	pag.	38
RESULTS	pag.	48
DISCUSSION	pag.	79
BIBLIOGRAPHY	pag.	86
SUPPLEMENTARY TABLES	pag.	93
<i>PUBLICATIONS AND COMMUNICATIONS INDEX</i>	pag.	96
PUBLICATIONS		

RIASSUNTO:

Lo studio della biologia molecolare comporta la dissezione dei sistemi biologici per individuare e isolare le singole molecole, delle quali si determinano le proprietà, cercando di dedurre dalla loro funzione e dalle loro caratteristiche il ruolo all'interno delle cellule.

Una volta definita la funzione di una singola molecola, ad essa si affiancano reti di relazione interazione-struttura-funzione, al fine di descrivere le interconnessioni che caratterizzano un sistema biologico.

E' noto però che i sistemi biologici sono complessi e il loro funzionamento dipende, in massima parte, dalle interazioni multiple che i singoli componenti stabiliscono tra loro in un determinato momento e in un dato contesto.

Dunque, questo approccio, definito di tipo riduzionistico, risulta essere poco utile in campi della biologia i cui fini ultimi consistono nella comprensione dell'evoluzione spaziale e temporale degli interattori molecolari.

Da questa osservazione emerge la necessità di guardare al "mondo cellula" con un nuovo approccio che miri a studiare gli organismi viventi in quanto sistemi che si evolvono nel tempo, ossia nell'interazione dinamica della parti di cui sono composti. A tale necessità è chiamata a dare risposta una nuova branca della Biologia, definita Biologia dei Sistemi.

La Biologia dei sistemi parte dalla conoscenza dei geni e delle proteine presenti nel corso del tempo in un organismo e utilizza tecniche di trascrittomica, metabolomica e proteomica per valutare i cambiamenti dinamici derivati da una perturbazione del sistema stesso. Tale disciplina utilizza ampiamente gli approcci della teoria dei sistemi, della bioinformatica e della matematica-statistica con l'obiettivo di creare un modello sempre più completo del funzionamento dei sistemi biologici.

Al contrario della biologia molecolare, che si focalizza sulle macromolecole biologiche, con particolare attenzione agli acidi nucleici e alle proteine, la Biologia dei Sistemi non si occupa del singolo meccanismo molecolare bensì delle interazioni dinamiche tra le varie molecole per formare nel corso del tempo un sistema.

L'aspetto dinamico, e cioè la forte dipendenza dal tempo dei programmi di formazione di strutture e processi biologici, è l'aspetto che fortemente caratterizza la biologia dei sistemi rispetto al resto delle scienze "omiche".

La novità che ha consentito l'inizio e lo sviluppo della biologia dei sistemi è l'introduzione di tecnologie *high-throughput* che permettono di studiare contemporaneamente una enorme varietà di molecole (mRNA, proteine, lipidi, metaboliti) coinvolte nei processi biologici e integrare i dati provenienti da diversi esperimenti in una visione unitaria.

Le caratteristiche che le tecnologie *high-throughput* devono possedere affinché possano essere integrate in un progetto di biologia dei sistemi sono: rapidità di esecuzione, simultaneità di esperimenti, elevato numero di dati derivanti dall'esperimento stesso.

Queste caratteristiche sono proprie della tecnologia Laser-ChIP attualmente in sviluppo nell'ambito della linea di ricerca "sviluppo di una sorgente laser ultra-breve per lo studio delle modifiche epigenetiche".

L'obiettivo principale della linea di ricerca "sviluppo di una sorgente laser ultra-breve per lo studio delle modifiche epigenetiche" è consistito nella messa a punto e nella successiva creazione di una piattaforma sperimentale che, tramite l'utilizzazione di una sorgente laser, sia in grado di indurre reazioni di crosslink tra DNA e proteine all'interno di cellule vive per studiare l'evoluzione nel tempo e nello spazio tanto del macchinario trascrizionale, tanto del codice epigenetico.

La necessità di tale apparecchiatura e tecnologia origina dal fatto che il rapido sviluppo della ricerca applicata nel settore “Biologia dei Sistemi” ha attualmente raggiunto un livello critico dal punto di vista tecnologico, poiché i metodi chimici convenzionali per l’induzione di legami covalenti tra DNA e fattori trascrizionali come passaggi preliminari di esperimenti di immunoprecipitazione della cromatina (ChIP, NChIP e XChIP) presentano una serie di limitazioni tecniche intrinseche per quanto riguarda la selettività, la sensibilità, la precisione, l’efficienza, la dinamica delle interazioni, il mascheramento e la modifica di alcuni epitopi.

Tale tecnologia Laser dunque si pone come valida alternativa ai suddetti metodi tradizionali poichè è in grado di indurre legami tra DNA e proteine in intervalli di tempo molto brevi e con efficienza di reazione abbastanza elevata.

L’idea che anima tale progetto è l’osservazione, confermata sia da dati sperimentali che in evidenze presenti in letteratura, che una sorgente laser UV ultrabreve è in grado di eccitare gli stati elettronici delle basi azotate che compongono il DNA e dei residui laterali amminoacidici delle proteine che legano il DNA stesso.

Una volta assorbita energia, il sistema DNA-proteina rilassa verso lo stato fondamentale tramite la formazione di un legame covalente (1-7).

La creazione di tale legame, ottenuto mediante una metodica “foto-fisica”, apre un ventaglio di possibilità per quanto riguarda studi di interazione in “*real time*” e la decifrazione di rapidi “cross-talk” tra fattori trascrizionali, *enhancer*, modulatori epigenetici e DNA.

La messa a punto della metodica Laser-ChIP ha previsto la definizione e la costruzione di una nuova sorgente laser, le cui caratteristiche meglio si coniugano alla tipologia di esperimenti *high-through-put*. In particolare la sorgente laser dedicata al progetto di ricerca produce impulsi di durata minore di 170 fs ad una lunghezza d’onda portante di 1030 nm con una eccellente qualità del fascio e una potenza media di 4 W nel *range* di frequenza di ripetizione di 50-350 kHz con una energia pari a ~0.7 mJ . Il sistema è dotato di cristalli generatori di armoniche che permettono di ottenere anche impulsi di circa 0.4 mJ a 515 nm, nel centro della banda visibile, e di circa 0.15 mJ a 260 nm, nell’UV. La durata degli impulsi nel verde e nell’UV si riduce a circa 120 fs.

Tale sorgente laser è implementata di un sistema in grado di generare impulsi “ a doppio colore” nello spettro dell’UV e del visibile per ridurre la probabilità di indurre danni al DNA e in generale al sistema cellulare in analisi. Tramite l’utilizzo di tale dispositivo viene infatti ridotta la quantità di fotoni altamente energetici che viene fornita al sistema nel quale si vuole indurre il crosslink.

La scelta di questo sistema laser impulsato è dettata dal fatto che ha caratteristiche di unicità tali da soddisfare i due requisiti essenziali per ottenere un crosslink DNA-proteina in modo rapido, altamente efficiente e che comporti un ridotto danno al DNA: un alto rapporto energia/impulso (alta intensità) e un’alta e variabile frequenza di ripetizione.

Il primo passo per confermare la possibilità di indurre un crosslink tra DNA e proteine con una sorgente Laser ultrabreve e per determinare le quali condizioni operative tale induzione di crosslink è ottimizzata, è stato la creazione di una linea cellulare in grado di esprimere la proteina di fusione ER α -GFP. ER α è un fattore trascrizionale il cui legame a particolari regioni del DNA (ERE, *Estrogen Responsive Element*) causa l’attivazione trascrizionale dei geni responsivi all’estrogeno. La presenza della *Green Fluorescence Protein* (GFP) consente di poter seguire in tempo reale l’avvenuto crosslink in cellule vive per mezzo di misure di fluorescenza. L’utilizzazione di queste cellule e la successiva messa a punto del protocollo di purificazione della cromatina

ha consentito di eseguire un numero elevato di esperimenti in un intervallo di tempo molto breve e, dunque, ha consentito di ricavare alcune informazioni importanti riguardanti il modo in cui una radiazione luminosa (in particolare di tipo UV Laser) interagisce con le cellule, gettando le basi per la comprensione del meccanismo che sottende all'induzione del cross-link stesso.

Nelle condizioni operative definite con questa tecnica sono stati effettuati esperimenti di immunoprecipitazione della cromatina (L-ChIP).

I risultati ottenuti hanno mostrato l'effettiva presenza di crosslink e, in aggiunta, hanno evidenziato il differente comportamento che singole proteine e regioni geniche hanno rispetto all'induzione di legami stabili ottenuta mediante una sorgente UV Laser.

Il primo vantaggio riscontrato dall'utilizzo della luce laser come induttore di crosslink è stato la progressiva diminuzione dei tempi di irraggiamento (che coincidono con i tempi di induzione dei legami stabili) che, al momento, sono di circa 1 minuto (contro i 15 minuti normalmente richiesti per l'induzione del crosslink ottenuta mediante trattamento delle cellule con formaldeide).

Questa diminuzione del tempo richiesto per la formazione di legami covalenti, consente di poter studiare interazioni tra proteine e DNA di un ordine di grandezza più rapide, nonché la presenza e la variazione nel tempo di particolari modifiche epigenetiche reversibili a carico della proteine istoniche.

Inizialmente l'attenzione è stata focalizzata su tre distinte combinazioni di *repetition rate* e energia per impulso: 2kHz 125μJ, 200Hz 125μJ e 20kHz 8μJ.

Dall'insieme dei dati ottenuti per queste 3 condizioni è emersa la necessità di studiare in modo approfondito l'effetto biologico che l'interazione tra luce UV e cellule viventi determina, in particolare considerando l'induzione del danno al DNA (sia come formazione di dimeri di timidine, sia come *double strand breaks*), attivazione di pathways di rilevamento di danno e di induzione di morte, nonché l'attivazione di programmi pro-apoptotici (come l'induzione delle Caspasi e dei ROS). L'idea sottesa alla scelta di effettuare queste analisi aggiuntive è la possibilità che informazioni sulla presenza di fenomeni quali la morte cellulare e il danneggiamento (sia delle proteine che del DNA), possono fornire indicazioni per quanto riguarda la scelta di nuove combinazioni dei parametri operativi del Laser (nonché parametri strettamente biologici e tecnici) in grado di massimizzare la resa di crosslink.

Da queste analisi è emerso che la quantità di fotoni rilasciata verso il sistema cellulare *in vivo*, benché in grado di indurre un crosslink tra istoni e regioni promotrici di diversi geni, eccede la dose richiesta in quanto il sistema cellulare stesso risulta danneggiato a seguito dell'irraggiamento.

Per questo motivo sono state analizzate altre combinazioni di frequenze di ripetizione e energia per impulso, andando progressivamente a scalare la quantità di energia totale fornita alle cellule.

Questo processo ha determinato la diminuzione sia delle percentuali di morte (e quindi di tutti i fenomeni cellulari e sub-cellulari che di essa sono la causa) sia una massimizzazione della quantità di crosslink ottenuta.

Il miglioramento sostanziale è stato ottenuto cambiando le caratteristiche della radiazione UV incidente, passando da un valore di 260nm a 300nm.

A 300nm i nucleotidi che compongono il DNA sono ancora in grado di assorbire energia, ma le timine non hanno il loro picco di assorbimento.

Questo determina una riduzione in formazione di dimeri di pirimidina e anche di danni strutturali alla fibra di DNA; il DNA integro assicura la migliore riuscita di un esperimento di ChIP, in quanto, molti dei passaggi della tecnica di

immunoprecipitazione della cromatina, sono affetti proprio dalla stabilità e qualità del DNA.

L'insieme dei dati mostrati e discussi in tesi suggeriscono che, come per ogni tecnica biologica condotta in vivo, per la definizione delle migliori condizioni in cui indurre un crosslink tra proteine e DNA molti parametri fisici e biologici devono essere tenuti in considerazione.

Prima di tutto, un ruolo chiave assumono le caratteristiche della radiazione UV laser incidente, per le quali è importante andare a definire il miglior equilibrio tra *repetition rate*, energia/impulso ed energia totale.

Anche alcuni accorgimenti strutturali possono influire sulla riuscita dell'esperimento di induzione del legame stabile e la ChIP a valle, tra cui la geometria dell'apparato Laser utilizzato, la velocità di agitazione del campione in cuvetta, il materiale di cui è composta la cuvetta stessa e la composizione delle soluzioni utilizzate in ChIP (in particolare prestando attenzione alla quantità di detergenti).

L'aspetto più importante da considerare resta comunque il modo in cui il sistema biologico risponde all'interazione con la luce UV, mediante l'attivazione di meccanismi di rilevamento e riparo del danno, nonché mediante l'induzione dei fenomeni di morte cellulare.

Al fine di creare legami stabili tra DNA e proteine, al sistema cellulare deve essere quindi fornita una quantità di energia sufficiente per promuovere l'attivazione elettronica delle basi del DNA e dei residui laterali della proteina, ma l'energia totale rilasciata non deve eccedere determinati valori per i quali i fenomeni distruttivi prevalgono su quelli culminanti con la creazione di legami covalenti.

BIBLIOGRAFIA:

1. M. J. Solomon and A. Varshavsky, Proc. Natl. Acad. Sci. USA **82**, 6470 (1985).
2. M. J. Solomon, P. L. Larsen, and A. Varshavsky, Cell **53**, 937 (1988).
3. L. Zhang, K. Zhang, R. Prändl, and F. Schöffl, Biochem. Biophys. Res. Comm. **322**, 705 (2004).
4. C. Russmann, M. Truss, A. Fix, C. Naumer, T. Herrmann, J. Schmitt, J. Stollhof, R. Beigang, and M. Beato, Nucleic Acids Res. **25**, 2478 (1997).
5. C. Russmann, J. Stollhof, C. Weiss, R. Beigang, and M. Beato, Nucleic Acids Res. **26**, 3967 (1998).
6. D. S. Gilmour and J. T. Lys, Mol. Cell. Biol. **5**, 2009 (1985).
7. D. S. Gilmour and J. T. Lys, Mol. Cell. Biol. **6**, 3984 (1986).

SUMMARY:

Establishing a stable covalent bond between proteins and nucleic acids, usually referred to as crosslinking is a powerful tool of molecular biology, which affords access to study otherwise transient interactions between bio-molecules. Crosslinking with fs- UV lasers has been presented in the literature as a revolutionary technique to increase the otherwise low process yield of conventional methods based on chemical catalysts, conventional UV sources, or longer UV pulses. It is known that crosslinking induced in cells by ultrashort laser pulses has a twofold advantage over conventional methods. (i) It binds only species that are in proximity (“zero length” covalent bond) of the absorbed photons rather than favoring unspecific bonds amongst many possible species in the cell. (ii) It should only operate until the radiation is incident on the sample, thus paving the way for time-resolved studies of transient interactions. Moreover, when combined with biochemical techniques such as Chromatin Immunoprecipitation (ChIP) to analyze the produced bonds, the UV laser method will make feasible the characterization of the dynamics of the transcription factors bindings on chromatin in living cells, thus overcoming the technical limitations of the current technologies. The aim of this research project was to find the best operating condition for the induction of crosslink between DNA and proteins in living human cells mediated by an UV laser source, by the exploration of ultra short laser characteristics. Particular attention was focalized on the role of laser repetition rate and on the total energy parameter. To screen in a easy and rapid way the possible combinations of both parameters a cellular model was construct, in which the crosslink yield is analyzed as readout of fluorescence signals. On the bases of so obtained informations, ChIP experiments were carried out against a specific epigenetic mark (Ch3K4H3) on different genetic promoter regions, coding for apoptosis involved protein (TRAIL), structural protein (H2B) and cellular trafficking involved one (SCAMP5). The response of human cells to UV laser radiation was also kept in consideration, looking at cellular mortality, cell phases distribution and DNA damages induction, in order to clarify the principles underpinning the crosslink induction processes. It was found that in some laser operating conditions, although the crosslink induction was still present, the DNA damages (and the consequent cell death) were too high to allow the ChIP experiment itself. Instead the conditions in which the cell viability was maximized, and so the apoptotic and pro-death cellular pathways minimized, fitted with effectively crosslinked experimental points (in terms of protein stability and DNA amplificability).

The set of data displayed and discussed in the thesis, suggests that as each *in vivo* technique, for the establishment of UV Laser mediated crosslink many physical and biological parameters need to be consider.

First of all, the UV Laser light characteristics assume key role in the setting of ChIP experiments by the definition of the better balance between total energy and repetition rate. Also some structural features are important: among them the apparatus’s geometry used for the irradiation, the material of the cuvette, the size of Laser beam, the speed of stirring. The most important thing to consider, however, is still the cellular behavior in response to the UV incident radiation and the way by which the crosslink could be formed.

To be sure that the creation of stable bonds between DNA and proteins is obtained, the cells must be hit with sufficient energy and the energy reaching the biological model does not disrupt the proteins or DNA itself.

Introduction

THE EPIGENETIC

Early advances in genetics led to the paradigm: phenotype (an organism characteristics/behaviour) is determined by genotype (its genetic make-up). This was later amended by the well-known formula $P = G + E$, encompassing the notion that the visible characteristics of a living organism (the phenotype, P) is a combination of hereditary genetic factors (the genotype, G) and environmental factors (E).

In the wake of early work by Waddington, more recent results have emphasized that the expression of the genotype can be altered without any change in the DNA sequence. This phenomenon has been tagged as “epigenetics”.

Epigenetics has been defined as “the study of stable alterations in gene expression potentials that arises during development and cell proliferation” {Jaenisch, 2003 #1} , or as “alterations in DNA function without alterations in DNA sequence” {Jones, 2001 #2}. The central idea behind the concept of epigenetics is that although the DNA sequence of almost all the nucleated somatic cells in the body of an adult mammal is identical (except some very specialized cells whose development requires DNA rearrangements), the phenotypes of those cells can be quite different because alternate subsets of genes are expressed at different times in development and during cellular differentiation. In other words, each cell type in an organism has its own epigenetic profile or signature {Morgan, 2005 #3}.

So, in contrast to many of the other ‘omics’ — proteomics, transcriptomics, metabolomics and so forth — epigenomics does not simply enhance genome sciences, but instead challenges the concept of the linearity between genome and phenotype: while information within the genetic material is not changed, instructions for its assembly and interpretation may be.

Modelling this new paradigm the equation is modified to $P = G + E + EpiG$.

Therefore the development of tissues and organisms depends upon the acquisition of distinct programs for gene expression among individual cell types. These programs are maintained in a heritable state by epigenetic mechanisms that impart cellular memory. At the core of such gene regulation are mechanistic pathways that affect the packaging of DNA into chromatin, thereby regulating the degree of DNA accessibility to transcriptional complexes. Clearly, the regulation of the chromatin structure is a complex and dynamic process. It is modulated at several levels by distinct mechanisms such as DNA methylation, nucleosome remodeling, histone post-translational modifications, incorporation of histone variants, and non-coding RNA. Aberrations in such epigenetic mechanisms are likely to impact gene expression as well as other physiologically critical processes such as chromosome condensation, segregation, and apoptosis.

Several lines of evidence indicate that tumorigenesis in humans is a multistep process in which a succession of genetic changes leads to the progressive conversion of normal cells. While genetic alterations can account for some of these changes, many of the alterations in gene expression observed in cancer are caused by epigenetic modifications. These observations highlight the relevance of epigenetic mechanisms toward the establishment of proper cellular function.

Alteration of these mechanisms cooperates with genetic mutations and contributes to the establishment and progression of neoplastic diseases.

Thereby epigenetics “provide a new paradigm for disease etiology and basic mechanisms in toxicology and evolution not previously appreciated.

The classical theory of recessive oncogenesis predicted a mutational mechanism for the inactivation of tumor suppressor (TS) genes. This prediction has been amply

confirmed, but an alternative, non-mutational, pathway for loss of TS gene activity has also come into focus. For some TS genes, this epigenetic pathway is more frequent than the mutational one” {Tycko, 2000 #4}.

Functionally, epigenetic marks act to regulate gene expression, silence the activity of transposable elements and stabilize adjustments of gene dosage, as seen in X inactivation and genomic imprinting .

In addition, epigenetic features may play a role in short-term adaptation of species by allowing for reversible phenotype variability. The modification of epigenetic features associated with a region of DNA allows organisms, on a multigenerational time scale, to switch between phenotypes that express and repress that particular gene. Whereas the DNA sequence of the region is not mutated, this change is reversible. It has also been speculated that organisms may take advantage of differential mutation rates associated with epigenetic features to control the mutation rates of particular genes.

From this argument seems evident that “epigenetic approach, which in some ways is a Lamarckian approach can be more informative than a purely genetic approach” {Jablonka, 1998 #5}. But comprehensively studying all the epigenetic and epigenomic factors related to a multitude of diseases and health conditions will take much more work.

A comprehensive Human Epigenome Project is a lot more complicated than a Human Genome Project. There is only one genome, but an epigenome varies in each and every tissue. The rapidly growing acceptance of epigenetics, a century after it first surfaced, is a huge step forward, in Jirtle’s opinion. “We’ve done virtually nothing so far,” he says. “I’m biased, but the tip of the iceberg is genomics and single-nucleotide polymorphisms. The bottom of the iceberg is epigenetics.” {Yoo, 2006 #6}

EPIGENETIC REGULATION OF CHROMATIN STRUCTURE AND FUNCTION

Chromatin is composed of both DNA and histone proteins, H1, H2A, H2B, H3, and H4. The repeating unit of chromatin is the nucleosome, defined as two of each of the core histones, H2A, H2B, H3, and H4 wrapped almost twice by approximately 146 base pairs of DNA (see figure 1 below).

The nucleosome establishes the first level of chromatin organization.

Nucleosomes themselves can be stacked and coiled to form higher order structures; one example of which is the 30 nm chromatin fiber.

Necessarily, wrapping of DNA as nucleosomes and compaction into higher order structures (see Figure 1 below), inhibits DNA-dependent nuclear processes. Accessing DNA, which is structured as chromatin, is a major challenge for transcription, replication and repair in all cells. Several mechanisms have evolved to allow access including chromatin remodeling by ATP-dependent protein complexes and enzymes that modify histone N-terminal tails.

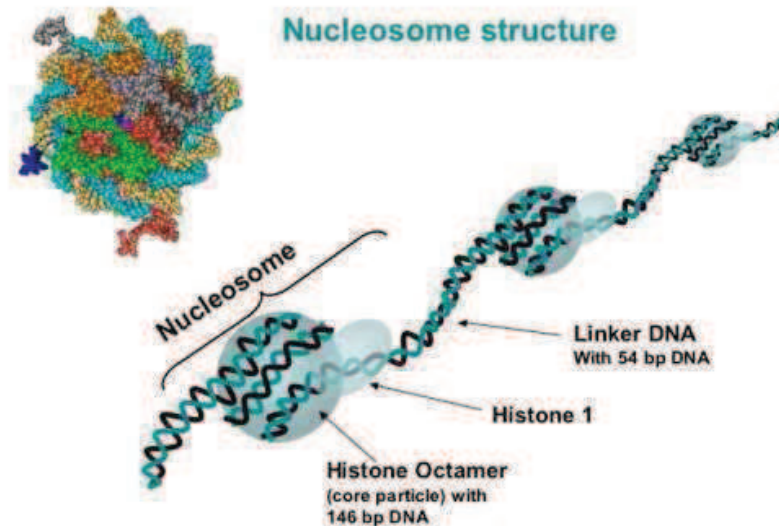


Fig 1: The repeating unit of the chromatin is the nucleosome, defined as two of each of the core histones H2A, H2B, H3 and H4 wrapped almost twice by approximately 146 base pairs of DNA

The histone proteins are highly conserved, essential proteins found in every eukaryotic organism.

The properties of these proteins are fundamental for the structure and function of chromatin overall. The core histones, H2A, H2B, H3, and H4 are low molecular weight (10-14 kDa) proteins {Johns, 1967 #7}.

Histone H1, the linker histone, is slightly larger than the core histones (21 kDa) and is found at half the molar concentration of H2A, H2B, H3, and H4 {Hayashi, 1978 #8}.

Extending from the central histone fold core domain of histones are the N-terminal tails. The crystal structure of the nucleosome lacks definition of the N-terminal tails outside of the nucleosome, leading to the conclusion that the tails are highly dynamic, exist in a random configuration and extend from the nucleosomal core {Luger, 1997 #10}.

These tail domains contain a number of conserved amino acid residues including lysine, arginine, and serine. Histone tails, which sustain a basic charge, can interact with the poly-anionic backbone of the core DNA, marginally contributing to nucleosome stability. Therefore, regulation of chromatin structure and transcription is often mediated through post-translational modifications that alter specific residues along these tails.

These post-translational protein modifications are acetylation, phosphorylation, ubiquitylation, methylation, and others, which can affect the accessibility of nuclear factors to DNA or induce the recruitment of such factors involved in transcription or chromatin assembly pathways.

Combinatorial patterns of these modifications are correlated with specific regulatory states and, as an informational mechanism for gene regulation, are called the "histone code" {Fischle, 2003 #11} {McGhee, 1980 #12}.

DNA-histone octamer interactions occur through the neutralization of negatively charged backbone phosphate groups by direct interactions and water-mediated hydrogen bonds with lysines and arginines. Additionally, hydrophobic interactions occur between residues such as threonine, proline, valine, and isoleucine and the deoxyribose groups of DNA {Luger, 1997 #10}. The lack of specific interactions with

the nitrogenous base pairs corresponds with the lack of nucleotide-sequence specificity of histone-DNA interactions.

This kind of interaction is extremely dynamic: DNA wrapped around a histone octamer can be blocked from interactions with proteins essential for transcription, replication and other nuclear processes.

Exposure of regulatory elements within DNA can occur either by sliding of nucleosomes, to position these sequences within linker DNA, or by transitionally lifting the DNA molecule off the nucleosome. The first process is actively regulated by chromatin remodeling complexes, while the second process occurs passively in solution {Kassabov, 2003 #13}.

Arguably, the most important function of chromatin may be repression and silencing of gene expression.

While repressed genes may share some of the characteristics of continuously silenced chromatin, defined as heterochromatin, they retain the potential for active transcription and are placed in the subdivision of chromatin known as euchromatin. The term "silenced" is used here with regards to a maintained absence of transcriptional activity, and "repression" for short-term or active down-regulation of transcription.

Silenced chromatin (versus repressed chromatin) can be further subdivided into constitutive, primarily at centromeric and telomeric regions, and facultative heterochromatin, such as the inactivated X-chromosome {Maison, 2002 #14} {Richards, 2002 #15}.

Briefly, both types of heterochromatin are present within highly condensed and pericentric regions of chromosomes, often consisting of long stretches of repeated elements. They also share the properties of widespread histone hypoacetylation, and DNA methylation. Additionally, recent results support the participation of unique, noncoding siRNAs and dedicated enzymatic complexes in the silencing of both constitutive and facultative heterochromatin {Grewal, 2002 #16}.

HISTONE ACETYLATION AND CHROMATIN REMODELLING

The organization of eukaryotic chromatin has a major impact on all nuclear processes involving DNA substrates. Gene expression is affected by the positioning of individual nucleosomes relative to regulatory sequence elements, by the folding of the nucleosomal fiber into higher-order structures and by the compartmentalization of functional domains within the nucleus.

Because site-specific acetylation of nucleosomal histones influences all three aspects of chromatin organization, it is central to the switch between permissive and repressive chromatin structure.

Acetylation is a dynamic phenomenon with the steady state mediated by the opposing activities of two classes of enzymes: histone acetyltransferases (HATs) and deacetylases (HDACs) {Jenuwein, 2001 #17} {Richards, 2002 #18} {Rabinowicz, 2003 #19 (see Figure 2)}.

These activities involve large regulatory complexes that are capable of responding to specific DNA sequences and can contain transcription factors, regulatory ligands, and signal transduction and cell cycle proteins.

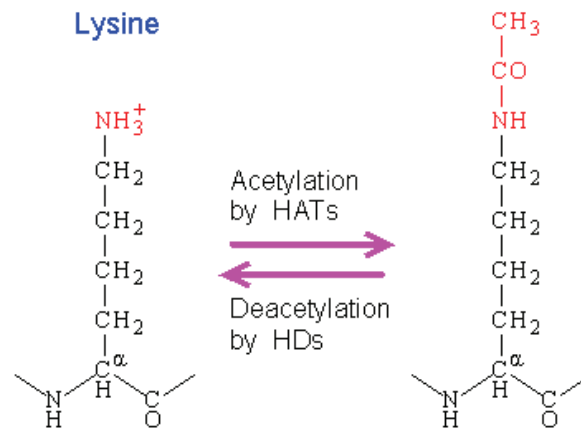


Fig 2: Acetylation is a dynamic phenomenon with the steady state mediated by the opposing activity of two classes of enzymes: histone acetyltransferase (HATs) and deacetylases (HDACs)

Histone acetylation occurs at the ϵ -amino groups of evolutionally conserved lysine residues located at the NH₂ termini of histones (see Figure 3).

All core histones are acetylated *in vivo*, but acetylations of H3 and H4 have been more extensively characterized than those of H2A and H2B.

HATs transfer acetyl moiety from acetyl CoA to the lysine residues; in the deacetylation reaction, HDACs catalyze the removal of acetyl groups from histones. Individual HATs and HDACs display distinct specificities in terms of the individual lysine residues and the particular histones they affect.

Whatever it is widely accepted that histone acetylation is essential to establish a transcriptionally competent state of chromatin {Kadonaga, 1998 #20} {Strahl, 2000 #21} {Tse, 1998 #22}.

However, the relation between chromatin conformation and histone acetylation is complex and three different effects could be important {Hansen, 1998 #24} {Hansen, 2002 #23}.

First of all, acetylation might modulate interactions between histone tails and the DNA.

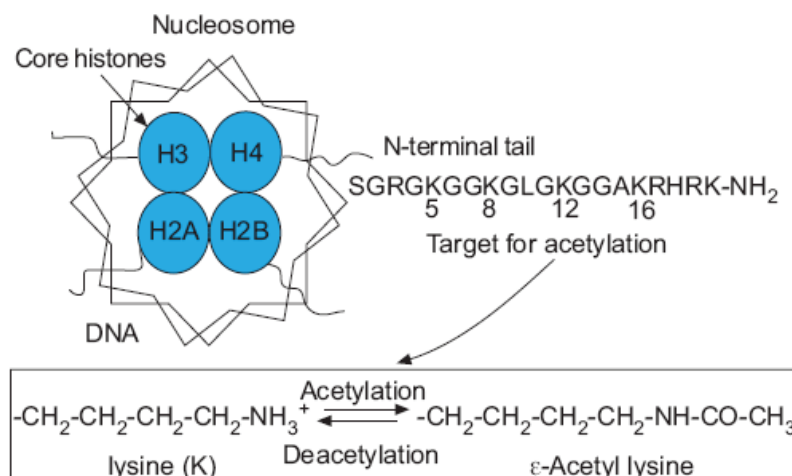


Fig 3: Histone targets of acetylation

Non-acetylated histone tails carry a large number of positively charged lysine and arginine residues (<100 per nucleosome) that interact with the negatively charged phosphate groups of the DNA backbone {Allan, 1982 #25} {Fletcher, 1995 #26} {Hansen, 1998 #24} {Hansen, 2002 #23}. These electrostatic interactions are highly dependent on ion concentration {Usachenko, 1994 #28}.

Moreover the histone tails could affect inter-nucleosomal association {Luger, 1998 #29}. An interaction between the positive N-terminal H4 tail and a highly negative region on the exposed H2A-H2B surface has been identified in the crystal structure of the nucleosome {Luger, 1997 #10}. Again, acetylation of the corresponding lysine residues is likely to weaken this interaction.

In the end the effect of acetylation *per se* on nucleosome structure appears rather modest {Wang, 2000 #30}. However, specific acetylation patterns displayed by the histone tails may also function to recruit further modulators of chromatin structure. The dramatic changes in promoter structure that accompany transcriptional activation are, therefore, presumably not the direct result of acetylation, but due to the synergistic actions of several factors. These include other covalent modifications such as phosphorylation, as well as the rearrangement of histones/nucleosomes relative to the DNA by nucleosome remodeling factors (as the proteins of the SWI2/SNF2 family). No matter how the acetylation of core histone allows the chromatin structure to transform from the resting closed conformation to an activated open form (see Figure 4, below). Thus, this allows binding of TATA box-binding protein (TBP), TBP-associated factors and, finally, RNA polymerase II, which initiates gene transcription. This molecular mechanism is probably common to all genes, including those involved in differentiation, proliferation and activation of cells {Lee, 1998 #27} {Vettese-Dadey, 1996 #31}.

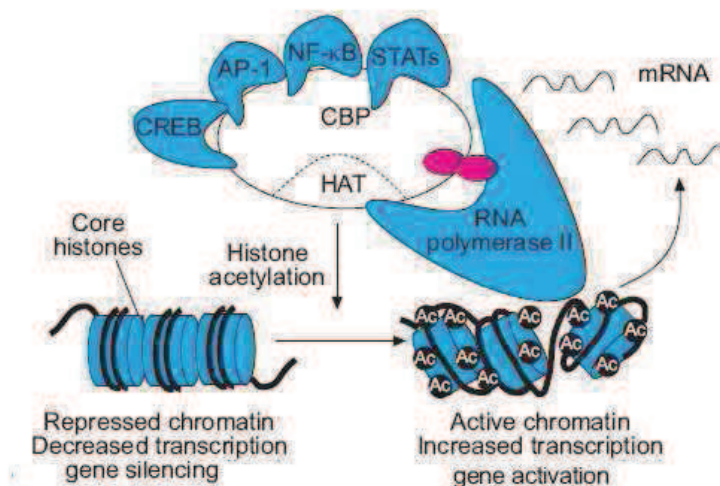


Fig 4: The acetylation of core histone allows the chromatin structure to transform from the resting closed conformation to an activated open form

From all exposed tell now it's evident, anyway, the importance that acetylation keeps in the maintenance of cellular homeostasis. Several lines of evidence indicate that tumorigenesis in humans is a multistep process in which a succession of genetic changes leads to the progressive conversion of normal cells. While genetic alterations can account for some of these changes, many of the alterations in gene

expression observed with cancer are caused by epigenetic modifications and, in particular, by an aberrant pathway of acetylation/deacetylation. Imbalance of histone acetylation/deacetylation in promoter regions contributes to the deregulation of gene expression and has been associated with carcinogenesis and cancer progression.

HATs and HDACs

Acetylation of histones is a reversible and dynamically regulated process controlled by a large family of enzymes termed histone acetyltransferases (HATs) and histone deacetylases (HDACs).

Currently, there are four groups of proteins with intrinsic HAT activity. They are as follows: GCN5 and P/CAF, which are related to the yeast HAT; the cyclic adenosine monophosphate response element-binding protein (CBP) and p300, which act as co-activators for a number of transcription factor complexes {Bannister, 1996 #32}; TAF250, a part of the basic transcription complex TFIID that binds with the TATA box; and finally SRC-1 and ACTR, which are coactivators for the ligand-activated nuclear receptors {Ogryzko, 1996 #33} {Mizzen, 1996 #34}.

With mounting excitement, researchers soon showed that several other known transcriptional coactivators possess HAT activity. These identifications directly linked the regulation of histone acetylation to the transcription machinery and provided a unifying model of transcriptional co-activators as histone-modifying enzymes.

So the acetylation allows greater access to the DNA by the general transcription machinery, helping it to initiate transcription (see Figure 5 below). Interestingly, many of the HATs also contain bromodomains, which have acetyllysine binding activity {Dhalluin, 1999 #35}. Bromodomains bind acetylated lysines on the histones, thus allowing the HATs to further acetylate their targets, creating a positive feedback system to efficiently activate transcription {Yang, 2002 #52}.

By its nature, reversible acetylation of a target implies that the acetyl group can also be removed. For every acetyltransferase that acetylates a substrate, there must be a deacetylase that does the reverse. Although prominent exceptions do exist, generally speaking, HDACs are anti-HATs: they are associated with transcription repression complexes and repressive chromatin states.

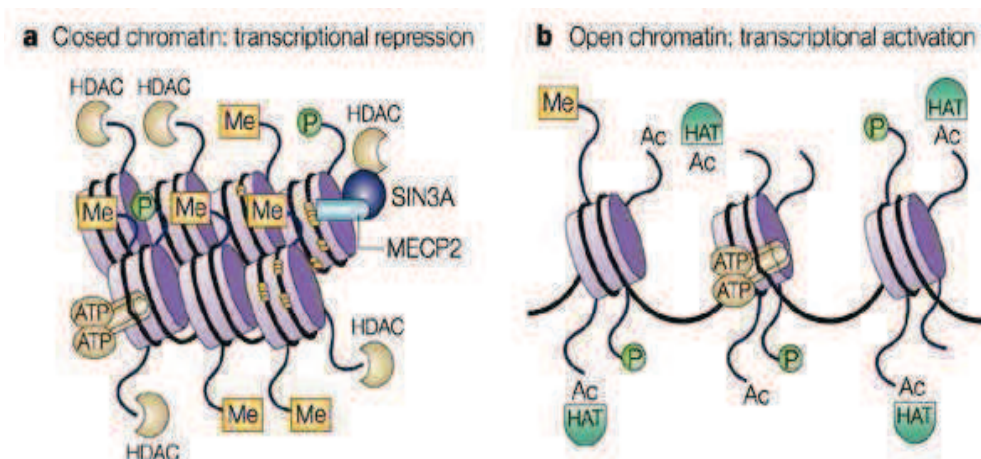


Fig 5: Transcriptional repression vs transcriptional activation

There are two protein families with HDAC activity (see Figure 6 below): the recently discovered SIR2 family of NAD⁺-dependent HDACs (this family will not be subject of discussion in this thesis), and the classical HDAC family. Members of the classical HDAC family fall into two different phylogenetic classes, namely class I and class II.

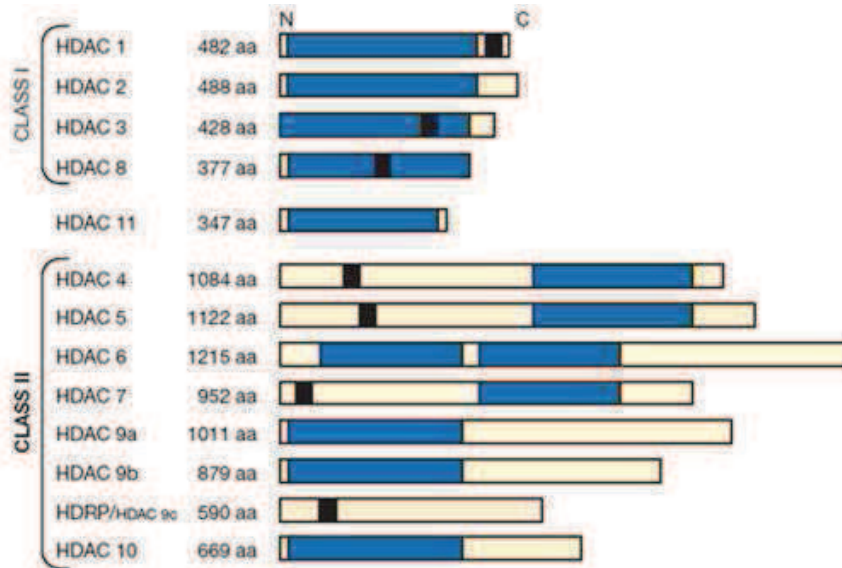


Fig 6: Schematic depiction of the different isoforms of HDAC. Bars depict the length of the protein. The catalytic domain is shown in blue.

Class I HDACs are significantly smaller than class II HDACs and are predominantly nuclear proteins (see figure 7 below), although a recent report has indicated that HDACs may be cytosolic in smooth muscle cells {Waltregny, 2004 #78} {Waltregny, 2004 #79}. Like some HATs, the class I HDACs generally function as part of protein complexes. The complexes include Sin3, NuRD, and CoREST {Heinzel, 1997 #36} {Humphrey, 2001 #37}.

Class II HDACs are further divided into subclasses IIa and IIb.

The class IIa HDACs consist of HDAC4, 5, 7, and 9 {Verdin, 2003 #38}. This subfamily of HDACs shares several unique properties. First, they all contain the N-terminal non-catalytic MITR (MEF2-interacting transcription repressor) homology domain. This domain serves critical functions as both a protein-protein interaction domain and a regulatory domain subject to phosphorylation {Miska, 1999 #39} {Grozinger, 2000 #40}. Second, they are all critical regulators of MEF2, a family of transcription factors important in muscle differentiation and neuronal apoptosis. Third and most importantly, they are all regulated by phosphorylation dependent subcellular trafficking {McKinsey, 2000 #41}. All of the class IIa HDACs are subject to nuclear export via a nuclear export signal at the C-terminus {Wang, 2001 #59} {McKinsey, 2001 #80}. The sub-cellular localization of these HDAC members is cell type-dependent and tightly regulated by specific signaling events.

Class IIb deacetylases include HDAC6 and HDAC10. They are characterized by a tandem repeat of complete (HDAC6) or partial (HDAC10) catalytic domains {Grozinger, 1999 #43} {Guardiola, 2002 #42}. HDAC6 and HDAC10 are also unique in their resistance to select deacetylase inhibitors, such as trapoxin B, which can potently inhibit the deacetylase activity of both class I and IIa.

Classification		Location		Function
Zn²⁺-dependent	Class I	HDAC1	Nucleus	Participate in Sin3, NuRD (nucleosome remodeling and deacetylation) and Co-REST complex
		HDAC2	Nucleus	
		HDAC3	Nucleus, rarely in cytoplasm	
	Class IIa	HDAC8	Nucleus	-
		HDAC4	Nucleus, cytoplasm	Interaction with SMRT/N-CoR and the co-repressors BcoR (Bel-6-interacting co-repressor) and CtBP
		HDAC5	Nucleus, cytoplasm	
		HDAC7	Nucleus, cytoplasm	
		HDAC9	Nucleus, cytoplasm	Muscle differentiation
	Class IIb	HDAC6	Cytoplasm	Tubulin deacetylase
		HDAC10	Nucleus, cytoplasm	Recruitment other HDACs
	Class IV	HDAC11	Nucleus, cytoplasm	-
Zn²⁺-independent	Class III	SIRT1-7		

Fig 7: Schematic classification of HDACs

Despite the presence of some class-specific sequence motifs and the generally low homology between classes, HDACs crystal structures confirm a highly conserved active site and substrate-binding pocket.

The conservation extends across classes I, II, and IV.

The catalytic domain of HDAC is formed by a stretch of C390 amino acids consisting of a set of conserved amino acids. The active site consists of a gently curved tubular pocket with a wider bottom. Removal of an acetyl group occurs via a charge-relay system consisting of two adjacent histidine residues, two aspartic residues (located approx. 30 amino acids from the histidines and separated by approx. 6 amino acids), and one tyrosine residue (located approx. 123 amino acids downstream from the aspartic residues). An essential component of the charge-relay system is the presence of a Zn²⁺ ion. This atom is bound to the zinc binding site on the bottom of the pocket.

So in the HDAC active site, a central motif of completely conserved residues coordinates a Zn ion and is complemented by a second group of highly conserved residues involved in the enzymatic reaction and substrate binding (see Figure 8). One of these residues, a Y, had been postulated to act as a transition-state stabilizer because of its position in various enzyme-inhibitor complexes.

Although generally highly conserved, this residue is substituted by H in all vertebrate class IIa HDACs. Examination of the available structures showed that H, a conservative substitution of Y, should not be able to act as a transition-state stabilizer, thus compromising enzymatic activity according to the observation that class IIa HDAC presents a low catalytic efficiency in comparison to class I HDAC.

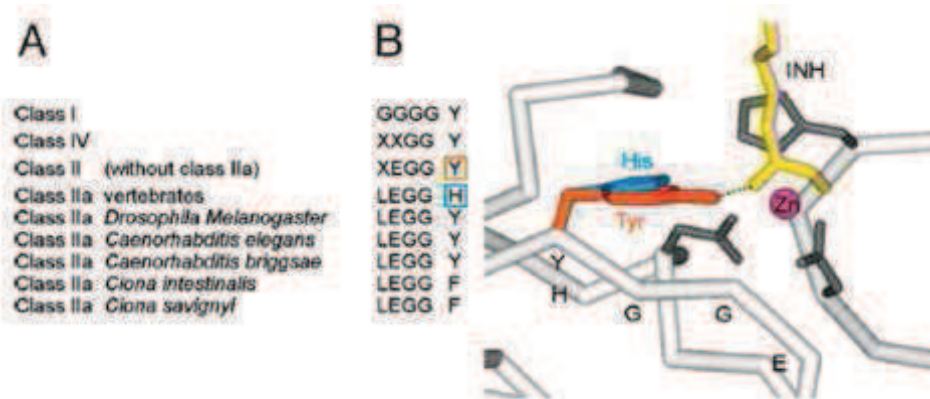


Fig 8: Sequence motif conservation (A) and active-site geometry (B)

To exert their function, HDACs need to be in the nucleus, where their predominant substrate is found. The nuclear localization of HDACs occurs via a nuclear localization signal (NLS) or via co-localization together with other proteins. Most HDACs contain a NLS, but some can be cytosolic as well (see Figure 7); this depends on other regulatory domains. Class I HDACs are found almost exclusively in the nucleus;

class II HDACs are able to shuttle in and out of the nucleus in response to certain cellular signals.

Extensive studies have shown that the change of the acetylation state of histone is correlated with dramatic biological consequences in the cell (see Figure 9 below).

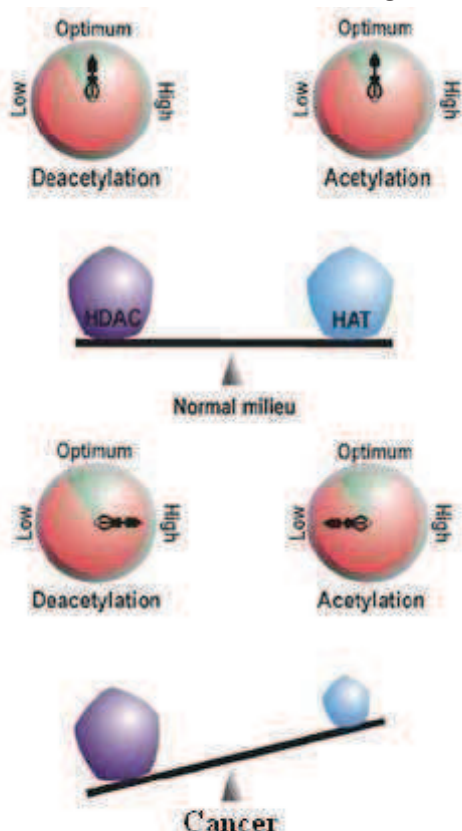


Fig 9: Unbalance between HDAC and HAT activity causes cancer disease (R.N SAHA et al., Cell death and differentiation 2006 Nature group editor)

Disruption of HAT and HDAC function is associated with the development of cancer, and malignant cells target chromatin-remodeling pathways as a means of disrupting transcriptional regulation {Mahlknecht, 2000 #45}.

Of the various hypotheses describing deregulation mechanisms, three have been put forth frequently:

- 1) disordered hyperacetylation could activate promoters that are normally repressed, leading to inappropriate expression of proteins
- 2) abnormally decreased acetylation levels of promoter regions could repress the expression of genes necessary for a certain phenotype
- 3) mistargeted or aberrant recruitment of HAT/HDAC activity could act as a pathological trigger.

Even though no direct alterations in HDAC genes have been demonstrated in cancer, the association of HDACs with various oncogenes and tumor suppressor genes is now well established, as is the potential for HDAC involvement in tumorigenesis {Kristeleit, 2004 #46}.

In acute promyelocytic leukaemia (APL), for

example, the oncoprotein produced by the fusion of the *PML* (promyelocytic leukaemia) gene and the retinoic acid receptor α (*RAR α*) a gene appears to suppress the transcription of specific genes through the recruitment of HDACs. Thus the cancer cell is unable to undergo differentiation, leading to excessive proliferation. Similar phenomena have been described for *RAR α* -PLZF (promyelocytic leukaemia zinc finger protein) fusion, AML1 (acute myelocytic leukaemia protein 1)-ETO fusion, and also in the Myc-Mad-Max signaling pathway involved in solid malignancies.

It is clear that HDAC enzymes seldom operate alone. Many proteins, with various functions such as recruitment, co-repression or chromatin remodelling, are involved in forming a complex that results in the repressor complex. The most important signal involved in the initiation process of repression is situated in the DNA. Methyl groups bound to the cytosine residues situated 5' to guanines in DNA, in so-called CpG islands, are directly responsible for the recruitment of the HDAC complex via proteins such as methylated-CpG binding proteins and methyl-CpG-binding-domain-containing proteins, or via the enzymes that methylate the CpG islands, the DNA methyltransferases.

Given these insights into the function of HDAC enzymes, it is not surprising that HDAC inhibitors are emerging as promising clinical therapeutics for cancer.

Indeed, HDAC inhibitors have been shown to result in the accumulation of hyperacetylated histones and to induce numerous anti-cancer effects including apoptosis, cytostasis, differentiation and inhibition of tumor angiogenesis in numerous cultured cell lines and in vivo.

HISTONE METHYLATION

Histone methylation is lagging behind acetylation in its characterisation, but is rapidly catching up {McBride, 2001 #47} {Zhang, 2001 #48}. In the past months, a number of methyltransferases have been discovered, proteins that read the methyl-lysine code have been identified, and a cross talk between methylation and phosphorylation has been recognised. The targeting of methyltransferases to specific promoters has been established as a crucial mode in their action and enzymes that either activate or repress transcription have been uncovered.

Histone methylation, perhaps more than any other form of modification, has demonstrated the power of modifications over DNA-based functions, regulating fundamental processes such as gene transcription and DNA repair. Furthermore, since the discovery of the first histone methyltransferase {Rea, 2000 #49}, the potential for the methylation 'mark' to control epigenetic events has caught the imagination of workers in this field. However, the recent discovery that methylation can be reversed {O'Carroll, 2000 #50} has shaken the dogma that a 'permanent' methylation mark is necessary for epigenetic control.

Histones may be methylated on either lysine (K) or arginine (R) residues. It is possible that methylation induces alterations in chromatin architecture, either condensing or relaxing its structure. However, a methyl group is relatively small and its addition to lysine or arginine residues does not neutralize their charge, so it is unlikely that methylation alone will significantly affect chromatin structure. It is more likely that it creates binding sites for regulatory proteins that contain specialized binding domains. Lysine side chains may be mono-, di- or tri-methylated, whereas the arginine side chain may be mono-methylated or (symmetrically or asymmetrically) di-methylated. At present, there are 24 known sites of methylation on histones (17 are lysine residues and 7 are arginine residues). If we take into consideration all

three possible methylation states of lysine and arginine, there are potentially 3×10^{11} distinct methylation states of histone proteins. Although all of this combinatorial specificity may not be used, this calculation highlights the vast potential for the regulation of function, and the enormity of the task of understanding how methylation works.

Lysine methyltransferase

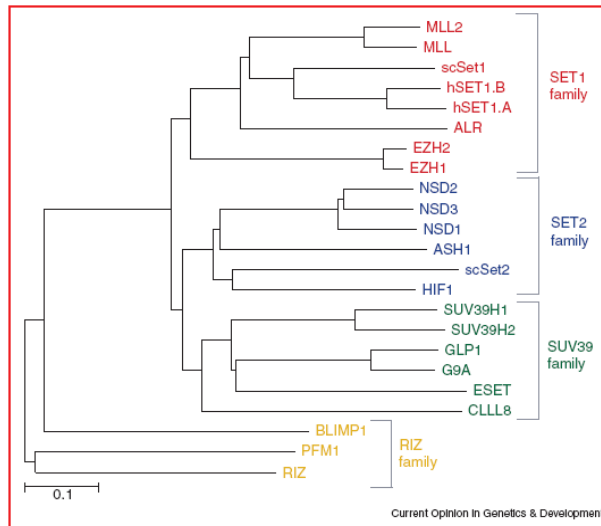


Fig 10: dendrogram of SET domain containing proteins

Methylation of lysines residues is known to occur on histone H3 (K4, K9 and K27) and H4 (K20). The SUV39 protein was the first histone methyltransferase to be discovered. The methyltransferase activity of SUV39 is directed against lysine 9 of histone H3 and its catalytic domain resides within a highly conserved structure, the SET domain. The sequences within the SET domain are not however sufficient for enzymatic activity. Methylation is only seen when two flanking cystein-rich sequences (PRE-SET and POST-SET) are fused to the SET domain.

Figure 10 shows a dendrogram of previously characterised human proteins that possess a SET domain, showing that they can be grouped into four classes. The classification is based on, first, the similarity between the human SET domains and, second, their relationship to SET domains in yeast (*S. cerevisiae*). Two groupings show similarity to either yeast SET1 or SET2, thus defining two of the classes (see Figure 10 above). Another class has SUV39 as its defining member and a fourth family represents homologues of the RIZ SET domain.

Arginine methyltransferase

Methylation at arginines occurs within the tails of histone H3 (R2, R17, R26) and H4 (R3). Arginines can be either mono-methylated or dimethylated on the guanidino nitrogen. Dimethylation can either be symmetric or asymmetric and enzymes are classified according to their ability to carry out one or the other reaction. There are five known arginine methyltransferases (Figure 11) that have a highly conserved catalytic domain. PRMT1, PRMT3 and PRMT4/CARM1 are classified as Class I enzymes as they can catalyse the formation of asymmetric dimethylated arginine whereas PRMT5/JBP1 is classified as a class II enzyme as it catalyses symmetric dimethylation. Remarkably there are very few recognisable domains outside the catalytic domains of these enzymes, unlike the case of lysine methyltransferases. The only features are a zinc finger structure in PRMT3 required to recognise RNA-associated substrates and an SH3 domain in PRMT2 that suggests a signalling role for this enzyme. Presumably the regions outside the catalytic domain are likely to dictate substrate specificity. To date, PRMT1 has been shown to modify histone H4 at Arg3 in vivo {Strahl, 2001 #58} {Wang, 2001 #59} whereas PRMT4/CARM1 has the potential to modify histone H3 at Arg2, Arg17, Arg26 and several unidentified carboxy-terminal residues in vitro {Chen, 1999 #60}. PRMT5 has a preference for H2A and H4 in vitro but the sites of methylation are as yet unknown.

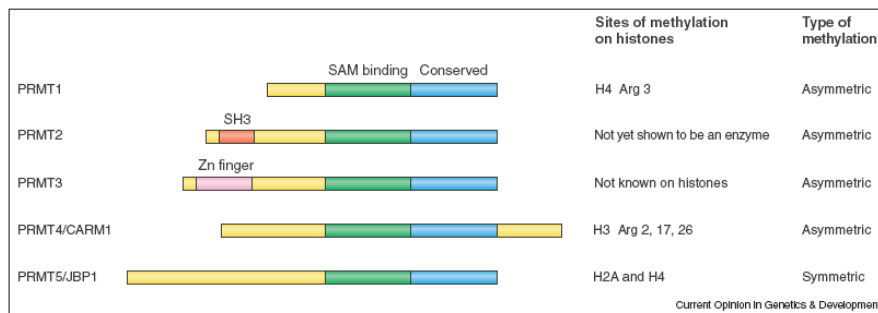


Fig 11: Arginine methyltransferases

Demethylation of lysines

Until recently, the methylation of histones was thought to be an irreversible process. The dogma surrounding this irreversibility of methylated lysines within histones came about from several lines of research. First, reports from over 30 years ago concluded that methylated lysines have the same half-life as histones. Second, the more recent discovery that methylation at H3K9 is responsible for forming and maintaining heterochromatin (a very stable and heritable chromatin state) bolstered the argument that methylation of histones is a permanent 'epigenetic' mark. Third, the mere fact that a demethylating enzyme had not been discovered, although many workers had searched for it, reinforced the view that methylation was a static process. This view had a chink in its armour from the very beginning: an enzyme with demethylase activity had been reported by Paik and Kim in 1973 {Paik, 1973 #61}, although this activity was never attributed to a particular protein. Indeed, the reversibility of methylation became apparent a few years ago when antibodies against methylated arginine or methylated lysine residues were used in chromatin immunoprecipitations. These experiments revealed that the methylation of histone residues appeared to be reduced under certain conditions. This prompted the idea that demethylation was a likely possibility, and a proposal was put forward which suggested that such an enzymatic activity would function through an amine oxidase reaction {Bannister, 2002 #62}. Recently, the enzyme LSD1 (lysine-specific demethylase 1; also referred to as BHC110 or p110b) was identified, which is able to demethylate a specific lysine (K4) within histone H3 using an amine oxidase reaction. This enzyme had previously been identified in a number of repressor complexes {Hakimi, 2002 #63}, a fact that fits well with its ability to demethylate the activating methylation site at H3K4. However, demethylation by LSD1 is limited to mono- or di-methylated H3K4: it cannot demethylate tri-methylated H3K4. This is precisely as predicted for an amine oxidase reaction, yet it is the tri-methylated state that is most associated with active genes. Because the transcription of many genes is dynamic, enzymes capable of removing the tri-methylated state should exist. In addition, enzymes that mediate tri-methylation, such as enhancer of zeste homolog 2 (EZH2), are implicated in cancer, so it is probable that the cell has enzymes to reverse this methylation and counterbalance this potentially dangerous methylation state. Demethylation of tri-methylated lysine would require a distinct set of enzymes to the amine oxidases. Such enzymes will most probably function through a pathway involving a hydroxyl radical attack.

Removal of arginine methylation

The search for arginine demethylases over the last few years has been fruitless. However, the fact that lysine demethylases such as LSD1 exist, makes it much more likely that there is an arginine demethylase. The amino oxidase reaction, through which LSD1 works, is predicted to be compatible with the demethylation of methylarginines as well as methyl-lysines. However, an alternative pathway for the reversal of arginine methylation has been proposed and recently shown to be operational on histones in mammalian cells. This pathway involves the removal of a methyl group from an arginine by the conversion of the methyl-arginine residue into citrulline. This process is termed deimination, since the methyl group is removed along with the imine group of arginine. The enzyme that mediates this reaction, peptidyl arginine deiminase 4 (PADI4), converts unmodified arginine and mono-methylated (but not di-methylated) arginine to citrulline at specific sites on the tail of H3 and H4. This activity of PADI4 is linked to the repression of an oestrogen-controlled gene, pS2 {Bannister, 2005 #64}.

THE APOPTOSIS PROGRAMM

Cell death can be classified into two forms based on morphologic and biochemical criteria: necrosis and apoptosis.

Necrosis is the non-physiologic or passive type of cell death that is usually caused by extreme trauma or injury to the cell; it generally affects cells in groups rather than single cells and evokes inflammation when it develops in vivo.

Necrotic cells cannot maintain proper plasma membrane function so they can no longer regulate osmotic pressure. The cells swell and rupture, spilling their cellular contents into the surrounding tissue, resulting in the nonspecific cellular destruction that leads to an inflammatory response necessary to remove the debris and begin tissue repair.

The other morphologic pattern of cell death is apoptosis which is a physiological process of cellular suicide required for the maintenance of cell homeostasis, embryonic development and for the differentiation and function of hematopoietic and lymphoid cells.

Morphologically, apoptosis is characterized by margination and condensation of nuclear chromatin (pyknosis), cytoplasmic shrinkage, nuclear fragmentation, and blebbing of the plasma membrane. The cell subsequently breaks up into membrane enclosed fragments, termed apoptotic bodies, which are rapidly recognized and engulfed by neighboring cells or macrophages. Considerable biochemical changes occur within the apoptotic cell to facilitate neat packaging and removal of apoptotic bodies by phagocytosis. Modifications of the cytoskeleton and the cytoplasmic membranes are required for cell shrinkage to occur.

From a biochemical, intracellular, point of view several major signaling pathways may lead to apoptosis in mammalian cells {Orrenius, 2003 #66} {Orrenius, #65} (see Figure 12 below). In the extrinsic, receptor-mediated pathway the ligation of surface receptors (e.g., CD95, TNFR1) is followed by the formation of the death-inducible signaling complex (DISC), resulting in the activation of procaspase-8. In type I cells, caspase-8 activates procaspase-3, which cleaves target proteins, leading to apoptosis. In type II cells, caspase-8 cleaves Bid, which, in turn, induces the translocation, oligomerization, and insertion of Bax and/or Bak into the mitochondrial outer membrane {Orrenius, 2003 #66}. This is followed by the release of several proteins from the mitochondrial intermembrane space, including cytochrome c, which forms a cytosolic apoptosome complex with Apaf-1 (apoptosis activating factor-1)

and procaspase-9 in the presence of dATP. This results in the activation of procaspase-9, which triggers the caspase cascade by activation of procaspase-3. In the intrinsic pathway, death signals act directly or indirectly on the mitochondria to cause the release of proapoptotic proteins from their intermembrane space. This cell death pathway is controlled by Bcl-2 family proteins (regulation of cytochrome c release), inhibitor of apoptosis proteins (IAPs) (inhibition of caspases), second mitochondrial activator of caspases (Smac), and Omi (negative regulation of IAPs). The intrinsic pathway may also operate via caspase-independent mechanisms, which involve the release from mitochondria and translocation to the nucleus of at least two proteins, apoptosis inducing factor (AIF) and endonuclease G (EndoG). Nuclear effects of AIF include chromatin condensation and formation of high-molecularweight DNA fragments. The role of EndoG in cell death is still unclear. When DNA damage is the trigger of the apoptotic response, the initially activated caspase is procaspase-2. Its activation also leads to the release of cytochrome c and apoptosome formation, although the precise mechanisms for this are unclear.

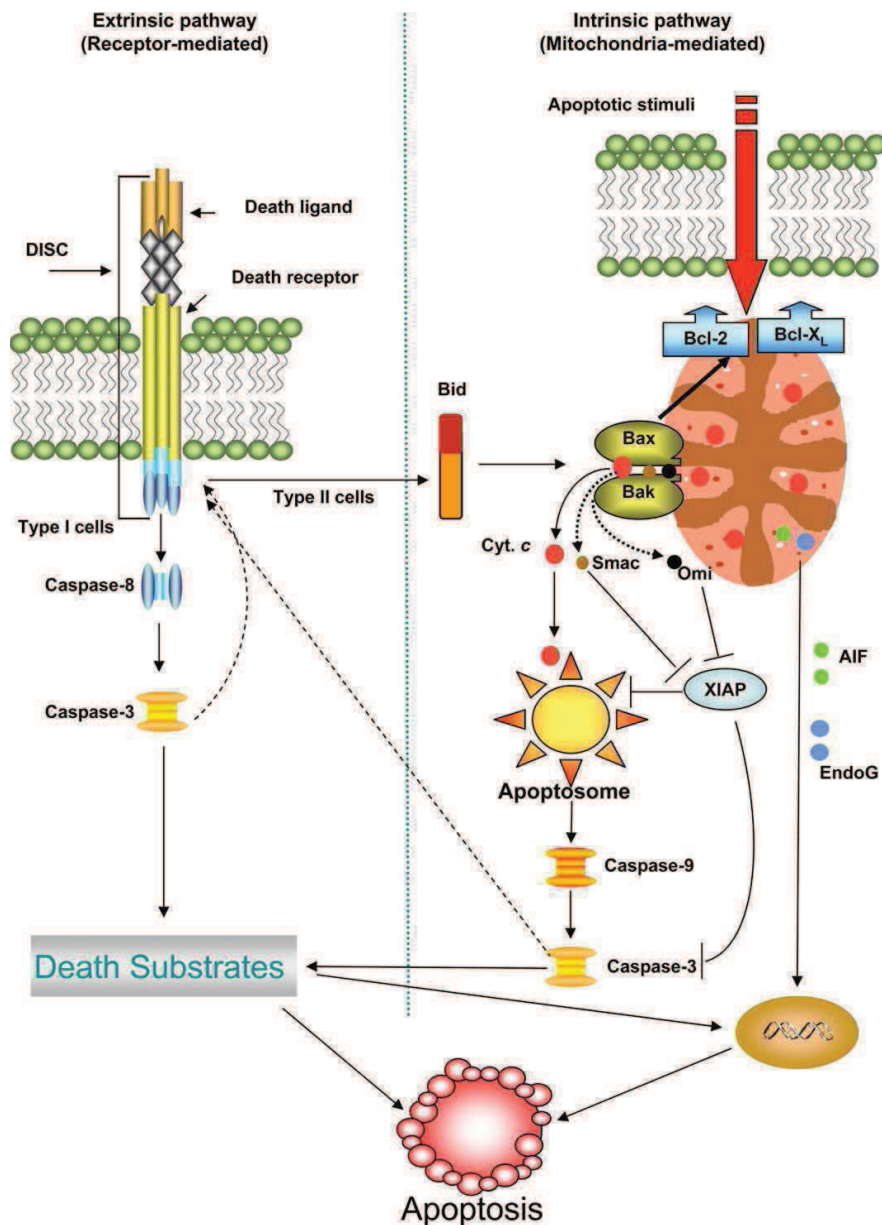


Fig 12: Major signaling pathways leading to apoptosis

IONIZING RADIATION, DNA DAMAGE AND CELLULAR DEATH

The genetic information required for the identity and function of eukaryotic cells resides within their DNA. During the lifetime of a cell, DNA can be continuously damaged from a variety of factors. As un-repaired or mis-repaired DNA damage can result in genetic or genomic instability, changes in cellular identity and function, cell death, and, in multi-cellular organisms, neoplastic transformation; eukaryotic cells have evolved efficient mechanisms to detect and repair DNA lesions induced within each phase of the cell cycle {Emanuel, 2007 #68}.

Ionizing radiation produces a wide spectrum of DNA lesions, such as: base damage (pyrimidine dimers formation), sugar damage, single strand breaks (SSB), double strand breaks (DSB), DNA-DNA and DNA-protein crosslinks. Both the spectrum of the induced lesions and their spatial distribution are affected by radiation quality. It is expected that densely ionizing radiation produces clustered ionizations with relative high efficiency. In addition to lesions correlated at very local scale (complex lesions), radiations quality may affect also the production of lesions correlated at larger distances. This is determinate by the interplay between the chromatin structure and the radiation track structure.

Exposure of DNA to UV radiation has a mutagenic effect on cellular systems.

Cyclobutane pyrimidine dimers (CPDs)¹ and pyrimidine (6-4) pyrimidone photoproducts [(6-4)PDs] are the two major stable photoproducts in UV-irradiated DNA (Figure 13). Their yield is dependent on the sequence {Haseltine, 1980 #70} {Sage, 1993 #71}, the methylation status of cytosines {Brash, 1982 #72} {Pfeifer, 1991 #73}, the DNA structure {Lyamichev, 1991 #74} {Tang, 1991 #75}, and the binding of sequence-specific proteins to DNA {Becker, 1984 #76} {Tornaletti, 1995 #77}. In order for dimerization to occur, adjacent pyrimidine bases must rotate substantially from their average B-form DNA conformation.

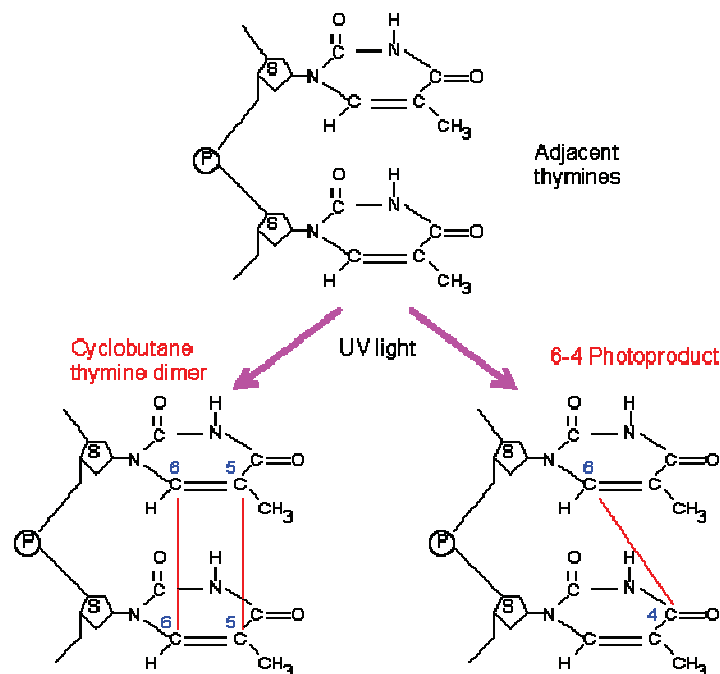


Fig 13: Photoproducts in UV-irradiated DNA

In order to understand how DNA lesions are repaired in eukaryotic cells, it is important to know how lesions are formed in chromatin and whether and how they affect chromatin structure. Some general principles are applicable:

- (i) Distortions of DNA structure introduced by folding into chromatin may affect damage formation.
- (ii) DNA structure may be fixed by protein-DNA interactions and, hence, prevent the conformational changes that are required for damage formation.
- (iii) Accessibility of DNA and, hence, DNA lesions is restricted on the chromatin surface by steric exclusion and, consequently, affects DNA-damage formation by bulky reagents or damage recognition by proteins.
- (iv) Dynamic properties of chromatin, such as dissociation/reassociation, nucleosome mobility, folding, and unfolding will affect DNA distortions and accessibility {Schieferstein, 1996 #69}.

Keeping in mind that a strong relationship between dimers formation, chromatin structure and protein-DNA interaction exists, two are the mainly cellular pathways to repair UV light induced dimers: the photoreactivation and nucleotide or base-excision repair pathways.

In the photoreactivation process, the Pyr-Pyr dimers are restored back into individual pyrimidine bases in a reaction catalyzed by the enzyme DNA photolyase. The commonly accepted model for the photorepair mechanism proposes that the dimer splitting is a consequence of a single electron transfer from the enzyme to the dimer; a mechanism recently verified by quantum chemical calculations.

Nucleotide excision pathway (NER) is the essential repair process for pyrimidine dimers adducts.

There are two NER sub-pathways: global genomic NER repair (ggNER) and transcription-coupled repair (TCR), which differ mainly in the step of recognition of the DNA lesions. TCR preferentially repairs the transcribed strand or transcribed genes compared to the untranscribed strand or silenced genes. In other words, the transcribed strand or genes that are undergoing transcription exhibit a faster rate of repairing DNA damage than the untranscribed strand and the overall genome. RNA polymerase II plays a critical role in the recognition of DNA damage in the TCR pathway.

The current TCR model proposes that RNA polymerase, stalled at a lesion point, directs the recruitment of repair enzymes to the transcribed strand of an active gene. This model assumes that RNA polymerase II must be removed from the lesion site of the transcribed strand to provide access for the repair complex, which initiates the repair process through unwinding the double helix at the damaged site, removal of the DNA terminus, and finally filling the gap and joining the DNA strands {An, #67}.

DNA damage triggers biochemical signals that activate, in addition to DNA repair, checkpoints responsible for delay in cell cycle progression that allows more time for DNA repair. If DNA damage cannot be repaired, checkpoints aim to induce permanent cell cycle arrest or cell death in the attempt to eliminate such severely damaged cells. Checkpoints at G1/S and S-phase prevent replication of damaged DNA and those at G2/M phase prevent segregation of damaged chromosomes.

Component of this complex signaling pattern have been classified as sensors of DNA damage, signal transducers and effectors (Figure 14).

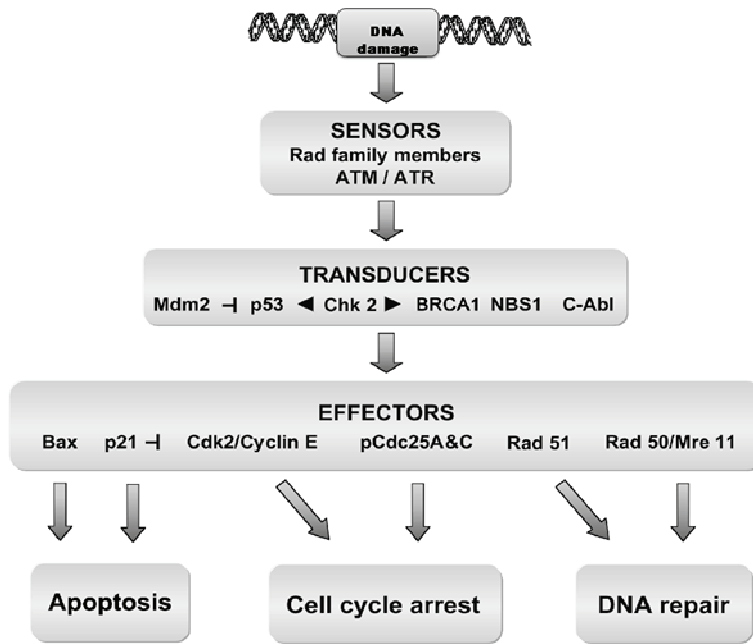


Fig 14: Components of signaling pathway involving in DNA damage recognition

This pathway is based on protein phosphorylation cascade.

Sensors scan chromatin for damage and translate it into biochemical signal that modulate the function of other proteins. Sensors include Rad1/Rad9/Hus1 complex, Rad27. Also ATM is close to the start of signaling pathway.

Downstream of sensors, signal transmission is accomplished by transducers, such as Chk2, p53, Brca1, Nbs1.

P53 induces genes such as p21 which is an inhibitor of Cdk-containing complexes,

essential for entry in S-phase, therefore inducing G1 arrest. Such a pause in cell cycling is welcome because it allows the cells enough time to repair the DNA damage inflicted by the mutagenic agent. This p53 also helps in the repair process directly by inducing the transcription of GADD45 (growth arrest and DNA damage), which encodes a protein involved in DNA repair. If during the pause in cell division the DNA damage cannot be successfully repaired, normal p53, induces apoptosis (Figure 15).

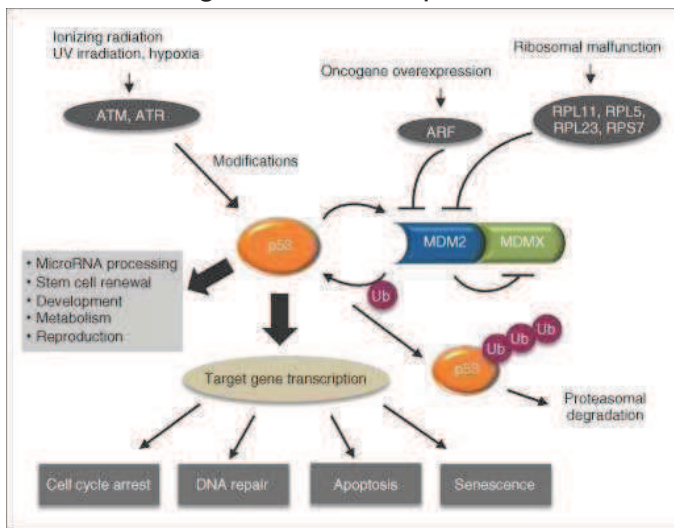


Fig 15: p53 and UV mediated DNA damage

CHIP PROCEDURE

Elucidating mechanisms controlling nuclear processes requires an understanding of the nucleoprotein structure of genes at endogenous chromosomal loci. Traditional approaches to measuring protein-DNA interactions *in vitro* have often failed to provide insights into physiological mechanisms.

Given that most transcription factors interact with simple DNA sequence motifs, which are abundantly distributed throughout a genome, it is essential to pinpoint the small subset of sites bound by factors *in vivo*.

Signaling mechanisms induce the assembly and modulation of complex patterns of histone acetylation, methylation, phosphorylation, and ubiquitination, which are crucial determinants of chromatin accessibility and in general, the assembly of these patterns acts as prelude for transcriptional activations.

These seemingly complex issues can be directly investigated by a powerful methodology termed the chromatin immunoprecipitation (ChIP) assay.

ChIP assay is a method used for experiments in molecular biology. The purpose of this assay is to determine whether proteins including (but not limited to) transcription factors bind to a particular region on the endogenous chromatin of living cells or tissues and, in reverse, to determine the genomic regions interact to specific proteins. The *in vivo* nature of this method is in contrast to other approaches traditionally employed to answer the same questions.

The target proteins of ChIP are histones (in a modified or native state) and transcription factors because these are responsible for the normal cellular functionality, including many processes as DNA synthesis, repair and assembly of transcriptional machinery. The chromatin immunoprecipitation (see figure 16 below) is able to provide a spatial and related temporal image of the chromatin state in a cell and, in addition, is able to determine in which way and in which position the transcriptional factors interact (directly or indirectly) with DNA.

The principle underpinning this assay is that DNA-bound proteins (including transcription factors) in living cells can be cross-linked to the chromatin where they are situated.

This is usually accomplished by a gentle formaldehyde fixation or through the exposure of living cell to UV light lamps. The next paragraph will be dedicated to the methods for the crosslink's induction.

Following the crosslink's induction, the cells are lysed and the DNA is broken into pieces 0.2-1 kb in length by sonication.

Once the proteins are immobilized on the chromatin and the chromatin is fragmented, whole protein-DNA complexes can be immunoprecipitated using an antibody specific for the protein in question.

The DNA from the isolated protein/DNA fraction can then be purified. The identity of the DNA fragments isolated in complex with the protein of interest can then be determined by PCR using primers specific for the DNA regions that the protein in question is hypothesized to bind.

From the short explanation it is clear the complexity of this method so it's important to evaluate step by step the ChIP protocol.

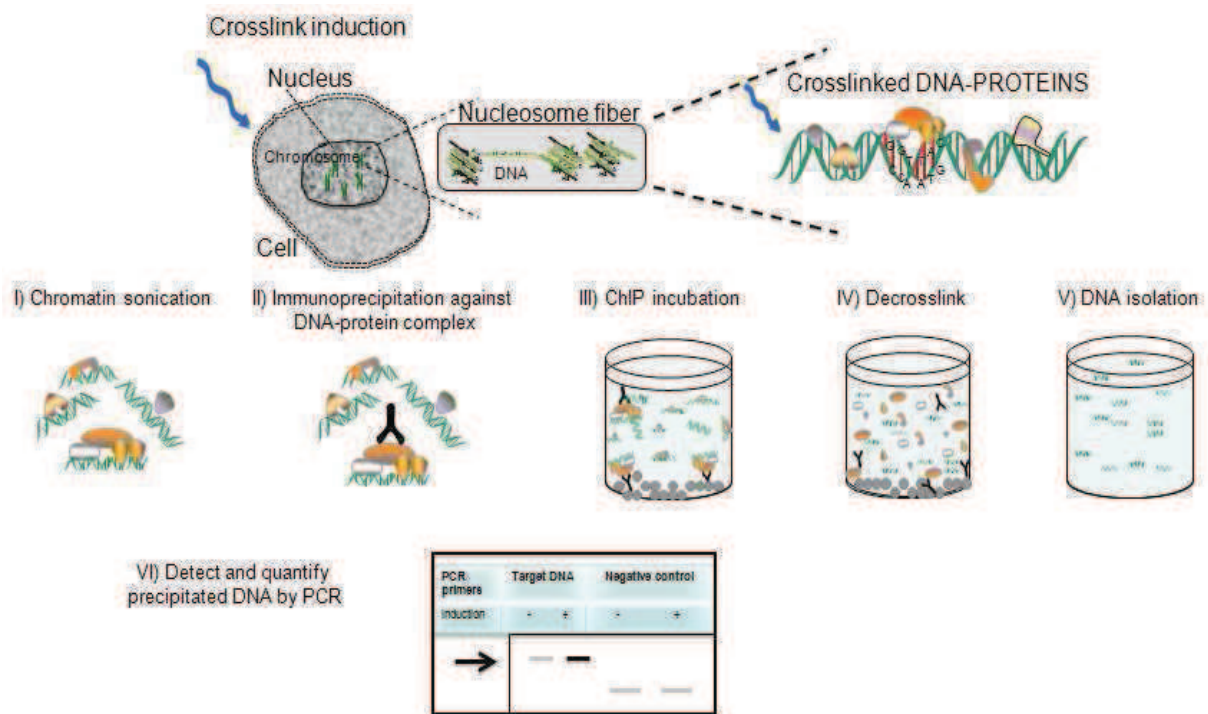


Fig 16: ChIP procedure

After the crosslink' s induction between amino acid residues of protein and nucleotide bases of DNA, the cytoplasmatic membrane of the cells must be destroyed and the nuclei sonicated.

Sonication is a rapid and straightforward way to shear the chromatin fragments and generate the smaller sized fragments desired. By controlling the sonication time and strength one can generate relatively uniform size populations and increase the resolution of the technique.

The treatment of nuclei in suspension with inaudible ultrasound (greater than about 18 kHz) results in their disruption.

Ultrasonication utilizes the rapid sinusoidal movement of a probe within the liquid. It is characterized by high frequency (18 kHz - 1 MHz), small displacements (less than about 50 μm), moderate velocities (a few m s^{-1}), steep transverse velocity gradients (up to 4,000 s^{-1}) and very high acceleration (up to about 80,000 g). Ultrasonication produces cavitation phenomena when acoustic power inputs are sufficiently high to allow the multiple production of microbubbles at nucleation sites in the fluid. The bubbles grow during the rarefying phase of the sound wave, then are collapsed during the compression phase. On collapse, a violent shock wave passes through the medium. The whole process of gas bubble nucleation, growth and collapse due to the action of intense sound waves is called cavitation. The collapse of the bubbles converts sonic energy into mechanical energy in the form of shock waves equivalent to several thousand atmospheres (300 MPa) pressure. This energy imparts motions to nuclei which disintegrate when their kinetic energy content exceeds the membrane strength.

Much of the energy absorbed by nuclei suspensions is converted to heat so effective cooling is essential during sonication procedure.

In addition it's important keep in mind that the presence of detergent (SDS) in the sonication buffer improves sonication efficiency considerably, but can induce foaming during sonication.

Foam makes the chromatin sample unsuitable for ChIP, probably as a result of the surface tension imposed by the foam, which can disrupt protein conformation. Foaming can be prevented by decreasing the sonication power.

Sonication is now used to disrupt the nuclear membranes and to fragment the cross-linked chromatin fibers. It is crucial to generate the appropriate length of chromatin fragments as it can greatly affect the read-out one obtains at the end of the procedure. Just think, excessive sonication could render a useful chromatin lysate completely useless. A length of ~500bp-1000bp is generally accepted as optimal. Unfortunately, it is very difficult to standardize the number of sonications required from laboratory to laboratory. Therefore, the procedure must be optimized in the individual laboratories and should be carefully performed for each lysate. When the chromatin is extracted from cells and fragmented, it is incubated with an antibody against specific transcriptional factors or histones.

Antibodies (Ab) are the most important factor for a successful ChIP experiment. In fact it is possible to detect only those proteins against which are commercially available Ab with high affinity and specificity and, in addition, different antibody preparations have distinct properties, which can affect the ChIP results. The affinity for epitopes differs between antibodies, affecting the resulting signal levels. For example, antibodies can differ in their sensitivity towards crosslinks or adjacent modifications and the crosslink's induction may cover up the epitope that the antibody is able to recognize on the protein linked to DNA resulting in a decrease in binding efficiency of the antibody when increasing the amount of crosslinked species.

At the last DNA isolated from the precipitated chromatin has to be analyzed to determine which DNA fragments are present in the precipitate. For the detection of specific DNA fragments, various methods are available, and the chosen method determines to what extent the data can be analyzed quantitatively. Commonly used analysis methods are conventional PCR and quantitative PCR. Alternative methods are microarray analysis and slot blotting.

Analyzing ChIP precipitates by quantitative real-time PCR (QPCR) has several advantages over conventional PCR. The QPCR technique does not quantify the amount of PCR product at the end of the PCR reaction, as with conventional PCR band densitometry. Instead, the initial amount of template DNA is calculated from the kinetics of the PCR reaction. During a QPCR run, the accumulation of PCR product is measured every cycle. The number of cycles needed to reach a certain amount of PCR product – 'Cycle threshold' or Ct value, and a calibration line, are used to calculate the initial amount of DNA template.

Quantitative PCR analysis for ChIP can be performed using DNA-dye based or probe-based PCR product detection chemistries. The most widely used DNA-dye based QPCR chemistry employs the fluorescent dye SYBRgreen for detection of the amplicon. SYBRgreen is only fluorescent when bound to double-stranded DNA (dsDNA), and the amount of fluorescence is proportional to the amount of dsDNA. SYBRgreen detects a PCR product independent of its DNA sequence, so this chemistry can be used for all primer sets.

In order to obtain high quality QPCR data, the primer sets used need to meet specific criteria. If primer sets are not optimized, this may result in amplification artifacts and/or an inaccurate quantification.

The amplification efficiency can be improved considerably by designing the length of the amplified fragment between 80 and 500 bp.

The ChIP and QPCR procedure consists of many steps that can influence the final results. Before the obtained data can be interpreted, the variation caused by all these

steps must be taken into account. The QPCR data have to be normalized for differences in the amount of input chromatin, precipitation efficiency and variation in the recovery of DNA after the ChIP.

Importantly, normalization only serves to correct for this technical variation, it should not affect biological variation.

These procedures to obtain the data's normalization involve the constitution of internal control during the development of the ChIP experiment.

The two internal controls are the so called INPUT and the so called NO ANTIBODY.

With the term input we refer to a part of sample which at the starting point is kept away from the rest and amplified with the same primers using in the ChIP.

The input sample will be indicative for the presence and amount of chromatin used in the ChIP reaction so this DNA sample should yield a PCR product with all primer sets used (the input is so a positive control).

The NoAb control is a chromatin sample to which nonspecific control serum is added instead of a specific antibody. The NoAb sample is treated the same way as the ChIP samples. The QPCR signals resulting from the NoAb samples indicate the amount of background signal generated by the chromatin preparations and ChIP procedure. Ideally, the washing steps remove non-specifically bound chromatin, resulting in an absence of QPCR signals for the NoAb samples. In reality however, it is not uncommon to find a PCR product for the NoAb control sample.

The NoAb is useful for the background subtraction.

With this method the background signals, as measured with the NoAb control, are subtracted from the signals obtained from the ChIP samples. It is assumed that by subtraction of the background signals only the true enrichment is shown. The major shortcoming of this method is the fact that the levels of background signal in the NoAb control samples may be different from those in the ChIP samples.

Finally the chromatin immunoprecipitation assay is important for understanding the molecular interactions' s role, but like other *in vivo* techniques it presents benefits and disadvantages.

Benefits:

- Good specificity
- It's a tool for the study of the mechanisms at the base of neoplastic processes *in vivo*
- Results with high scientific value

Disadvantages:

- The antibody is the technique's limiting condition
- The protocol is complex and hard-working
- It's more expensive

THE CROSSLINK INDUCTION

Protein–DNA interactions play a major role in molecular biology. They are involved not only in structural organization of the DNA within the cell nucleus, but also in DNA replication, DNA recombination and repair, as well as in gene regulation and transcription. Chemical and enzymatic methods have been developed to study protein–DNA interactions *in vitro* and, more recently, also *in vivo* by genomic footprinting . However, many protein–DNA interactions are not strong enough to be detectable with available techniques of genomic footprinting. Therefore, several methods have been used to stabilize these interactions, including chemical and UV light crosslinking.

The UV light is able to excite the electronic state of proteins and DNA which relax by means of the formation of a covalent bond.

However, this reaction is relatively inefficient and the formation of a photo-induced product is strongly dependent on structural parameters such as the proximity of reactive amino acids and base.

Not all amino acids and bases are equivalent with respect to this photo-induced reaction. So the amino acids more responsive to UV crosslink's induction possess an aromatic ring in its structure or, in general, many free electrons.

Irradiation with UV creates covalent bindings between the reactive groups of DNA and amino acids such as thymine and cysteine, serine, methionine, lysine, arginine, histidine, tryptophan, phenylalanine or tyrosine.

Usually the UV crosslink is obtained with UV lamps which can induce a stable bond between DNA and proteins in vitro but also in living cells. Irradiation of living cells with UV light lamps of wavelength near 260 nm produce covalent bonds at contact points of nucleic acids and protein (mainly transcriptional factors and histones which are already tightly associated with DNA in the nucleus). The proximity in fact affects mainly the method's efficiency because UV light is a zero length crosslinker so theoretically, is able to induce the bond's formation only between proteins and DNA's bases which are jet close together. So the occurrence of a crosslink must depend on a combination of factors, including the inherent photoreactivity of the nucleotides that are joined, the correct distance and geometrical arrangement of the nucleotides and the molecular dynamics at the site of the crosslink.

In addition photo-crosslinking with low power UV lamps requires long exposures to obtain even low levels of crosslinking and could cause enough photo-damage to the DNA to cause redistribution of proteins. The most common change on DNA is represented by the production of pyrimidine dimers. The formation of pyrimidine dimers is associated with the excitation of the triplet state of the DNA base.

For these reasons often the UV method is replaced to the chemical crosslink's procedure that employs like bifunctional reagent the formaldehyde.

Formaldehyde is the cross-linking agent of choice for the experiments on the chromatin's structure. The reaction of formaldehyde with proteins has been extensively investigated, although the general picture is not yet clear since the nature of the reaction is dependent on the conditions employed.

It is easy to handle, water-soluble, and active over a wide concentration range. Most importantly, it readily traverses biological membranes, allowing cross-linking to be performed on intact cells. Formaldehyde crosslinks primary amino groups such as those on lysines and the bases adenine, guanine and cytosine forming methylene bridges. For its chemical quality the formaldehyde is able to induce the crosslink as between DNA and proteins, as between proteins and proteins.

Protein-protein and protein-DNA crosslinks are formed between groups within distances of approximately 2 Å. These modifications are reversible: extended incubation at 65°C breaks the protein-DNA bonds while the protein-protein crosslinks can be reversed by boiling.

The crosslink's reaction is a double-steps process the formation which involves the creation of a Schiff base because of the interaction of the imino and amino groups on the proteins with the formaldehyde (figure 17 below).

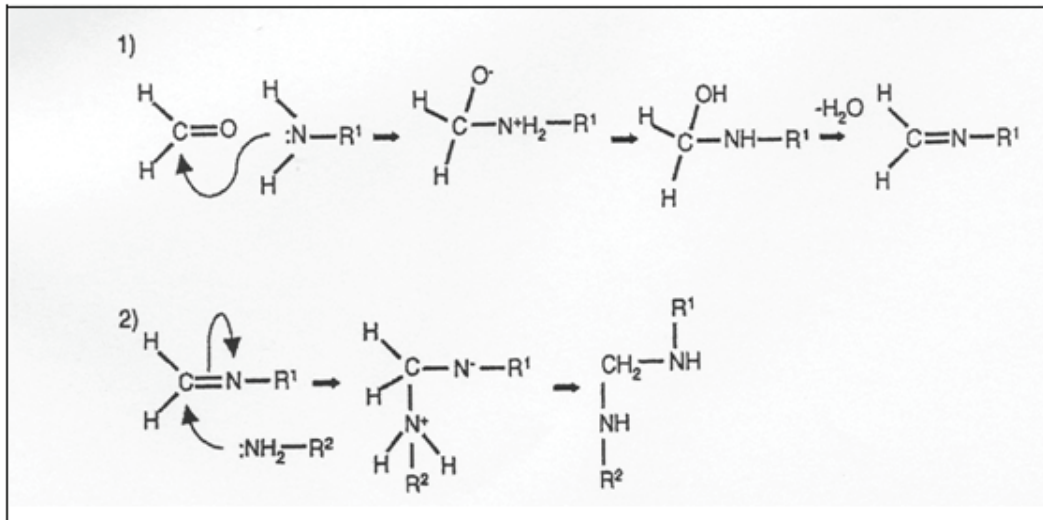


Fig 17: The crosslink's reaction with formaldehyde is a double-step process

In the second step, this activated compound is able to connect another amino group forming a stable bridge. Interestingly because formaldehyde efficiently produces protein-nucleic acid as well as protein-protein crosslinks, this method can, in principle, be utilized to detect proteins that bind DNA directly as well as those that bind DNA through other factors. This feature is at the same time, the great advantage and disadvantage of formaldehyde crosslink's induction.

In fact in ChIP experiments it's important that are able to link the DNA much transcriptional factors as possible, but at the same time it's fundamental that positive false are minus as possible. Inducing protein-protein bonds formaldehyde is able to connect large transcriptional multicomplex to related DNA regions but in this complex it might include physiological extrain proteins.

However, because chemical crosslinking usually changes protein charge, creates protein-protein crosslinks and is a multi-step process that produces chemical bridges of significant length, perturbations in structure can result.

In conclusion the chemical methods, however, disturb the equilibrium within the cell due to the general reactivity of the chemical agents and UV light generates heat, which can also perturb the interactions under study. Furthermore, both methods are slow, requiring times in the range of minutes. Therefore, they are not suitable for the study of rapid binding kinetics. In fact the proteins-DNA interactions are dynamic in vivo and their study needs to the rapid freezing of the interaction at a particular step during the assembly of the complex. To meet this requirement it's under investigation the development of a new tool that induces UV light crosslink mediated by UV laser pulsed system.

UV LASER CROSSLINK

Biomolecules never function in isolation. In living systems, proteins, nucleic acids, carbohydrates, lipids, and metabolites crowd together. Specific interactions occurring within this melange are the basis of biological function and regulation.

Ideally, the scientist could peer inside the cell and observe interactions in their native setting. Since nonperturbing nanoscopic vision does not (yet) exist, alternative approaches are needed. Historically, biochemists often employed a reductionist strategy: remove a molecule from the cellular milieu and study its behavior in a test tube environment of defined composition. More recently, methods have been

developed to probe the cellular environment surrounding a specific biological molecule. In particular, for the study of the transcription factors-DNA complexes many methods are now available.

These techniques such as immunoprecipitation of native nucleoprotein complexes attempt to 'capture' the native proteins bound to specific sequences. These methods have the potential to give artificial results, because the proteins are non-covalently bound to DNA and are subject to redistribution during chemical treatment, isolation or immunoprecipitation of the DNA-protein complex.

So, these types of experiments generally disrupt the highly organized cellular context. Such a deconstructionist approach can lead to false positive results, where molecules appear to interact with partners they would not normally encounter, and to false negative results, when low-affinity interactions fail to survive disruptive washing steps. This kind of problem can be overcome by chemical or UV-light induced crosslinking to 'freeze' DNA-protein interactions. Chemical crosslinking with formaldehyde has been extensively used to prepare samples for electron microscopy, and study the distributions of histones and other proteins along DNA. However, because chemical crosslinking usually changes protein charge, creates protein-protein crosslinks and is a multi-step process that produces chemical bridges of significant length, perturbations in structure can result. Also, because chemical crosslinking is slow it cannot be used for kinetic studies and might trap unlikely interactions.

However photochemical crosslinking of proteins to the nucleic acids has been applied to study a variety of nucleic acid binding proteins. Irradiation with UV light of wavelength near 260 nm produces a 'zero length' covalent bond between contact points of nucleic acid and protein and it occurs in the time scale of μ seconds.

Therefore, it is believed to produce less perturbation to structure than chemical crosslinking. In addition, 266 nm laser light could reduce the production of protein-protein crosslinks. Photo-crosslinking with low power UV lamps requires long exposures to obtain even low levels of crosslinking and could cause enough-photo damage to the DNA to cause redistribution of proteins.

Some of these problems can be avoided using high powered UV lasers (for the Laser theory principles, look at the next paragraph), which achieve high efficiency of crosslinking, sometimes in a single pulse.

So crosslinking by short pulsed UV lasers is a potentially powerful tool to investigate such DNA-protein interactions, especially transient interactions and binding kinetics, because the number of photons required for covalent complex formation can be delivered very rapidly, in nano-, pico- or even femtosecond intervals, and the high energy of the pulses should result in efficient crosslinking.

The mechanism leading to UV laser crosslinking induces the excitement of the electronic state of the biomolecules which culminates with the creation of a stable bond between them.

This mechanism can be understood as a two photon process. In particular, regard to the DNA-proteins interaction we can observe the excitement, indifferently, of the DNA bases or of the aminoacid side chains. This occurs because both possess a delocalized electronic system which can be excited with a radiation of suitable wavelength.

Clearly the aminoacid side chains which preferentially undergo to the photo-laser induction are the aromatic ones (mainly tyrosine, phenylalanine and tryptophane).

If we are watching to DNA (but the same is valid for a protein system) there are two possibilities for a two photon transition which leads to crosslinking (see Figure 18 below).

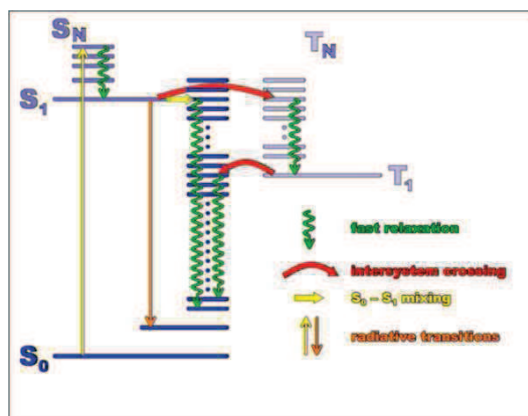


Fig 18: Crosslink induction mediated by UV laser: energy diagram

In both cases the first photon excites the S₀–S₁ transition. From the S₁ state a second photon can directly promote the excited DNA base to the high singlet level S_N, which causes crosslinking. As there is a certain probability for intersystem crossing (typical intersystem crossing rates are $k_{isc} = 10^9/s$), a fraction of the excited molecules will relax to the first excited triplet state T₁. From T₁ a second photon can lead to excitation of high triplet states T_N, which can also cause crosslinking. The ratio $m(S_1/T_1)$ between excitation via the singlet or triplet path depends on the pulse length of the exciting laser, the effective lifetime of the excited singlet state S₁ and the intersystem crossing rate.

In practice only very few crosslink events are due to the excitation via two photons at the singlet state. In fact, the critical parameter in UV laser crosslinking of proteins to DNA is not the total amount of energy but a combination of intensity and pulse length. Pulse length determines which path is used to initiate crosslinking. Although the singlet path is more efficient, it is difficult to achieve singlet excitation because of the very short effective lifetime in the singlet state S₁.

Pulses with a pulse length well below the effective lifetime of S₁ should lead to pure singlet-mediated DNA–protein crosslinking.

The triplet state T₁ is more stable of the S₁ state and its longest lifetime increases the possibility that a second photon is able to excite the transition to T_n state.

The T_n state (like also S_n state) possess enough energy for the crosslink' s induction. So, if we know the lifetime of the two transition state S₁ and T₁ which is fixed because is dependent to the chemical species in exam, the crosslink's yield depends on the intensity and length of the applied UV laser pulses.

By changing the pulse length the path leading to crosslinking can be chosen. For a pulse length shorter than the intersystem crossing rate constant, singlet-mediated crosslinking dominates, whereas pulses which are long compared with the intersystem crossing rate constant lead to crosslinking via the triplet channel.

One problem with UV laser crosslinking is the difficulty of comparing results obtained with different proteins and different DNA sequences. This is due to differences in the nature and strength of the interaction and to the involvement of different amino acid side chains and DNA bases. In some cases water molecules mediate the contacts between amino acids and DNA bases.

In addition the great capability of UV laser crosslink is the possibility, that it offers, to study the molecular interactions in vivo.

So at the UV laser pulsed systems are submit living cells or nuclei.

However, there could be fundamental differences between the results of crosslinking in cells or nuclei compared to crosslinking isolated nucleoproteins, as done in most

studies. First, suspensions of cells or nuclei scatter significant amounts of the incident light, reducing the intensity of the light within the samples. Second, the local concentration of DNA in nuclei is very high, leading to an internal filtering effect that could also decrease the effective intensity of the light. Third, the high local concentration of DNA in nuclei might trap free radicals that could increase photochemical degradation of the DNA and proteins.

LASER THEORY

A laser is an electronic-optical device that emits temporally and spatially coherent, nearly monochromatic light radiation. The term "laser" is an acronym for *Light Amplification by Stimulated Emission of Radiation*.

From its name it's clear that the stimulated emission's rule is fundamental for its functionality. Before coming to the stimulated emission phenomenon it's worth recalling a few basic principles of quantum physics. The atomic populations of any system at equilibrium in nature, without an external source of energy, stabilize to values predicted by the Boltzmann's distribution. This distribution predicts an exponential drop in atomic population with increasing energy. Let's recall a central concept of quantum mechanics: atomic energies are confined to certain allowed, discrete values. By applying the Boltzmann's law, we may predict the population of atoms for each discrete energy state. So, if the temperature of the entire system was raised, the atomic distribution would shift towards higher energies. However, the population of a lower energy level will always exceed that of a higher level.

The energy difference between the upper and lower energy states of any radiative transition is manifested as the photon energy and, hence, the wavelength of the emitted (decay to the lower level) or the absorbed (jump to the higher level) light.

Normally, emission of light is mainly the result of a spontaneous decay from excited to low-lying energy states until the ground state of the system is reached. During such a decay process the exceeding energy of the system is emitted as light in the so-called SPONTANEOUS EMISSION (see Figure 19).

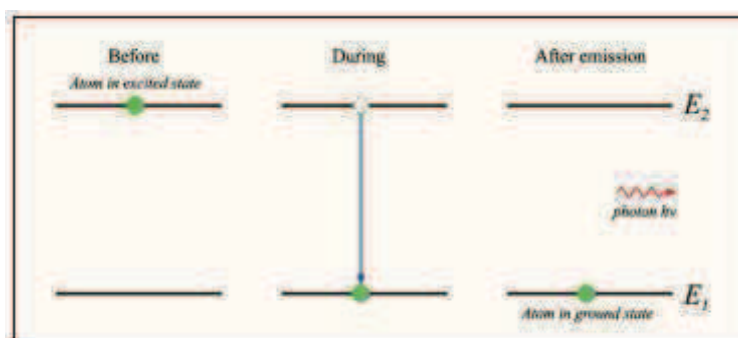


Fig 19: Spontaneous emission

Another mechanism, known as STIMULATED EMISSION also takes place; this is not dominant over the spontaneous emission until the atomic population of the ground state exceeds the population of any excited state. Stimulated emission occurs when an external radiation source, having a wavelength resonating with that of photon associated to an atomic transition, finds an atom in the excited state. Then, there is a finite probability for the external radiation field to induce a transition to the atomic ground state while a photon is emitted, identical to the incident radiation photons in energy and direction, for energy and momentum conservation. The fact that these two photons are identical makes the radiation emitted by stimulated emission coherent and monochromatic, two key properties of laser light. Additionally, the fact

that the two photons are emitted in the same direction will play a role—along with a well-aligned cavity—in making the light collimated, another key property of laser light. In essence, the original photon is amplified by this process; this is the reason for which it is called stimulated emission (see Figure 20).

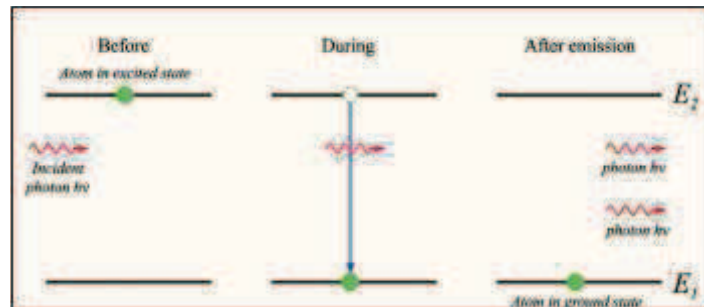


Fig 20: Stimulated emission

Let us now consider a situation where energy is injected into a system at thermal equilibrium to cause a population of atoms at a higher energy level to be larger than that of a lower level (PUMPING). Such a non-equilibrium condition is, indeed, required for lasing action in almost all lasers. Energy may be injected selectively to pump an upper energy level from which transitions occur to a lower level.

Pumping may be realized in several ways, including electrical, thermal, optical, chemical, or nuclear. Lasers often utilize electrical or optical pumping. In the latter case, when the medium where lasing action takes place (ACTIVE MEDIUM) is a solid material, light from a flash-lamp or an arc-lamp is focused onto a rod containing the lasing atoms.

Commonly used solid state laser active media include ruby (chromium ions in an aluminum oxide host glass) and YAG (neodymium ions in an yttrium–aluminum–garnet host glass).

The lasing atoms absorb photons of incident pump light and become excited to upper energy levels.

Regardless of the method, the end goal of pumping is to excite high-energy states within the lasing medium so that the population of atoms at a high-energy state is greater than the population of atoms at a low-energy state for the lasing transition.

This population inversion is a pre-requisite for the laser action to occur: if it is not maintained, atoms will absorb rather than emit photons and the light intensity will decrease rather than being amplified while traveling through a medium.

THREE AND FOUR LEVELS LASER

Lasers are classed by the number of energy levels involved in the actual lasing process as three- or four-level lasers. In a three-level system (see Figure 21 below), energy injected into the gain medium excites atoms to a pump level above the upper lasing level.

From there atoms very quickly decay to the upper lasing level, with no radiation emission (non-radiative transition). This upper level has a lifetime sufficiently long so as to ensure population inversion. The lasing transition now occurs between the upper level and the ground state, which plays the role of lower level in the lasing transition, with consequent laser light emission in the process.

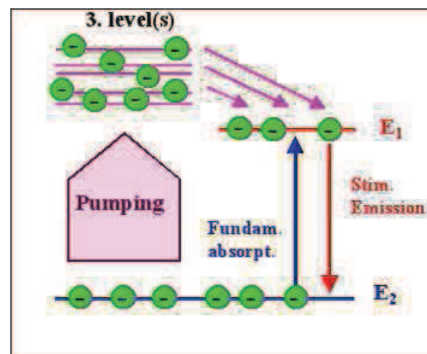


Fig 21: Three levels laser system

An improvement of this scheme is obtained with a four-level structure, where the laser transition takes place between the third and second excited states on the energy axis (see Figure 22). Decay of the lower laser level must be much more rapid than the lasing transition to ensure a good population inversion and, consequently, an efficient lasing action.

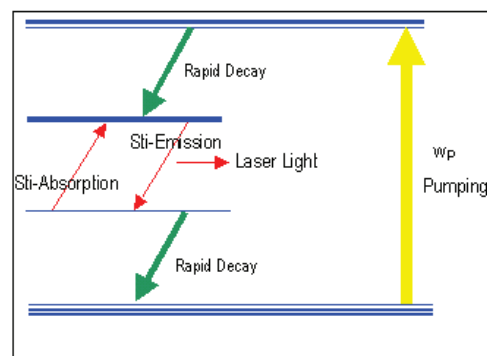


Fig 22: Four levels laser system

In fact, in a four-level system, laser gain is realized as soon as pumping is applied to the system. Pump energy is injected into the pump level, which decays, in most cases, almost instantaneously to the upper lasing level. The active medium is such that the upper level has a longer lifetime than the lower one, therefore a population inversion occurs almost immediately after pump energy is injected. For the above reason four-level systems are more efficient than three level ones, and by far the most commonly used.

LASER COMPONENTS

A laser source is an optical cavity, constituted by an active medium between two mirrors, pumped by an external energy source (see the Figure 23 below).

This pump source can be a flash-lamp or an electrical power supply, or chemical reaction or another laser, depending on the specific system in use.

The pumping energy is directed into the gain medium, namely the material which gives different lasers their individual characteristics. There are many different materials used as active/gain media including crystalline solids usually doped with transition metal or rare earth ions, gases such as CO₂ or He and Ne, semiconductors such as gallium arsenide and liquids dyes.

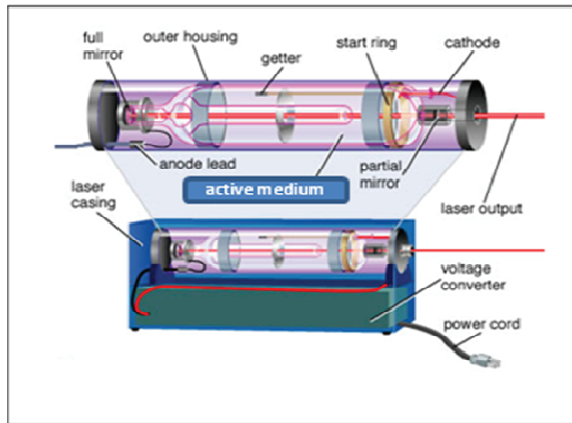


Fig 23: Laser components

When energy is pumped into the gain medium it causes population inversion and the release of a great number of photons via stimulated emission. A pair of mirrors are placed at the front and back of the gain medium, respectively, to constitute a closed optical cavity.

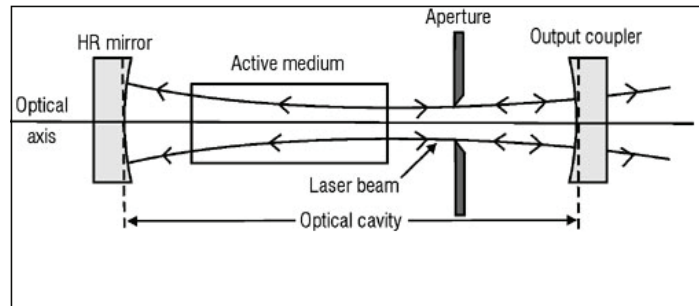


Fig 24: Light amplification in laser active medium

One of the two mirrors is fully reflective (HR), whereas the other one is only partially reflective (output coupler). Photons emitted due to stimulated emission pass through the medium many times getting more and more (light amplification) until they pass through the output coupler and escape from the laser cavity to form the output laser beam (see Figure 24).

Aim of the thesis

AIM OF THE THESIS

The study of molecular biology involves the dissection of biological systems to identify and isolate individual molecules, determine their characteristics by which to understand what is their role and function inside the cells. Once defined the function of a single molecule, it is joined by networks of interaction-structure-function, in order to describe the interconnections that characterize a biological system.

But it is known that biological systems are complex and their function depends, mostly, from the multiple interactions that determine the individual components together in a given time and in a given context. Therefore, this approach, called reductionist, turns out to be very useful in fields of biology whose ultimate goals are to understand the spatial and temporal evolution of molecular interactors.

From this observation emerges the need to look at the "cellular world" with a new approach that aims to study living organisms as systems that evolve over time, ie dynamic interaction of parts in its composition. In this need is called to answer a new branch of biology, called Systems Biology.

Systems biology begins with the knowledge of genes and proteins present in the time thing in an organism, and uses techniques of transcriptomics, metabolomics and proteomics to assess the dynamic changes resulting from a perturbation of the system itself. This discipline makes extensive use of the approaches of systems theory, bioinformatics and mathematics-statistics with the aim of creating a more complete model of the functioning of biological systems. Instead of molecular biology, which focuses on biological macromolecules, with particular attention to the nucleic acids and proteins, systems biology is not concerned with the individual but the molecular mechanism of the dynamic interactions between different molecules to form a system over time. The dynamic aspect, namely the strong dependence on the time of the training programs of biological structures and processes, is the aspect that strongly characterizes the systems biology science than the rest of the "omics".

The innovation that has enabled the birth and development of systems biology is the introduction of high-throughput technologies that allow us to study simultaneously a wide variety of molecules (mRNA, proteins, lipids, metabolites) involved in biological processes and integrate data from different experiments in a unified vision. The features that must have high-throughput technologies that can be integrated into a systems biology project are: speed of execution, simultaneous experiments, large amount of data resulting from the experiment itself. These characteristics are inherent in ChIP-laser technology currently under investigation in the research line "development of an ultra-short laser source for the study of epigenetic modifications on chromatin. The main objective of the research line "development of an ultra-short laser source for the study of epigenetic modifications on chromatin" consists in the development and subsequent creation of an experimental platform that, through the use of a laser source, both in able to induce cross-link reactions between DNA and proteins within living cells to study the evolution in time and space of both the transcriptional machinery, much of the epigenetic code.

The need for such equipment and technology arises from the fact that the rapid development of applied research in the field of "Systems Biology" has now reached a critical level in terms of technology, as conventional chemical methods for the induction of covalent bonds between DNA and transcriptional factors as steps preliminary experiments of chromatin immunoprecipitation have a number of inherent technical limitations with regard to selectivity, sensitivity, precision, efficiency, dynamic interactions, masking and modification of certain epitopes.

This laser technology, therefore, is a valid alternative to these traditional methods as it is able to induce links between DNA and proteins in very short intervals of time and with high efficiency of reaction. The idea that drives this project is the observation, confirmed by experimental data that evidence in the literature, that an ultrashort UV laser can excite the electronic states of nitrogenous bases composing the DNA and amino acid side residues of proteins that bind DNA itself.

Once absorbed energy, the system DNA-protein relaxes to the ground state via the formation of a covalent bond. The creation of this link, obtained by a method "foto-physic", opens up a range of possibilities for study of interaction in "real time" and rapid decoding of "cross talk" between transcription factors, enhancers, epigenetic modulators and DNA.

The reducing time scale of crosslink induction increases the number of proteins-DNA interaction that can be analyzed by "omic" science, and in general helps to clarified the temporal sequence of the events constituting the biological phenomenon (for example the epigenetic code variation).

Materials and Methods

MATERIALS AND METHODS

Cell lines.

MDA-MB231 and MCF7 were cultured using standard procedures. Both cell lines were cultured in Dulbecco's modified Eagle's medium (DMEM-Euroclone) supplemented with 10% FCS (Sigma), 50µg/ml penicillin-streptomycin (Gibco) and 2mM glutamine (Gibco). Cell lines were maintained at 37°C in a humidified atmosphere of 95% air, 5% CO₂ as previously reported.

Trypan Blue staining

Cells treated and un-treated were seeded at an initial concentration of 1×10^6 cells/ml cells in 6-well tissue culture plates.

After 24 h, cells were collected by trypsinization and counted in duplicate; Trypan blue (Euroclone) dye exclusion was used to determine a cell growth curve. The number of cells was reported in comparison to a control-non treated samples.

Optical microscope observation and cell images capture

Treated and un-treated cells were analysed with phase-contrast optic microscope (EVOS) and cellular images were capture with camera integrated inside the microscope.

Each experimental point was carried out in triplicate.

Western blotting analysis and antibodies.

For immunoblotting, MDA-ERalpha-GFP cells were lysed (50mM Tris-HCl pH 8.0, 150mM NaCl, 1% NP-40, 10µM NaF, 0.1mM Na₃VO₄), 40µg/ml PMSF and protease inhibitors (SIGMA). Insoluble material was removed by centrifugation, and protein concentration was determined by Bio-Rad assay (Biorad). Lysates (30µg protein) were loaded onto SDS-PAGE gels and proteins were transferred to nitrocellulose membranes (Schleicher and Schuell, Dassel, Germany) and recognized by specific antibodies. The antibody against total p53 (1:1000) was purchased from BD Transduction Laboratory (BD) {Bontempo, 2009 #85}.

The antibodies against phS1981 ATM (1:1000) and phS139 H2AX (1:1000) were acquired from Abcam.

The antibody against Ack373-382 p53 (1:500) is made from Upstate; NBS1 (1:1000) is an antibody product by R&D Systems, while ERKs (1:1000) is a Santa Cruz one. Primary antibodies were detected using horseradish peroxidase-linked anti-mouse or anti-rabbit (Amersham Biosciences), conjugates as appropriate and visualized using the ECL detection system (Amersham Biosciences).

Histone detection

MDA-ERalpha-GFP cells were harvested and washed twice with ice-cold PBS 1x (Euroclone). Then cells were lysed in Triton Extraction Buffer (TEB: PBS containing 0.5% Triton X 100 (v/v), 2mM phenylmethylsulfonyl fluoride (PMSF), 0.02% (w/v) Na₃N) at a cellular density of 10⁷ cells per ml for 10 minutes on ice, with gentle stirring. After a brief centrifugation at 2000 rpm at 4°C, the supernatant was removed and the pellet was washed in half the volume of TEB and centrifuged at before. The pellet was resuspended in 0.2M HCl at a cell density of 4x10⁷ cells per ml and acid extraction was proceeded over night at 4°C on rolling table. The day after the samples were centrifuged at 2000 rpm for 10 minutes at 4°C, the supernatant was removed and protein concentration was determined using the Bradford assay. About

10 µg of acid-extracted protein were loaded on 15% SDS-polyacrylamide gel electrophoresis (SDS-PAGE) and transferred to nitrocellulose. The nitrocellulose was incubated with anti phS139H2AX (Abcam) and the analyses were performed according to the supplier's suggestions. Ponceau red staining was used to normalize for equal loading {Garcia, #82}.

Cell cycle analysis

The cells were harvested and resuspended in staining solution containing RNase A, propidium iodide (50 µg/ml), sodium citrate (0.1%), NP40 (0.1%) in PBS 1X for 30 min in the darkness. Cell cycle distribution was assessed with a FACScalibur flow cytometer using the Cell Quest software (Becton Dickinson, Milan, Italy) and analyzed by standard procedures using the same software and the ModFit LT version 3 Software (Verity, Topsham, ME, USA) {Milite, #81}.

Cell death analysis

For cytofluorimetric analysis, cells were cultured and irradiated in specific LASER operating condition. Then cells were collected in 0.1% sodium citrate and 50 µg/ml propidium iodide (PI). After 30' incubation, the percentage of cells with sub-G₁ DNA was evaluated for flow cytometry with a FACS analyzer (FACScalibur; BD Biosciences, San Jose, CA) {Souto, #83}.

ROS production Analysis

To measure intracellular ROS levels, cells grown at 70% confluence were collected and suspended in PBS. After the crosslink induction performed with LASER device in the selected conditions, the oxidation sensitive fluorescent probe dihydroethidium (DHE, Invitrogen, Carlsbad, CA, USA) was added at 5 µM. After 30 min of incubation under protection from light, the cell suspension was subjected to flow cytometry analysis.

DNA extraction and purification

DNA extraction and purification was obtained by using Qiagen kit, following the directions provided.

Caspases3/7 activation assay

Cellular damages and so apoptosis was detected by examining caspase 3/7 activity following the manufacturer's instructions (B-Bridge). The methodology is based on a fluorochrome inhibitor of caspases (FLICAs). The detection of caspases 3/7 activity is based on an inhibitor peptide sequence (DEVD) targeted by both caspase 3 and caspase 7. The red probe is sulforhodamine B (SR).

The probes also contain a fluoromethyl ketone group (FMK), which forms a covalent bond with the active caspase enzyme; because of the non-polar nature and relatively small molecular weight of these FLICA probes, they are cell-permeant. Because the SR-DEVD-FMK FLICA reagent becomes covalently coupled to the enzyme, it is retained within the cell while any unbound SR-DEVD-FMK FLICA reagent diffuses out of the cell and is washed away.

After 1 h of incubation of a sample of 1×10^6 cells with the caspases 3/7 SR-DEVD-FMK substrate and two washings in PBS, all samples were analyzed by FACS using a FACScalibur (Becton Dickinson, NJ) and the Cell Quest Technology (Becton Dickinson, NJ).

Immunoprecipitation assay (IP).

Cell extract was prepared from pellets of MDA-ERalpha-GFP cells to 80% confluence in 150-mm tissue culture plates. Proteins were extracted in buffer containing NP-40 (0.5%), Tris-HCl pH 8.0 (20mM), NaCl, (150mM), PMSF (1mM), Glycerol 10%, EDTA (1mM) and 1X Complete protease inhibitor mixture (SIGMA) for 20 minutes on ice. Cell debris was removed by centrifugation for 10 minutes 12,000 ×g and the soluble material was incubated with the antibodies against ERalpha (Santa Cruz) and GFP (Abcam) at the recommended concentrations overnight at 4°C. The immune-complexes were precipitated with Sepharose-protein A/G Plus (Santa Cruz Biotechnology) for an additional 2 hours at 4°C. After four washes in lysis buffer and two in PBS, the proteins bound to beads were eluted and resuspended in SDS-PAGE sample buffer and analyzed by Western blot to verify specific IP.

Transfection of pERalpha-EGFP-C1 in MDA-MB231 cells

pERalpha-EGFP-C1 vector (kindly provided by Ken-Ichi Matsuda, Department of Anatomy and Neurobiology, Kyoto Prefectural University of Medicine) {Matsuda, 2002 #84} was transfected into MDA-MB231 cells thanks to Lipofectamine™ 2000 Transfection Reagent (Invitrogen). First of all 2×10^5 cells were plated in each well of a 12-well plate. After the cells have been adhered we proceed to prepare the lipofectamine reaction mixture, composed of 1 ml of Opti-MEM (Invitrogen) plus 4 µl of Lipofectamine Reagent and we left it at RT for 5 minutes, shaking every 30 seconds. Then the DNA mix was set: 1 µg of plasmid up to 30 µl with sterile TE 1X. At this point the Lipofectamine mixture was combined with DNA solution and was incubated for 20 minutes at RT, shaking every 2 minutes. In the end the cells were washed with sterile PBS twice and the final mixture was added them gently; after 6 hours complete D-MEM medium (Euroclone) was supplied to MDA-MB231 cells

Transfection efficiency evaluation

The efficiency of transfection was calculated through FACS (FACScalibur; BD Biosciences, San Jose, CA) analysis looking at GFP presence inside MDA-MB231 transfected cells. The percentage of GFP-positive cells was analyzed as shift along FL1 channel, in comparison with un-transfected cells

Cell sorting

The cytofluorimeter used to sort MDA-ERalpha-GFP cells is FACS ARIAll (Becton Dickinson). Data were analysed with Diva 6.1 software.

After the construction of G1 gate on the base of physical parameters (FSC and SSC) to isolate an homogeneous cell population, the dot-plot of GFP-positive cells was obtained. The FACS calibration was carried out through Accudrop beads, all the needles and connection were sterilized with 70% ethanol and washed with 1x sterile PBS.

The threshold of GFP positive cells was set on G2 gate and the cells were collected.

Pyrimidine dimers formation assay

The pyrimidine dimers formation, after the exposure of living cells at UV LASER radiation, was evaluated and measured following the manufacturer's instructions (Abnova).

The Abnova cellular UV-Damage Detection kit based on the formation of CPDs on the genomic DNA that was detected by anti-CPDs antibody.

To enable antibody binding to CPDs on the genomic DNA, cell must be fixed, permeabilized and DNA denatured. Detector anti-CPDs antibody is pipetted into the wells and allowed for 1 hour, during which time it binds to any CPDs. Unbound antibody is washed away and horseradish peroxidase-conjugated secondary antibody is added, which binds to the detector antibody. The horseradish peroxidase catalyzed the conversion of the chromogenic substrate tetra-methylbenzidine (TMB) from a colorless solution to a blue solution (or yellow after the addition of stop reagent). The colour is quantified by spectrophotometry (Abs 450nm) and reflects the relative amount of CPDs in the cells.

Comet Assay

Trevigen's CometAssay, or single cell gel electrophoresis assay, provides a simple and effective method for evaluating DNA damage in cells. Alkaline Comet assay is used to detect small amount of damage including single and double stranded DNA breaks.

First of all 1×10^5 cells (treated and untreated with LASER device) are immobilized on a bed of low melting point agarose and then gently lysed (Lysis Solution cat: 4250-050-01).

The assay is performed in alkaline conditions (0,4g NaOH, 200mM EDTA) to unwind and denature the DNA and to hydrolyze sites of damages.

The remaining nucleoids are subjected to electrophoresis in an Alkaline Electrophoresis Solution pH > 13 (8g NaOH, 500mM EDTA pH8) and subsequent staining with a fluorescent DNA intercalating dye (SYBR Green staining solution).

The Comet visualization is performed with epifluorescence microscope (Zeiss).

In Fluorescence Experiments

Cells transfected and irradiated were gently lysed to preserve the integrity of nuclear membranes.

Then they are sonicated and the DNA was recovered with Qiagen DNA extraction kit, following manufacture's instructions. The protein ERalpha-GFP linked to DNA (on ERE sequences) was purified and the quantity of GFP signal (related to the amount of crosslink induction) was measured with fluorescence scan plate reading (TECAN INFINITE 2000).

ChIP experiments

The antibody used in ChIP experiments was :3CH3K4H3 (Abcam). The analysed genomic regions were:

H2B Prom F	TGTA CTTGGTGACGGCCTTA
H2B Prom R	CATTACAACAAGCGCTCGAC
TRAIL Prom F	AGTTTCCCTCCTTTCCAACG
TRAIL Prom R	CACTGAAGCCCTTCCTTCTCT
Myog F	AAGTTTGACAAGTTCAAGCACCTG
Myog R	TGGCACCATGCTTCTTTAAGTC
SCAMP5 F	GAACTAGCACCTCGGACAGC
SCAMP5 R	AGGAGGAGCAGCCTTAGGAG

The MDA-ERalpha-GFP cells were crosslinked with formaldehyde (positive control) and with Laser device at different combinations of repetition rate, energy for pulse, time duration and UV light output.

Then the cells were lysed (Buffer B: 20 mM HEPES pH 7.6, 10 mM EDTA, 0.5 mM EGTA, 0.25% triton-x100; Buffer C: 50 mM HEPES pH 7.6, 150mM NaCl, 1mM

EDTA, 0.5mM EGTA) and sonicated in a specific Buffer D (20mM HEPES pH 7.6, 1mM EDTA, 0.5mM EGTA)+ 0.05% SDS + protease inhibitors.

The sonicator employed was Bioblock Vibra Cell 72434.

The chromatin immunoprecipitation was carried out over night at 4°C in ChIP mix (PIC, MQ water, Incubation Buffer, chromatin, antibody, blocked beads). The Incubation Buffer contains: 10 mM Tris pH 8.0, 150 mM NaCl, 1mM EDTA, 0.5 mM EGTA, 0.15% SDS, 1% triton-x100 and protease inhibitors

The beads were washed, the crosslink reversed and the purified DNA was analyzed by RealTime-PCR, looking at specific regions of DNA.

Immunofluorescence experiment

MDA-ERalpha GFP cells were treated as suggested to manufacture antibodies suppliers.

In particular the antibody was against ER-alpha (Santa Cruz) and revealed with Texas Red conjugated anti-rabbit.

Nuclei were stained with Hoechst for 10 minutes; images were analyzed with fluorescence microscope (ZEISS).

Laser apparatus

PHAROS is a custom, versatile femtosecond laser as a source of UV/visible ultrashort pulses. It is based on the new active medium Ytterbium tungstate (Yb:KGW) that shows several distinctive features which make it an attractive alternative to Ti:sapphire based system. Yb: KGW, having broad enough emission spectrum to support <200 fs pulse generation, can be directly pumped by diode lasers at 980 nm making the system less complex and more reliable. Due to high pump absorption cross section and low heat emission/power consumption rate Yb:KGW systems offers high output power and near-diffraction limited beam quality. The PHAROS Laser is able to deliver high-energy UV- fs-pulses in the energy range 10-150 microjoule per pulse at a repetition rate variable within almost six orders of magnitude, between 1 Hz and 200 kHz. The carrier wavelength of such pulses is 263 nm, in order to match the first UV absorption band window of DNA bases which covers the 250-280 nm range.

This laser utilizes the chirped pulse amplification technique (CPA) to deliver ultra-short, ultra-intense pulses with no damage to the employed optics. Hence, it is made of four parts:

- Laser Oscillator
- Pulse Stretcher
- Regenerative amplifier
- Pulse Compressor

The oscillator includes two active medium rods and it's optically pumped by Xe flash-lamps. After the pumping, the modes are locked (Kerr lens mode-locking) so that a train of equally spaced pulses— with energy of ≈ 1 nJ and duration of ≈ 100 fs - is produced, the time distance between two pulses being approximately 15 ns. The pulse energy is low enough to prevent the occurrence of self-induced phenomena in the active medium and damaging of all the crossed optics in the oscillator. To keep the intensity low the Chirped Pulse Amplification technique is adopted (see the figure I below concerning the scheme of principle of the CPA technique).

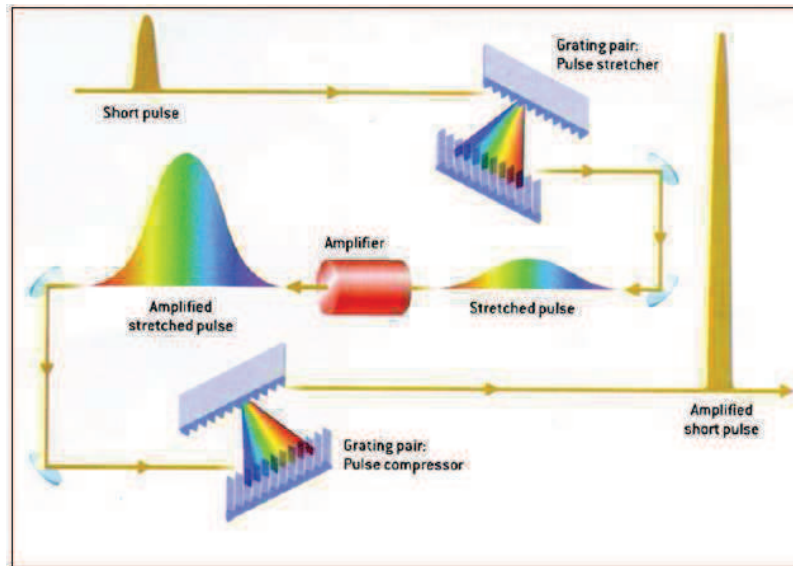


Fig I: CPA technique

The pulse is stretched by a pair grating to extend the pulse duration thereby reducing the peak power. It acts by inducing spatial dispersion in the pulse so that different spectral components travel different paths and are lined up at the stretcher exit.

Peaks with low power are then amplified in the regenerative amplifier with no risk of damages for the active medium and the optics of the regenerative amplifier. The pulse leaving the stretcher lasts ≈ 300 ps and enters the regenerative amplifier. The regenerative amplifier is a laser cavity itself. The pulse coming from the stretcher acts as a seed for the lasing action into the amplifier cavity and gets strongly amplified by passing back and forth into the amplifier laser rod, thus taking all the gain acquired in the pumped amplifier active medium. The pulse oscillates within the amplifier cavity until it becomes amplified by a factor of about 10^6 . It is, then, extracted from the regenerative amplifier cavity by means of an electro-optic ultra-fast switch. The compressor is made by a second pair grating and works in the opposite way with respect to the stretcher, so it compensates for the dispersion introduced by the stretcher through two diffraction gratings. In the compressor the colours which traveled a longer distance into the stretcher and were, , delayed take a shorter path and are re-phased in time with colours that arrive first.

The compressor is made of all-reflection optics so it can generate a pulse with a peak great power with no risk of damages.

The recompressed pulse has a duration of 130 fs an energy of about 4 mJ at a repetition rate of 2 kHz. The repetition rate can be as high as 200 kHz at the expenses of the pulse energy.

Such laser source is followed by a series of harmonic generator contained in a case ("HIRO", Light Conversion).

The FHG (see the Figure II) is able to generate a UV femtosecond pulses starting with a near-infrared laser source.

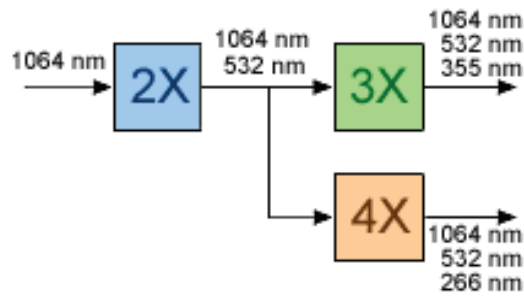


Fig II: Harmonic generation principles

The second harmonic generation is achieved by non-linear crystals which have a small group velocity difference between the fundamental and the harmonic wave, a large non linearity and exhibit no absorption at both the fundamental and harmonic wavelength. These crystals need to be also transparent at twice the harmonic frequency to avoid two photons absorptions.

For the above reasons the typical choice, in this case, is KDP.

“HIRO” is the harmonics generator for “PHAROS” laser providing conversion to 515 nm, 343 nm and 258 nm wavelengths.

With its small foot print – 155x325mm – and a wide variety of fixing methods “HIRO” fulfills the need of all – OEM, industrial and scientific users. Depending on the model of “HIRO” it can provide the second and the fourth or the second, the third and the fourth harmonic. The active harmonic is selected by manual rotation of the knob – changing the harmonics will never take longer than a few seconds.

“HIRO” shows a lot of features:

- High conversion rate to the second/third/fourth harmonic
- Easy switching between active harmonic
- Small footprint
- Integrated separation of the harmonics
- Flexible in fixing and easily customized to include additional options such as splitting the harmonics, continuum generators, beam expanders/down-collimators

The principal of operation of “HIRO” is based on collinear generation of the higher harmonic of laser radiation in angle-phase-matched nonlinear crystals. The optical layout of “HIRO” also includes the beam size reduction and collimation optics to ensure highest conversion efficiency into the harmonics. One active harmonic can be selected from the “HIRO” at a time. However the residual lower harmonics can be also accessed through the output ports. All the harmonics exit the housing already separated from the lower ones by a couple of dichroic mirrors.

Alternatively the output of “PHAROS” laser device could be sent to “ORPHEUS” device to convert the infrared pulses in visible light.

“ORPHEUS” is a collinear optical parametric amplifier of white-light continuum pumped by “PHAROS” laser. It shows high output stability throughout the entire tuning range, high output pulse and beam quality, full computer control via USB port as well as lots of optional frequency mixers to extend the tuning range from UV up to mid-IR ranges.

It can also operate at wide range of repetition rates from 1 kHz up to 1 MHz.

Parametric amplification is performed with the second harmonic of pump laser. 515 nm pump beam is generated inside of OPA unit with computer controlled angle

adjustment. Fresh/residual fundamental and second harmonic radiation (1030 nm and 515 nm respectively) are accessible from dedicated output ports.

ORPHEUS provides tunable OPA output (630-2600 nm) with residual second harmonic and fundamental radiation beams at the same time. Collinear optical parametric amplification (OPA) has been used for more than a decade to generate ultra-broadband pulses in the visible frequency range (~300-750 nm).

The basic idea behind the concept of OPA is illustrated in Figure III below.

Briefly, when the signal and pump are collinear so that it is only possible to amplify a relatively narrow range of frequencies at once.

However, at certain non-collinear angle α between pump and signal beams, the phase matching curve becomes essentially flat in a broad frequency range over which simultaneous amplification of signal frequencies is possible.

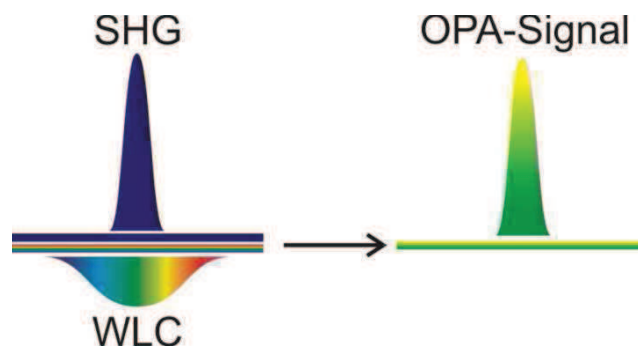
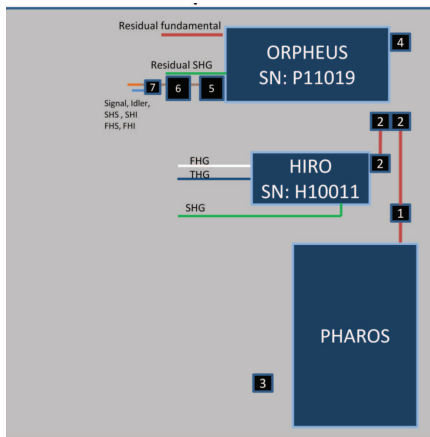


Fig III: OPA

In the schematic Laser configuration below (Figure IV), the possibility to switch from “PHAROS”-“HIRO” to “PHAROS”-“ORPHEUS” is explained.

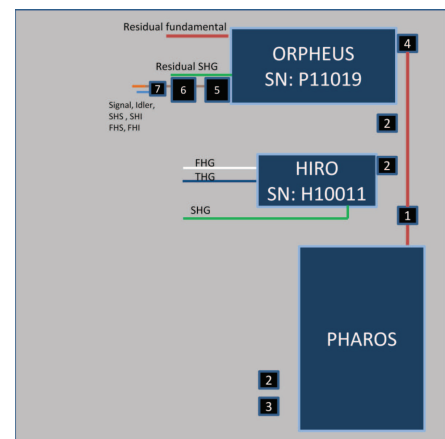
System layout

1. Full PHAROS output to HIRO



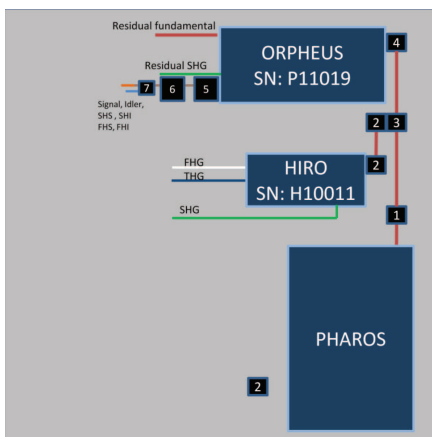
- 1 – Periscope (70mm->125mm)
- 2 – Beam routing mirror
- 3 – Beam splitter (50%)
- 4 – Beam routing mirror with shutter
- 5 – Mixer 1 (external frequency mixing stage)
- 6 – Mixer 2
- 7 – Wavelength separator

2. Full PHAROS output to ORPHEUS



- 1 – Periscope (70mm->125mm)
- 2 – Beam routing mirror
- 3 – Beam splitter (50%)
- 4 – Beam routing mirror with shutter
- 5 – Mixer 1 (external frequency mixing stage)
- 6 – Mixer 2
- 7 – Wavelength separator

3. 50% to HIRO



- 1 – Periscope (70mm->125mm)
- 2 – Beam routing mirror
- 3 – Beam splitter (50%)
- 4 – Beam routing mirror with shutter
- 5 – Mixer 1 (external frequency mixing stage)
- 6 – Mixer 2
- 7 – Wavelength separator

Fig IV: Schematic Laser configuration

In the configuration 2 (Full PHAROS output to ORPHEUS) only some combination of repetition rate and energy for pulse are allowed, as shown in the figure V immediately below.

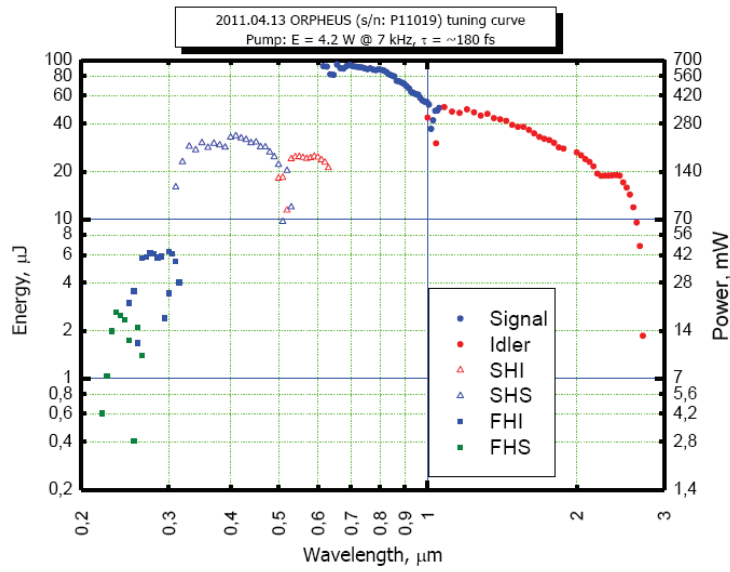


Fig V: ORPHEUS tuning curve

It is interesting to note that a third configuration also exists, by which the output of PHAROS could be spitted 50% to HIRO and 50% to ORPHEUS. This configuration will be an useful tool to perform “double colors” crosslink experiments. The rationale of two colors experiments is reported in the Supplementary table 2, in attach at the end of the thesis.

Results

RESULTS

Establishing a stable covalent bond between proteins and nucleic acids, usually referred to as crosslinking {Solomon, 1985 #86} is a powerful tool of molecular biology, which affords access to study otherwise transient interactions between biomolecules. Crosslinking with fs- UV lasers has been presented in the literature as a revolutionary technique to increase the otherwise low process yield of conventional methods based on chemical catalysts, {Solomon, 1988 #87} conventional UV sources, {Zhang, 2004 #88} or longer UV pulses {C. Russmann, 1997 #89}.

It is known that crosslinking induced in cells by ultrashort laser pulses has a twofold advantage over conventional methods. (i) It binds only species that are in proximity (“zero length” covalent bond) of the absorbed photons rather than favoring unspecific bonds amongst many possible species in the cell. (ii) It should only operate until the radiation is incident on the sample, thus paving the way for time-resolved studies of transient interactions. Moreover, when combined with biochemical techniques such as Chromatin Immunoprecipitation (ChIP) to analyze the produced bonds, the UV laser method will make feasible the characterization of the dynamics of the transcription factors bindings on chromatin in living cells, thus overcoming the technical limitations of the current technologies {Lis, 1985 #90}.

The first step in the project has consisted in testing a femto-second laser system (PHAROS) with the aim to optimise UV-laser photo-induced cross-linking with high efficiency. The PHAROS in use is able to deliver high-energy UV- fs-pulses (in the energy range 10-150 microjoule per pulse) at a repetition rate variable within almost six orders of magnitude, between 1 Hz and 200 kHz. The carrier wavelength of such pulses is 263 nm, in order to match the first UV absorption band window of DNA bases which covers the 250-280 nm range. These characteristics offer the advantage of making such laser source particularly suitable for the project purpose as it has (i) high energy/pulse and (ii) high and variable repetition rate, thus looking promising for fast, highly-efficient, damage controlled laser induced DNA-protein cross-link.

In order to evaluate the capability of this UV laser source to induce the cross-link between DNA and proteins and for understanding the optimum conditions in which this cross-link can be obtained, a vast range of biological experiments have been made next to General Pathology Department of S.U.N. University.

First of all a fast and highly powerful method has been creating to test a variety of macroscopic parameters characterizing the DNA-proteins interaction *in vivo* mediated by laser light (see Supplementary Table 2 to the summarize of the method). These test responses are not referred to a single cell typology or a unique DNA-transcriptional factor interaction, but they provide a great number of technical and biological data suitable for Laser-ChIP (L-ChIP) technique development. The key point in the experimental data-set has been the creation of a stable cell line expressing a transcriptional factor linked to the GFP protein; to ensure a homogeneous starting fluorescent clone population the cells have been selected with a cell sorter (FACS AriaII). For this purpose MDA-231 cells (that are Estrogen Receptor negative Breast Cancer cells) have been transfected with a vector coding for Estrogen Receptor α , linked to Green Florescent protein (ER α -GFP). The Estrogen Receptor α is a ligand-activated receptor that is a member of the steroid/nuclear receptor (NR) superfamily and acts like a transcriptional factor when binding particular DNA regions (ERE: Estrogen Responsive Elements). The NR ER α is recruited on the minimal consensus ERE sequence that is a 13 bp palindromic inverted repeat sequence (IR): 5'-GGTCAnnnTGACC-3' and though an highly

conserved C domain (comprised of two functionally distinct zinc fingers) it interacts directly with the DNA helix. Even though MDA-231 are ER-negative cells in their DNA are present the ERE sequences; so in the obtained ER-GFP clones is possible to observe a green fluorescent signal (with an emission wavelength at 510 nm) directly on the chromatin.

So first of all, the MDA-MB 231 cells were transfected with pERalpha-EGFP-C1vector and the efficiency of transfection was measured at FACS looking at the percentage of GFP fluorescent signal present inside the cells.

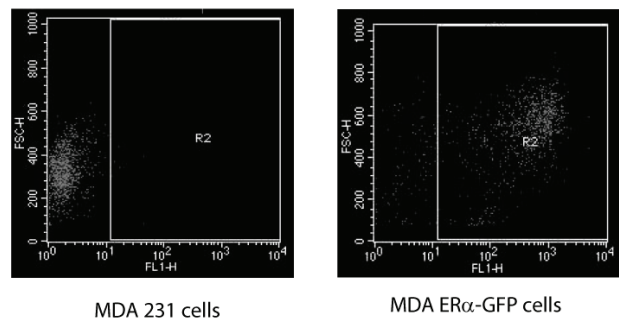


Fig 25: FACS Transfected GFP positive cells. The data are referred to the parental MDA-MB231 cell line

In the figure 25 above is possible to observe the shift of cellular population along the FL1-H (the green channel of FACScalibur station).

Another experiment to confirm the transfection and the production of fusion protein Erα-GFP was the immunoprecipitation one.

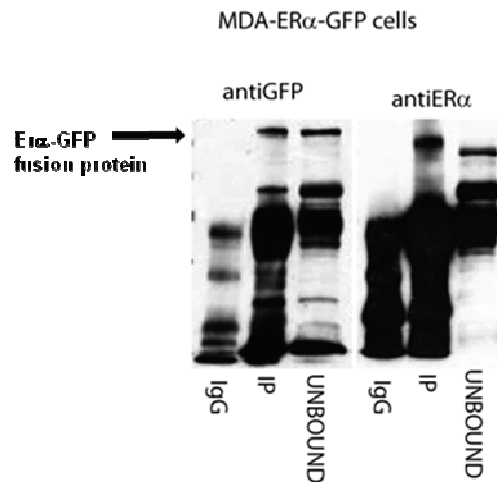


Fig 26: Immunoprecipitation analysis bringing out with Erα antibody and GFP antibody. The protein in the cellular extract was precipitated with a resin coupled with ERα antibody and the bound fraction was loaded on a polyacrylamide gel after blotted against ERα and GFP

In the figure 26 is reported the immunoprecipitation experiment, using two different antibodies against the protein ERα and against GFP.

As it is possible to note, the signals of both antibodies perfectly merge, as demonstration of fusion protein expression inside the cellular model.

Confirmed the expression of fusion protein, the transfected cell line was sorted in order to obtain an homogeneous clone. As reported in figure 27, the sort experiment

was carried out using control (non fluorescent) parental MDA-MB231 cell and setting the threshold value for GFP presence at very high intensity.

After the sorting session, from a percentage of GFP-positive cells equal to 29,1%, the transfected cell line presented then a GFP positive percentage of about 90%.

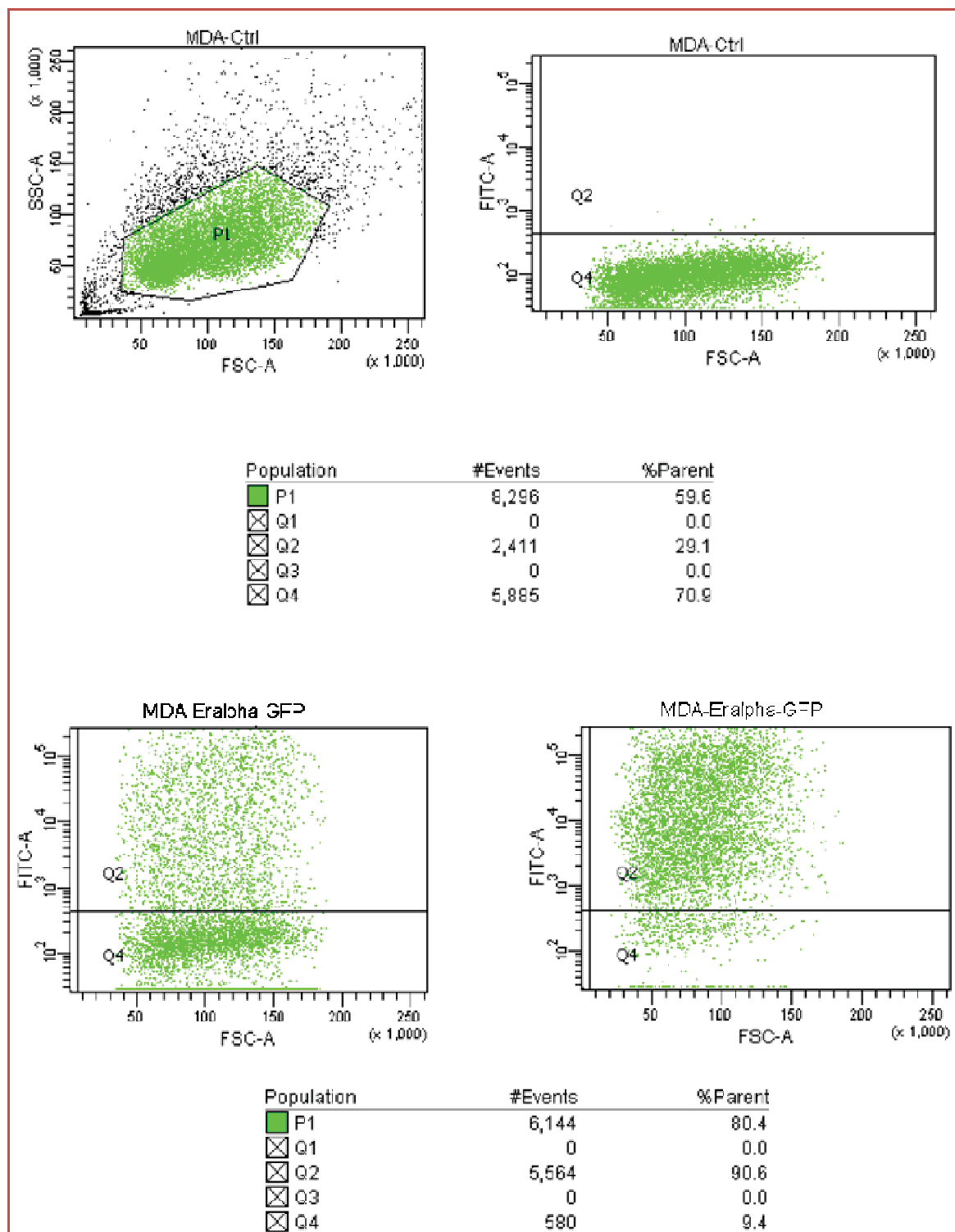


Fig 27: Cell sorting images obtained with FACSaria and analyzed with Diva 6.1 softwear. The data are referred to the parental cell line

The localization of the fusion protein was also determined by experiments of immunofluorescence, staining the transfected cells with an antibody specific for the Estrogen Receptor α and looking at the GFP signal.

As it is possible to note from figure 28 both colors (red caused by Texas Red conjugated secondary antibody and green related to GFP presence) co-localize in the nuclear and peri-nuclear cellular region.

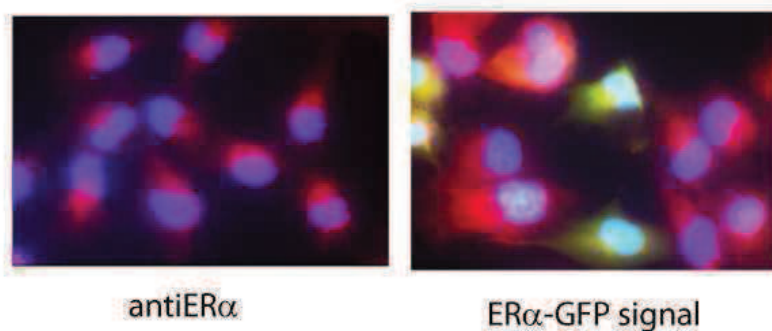


Fig 28: immunofluorescence images obtained by staining the transfected cells with ER α (red color) and looking at the GFP signal (green color)

Verified the ER α -GFP production and the suitability of the method, MDA ER α -GFP cells constitute the starting biological material for optimising the laser source parameters and then utilizing the established settings for experiments of ChIPs.

1×10^6 cells/point in a volume of 20 μ L of saline solution have been irradiated with the PHAROS pulses in a 96 MW support. A specific protocol for chromatin extraction and purification has been set up thereby allowing the measurement of GFP as readout of cross-link (see Supplementary Table 2 to the scheme of “in fluorescence” protocol).

Chemically induced crosslinkink called “positive control” in the following, in which the covalent bind between DNA and proteins is obtained by using formaldehyde as in vivo chemical bi-functional reagent, has been compared to photo-induced crosslink obtained with several different sets of the laser source parameter value.

The “negative control” in the following, instead, represents the case when the same amount of cells is analysed without being treated for the cross-link induction (neither trough the chemical way, nor with the laser methodology), therefore acting as a background remover.

As the critical parameter in optimising UV laser cross-linking of proteins to DNA is probably not only the total amount of light energy absorbed by the target, but a combination of light intensity [energy/(duration x unit area)], pulse length, irradiation time, and repetition rate a great number of irradiation conditions have been evaluated and are currently under evaluation.

It is worth stressing that the above interplay amongst several parameters of the laser source setting is not known neither on empirical basis, nor from the microscopical point of view.

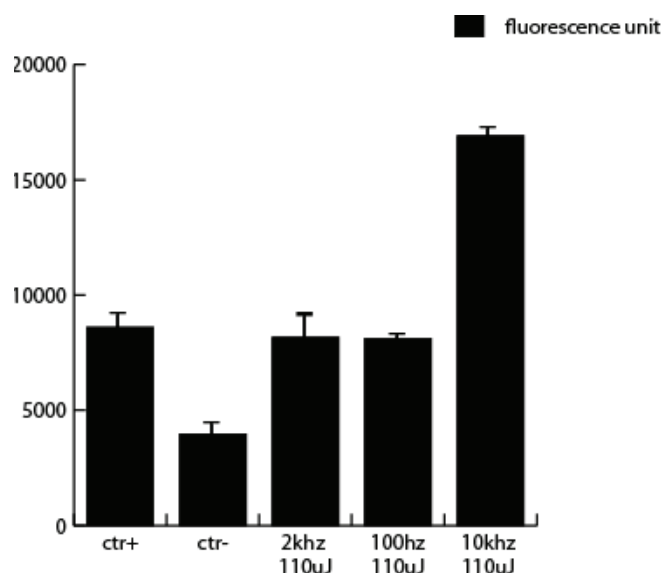


Fig 29: Fluorescent scan methodology at three different Laser operative conditions. The data are reported by comparing with a negative and a positive ctr. The vale are average of 4 tests

Figure 29 above shows the results obtained in three distinct laser source conditions, namely, when keeping constant the laser pulse energy and the irradiation time, equal to 110 μ J, for 1 minute, but varying repetition rate. Experiments are averages over four points.

As it possible to note, by increasing the repetition rate, at the same value of energy/pulse, the florescence increases. As the florescence value is related to stable bonds induction, the yield of crosslink improves by increasing the repetition rate.

The same experimental protocol has been applied for the set of data shown in fisure 30.

In this figure it is possible to observe that, with cells irradiated with the maximal pulse energy currently available, corresponding to 140 μ J, a correlation exists between irradiation times and repetition rates; the florescence recovery is larger when the laser induction is shorter in time (probably due to the small value of irradiated cell disk).

It is intresting to note that when the energy/pulse value is equal to 140uJ (no more 110uJ), the differences among repetition rates are negligible (the value of florescence recovery is always simillar despite the variation of Hz).

In addition, many different laser conditions have been able to yield a fluorescent recovery higher than the positive control (chemical cross-link).

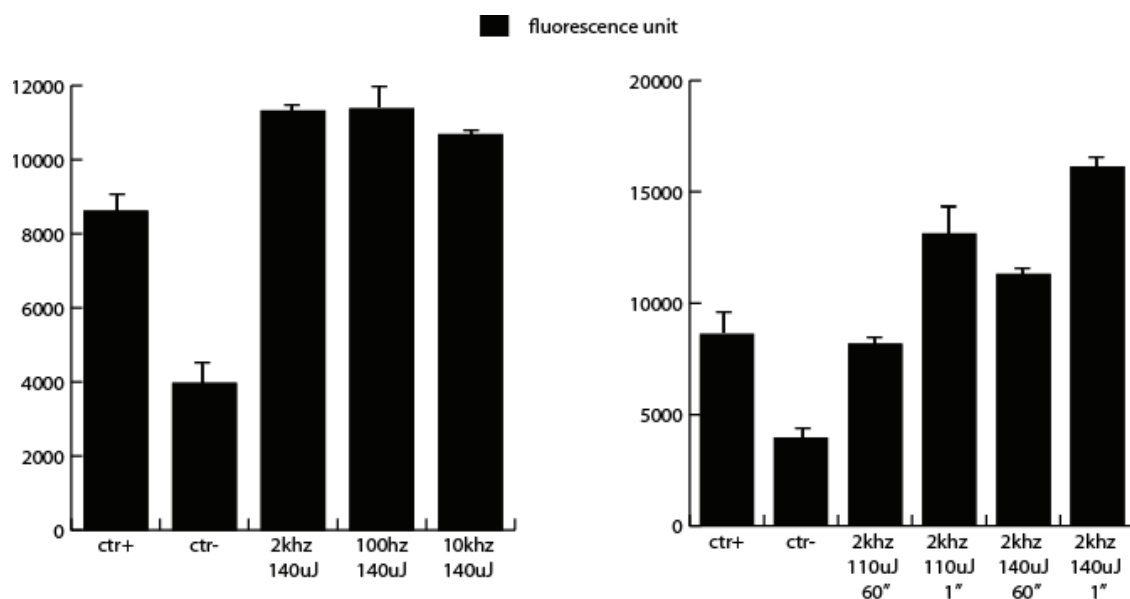


Fig 30: In fluorescence experiments carried out maintaining constant the energy/pulse parameters and varying the time of exposure to the UV Laser light

These laser conditions differ mainly for the repetition rates, that is the number of pulses per second that hits the biological samples.

In the figure 31, results relative to a comparison between irradiation performed with laser beams having two different sizes were reported: crosslink obtained with the ordinary output beam, which has a diameter of about 2.5 mm and does not match the well size of the target has been compared with crosslink obtained, in the same conditions, but using an enlarged beam size (a diameter of approximately 6 mm) which exactly matches the well size.

This test has the aim to optimise the irradiated volume of the sample. Indeed, the ordinary laser beam dimension is not large enough to couple the entire well used as experimental support; so, when the laser beam is in its "normal state" only about 1/3 of the cells are actually irradiated.

When the laser beam is enlarged, by simply using an optical lens, up to the well dimension, it shines the entire air-solution contact surface. It is worth mentioning that the irradiated volumes are very small, amounting to about 20 μ l, which implies a very thin disk to irradiate, having a height of about 1 mm.

This reduced thickness to travel through minimises light absorption and scattering which might cause a lower light fluence to be available for the irradiation of the deeper solution layers.

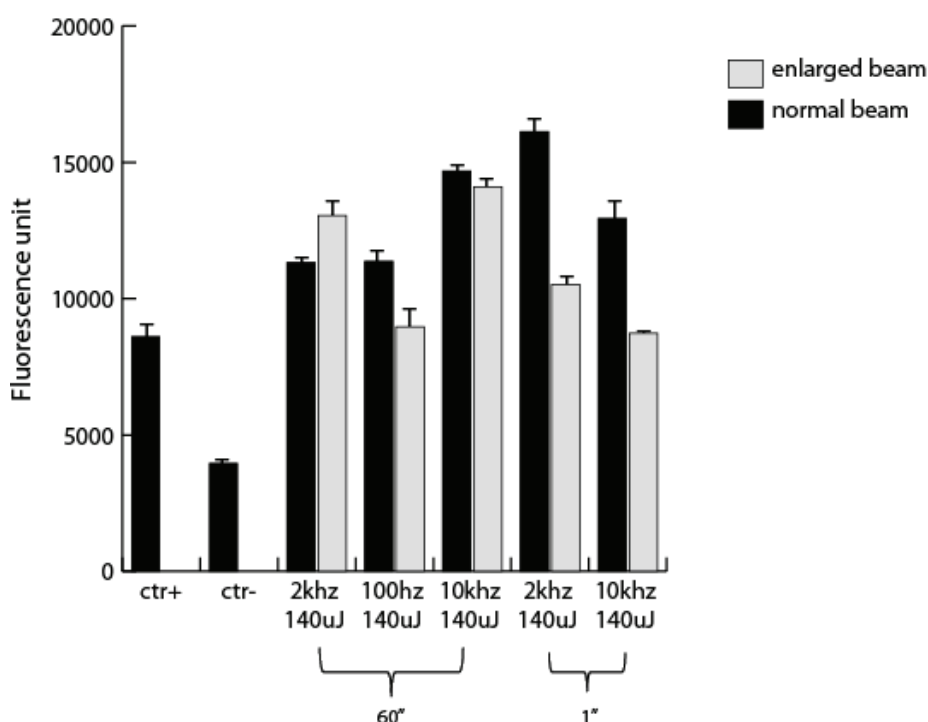


Fig 31: Comparison between two different Laser output sizes to merge the sample in an effective way

However, beam enlargement is obtained only by paying the price of a reduction of the pulse intensity. In fact, the same nominal amount of power is spread out over a wider surface.

Moreover, in practice, enlarging the beam implies also a reduction of the overall pulse energy due to reflection losses from the lens.

Due to this, an about 25% energy loss is measured in the enlarged compared to the ordinary beam.

The above two reasons could explain why the fluorescent recovery, in the enlarged case, is generally lower than in the normal one (see in figure 31 the grey bars compared with black bars).

However, also in this last experiment it is possible to note the complex interplay that occurs among the several physical parameters of the laser source which affects the response of the biological sample.

It is also important to keep in mind that no use of any device has been done so far to mix up the solution while irradiating. This choice is motivated by two reasons:

- (i) some irradiation times are so short that no mix can be successfully performed
- (ii) the solution volume used so far is very small and thin, making hard to employ any such mixing tools.

To overcome these limitation, another procedure to irradiate the cells was set, in which living cells were resuspended in 1ml of buffered saline (PBS) and solution was stirred (Figure 32 below).

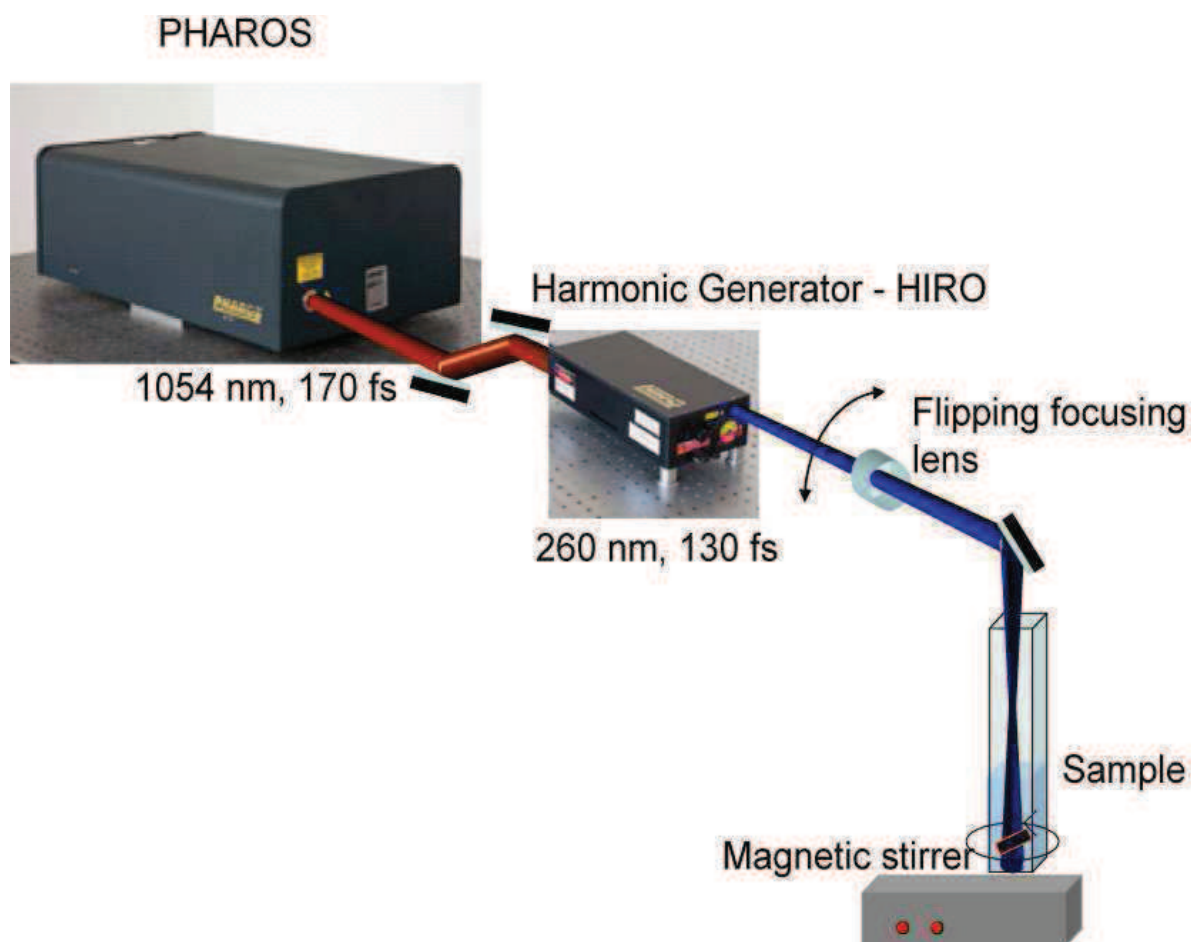


Fig 32: Geometry of Laser apparatus device coupled with for cell irradiating support.

When compared to the initial procedure performed into a volume of $20\mu\text{L}$, in a 96Mw support, this procedure showed a clear advantage most likely due to the different concentration of the cells as well as to the possibility to irradiate the target in a very uniform way, what was a problem, instead, with the previous configuration that used $20\mu\text{L}$ droplets.

In fact, when using droplet targets, a peripheral, non-negligible region of the target volume contained in the well is not properly irradiated. This causes a systematic error in under-estimating the photo-induced cross-link.

As expected, the 'GFP-method' allows to screen a lot of conditions simultaneously. In figure 33 are reported the data obtained in different experiments in which laser repetition rate and its energy/pulse have been changed.

Also for this new setting in a large volume and at low cellular concentration, the contribution of repetition rate, energy /pulse and time of irradiation were estimated.

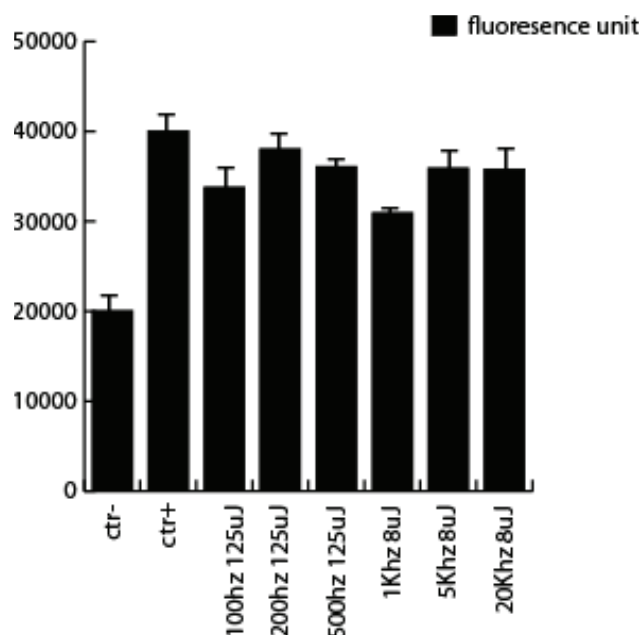


Fig 33: "In fluorescent" experiments done with 1ml cuvette geometry

The repetition rates spare from 100Hz to 20KHz to cover the total range of laser PHAROS operative conditions.

The values of energy/pulse parameter were instead chosen in accordance with the characteristics of Laser device in use.

In every case the yield of crosslink induction, expressed as fluorescence readout, is comparable to the chemical experimental point and very reproducible as demonstrated by the low standard deviation (SD have been calculated on sestupicates).

To better understand the role of repetition rate and the energy, attention was focused on two 'extreme' conditions: 200Hz with 125micro joule and 20KHz with 8 micro joule.

To date is still unclear what is the key mechanism by which the amount of obtained crosslink induction is similar in the two under-study operative modes, although the employing Laser parameters are so different one from each other.

On the base of these preliminary observations was under investigation the rule of cellular concentration and time of irradiation as key factors for the crosslink induction. As the cellular concentration is concerned it was (data not shown) evident that, when number of cells is too high, the laser beam is not able to penetrate deep inside the solution, causing a decrease in the crosslink yield. Hence the necessary of the stirring, jet explained above

To check different irradiation times, in the same operating laser conditions and with the same amount of cell, equal to 1 million, two different times of irradiation were been tested.

Figure 34 shows that also with 1 minute of irradiation the crosslink induction is good enough to be comparable to the chemical experimental point.

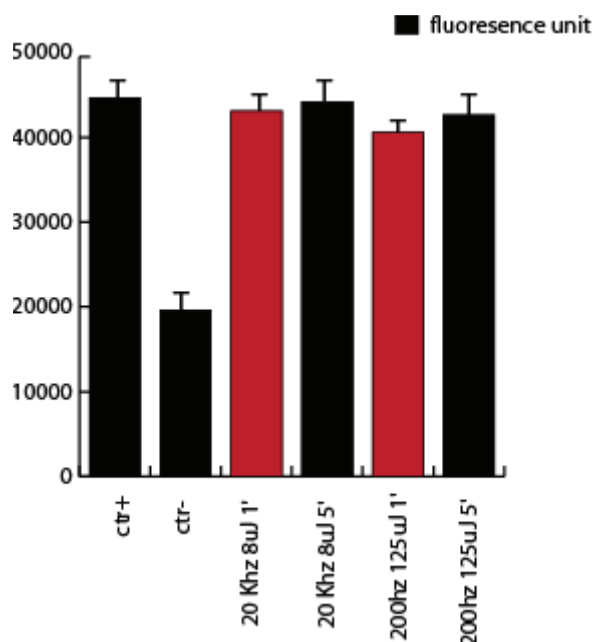


Fig 34: Role of time of irradiation in “in fluorescence experiments”

The encouraging results, obtained with the ‘GFP-method’, suggested the set up of others experimental conditions.

In particular at the total amount of the energy for pulse/repetition rate combinations the Laser setting 2KHz 125 μ J was added because, in term of repetition rate, it is the “natural output” of the PHAROS Laser device.

One of the drawbacks arising from the interaction between a cellular model and an UV radiation was the estimation of damages inside the cells, looking at DNA integrity, proteins stability and cellular viability.

For this reason a lot of experiments were done; all of these experiments may help to elucidate the molecular bases of the crosslink reaction inside living cells.

In particular, the presence of cellular death (that is an expression of to cellular damage) could be important parameter to choice the best conditions to achieve the crosslink induction.

As it is shown in the figure 35 below, in the three selected laser conditions (2KHz 125 μ J, 200hz 125 μ J, 20KHz 8 μ J) a study on cellular viability was performed using the ability of Propidium iodide (PI) to selectively enter inside death cells.

On the same experimental points, also analysis of cell cycle progression and fluorescence recovery (obtained with “GFP-Method”) were done.

All these data are shown on the panel 35, in the next page.

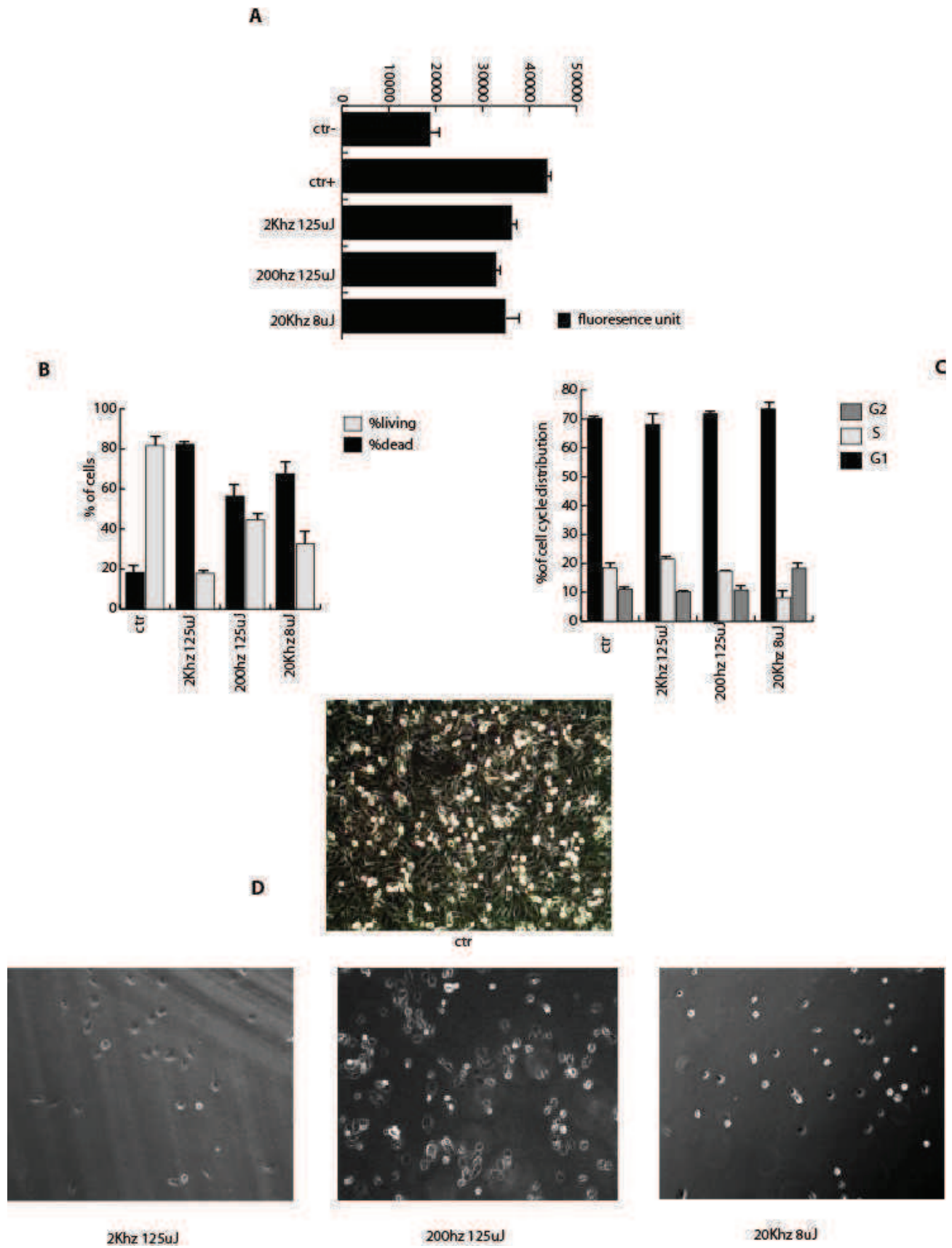


Fig 35: In fluorescence experiment (A), PI incorporation (B), cell cycle analysis (C) and image capture (D) in three different Laser conditions

As additional proof of cellular death, the viability of irradiated cells was also estimated by microscope observation (Fig 35, panel D).

Also in this case, the data suggest that the Laser irradiation of living cells cause some dramatic changes inside the cells bring them to dead.

At the same time also a study on cell cycle distribution of the irradiated cells, compared with control ones, was carried out to analyze if the UV Laser Light lead to the accumulation of cells in one of the cell cycle checkpoints.

As it possible to note from figure 35 no accumulation in a particular cell cycle phase is induced. So, probably the observed death is a very rapid phenomenon not closely related to cell phase checkpoints.

To verify the DNA damage that might be produced by the irradiations the activation of pathways known to respond to DNA damage and apoptosis cascade activation have been tested. Following the UV exposure, the cell reacts by the activation of some pro-apoptotic pathways in which the induction of p53 and p53-regulated proteins is observed. The p53 tumor suppressor protein, a key regulator of cellular responses to stress, is stabilized and activated after DNA damage. The rapid activation of p53 by ionizing radiation is largely dependent on the ATM kinase. p53 is phosphorylated by ATM shortly after DNA damage, resulting in enhanced stability and activity of p53. The cross-talk between p53 and ATM is, for this reason, the starting point to check the presence of UV induced DNA damage. Also the presence of histone H2AX phosphorylated on S139 is a marker of DNA damage and has been evaluated.

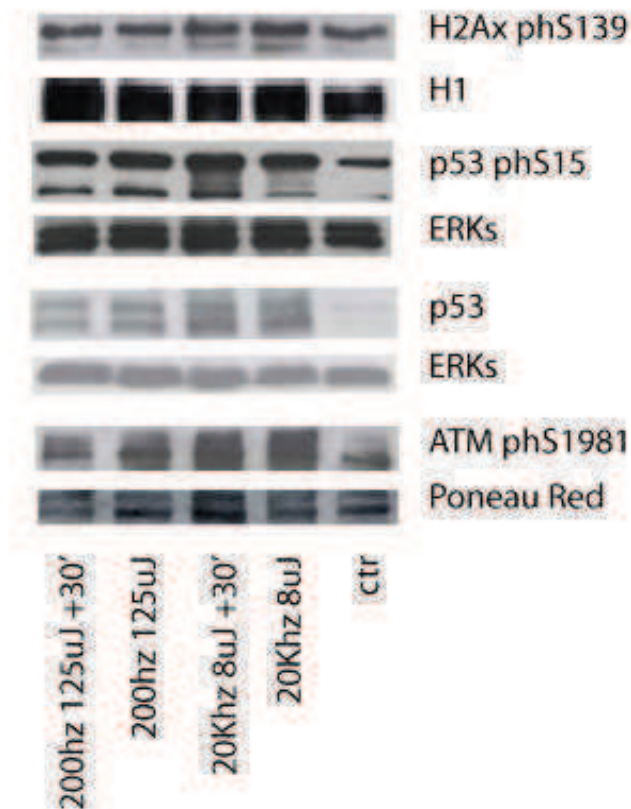


Fig 36: Western Blot panel for proteins involved in DNA damage recognition.

MDA231-Er α -GFP cells have been irradiated with an UV laser source in the two different 'extreme'-operating conditions. For each laser condition, additional points have been carried out in which the cells have been kept at room temperature for a time of 30 minutes after irradiation (cells with waiting time). Indeed, during the 30 minutes the DNA repair mechanisms and DNA damage signalling pathways, in a cell, are normally activated. Western blot analysis shown in Figure 36, reveals that the UV damage-response pathways are only partially activated in the cellular model used, after the exposure of cells at an UV source for the irradiation time of 1 minute. In particular, H2AX phosphorylation is few altered, whereas p53 and ATM phosphorylations seem to be induced but no real difference has been detected between the irradiated samples with waiting time. This last observation confirms the idea that the observed cellular death is an early event.

Despite the time in which the cellular death occurs, from the figure 37 below it is clear that happens through the activation of caspases 3/7 and the production of reactive oxygen species (ROS).

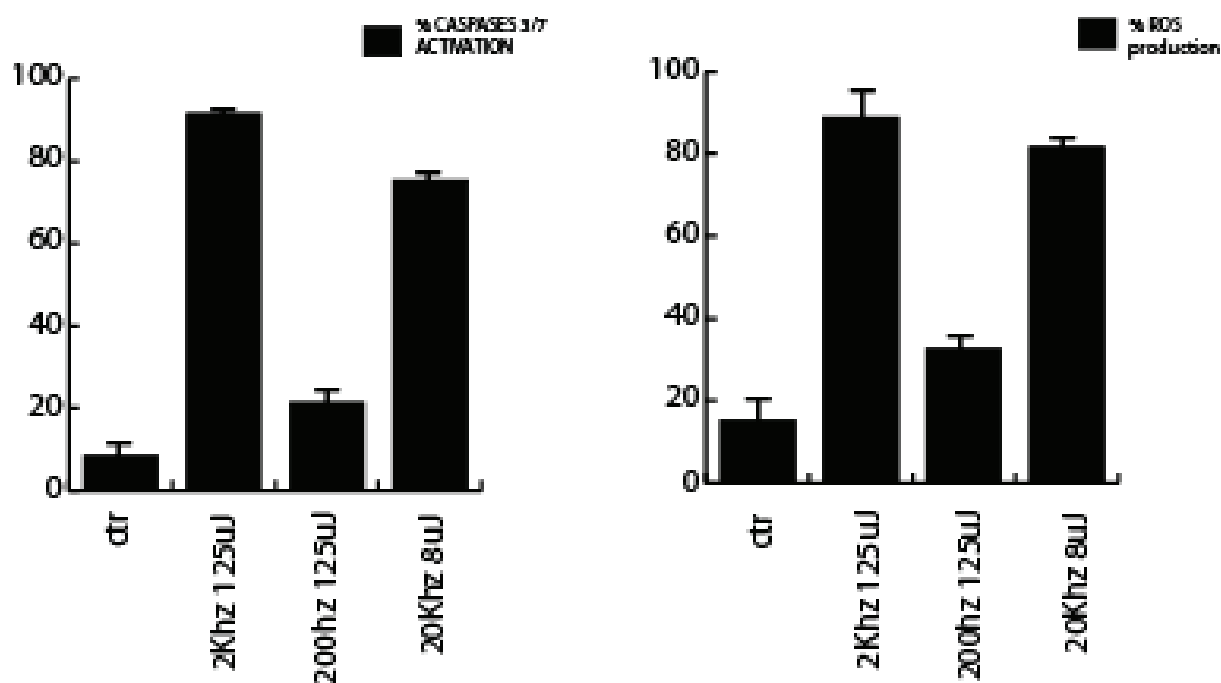


Fig 37: ROS and Caspases 3/7 activation assay in the three selected conditions.

Caspases are aspartate-specific cysteine (interleukin-1 β converting enzyme/CED-3) proteases present in cells as inactive or low activity proenzymes (zymogens) that are sequentially activated to promote apoptosis.

The caspases most often associated with apoptosis are caspases 2, 3, 6, 7, 8, 9 and 10. Caspase cascades are composed of upstream (initiator) caspases (caspase 2, caspase 8, caspase 10), which are activated by death receptor signalosomes (DISC); caspase 9, which is activated by the mitochondrial cytochrome C/Apaf-1 derived apoptosome; and downstream (effector) caspases (caspase 3, caspase 6, caspase 7) that cleave proteins involved in programmed cell death events. Caspase 2, caspase 8 and caspase 10 are activated by death receptor signalosomes (death-inducing signaling complex (DISC)).

In addition to activating caspase-3, caspase-6 or caspase-7 directly, caspases 8 or 10 activates pro-apoptotic factors such as BID that induce the release of cytochrome C from the mitochondria. Caspase 9 is activated by the mitochondrial release of cytochrome C. Cytosolic cytochrome c binds and induces oligomerization of apoptotic protease activating factor 1 (APAF-1) followed by recruitment of procaspase-9 to form an apoptosome. Apoptosome-associated procaspase-9 self-activates and then activates downstream caspase 3 and/or caspase 7.

The downstream executioner caspases (3,6,7) cleave: proteins involved with DNA processing such as DNA fragmentation factor (DFF-45); the DNA repair enzymes poly(ADP-ribose) polymerase (PARP); and DNA fragmentation factor 45 kDa subunit (ICAD); signaling molecules such as the Rho-GTPase GDP dissociation inhibitor (D4-GDI); enzymes protein kinase Cd (PKCd), cytosolic phospholipase A2 (cPLA2); sterol-regulatory element-binding proteins (SREBP); p21-activated kinase 2 (PAK2); and DNA-dependent protein kinase catalytic subunit (DNA-PKcs); and structural proteins such as α -fodrin, actin, and lamin.

As reported in literature, the reactive oxygen species are produced instead, after the exposure to UV radiations. High levels of ROS cause oxidative stress inside the cells bringing them to death.

So both data shown in figure 37 are consistent one with another.

With some of the operating Laser conditions an experiment of chromatin immunoprecipitation (ChIP) was also done, to confirm that the selected combinations of repetition rate and energy for pulse were also able to induce the crosslink between DNA and proteins in the cellular model (see figure 38).

Among the three combinations of energy and rep/rate discussed at now, only two of these (2Khz 125uJ and 200Hz 125uJ) were employed in the ChIP experiment as the minimum and the maximum value of live/death cells.

In this ChIP experiment an antibody against 3CH3K4H3 histone was employed to pull down the TRAIL promoter region in MDA-ER α -GFP cells. In the figure 38 is reported the genome browser data related to the occurrence of this histone mark on the specific selected region in different cell lines.

The second amplified gene, called in figure 38 below Myo, represents the negative control of the data set because is not specific per the histone mark selected, and so the value of recovery remains unchanged among the different experimental points.

Although the signal of recovery obtained with chemical experimental point is greater than the physics, it is also possible to note that, particularly for the point 2khz 125uJ the recovery of 3CH3K4H3 is good enough and it is due with a time of exposition 1 order of magnitude minor than chemical.

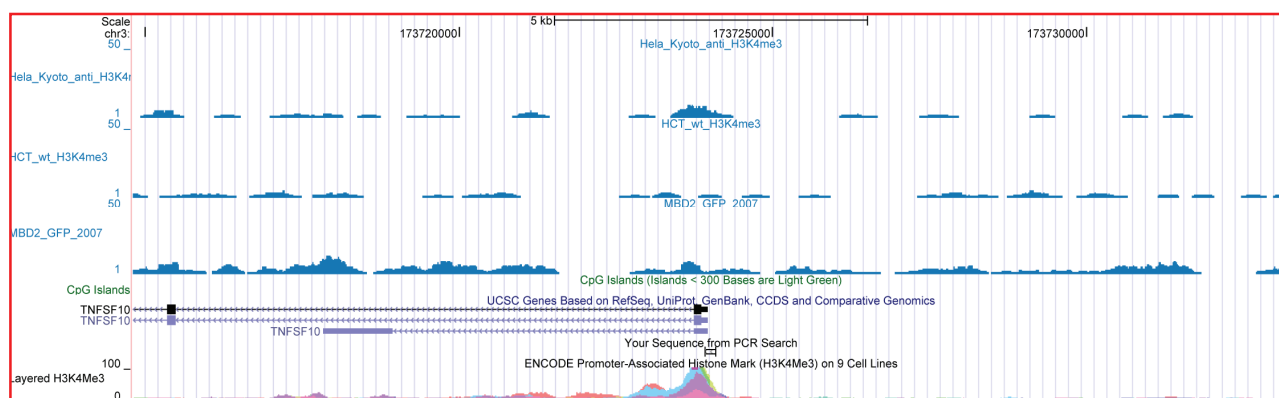
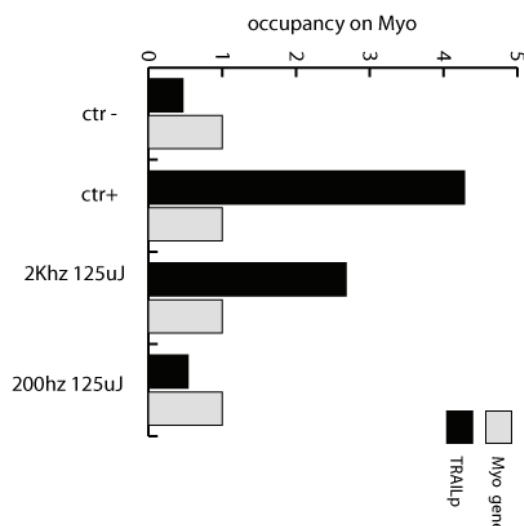


Fig 38: ChIP experiment employed 3CH3K4H3 antibody, The amplified genetic region is TRAIL promoter one. In the Panel above is reported the genome browser analysis to confirm the presence of the epigenetic mark on TRAIL pReg.

As more than once, reference was made to cellular damages induced by incident UV radiation, the recovery values after ChIP experiment on TRAIL promoter region lowest than chemical could be caused by photoproducts presence or DNA structural damages.

So, looking at all the results, another question kept in consideration was if the DNA itself, after the laser crosslink induction, could be damaged and if this damage could cause problems for the ChIP experiment and subsequent DNA amplification.

So the presence of pyrimidine dimers was evaluated, at the first, for the three employed conditions (Figure 39).

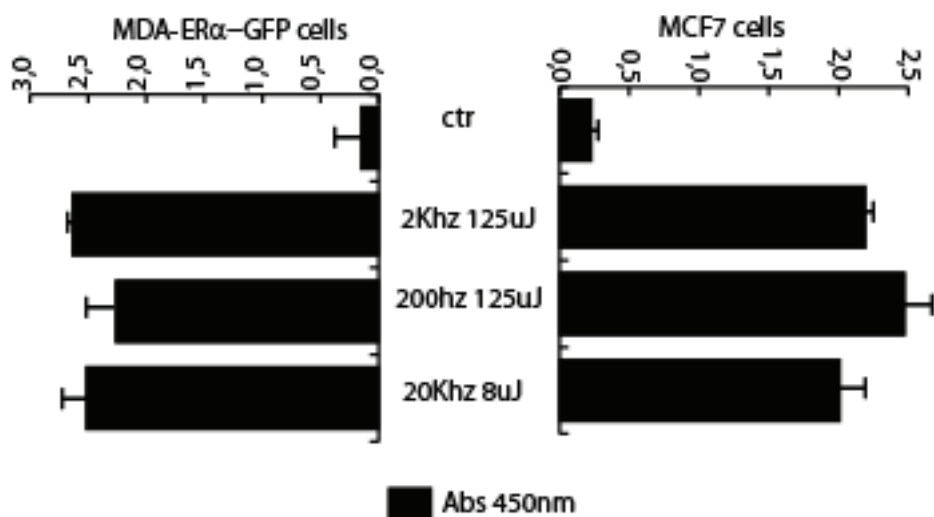


Fig 39: Pyrimidine dimers formation assay carried out on two different tumoral cell lines

This experiment was done in two different cell lines, to exclude that the previous manipulation of MDA-ER α -GFP (e.i. transfection) could interfere with the DNA stability.

As it is possible to note from figure 39, both cell lines react in the same way at the Laser treatment, with value of pyrimidine dimers formation more or less equal.

The preliminary data regarding the photo-products formations in irradiated living cells were the input to keep lower the energy.

In fact if an high dose of very energetic photons is able to induce the crosslink formation between DNA and proteins, too much energy could damage the interacting system up to be a limitation for CHIP study itself and CHIP-seq downstream analysis.

So other combinations of laser operating modes were explored, with the idea of the minimization of DNA damage but at the same time, an optimization of the crosslink yield.

As shown in figure 40 below, additional experimental points were carried out in which the amount of total energy results to be different to the three ones tested until now.

In particular, 2khz 125uJ condition was maintained and other experimental points differing for total energy were added.

These experimental points were obtained keeping constant the repetition rate but varying the energy/pulse value (starting from 90uJ up to 30uJ)

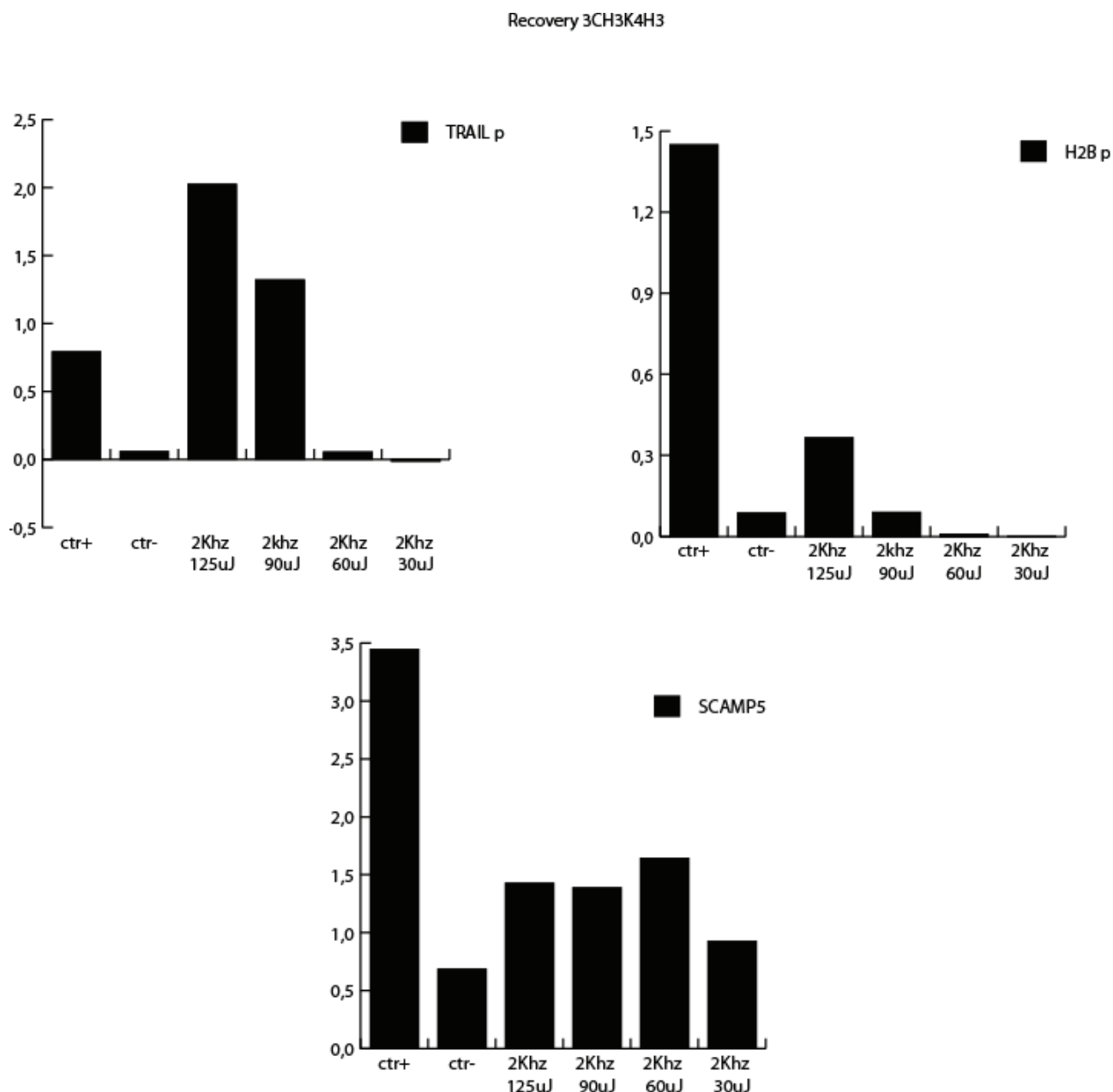


Fig 40: ChIP experiment on scaling energy experimental points, Also in this case the antibody was 3CH3K4H3 and the amplified regions were: TRAIL promoter, H2B promoter, Scamp5 promoter.

In this ChIP experiment additional genomic regions were analyzed by Real Time-PCR after immunoprecipitation of chromatin. Indeed, the data were compared to a negative and a positive (chemically induced crosslink) experimental points.

As it is possible to observe each gene reacts in a different manner at the same irradiation session, indicating that a preferential behavior exists in relation to Laser crosslink induction.

As the crosslink induced by UV Laser is a “zero length” reaction independent of reactivity and length of bi-functional reagents, some changes to the protocol for ChIP experiments were done, for promoting the permanence of only stable links between DNA and proteins.

Increasing the percentage of detergents (e.g. SDS) the recovery related to 3CH3K4H3 is improved for the TRAIL genetic region comparing to the one shown in figure 38.

Regarding the region of H2B, it seem to be negative for the crosslink induced in the presented Laser conditions, instead for the region of SCAMP5 is always present a detectable recovery.

Also in this case, the genome browser of selected genic regions were shown (see fig 41).

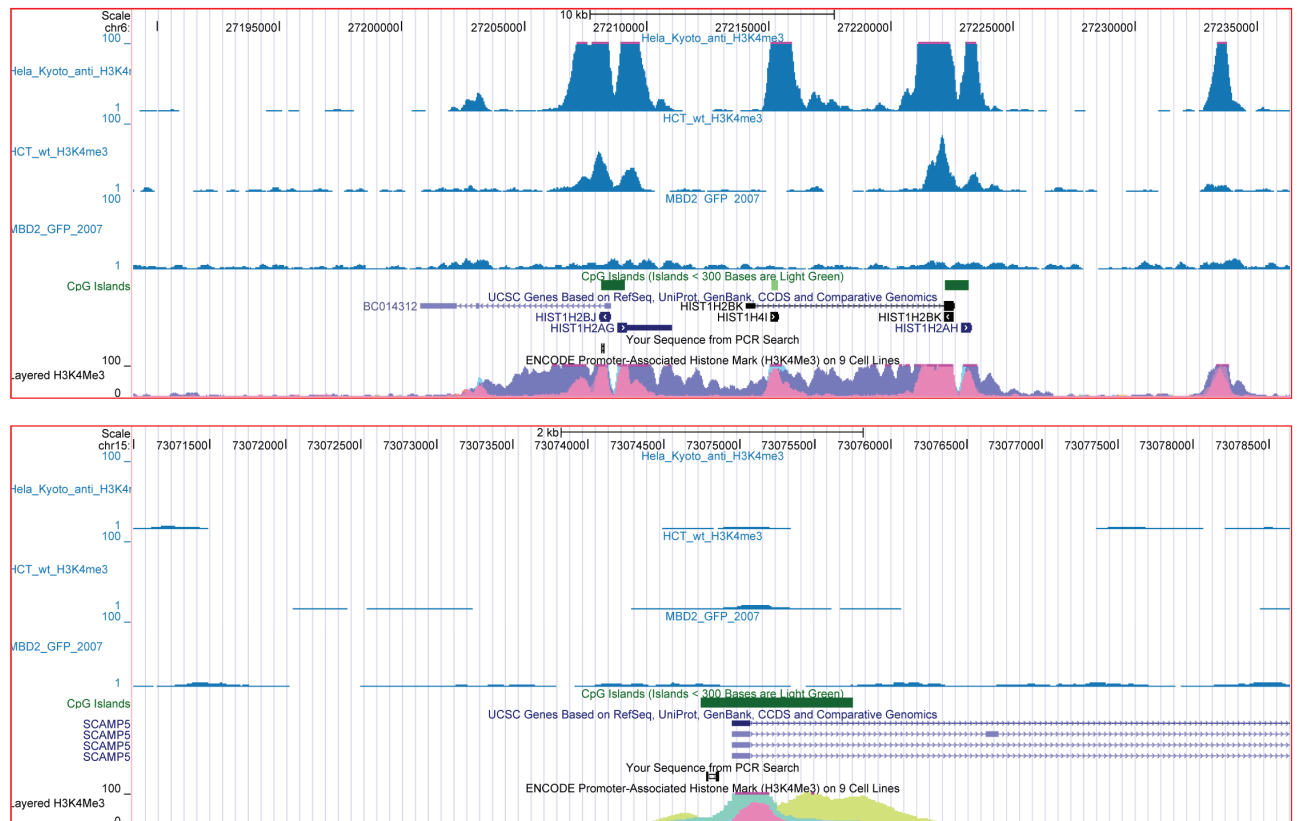


Fig 41: Genome browsers panel for H2B SCAMP5 promoter regions in relation to the specific epigenetic mark.

With high energies of Laser device a preferential crosslink is thus induced but it is plausible that the quantity and quality of crosslink could be improved by varying the Laser energy and the way by which this energy is supplied to the biological system.

Also for these experimental points an analysis of mortality and cell cycle distribution, after the irradiating session, was been made.

As shown in figure 42 by scaling the total energy, a reduction of mortality is visible.

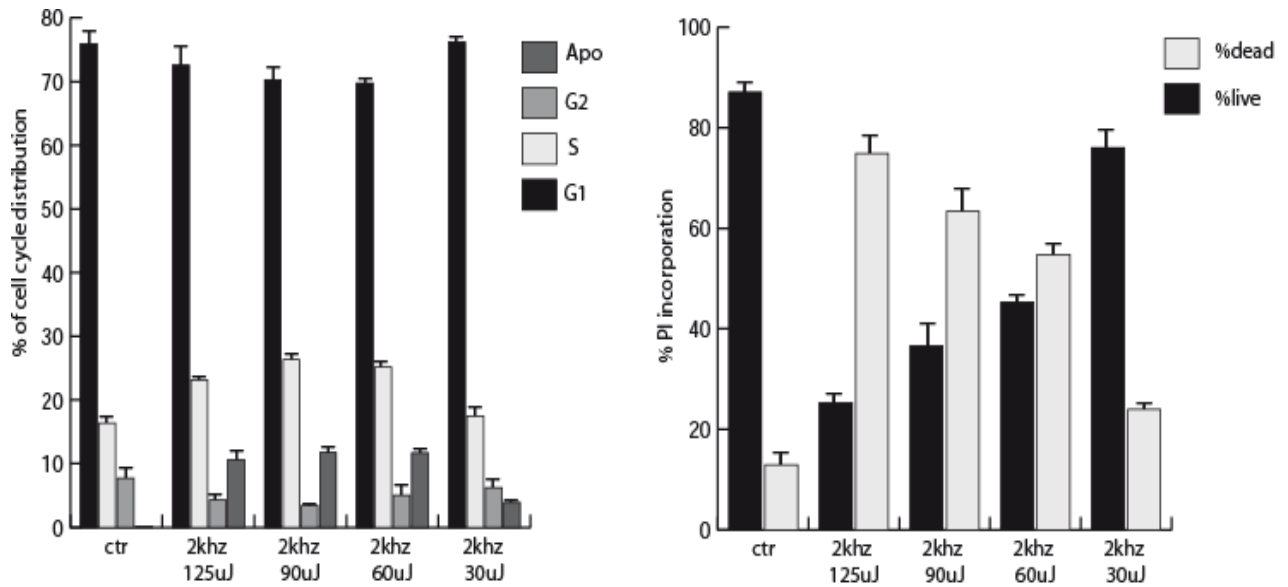


Fig 42: cell cycle progression and PI incorporation experiments

The figure 42 shows that the cells die because their cell membrane is permeable to staining with PI, but the activation of apoptosis (detected with FACS analysis) is only quite present after few hours from the irradiating session. Consistent with this idea the expression of pro-apoptotic proteins and the related percentage of cellular death was analyzed, scaling the quantity of total energy for each experimental point.

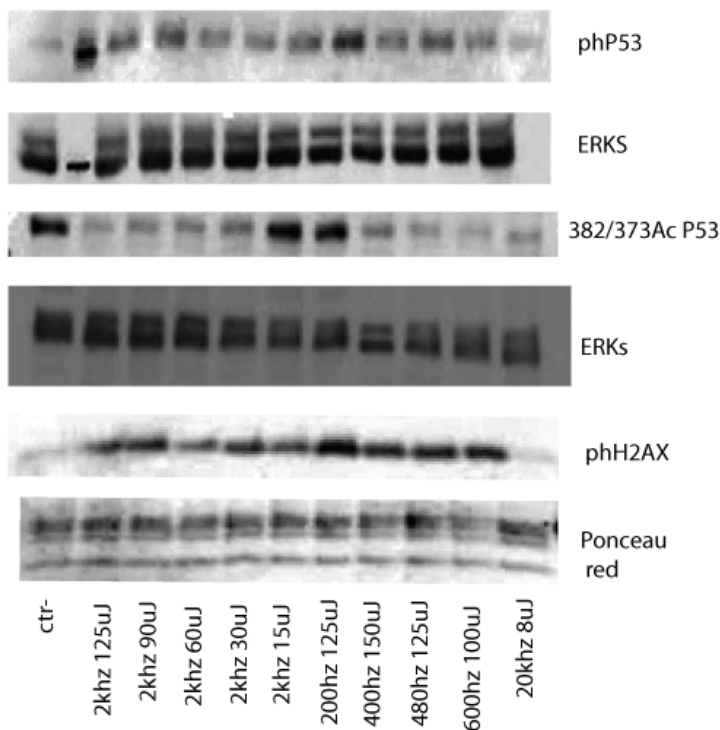


Fig 43: Western blot panel of pro-apoptotic proteins

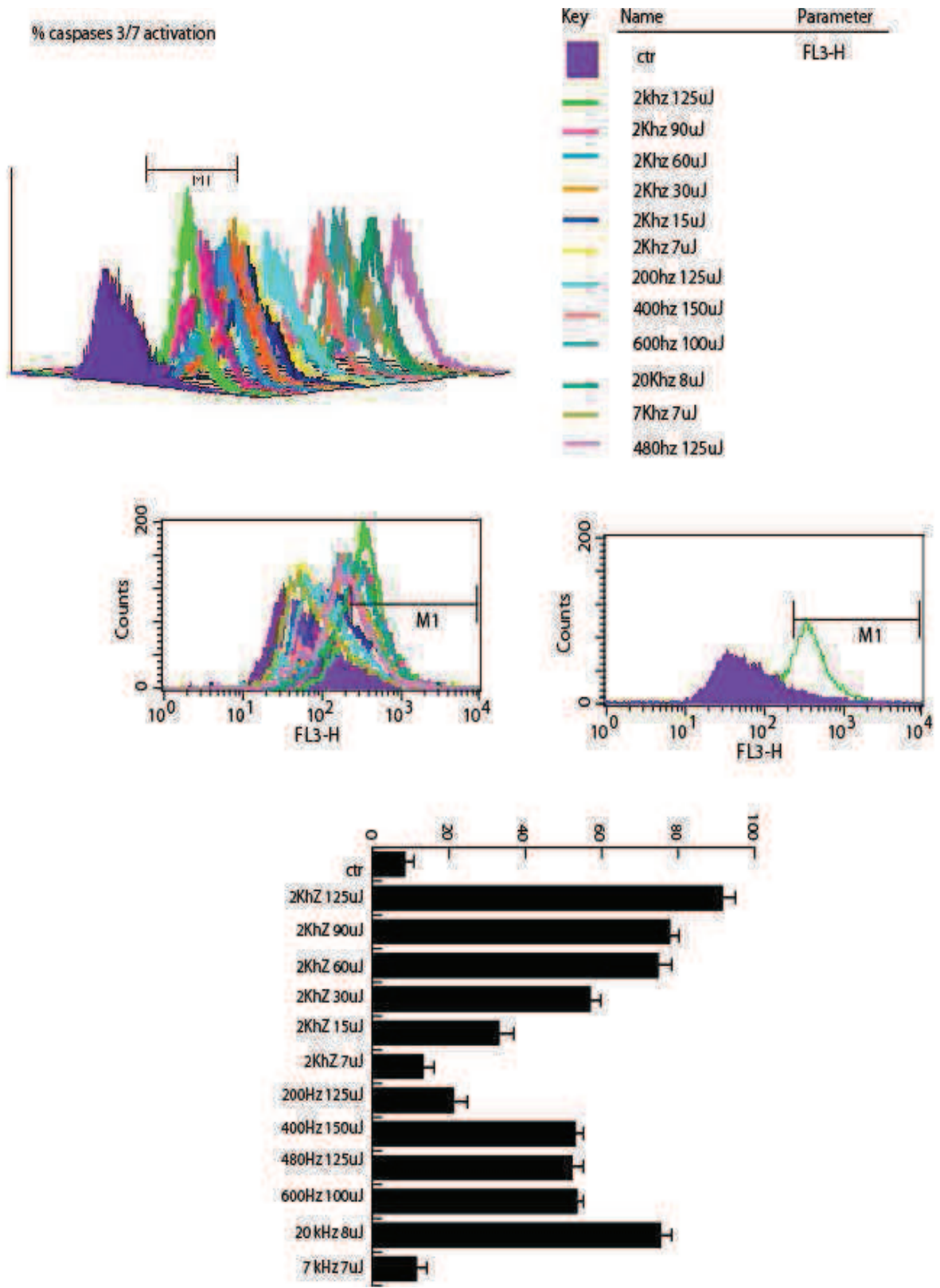
From the data presented in figure 43, some key proteins in the pathway leading to apoptosis (but in general also in other forms of cellular death) are inducing and this induction is caused by the total amount of energy in the time unit, but also by the way in which this energy is supplied to the cells.

In fact many of the case shown in the figure posses the same quantity of energy released to the cellular model in the time of 1 minute, but by varying the combination of energy for pulse and repetition rate; the biological effect is not the same for all and it is greater in the “not extremely stressed” conditions (see table 1 below).

HZ	ω	seconds	total energy*1000	nuber of hits
2000	125	60	15000	120000
2000	90	60	10800	120000
2000	60	60	7200	120000
2000	30	60	3600	120000
2000	13	60	1560	120000
2000	7	60	840	120000
200	125	60	1500	12000
400	150	60	3600	24000
480	125	60	3600	28800
600	100	60	3600	36000
20000	8	60	9600	120000
7000	7	60	2940	420000

Table 1: Characteristics of employed laser conditions

In the same conditions the caspases3/7 activation and the ROS production were also tested (see figure 44 below).



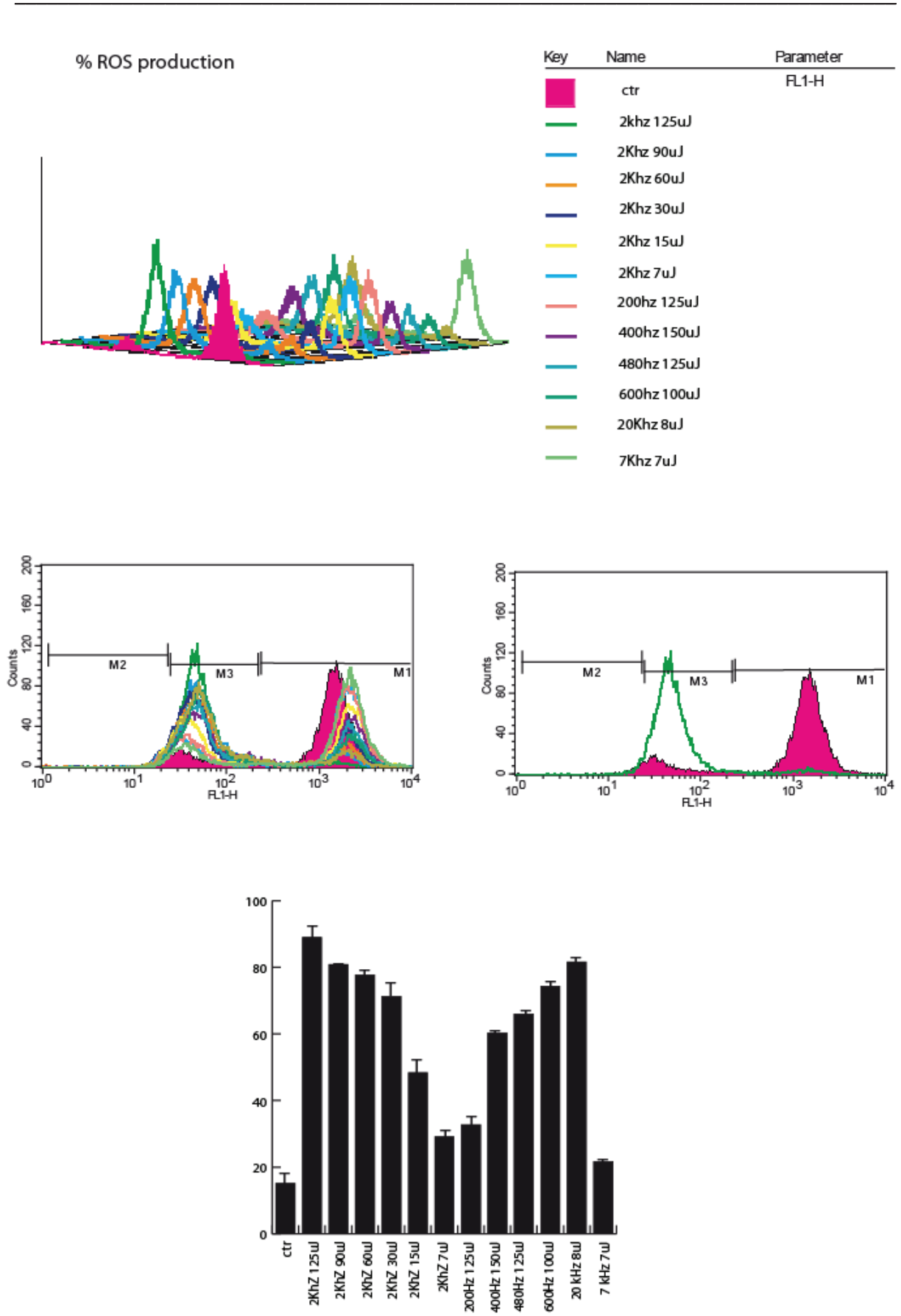


Fig 44: Caspases 3/7 activation (A) and ROS production (B) assays

It is interesting to note that both assays show the same trend, demonstrating the enormous biological effect induced by UV laser device. Looking at the data, the observed cellular death is due to a complex system of activation involving ROS production and caspases cascade, but the final step in this complex process culminates to cellular death.

The cellular death was quantified by FACs analysis, and as shown in figure 45, it is clear that a correlation between energy released and death exists.

Analyzing all the data concerning the wbs, caspases and ROS production, it is easy to note that extreme conditions of repetition rate and energy/pulse activate the same way the pathways of cell damage. By focusing on the group of experimental points that has total energy equal to 3600 mJ you can see the different behavior with regard to protein expression. In addition these 3 experimental points induce, in the same manner, the caspases 3/7 but differently the ROS production. This trend could suggest an non linear response of cellular system to UV laser treatment. The experimental point in which is low enough the activation of caspases and ROS is 200hz 125uJ (total energy= 1500). For this condition however, the stronger induction of protein-induced by damage is observed. The total energy of this point is similar to the energy of the condition 2khz 15uJ (1500 vs 1800) but the biological effects are very different between them, with a percentage of ROS and caspases activation bigger than twice.

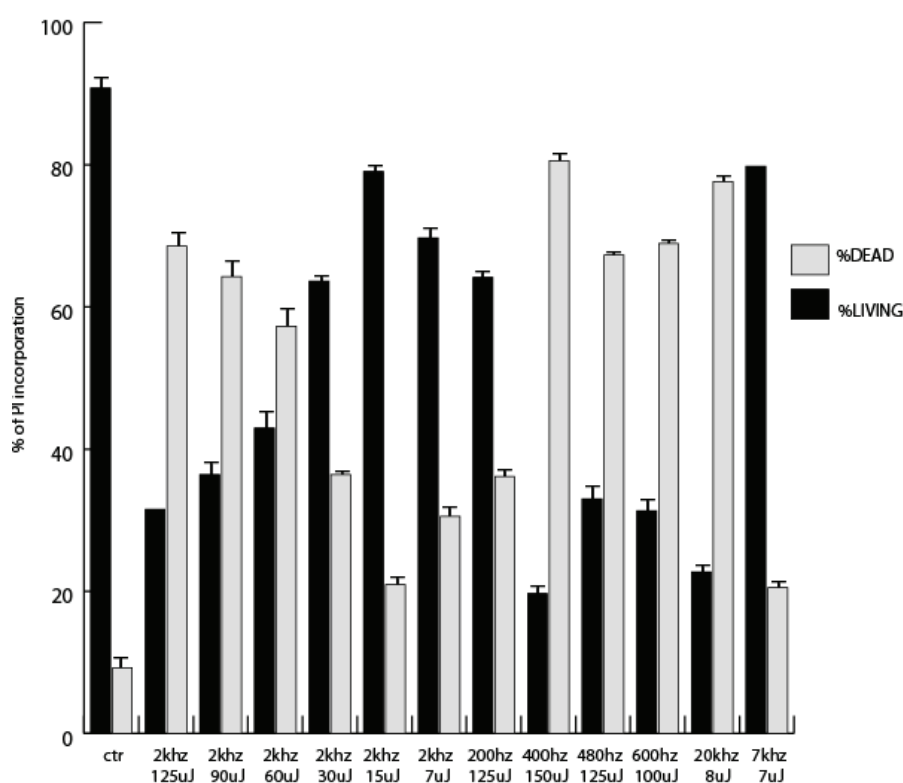


Fig 45: PI incorporation analysis

It is interesting to note that, in the two different conditions mainly analyses at now (2khz 125uJ and 20Khz 8uJ), the percentage of cellular death is quite similar though the quantity of energy scales among them. It could suggests that a threshold value exists exceeded it the biological effect is the same.

Confirming this hypothesis there is also the data regarding the points 2khz 30uJ and 200hz 125uJ. For these the total energy is, respectively, 3600 and 1500 but the percentage of cellular death remains unchanged.

The cellular death was also confirmed by microscope observation and images capture. The figure 46 shows that after the UV laser crosslink induction the cells lose the ability to link them selves at the plate and at 24h from laser treatment they are mostly dead. The images are referred only to few experimental points (other laser conditions are data not shown).

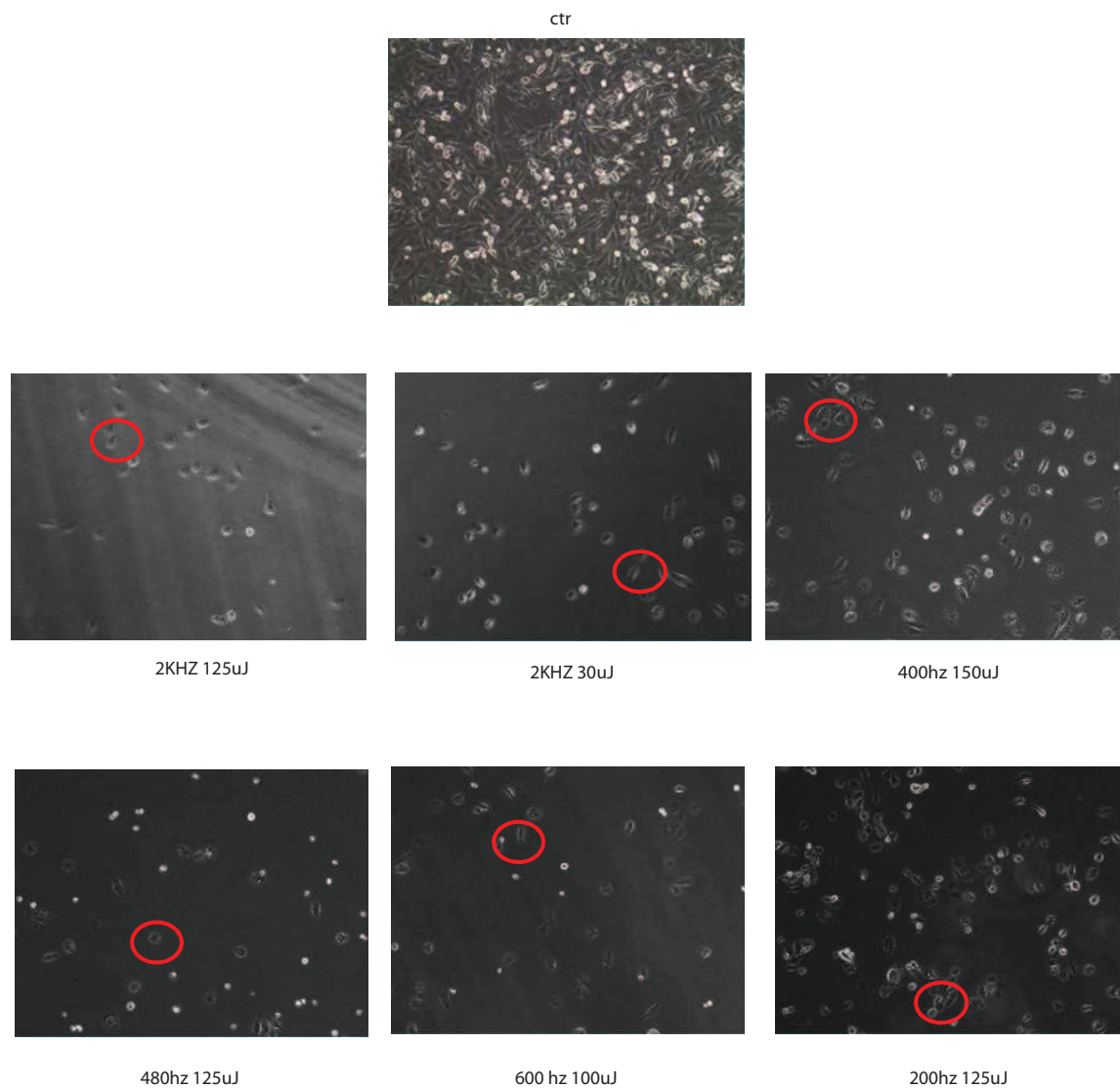


Fig 46: Images captures of cells after irradiation

Probably the cellular death is also due to DNA fragmentation, induced by the UV exposure and thought the activation of pro-apoptotic pathway (keep in mind the caspases 3/7 activation) as show in figure 47.

In the panel below some images of comet assay are presented in the laser condition in which caspases and ROS activation was detect. Also in this case, the data are compared with a negative control (without tail); each laser condition induces DNA fragmentation and the length of tails is related to the percentage of damage itself. As yet explained below the damage is function of quantity of energy released to the cells.

In the panel of comet assay images only few laser conditions are reported with the aim of showing the rationale of the experiments. the other laser setting are included in the Table Supplementary 3, in attach at the end of thesis.

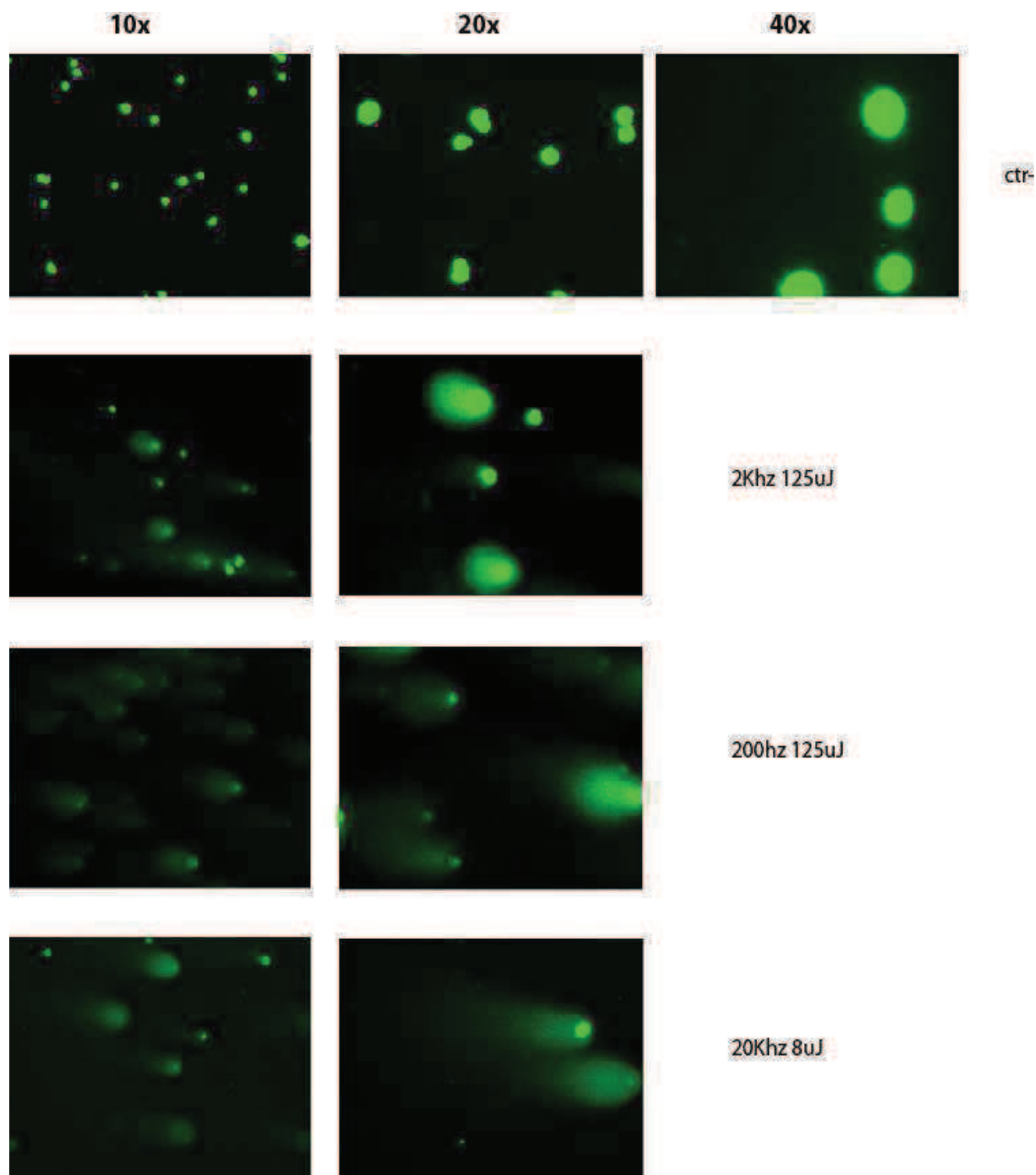


Fig 47: Comet assays

In the same conditions, an evaluation of the quantity of pyrimidine dimers formation was carried out and the obtaining results were shown in the figure 48 below. In each tested condition is present the positive signal to the pyrimidine formation with no significant differences among each experimental point.

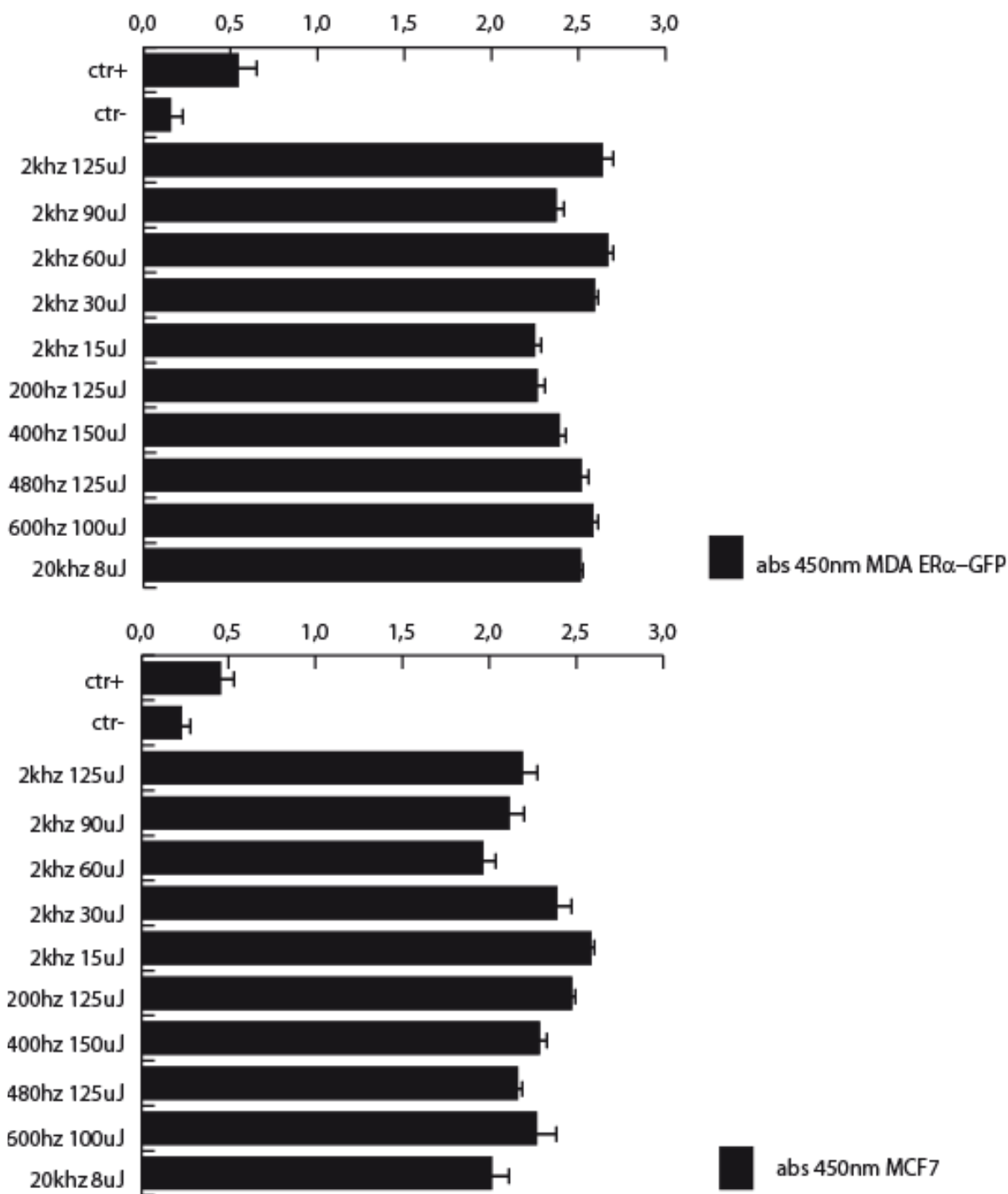


Fig 48: Dimers production assay carried out in two different cell lines

Since the presence of DNA damage, as already explained above, may be a limitation for the downstream analysis, also other laser settings were tested to reduce the cellular death (that could be directly related to DNA damages). In the next figure (Figure 49, below), the data related to cellular death were reported, in which the cells were irradiated with very few total energy.

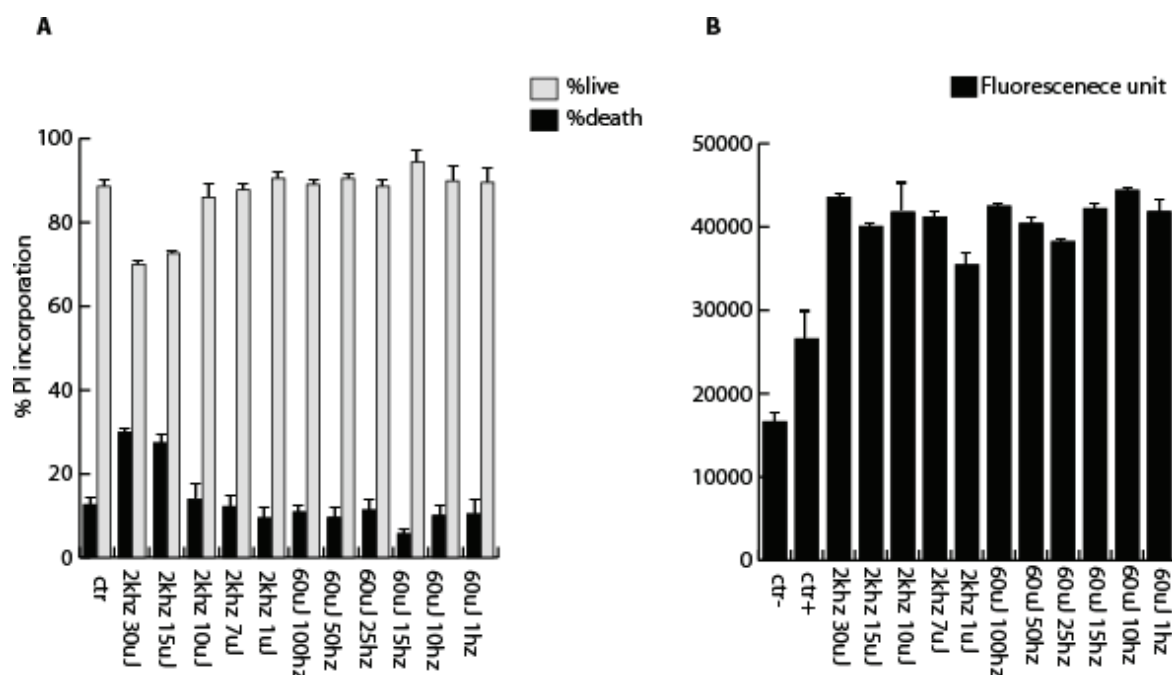


Fig 49: PI incorporation at low energy values (A) and "In Fluorescence" experiments (B)

HZ	uJ	T=seconds	TOTAL ENERGY*1000	NUMBER OF HITS
2000	30	60	3600	120000
2000	15	60	1800	120000
2000	10	60	1200	120000
2000	7	60	840	120000
2000	1	60	120	120000
100	60	60	360	6000
50	60	60	180	3000
25	60	60	90	1500
15	60	60	54	900
10	60	60	36	600
1	60	60	3,6	60

Table 2: Characteristics of employed laser conditions

So, in the first panel some additional points were shown and it is immediately evident that low energies (listed in the Table 2, above) correspond to low level of death. Some of these points were also analyzed for the ROS production, and also in this case the percentage of ROS inside the cells decreases in a proportional way to the decrement of energy (see fig 50)

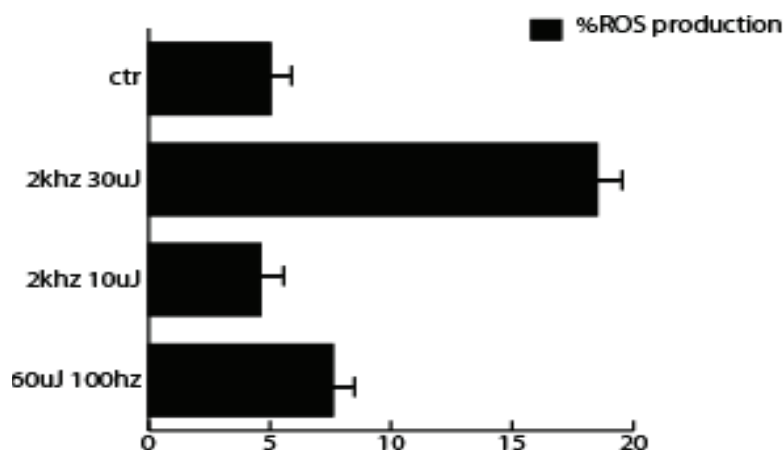


Fig 50: ROS production assay

Though in the employed conditions the rate of cellular death and the production of ROS decreases, the energy released to the cellular system is enough to promote the crosslink reaction between proteins and DNA (ER α -GFP protein and ERE sequences) as shown in the figure 49, panel B.

Continuing on this idea, the final UV laser wavelength was changed, from the 260nm to 300nm, to reduce the absorption of energy to the thymines that constitute the candidates to the pyrimidine dimers formation and usually are present in the regions of DNA breaks (figure 51, below).

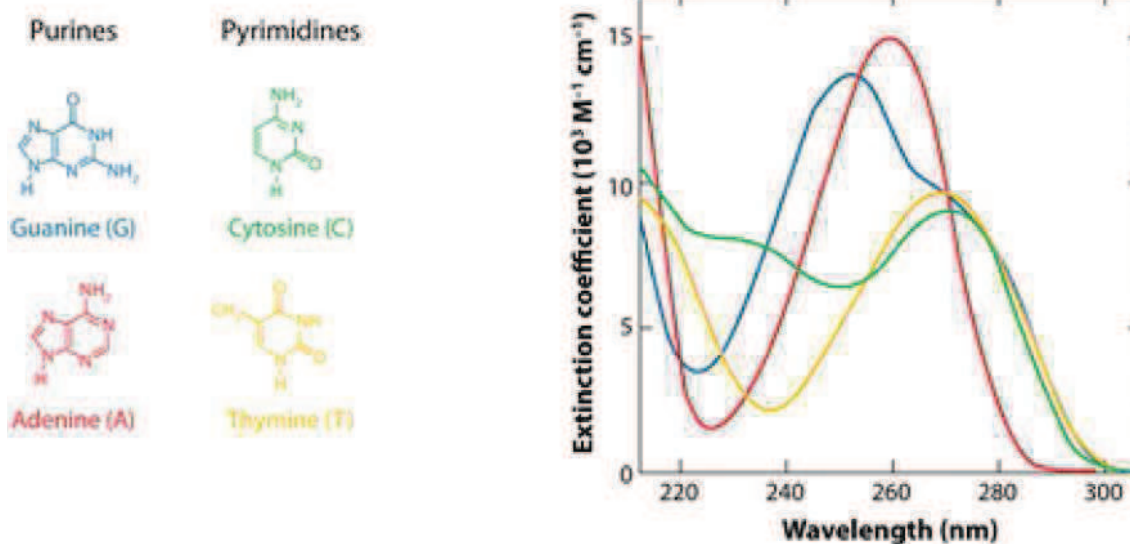


Fig 51: Spectral absorption of DNA bases

To verify the reduction of DNA damages and to analyze the global effect on living cells, first of all an experiment of PI incorporation was done.

In figure 52 is reported the comparison between the two different wavelengths.

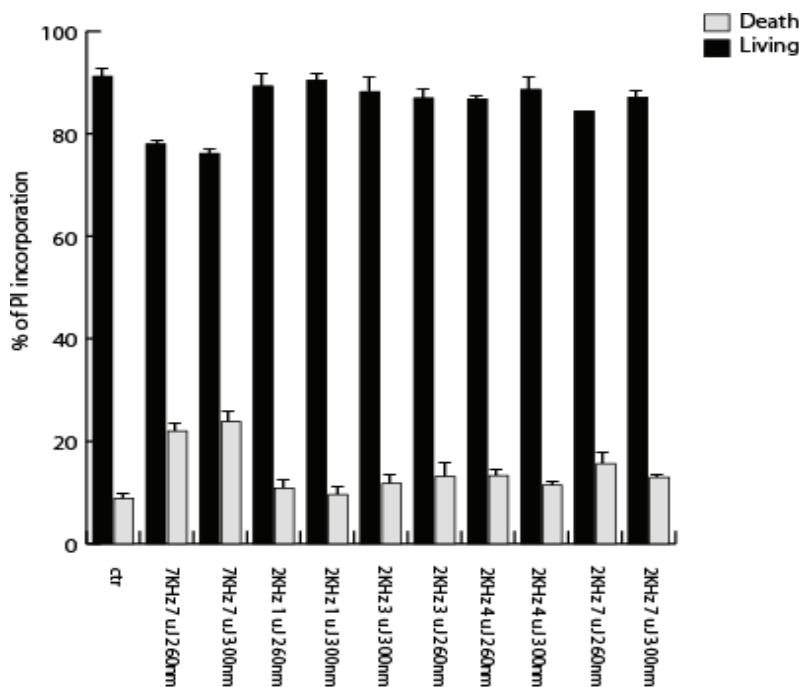


Fig 52: PI incorporation at different UV Laser outputs (260nm and 300 nm)

As previous shown, at the low energies with wavelengths equal to 260nm no cellular death is immediately appreciable. The same is true also with the wavelength output of 300nm. But looking at the percentage of dimers formation the question is quite different (se figure 53).

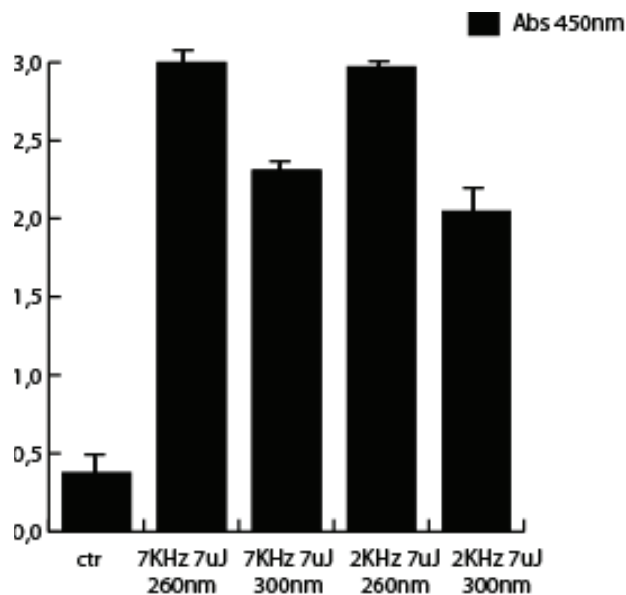


Fig 53: Dimers formation assay at 260nm and 300nm

Especially for the 2khz 7μJ experimental point is present a strong reduction in dimers formations (which is still evident also in the 7khz 7μJ condition).

The decrease of dimers formation and the absence of cellular death after few minutes from the irradiating session doesn't exclude the cellular death after 24h from the laser treatment, as shown in figure 54.

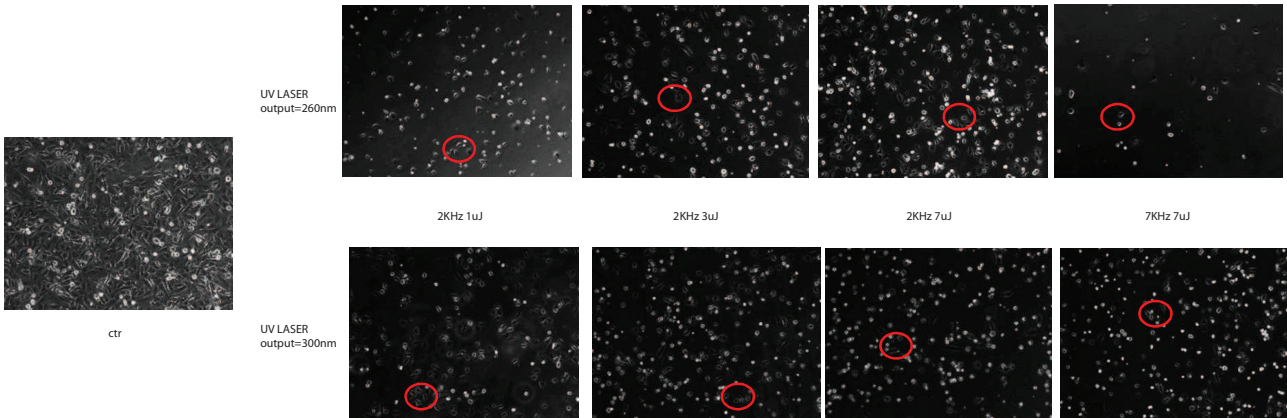
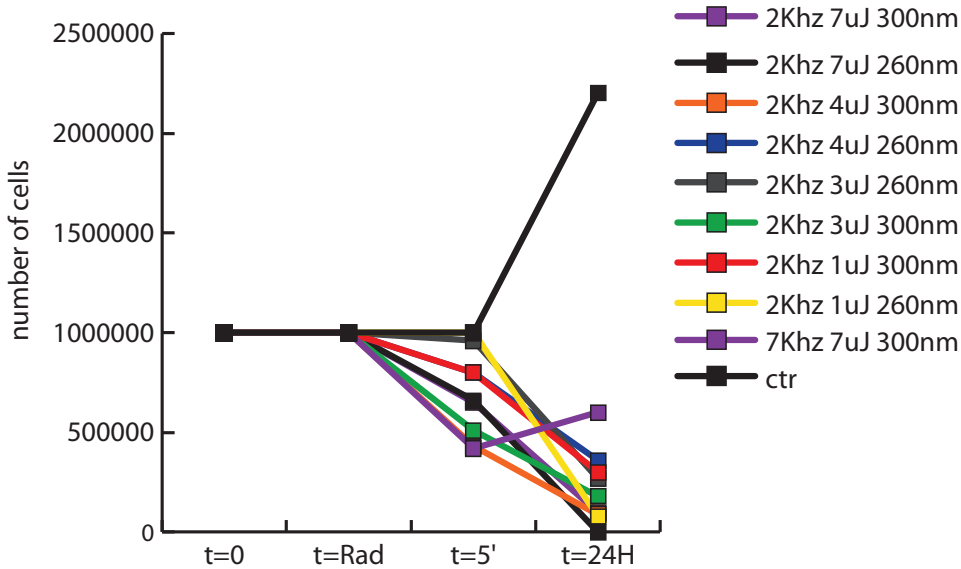


Fig 54: Cell count with Trypan blue staining and images capture after irradiation

In both these selected conditions the CHIP experiment was done. As shown in figure 55 the recovery of DNA is good enough in both conditions. Also in this experiments different genic regions were analyzed and they show a different behavior if compared with the same genetic regions analyzed after high energetic UV exposure.

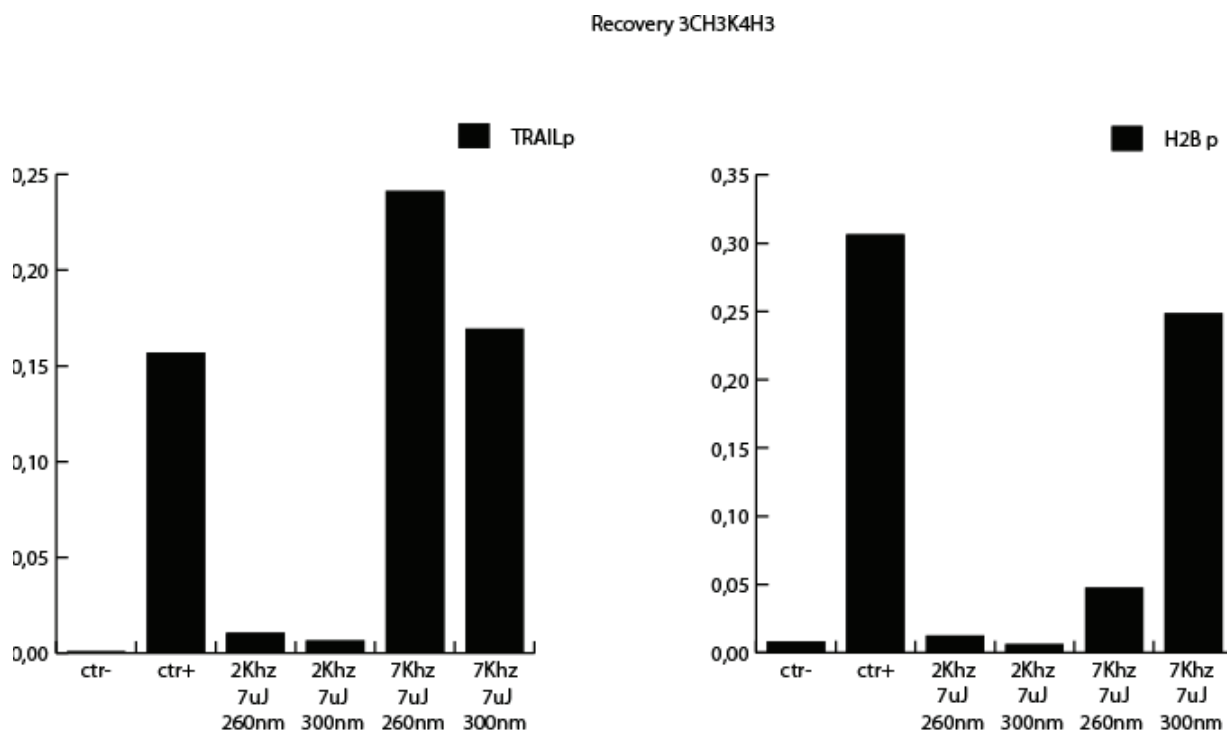


Fig 55: ChIP experiment

For the 7Khz 7µJ point a good recovery was obtained in 260nm condition but also with UV output near the 300nm.

An interesting improvement in this ChIP experiments is the recovery value for the H2B promoter region for which, in the previous experiments (compare figure 40 with figure 55) at high intensity of energy, no signal was obtained.

One of the possible explanations for this trend could be the sequence of the analyzed promoter regions. In fact by using low energetic laser conditions the DNA damage is minimized and an UV output of 300nm is only quite absorbed by thymines, so DNA sequences with a reduced content of paired T residues can react at the crosslink induction better than others.

Gene	Ampl	R primer	F primer	PairedT
H2B promoter	121bp	CATTACAACAAGCGCTCGAC	TGTA CTGGTGACGGCCTTA	10
TRAIL promoter	184bp	CACTGAAGCCCTTCTCTCT	AGTTTCCCTCTTCCAACG	30

H2Bp 121bp

TGTAC TGGTGACGGCC TAGTACCCTCGGACACGGCGTGC TGGCCA ACTCCCCAGGCAGCAG
CAGGCGCACGGCCGTCTGGATCTCCCTGGAGGTGATGGTCTGAGCGC GTGTGTAATG

TRAILp184bp

CACTGAAGCCC TCC TCTCTA TCTTT ATAGTCAGTGAGGAAATGAAAGCGAATGAG TGTCTT
TCTGGG TCTGTGGCC TGGCCCCACCCACATCTA TGAACCTGCAACTGTCCCTCCCC TCTCT
ACTGCCAGGGACAGCTC TGTCTCAAAGTAGTC TGGAAAGGAGGGAAACT

Table 3: Characteristics of amplified regions after ChIP experime

Discussion

DISCUSSION

The availability of the DNA sequence of many eukaryotic genomes and the generation of high density tiling arrays covering such entire genomes has made it possible to decipher the regulatory principles that are based on the interplay of *trans*-regulatory TFs and their cognate *cis*-regulatory DNA recognition sequences at genome-wide level. At the chromatin level a mutual interplay between TFs and epigenetic modifiers (DNA and histone modifying machineries) sets up determinants of regional gene (in)activity.

The ensemble of histone modifications at a given gene locus has been proposed to establish an “epigenetic code” of great complexity. Irrespectively of whether such a code does exist or whether chromatin modifications rather constitute a step in signal transduction, it has become increasingly clear that chromatin modifications constitute docking sites for regulatory factors. Thus, decryption of the information encoded by genomes requires a deconvolution of the genetic and epigenetic programs and the interplay between these two regulatory levels. In addition to their enormous potential and power for the study of gene regulation mechanisms such analyses will also provide important tools for diagnosis, prognosis, and therapy of diseases.

The chromatin immune precipitation (ChIP) technique is the tool of choice for analysis in which is important to isolate the DNA-transcription factors complexes.

To face limitations of conventional ChIP, a ChIP in which the binding between DNA and transcriptional factors is obtained by the use of a laser system (photo-induction) has been set-up.

The overall objective of the work has been to establish a novel ChIP technology that is based on highly efficient, precise, robust and reproducible laser-assisted DNA-protein photo-crosslinking (termed “LChIP”).

LChIP may overcome the limitations of the formaldehyde-based crosslinking and allows deciphering genomic information into TF and epigenetic mediator-modulated networks with unprecedented accuracy, sensitivity and precision at a dynamic range of magnitudes larger than possible with XChIP. In the future LChIP will be established for genome-wide studies.

UV laser crosslink DNA and proteins is generally regarded as a two-step process, even though recent studies suggest that one UV-photon process can be the dominant mechanism for cross-linking nucleic acid bases with proteins *in vitro*. Nevertheless, due to their complexity, interactions in living cells follow reaction paths not easily reproducible *in vitro*, and results obtained *in vivo* clearly show the non-linear response of the living cells to a high-intensity laser.

Within the two photon excitation scheme a first UV photon excites the DNA base from the singlet S_0 ground state to the first excited S_1 manifold. From the second S_1 level the molecule can absorb a second photon, which promotes the DNA base to high lying singlet S_N levels above the ionization limit (I.L.).

The generated cation radical and the electron may recombine and possibly initiates crosslinking with hydrogen-bonded amino acids. There is, however, a finite probability for an intersystem crossing (I.C.) to the triplet T_1 manifold, which has a long lifetime compared to the singlet S_1 level. Absorption of a second photon then leads to a transition to high lying T_N levels above the ionisation limit. The ions produced via the triplet channel can also initiate crosslink to the contacting proteins. Processes leading to DNA damage can be initiated at any of the four excited states

S_1 , S_N , T_1 , and T_N , but only S_N and T_N lead to crosslinking. Thus, to reduce DNA damage the population times in the non-productive states S_1 and T_1 should be minimized. From this point of view singlet channel to crosslink (via S-states) is to be favored to triplet channel (via T-states) as it is much faster thus reducing residence time in the intermediate, excited state which leads to cell damage without directly contributing to crosslink.

In this process the crosslinking yield strongly depends on pulse intensity and pulse length.

By changing the pulse length the path leading to crosslinking can be chosen. For a pulse length shorter than the intersystem crossing rate constant, singlet-mediated crosslinking dominates, whereas pulses which are long compared with the intersystem crossing rate constant lead to crosslinking via the triplet channel.

The induction of UV laser crosslink between DNA and proteins presents, respect to the conventional chemical crosslink formation, the following advantages:

- Shorter times of exposure
- Reduced protein-protein bonds formation
- Good yield
- Possibility to analyze the kinetic of TFs and DNA binding in real time

So crosslinking by short pulsed UV lasers is a potentially powerful tool to investigate such DNA–protein interactions, especially transient interactions and binding kinetics, because the number of photons required for covalent complex formation can be delivered very rapidly, in nano-, pico- or even femtosecond intervals, and the high energy of the pulses should result in efficient crosslinking with no formation of a-specific products.

So, even though the conventional ChIP is a excellent technique to study the binding events to DNA, the Laser-ChIP is able to surpass the technical limitations of the original bottom-up process.

These intrinsic limitations comprise:

Selectivity: Formaldehyde introduces covalent bonds between protein-DNA and protein-protein complexes. Transcription factors (TFs) are generally embedded within complexes/machineries that display multiple interaction surfaces (with DNA or between subunits). This has two consequences: (i) factors that bind DNA directly or indirectly via protein-protein interactions with chromatin components will be crosslinked with vastly different efficiencies depending on the stability of the interaction and (ii) a single protein/complex can be crosslinked to more than one site in the genome e.g. in the case of enhancer-promoter looping. Native-ChIP can only be employed efficiently for very stable interactions, predominantly histone (nucleosome)-DNA interactions. The novel Laser-ChIP technology will identify direct protein-DNA contacts preferentially if not exclusively under certain conditions (wavelength, repetition rate, energy/pulse).

Accuracy and efficiency: The overall performance of conventional ChIP depends critically on the efficiency of the first step, the crosslink of factors to DNA by formaldehyde exposure of intact cells. However, chemical crosslinking is diffusion-controlled and varies considerably with cell type, manipulation, storage and purity of the chemical. Due to the progressively increasing non-specific crosslink by chemical crosslinkers, formaldehyde crosslinking has to be stopped long before a maximal crosslinking of DNA to protein has been reached. This implies low efficiency of the subsequent immunoprecipitation. L-ChIP involves ultra-fast physical crosslinking by femtosecond UV lasers specifically designed for highly efficient DNA-protein

crosslinking. Once calibrated it operates fully reproducible and highly accurate, and is cell and operator independent.

Dynamics and half-lives of DNA interactions: TFs bind with highly different kinetics/half-lives to DNA/chromatin. Current technologies do not allow studying very short-lived interactions. Due to its ultra-fast crosslinking, LChIP will allow fundamental studies on the mechanisms of DNA/chromatin recognition by DNA-binding regulatory factors.

Sensitivity: Conventional XChIP requires large amounts of cells (about 10^6 to 10^8 cells) as starting material. Given its high efficiency documented in proof-of-principle experiments, LChIP in its current state of development already provides the sensitivity for regular TF analyses thus facilitating the analysis of very small numbers of cells (e.g. from patients samples) and subpopulations (e.g. hematopoietic cells).

Single cell, tissue crosslinking and sorting: Current ChIP technologies do not permit crosslink of selected individual cells or frozen tissue slides and subsequent analyses of defined population. LChIP linked to with microscopic and cell-sorting platforms using microfluidic systems will permit to photo crosslink subsets of cells 'on-the-fly', crosslink cells in particular phases of the cell cycle, or leukemia blasts for genome-wide analyses.

Epitope masking and modification: Formaldehyde crosslinking alters lysine residues, which can be part of antibody epitopes in targeted DNA binding proteins, particularly in modified histones. This has several serious drawbacks: (i) it reduces substantially the IP efficacy in epigenetic studies and yields $\ll 1\%$ are commonly observed, (ii) due to the covalent stabilization of entire complexes, antibody epitopes may reside inside a complex, which would become accessible due to dissociation if only DNA crosslinks would occur, (iii) epitope-tagging is limited to peptides that are not modified by formaldehyde. LChIP will not affect protein epitopes and hence have a dramatically higher IP efficacy allowing the use of epitope-tagging approaches with highly efficient antibodies independent of the presence of lysines.

The rationale at the bases of the entire experimental data set was:

- the creation of a powerful tool (ER α -GFP methodology) to analyze in a short time the best conditions for the UV Laser crosslink induction
- the validation of the method by performing ChIP analysis
- the evaluation of cellular behavior in response to Laser treatment
- the correction of the starting hypothesis on the bases of obtaining results

Regarding to the first point the establishment of a rapid methodology to start the screening of Laser conditions was necessary to have an idea of the direction in which to move the first passes. As jet explained below, the setting of Laser device is composed by a lot of parameters to manage. Among them the energy/pulse, the repetition rate of photons, the time of irradiation, the total released energy, the number of hits and the wavelength of UV output Laser light.

The combination of all these parameters increases strongly the number of biological proofs that are important to realize the setting.

For this reason the availability of a screening test that links in a direct way the crosslink yield to the fluorescence signal was suitable for the purpose.

With this test, whose principles were already been explained in the chapter Results, a lot of experimental conditions were tested simultaneously by varying the proper Laser parameters but also several technical and biological terms, as cellular concentration and typology of saline buffer.

At the end of this preliminary session of data, as expected, some operative conditions were discovered in which the protein ER α -GFP was crosslinked to DNA fiber.

This conditions correspond to: 2Khz 125uJ, 200hz 125uJ and 20Khz 8uJ; the irradiation time was fixed to 60", though in some conditions, and with the 20ul configuration, after a second of irradiation the recovery of crosslink was quite similar to 60" ones.

It is important to keep in mind that, for the characteristic of this assay, the obtaining data constituted only a preliminary idea on the "final" L-ChIP establishment.

In fact with this methodology was not considered the amplificability of DNA and the stability of crosslinked proteins but it only confirmed the capability to interfere with cellular processes (e.s the transcription and the epigenetic code) by the creation of stable bonds between DNA and proteins (transcriptional factors in particular). This factor explains also the motivation to choice time of irradiation that are lower than the chemical one but not very short for a ChIP experiments.

In addition, because its technical simplicity, the ER α -GFP test is not affected by variability and it is quantitative if reported to a negative and positive control.

In some of selected conditions founded through ER α -GFP method, the ChIP analysis was done. The conditions were: 2Khz 125uJ and 200hz 125uJ, chosen on the bases of value of cellular mortality (in particular, among the three different conditions previous listed, the one with the highest value of % cellular death and the lower one).

As shown in Results, the ChIP experiment was performed looking at the trimethylation of lysine 4 of histone H3 and the % of chromatin immunoprecipitation (related to the quantity and quality of crosslink induction) was expressed as % of recovery of TRAIL promoter region sequence of DNA.

The choosing to amplify the TRAIL promoter region could be justify with different motivations: i) TRAIL is an important protein involved in cell death and tumor fighting, ii) the TRAIL promoter region is affected by many epigenetic modifications and iii) its promoter region was extensively studied by the work group in the Department of General Pathology of SUN, Naples.

The recovery in this ChIP experiment did not reach the value of the chemical one, but it was, however, good enough to continue the study.

In particular, it is worth pointing out that a result comparable with the chemical crosslinked point was achieved through a decreasing in time of 1 order of magnitude (15 minutes versus 1 minute).

The decrease of the induction time to obtain the crosslink allows to study a wider range of biological phenomena involving the interaction between DNA and proteins and the methods could be useful for study the time scale of all the interactions that occur on a specific region of DNA.

The crosslink obtained with Laser source is a "zero-length" reaction, so, compared with the chemical methodology, it is less susceptible to the downstream conditions of ChIP experiments.

For this reason, by vary a bit the protocol for the immunoprecipitation reaction (e.i increasing the % of detergents) the recovery of 3CH3K4H3 far exceeded the value of the positive control.

The idea was to promote the stay of direct bounds between DNA and proteins comparing with a chemical link mediated by the insertion of a bi-functional reagent interacting with protein and DNA respectively.

The most interesting thing is however the selectivity and preferential behavior of different genetic region to the crosslink induction with UV Laser light.

As shown in Results, each DNA region analyzed by ChIP experiments acts as unique, though all of them are immunoprecipitated with the same antibody and the particular epigenetic mark is present on their promoter regions.

It could be justified by the characteristics of the DNA sequence composing the amplified regions (TRAIL, H2B and SCAM5 promoters) or by the way by which the protein 3CH3K4H3 interacts with them (e.i. the orientation of DNA on the histone core, if the DNA regions protrude outward the histone or the region of crosslink resides in an area not accessible or poorly accessible to the photons released to the Laser device).

To clarify this aspect it is need to study the 3D structure of wrapped DNA containing these regions, in relation to the particular epigenetic mark.

One problem with UV laser crosslinking is the difficulty of comparing results obtained with different proteins and different DNA sequences. This is due to differences in the nature and strength of the interaction and to the involvement of different amino acid side chains and DNA bases. In some cases water molecules mediate the contacts between amino acids and DNA bases.

It's important to keep in mind that the Laser-ChIP is an *in vivo* technique.

However, there could be fundamental differences between the results of crosslinking in cells or nuclei compared to crosslinking isolated nucleoproteins, as done in most studies. First, suspensions of cells or nuclei scatter significant amounts of the incident light, reducing the intensity of the light within the samples.

Second, the local concentration of DNA in nuclei is very high, leading to an internal filtering effect that could also decrease the effective intensity of the light. Third, the high local concentration of DNA in nuclei might trap free radicals that could increase photochemical degradation of the DNA and proteins.

These considerations underline the necessity of a thorough study regard the quantistic principles that rule the photo-crosslink induction.

The synergy between theoretical calculations and experiments on chemical models together with the structural characterization of the photo-crosslinked products will help to understand the chemical principles governing the reactivity of DNA and proteins.

Thus, the factors effecting the excitation of the DNA and the protein, the formation of intermediate reactive species, and the creation of the new DNA-protein bonds will be studied and this detailed description of the photochemical behavior of DNA in a protein environment will provide the knowledge needed for rational design and optimization of the crosslink experimental conditions. The identification of the electronic states of the DNA bases and the corresponding intermediate species involved in the DNA-protein bond-making process will also open the possibility of fine-tuning the laser wavelength in the visible range to selectively link the desired fragments.

The DNA's stability is a crucial factor for the success of a ChIP experiment because the fragility of its structure could interfere with the sonication step (bringing to the production of too short in length DNA fragments) that is fundamental for the precipitation mediated by the antibody and so for the amplification by PCR or *in Real Time-PCR*.

From sonication tests (data not shown) performed on irradiated cells by varying the time of exposure to UV Laser treatment and by varying the conditions of sonication (in time of minute, amplitude, volume and etc..) was immediately evident the irradiated cells behaved differently.

This observation was the first proof to the understanding of the possible DNA structural damage presence in the cellular model.

To better understand the cellular behavior in response to the Laser treatment a lot of experiments were done, looking at cellular viability/mortality, the activation of

pathways of DNA damage recognition and repair, the cell cycle progression and the integrity of DNA itself.

The idea was to discover a Laser condition by which the energy released to the cells was strong enough to promote the crosslink induction but not too hard to disrupt the DNA and to kill all of cells.

So the first passage was to study in particular one condition (2khz 125uJ) keeping constant the repetition rate (equal to 2khz) and varying the parameter of energy to obtain, in the time unit of 1 minute, a scalar decrement of total energy.

At this experimental points were also added some additional conditions, choosing the combination of rep rate and energy/pulse to achieve the same total energy (3600 mJ) of the experimental point 2khz 30uJ.

For each point was analyzed first of all the cellular mortality, measured as capability of PI to pass through the cellular membrane of dead cells.

From the total amount of data, the presence of two concomitant types of cellular death was discovered after the crosslink induction with the Laser device. One of this is active in the first minutes after the irradiation session, and culminates with a strong reduction in cell number after few hours past treatment.

In cells that remain alive after treatment, the apoptotic pathway was activate, as demonstrated by caspases 3/7 activation, ROS production and the expression of some characteristic proteins.

It is interesting to note that the activation of apoptotic pathway is mostly linked to the total energy released to Laser and absorbed by the cells. So the induction of apoptosis scales with the decrease of the total energy.

The concomitant subsistence of both ways bringing to cellular death ensures that the geometry of irradiation (1 million of cells in 1 ml of PBS in a 1mm diameter quartz cuvette, in stirring) allows to hit all the cells present in.

This is an additional proof of the improvement achieved by passing to a volume of 20ul (with the same cellular concentration) to a volume of 1ml.

It is interesting to note that for the experimental point at same total energy (2khz 30uJ, 400hz 150uJ, 480hz 125uJ and 600hz 100uJ) the percentage of cellular death is different, as so the percentage of caspases activation, ROS production and protein expression.

In fact it seems that an higher number of hits, with low energy each, affects less the cellular vitality in comparison to experimental points in which the same energy is released with fewer high energetic hits.

This trend is also observed with regard to the expression of marker of damage proteins.

The evaluation of cellular damages was also carried out looking at the presence of DNA dimers formation and double/single strand breaks.

Both DNA lesions are present on the chromatin fiber, as confirmed by Comet assay and evaluation of bases dimers. The Comet assay, done on each experimental points, shows the production of DNA tails as function of damage (double strand breaks, in particular) that is, in turn, function of energy absorbed by the samples.

The same is true for the dimers formation experiment, although the percentage of dimers is quite similar in all samples, indicating that in all conditions, the energy supplied is too much. Clearly the formation of adducts between TT bases requires less energy than one required for to break DNA strands and this could justify the data.

Once understand that, in the used conditions, the DNA inside the cells was damaged and this damage could interfere with the downstream analysis, the next step (in the

definition process bringing to ChIP's best conditions definition) was to progressively lower the energy, both for total number of photons, both for repetition rate.

As confirmed by data regarding PI incorporation and ROS production, keeping lower the energy, the cells remain alive after the irradiating session, and this aspect is related to the reducing of DNA damage.

To confirm that a low energy the crosslink induction was optimized, the Laser setting utilized for the ChIP experiment were 7Khz 7uJ and 2khz 7uJ.

Regarding the condition 7khz 7uJ, the energy was scaled of a factor of 5, comparing to the previous analyzed 2khz 125uJ.

Moreover the repetition rate was increased (passing from 2khz to 7khz) because, high rep/rate value with low energy for pulse seems to be preferred by the cells (as explained jet above).

It is also important to note that in the condition 7Khz 7uJ, the ROS and caspases activation was very low, as soon as the percentage of cellular death.

So the choice of this condition was been made because it combines some requirements for a theoretical good yield of crosslink formations: low value of cellular mortality, low percentage of ROS and caspases 3/7 activation but, however a not too reduced energy.

The recovery of ChIP experiment in this condition was bigger than the positive control for the region of TRAIL promoter, instead for the genomic region H2B promoter the signal is still too low, but anyway present if compared with negative control.

The trend of ChIP experiment is different when the output of Laser device is setting on a wavelength of 300nm.

With the UV wavelength of 300nm is reduced the absorption of T and C residues, so theoretically the formation of dimers could be reduced and structural damages could be avoided; as confirmed by data, the pyrimidine dimers are still present also in this conditions, but in less percentage, comparing with the same experimental point in which the output UV is set on 260nm (corresponding to the spectral region in which the absorption of T and C is greatest).

H2B promoter region seems to be crosslinked to 3CH3K4H3 in a better way, when the UV output is 300nm (referred to negative and positive experimental point) and the value is approximately equal to the chemical one.

Regarding the TRAIL promoter region, instead, it seems to be less susceptible to vary the UV wavelength, as emerged looking at the recovery values, that are similar in the condition 260 and 300nm.

The set of data displayed and discussed at now, suggests that as each *in vivo* technique, for the establishment of UV Laser mediated crosslink many physical and biological parameters need to be consider.

First of all, the UV Laser light characteristics assume key role in the setting of ChIP experiments by the definition of the better balance between total energy and repetition rate.

Also some structural features are important: among them the apparatus's geometry used for the irradiation, the material of the cuvette, the size of Laser beam, the speed of stirring.

The most important thing to consider, however, is still the cellular behavior in response to the UV incident radiation and the way by which the crosslink could be formed.

To be sure that the creation of stable bonds between DNA and proteins is obtained, the cells must be hit with sufficient energy and the energy reaching the biological model does not disrupt the proteins or DNA itself.

Bibliography

BIBLIOGRAPHY

Allan, J., Harborne, N., Rau, D.C. and Gould, H. (1982) Participation of core histone "tails" in the stabilization of the chromatin solenoid. *J Cell Biol*, **93**, 285-297.

An, J., Yang, T., Huang, Y., Liu, F., Sun, J., Wang, Y., Xu, Q., Wu, D. and Zhou, P. Strand-specific PCR of UV radiation-damaged genomic DNA revealed an essential role of DNA-PKcs in the transcription-coupled repair. *BMC Biochem*, **12**, 2.

Angrand, P.O., Apiou, F., Stewart, A.F., Dutrillaux, B., Losson, R. and Chambon, P. (2001) NSD3, a new SET domain-containing gene, maps to 8p12 and is amplified in human breast cancer cell lines. *Genomics*, **74**, 79-88.

Arents, G. and Moudrianakis, E.N. (1995) The histone fold: a ubiquitous architectural motif utilized in DNA compaction and protein dimerization. *Proc Natl Acad Sci U S A*, **92**, 11170-11174.

Bannister, A.J. and Kouzarides, T. (1996) The CBP co-activator is a histone acetyltransferase. *Nature*, **384**, 641-643.

Bannister, A.J. and Kouzarides, T. (2005) Reversing histone methylation. *Nature*, **436**, 1103-1106.

Bannister, A.J., Schneider, R. and Kouzarides, T. (2002) Histone methylation: dynamic or static? *Cell*, **109**, 801-806.

Becker, M.M. and Wang, J.C. (1984) Use of light for footprinting DNA in vivo. *Nature*, **309**, 682-687.

Bontempo, P., Mita, L., Doto, A., Miceli, M., Nebbioso, A., Lepore, I., Franci, G., Menafra, R., Carafa, V., Conte, M., De Bellis, F., Manzo, F., Di Cerbo, V., Benedetti, R., D'Amato, L., Marino, M., Bolli, A., Del Pozzo, G., Diano, N., Portaccio, M., Mita, G.D., Vietri, M.T., Cioffi, M., Nola, E., Dell'aversana, C., Sica, V., Molinari, A.M. and Altucci, L. (2009) Molecular analysis of the apoptotic effects of BPA in acute myeloid leukemia cells. *J Transl Med*, **7**, 48.

Brash, D.E. and Haseltine, W.A. (1982) UV-induced mutation hotspots occur at DNA damage hotspots. *Nature*, **298**, 189-192.

Buyse, I.M., Shao, G. and Huang, S. (1995) The retinoblastoma protein binds to RIZ, a zinc-finger protein that shares an epitope with the adenovirus E1A protein. *Proc Natl Acad Sci U S A*, **92**, 4467-4471.

C. Russmann, M.T., A. Fix, C. Naumer, T. Herrmann, J. and Schmitt, J.S., R. Beigang, and M. Beato. (1997) Two wavelength femtosecond laser induced DNA-protein crosslinking. *Nucleic Acids Res.*, **25**.

Chen, D., Ma, H., Hong, H., Koh, S.S., Huang, S.M., Schurter, B.T., Aswad, D.W. and Stallcup, M.R. (1999) Regulation of transcription by a protein methyltransferase. *Science*, **284**, 2174-2177.

Cohen, T. and Yao, T.P. (2004) AcK-knowledge reversible acetylation. *Sci STKE*, **2004**, pe42.

Dhalluin, C., Carlson, J.E., Zeng, L., He, C., Aggarwal, A.K. and Zhou, M.M. (1999) Structure and ligand of a histone acetyltransferase bromodomain. *Nature*, **399**, 491-496.

Emanuel, P. and Scheinfeld, N. (2007) A review of DNA repair and possible DNA-repair adjuvants and selected natural anti-oxidants. *Dermatol Online J*, **13**, 10.

Fischle, W., Wang, Y. and Allis, C.D. (2003) Histone and chromatin cross-talk. *Curr Opin Cell Biol*, **15**, 172-183.

Fletcher, T.M. and Hansen, J.C. (1995) Core histone tail domains mediate oligonucleosome folding and nucleosomal DNA organization through distinct molecular mechanisms. *J Biol Chem*, **270**, 25359-25362.

Garcia, J., Franci, G., Pereira, R., Benedetti, R., Nebbioso, A., Rodriguez-Barrios, F., Gronemeyer, H., Altucci, L. and de Lera, A.R. Epigenetic profiling of the antitumor natural product psammaphin A and its analogues. *Bioorg Med Chem*, **19**, 3637-3649.

Grewal, S.I. and Elgin, S.C. (2002) Heterochromatin: new possibilities for the inheritance of structure. *Curr Opin Genet Dev*, **12**, 178-187.

Grozinger, C.M., Hassig, C.A. and Schreiber, S.L. (1999) Three proteins define a class of human histone deacetylases related to yeast Hda1p. *Proc Natl Acad Sci U S A*, **96**, 4868-4873.

Grozinger, C.M. and Schreiber, S.L. (2000) Regulation of histone deacetylase 4 and 5 and transcriptional activity by 14-3-3-dependent cellular localization. *Proc Natl Acad Sci U S A*, **97**, 7835-7840.

Guardiola, A.R. and Yao, T.P. (2002) Molecular cloning and characterization of a novel histone deacetylase HDAC10. *J Biol Chem*, **277**, 3350-3356.

Hakimi, M.A., Bochar, D.A., Chenoweth, J., Lane, W.S., Mandel, G. and Shiekhhattar, R. (2002) A core-BRAF35 complex containing histone deacetylase mediates repression of neuronal-specific genes. *Proc Natl Acad Sci U S A*, **99**, 7420-7425.

Hansen, J.C. (2002) Conformational dynamics of the chromatin fiber in solution: determinants, mechanisms, and functions. *Annu Rev Biophys Biomol Struct*, **31**, 361-392.

Hansen, J.C., Tse, C. and Wolffe, A.P. (1998) Structure and function of the core histone N-termini: more than meets the eye. *Biochemistry*, **37**, 17637-17641.

Haseltine, W.A., Gordon, L.K., Lindan, C.P., Grafstrom, R.H., Shaper, N.L. and Grossman, L. (1980) Cleavage of pyrimidine dimers in specific DNA sequences by a pyrimidine dimer DNA-glycosylase of *M. luteus*. *Nature*, **285**, 634-641.

Hayashi, K., Hofstaetter, T. and Yakuwa, N. (1978) Asymmetry of chromatin subunits probed with histone H1 in an H1-DNA complex. *Biochemistry*, **17**, 1880-1883.

Heinzel, T., Lavinsky, R.M., Mullen, T.M., Soderstrom, M., Laherty, C.D., Torchia, J., Yang, W.M., Brard, G., Ngo, S.D., Davie, J.R., Seto, E., Eisenman, R.N., Rose, D.W., Glass, C.K. and Rosenfeld, M.G. (1997) A complex containing N-CoR, mSin3 and histone deacetylase mediates transcriptional repression. *Nature*, **387**, 43-48.

Huang, N., vom Baur, E., Garnier, J.M., Lerouge, T., Vonesch, J.L., Lutz, Y., Chambon, P. and Losson, R. (1998) Two distinct nuclear receptor interaction domains in NSD1, a novel SET protein that exhibits characteristics of both corepressors and coactivators. *Embo J*, **17**, 3398-3412.

Humphrey, G.W., Wang, Y., Russanova, V.R., Hirai, T., Qin, J., Nakatani, Y. and Howard, B.H. (2001) Stable histone deacetylase complexes distinguished by the presence of SANT domain proteins CoREST/kiaa0071 and Mta-L1. *J Biol Chem*, **276**, 6817-6824.

Jablonka, E., Lamb, M.J. and Avital, E. (1998) 'Lamarckian' mechanisms in darwinian evolution. *Trends Ecol Evol*, **13**, 206-210.

Jaenisch, R. and Bird, A. (2003) Epigenetic regulation of gene expression: how the genome integrates intrinsic and environmental signals. *Nat Genet*, **33 Suppl**, 245-254.

Jenuwein, T. and Allis, C.D. (2001) Translating the histone code. *Science*, **293**, 1074-1080.

Johns, E.W. (1967) A method for the selective extraction of histone fractions f2(a)1 and f2(a)2 from calf thymus deoxyribonucleoprotein at pH7. *Biochem J*, **105**, 611-614.

Jones, P.A. and Takai, D. (2001) The role of DNA methylation in mammalian epigenetics. *Science*, **293**, 1068-1070.

Kadonaga, J.T. (1998) Eukaryotic transcription: an interlaced network of transcription factors and chromatin-modifying machines. *Cell*, **92**, 307-313.

Kassabov, S.R., Zhang, B., Persinger, J. and Bartholomew, B. (2003) SWI/SNF unwraps, slides, and rewraps the nucleosome. *Mol Cell*, **11**, 391-403.

Kouzarides, T. (2002) Histone methylation in transcriptional control. *Curr Opin Genet Dev*, **12**, 198-209.

Kristeleit, R., Stimson, L., Workman, P. and Aherne, W. (2004) Histone modification enzymes: novel targets for cancer drugs. *Expert Opin Emerg Drugs*, **9**, 135-154.

Lee, K.M. and Hayes, J.J. (1998) Linker DNA and H1-dependent reorganization of histone-DNA interactions within the nucleosome. *Biochemistry*, **37**, 8622-8628.

Lis, D.S.G.a.J.T. (1985) RNA polymerase II interacts with the promoter region of the noninduced hsp70 gene in *Drosophila melanogaster* cells. *Mol Cell Biol*, **6**(11).

Luger, K., Mader, A.W., Richmond, R.K., Sargent, D.F. and Richmond, T.J. (1997) Crystal structure of the nucleosome core particle at 2.8 Å resolution. *Nature*, **389**, 251-260.

Luger, K. and Richmond, T.J. (1998) DNA binding within the nucleosome core. *Curr Opin Struct Biol*, **8**, 33-40.

Lyamichev, V. (1991) Unusual conformation of (dA)_n.(dT)_n-tracts as revealed by cyclobutane thymine-thymine dimer formation. *Nucleic Acids Res*, **19**, 4491-4496.

Mahlknecht, U. and Hoelzer, D. (2000) Histone acetylation modifiers in the pathogenesis of malignant disease. *Mol Med*, **6**, 623-644.

Maison, C., Bailly, D., Peters, A.H., Quivy, J.P., Roche, D., Taddei, A., Lachner, M., Jenuwein, T. and Almouzni, G. (2002) Higher-order structure in pericentric heterochromatin involves a distinct pattern of histone modification and an RNA component. *Nat Genet*, **30**, 329-334.

Matsuda, K., Ochiai, I., Nishi, M. and Kawata, M. (2002) Colocalization and ligand-dependent discrete distribution of the estrogen receptor (ER)α and ERβ. *Mol Endocrinol*, **16**, 2215-2230.

McBride, A.E. and Silver, P.A. (2001) State of the arg: protein methylation at arginine comes of age. *Cell*, **106**, 5-8.

McGhee, J.D. and Felsenfeld, G. (1980) The number of charge-charge interactions stabilizing the ends of nucleosome DNA. *Nucleic Acids Res*, **8**, 2751-2769.

McKinsey, T.A., Zhang, C.L., Lu, J. and Olson, E.N. (2000) Signal-dependent nuclear export of a histone deacetylase regulates muscle differentiation. *Nature*, **408**, 106-111.

McKinsey, T.A., Zhang, C.L. and Olson, E.N. (2001) Control of muscle development by dueling HATs and HDACs. *Curr Opin Genet Dev*, **11**, 497-504.

Milite, C., Castellano, S., Benedetti, R., Tosco, A., Ciliberti, C., Vicidomini, C., Bouilly, L., Franci, G., Altucci, L., Mai, A. and Sbardella, G. Modulation of the activity of histone acetyltransferases by long chain alkylidenemalonates (LoCAMs). *Bioorg Med Chem*, **19**, 3690-3701.

Miska, E.A., Karlsson, C., Langley, E., Nielsen, S.J., Pines, J. and Kouzarides, T. (1999) HDAC4 deacetylase associates with and represses the MEF2 transcription factor. *Embo J*, **18**, 5099-5107.

Mizzen, C.A., Yang, X.J., Kokubo, T., Brownell, J.E., Bannister, A.J., Owen-Hughes, T., Workman, J., Wang, L., Berger, S.L., Kouzarides, T., Nakatani, Y. and Allis, C.D.

(1996) The TAF(II)250 subunit of TFIID has histone acetyltransferase activity. *Cell*, **87**, 1261-1270.

Morgan, H.D., Santos, F., Green, K., Dean, W. and Reik, W. (2005) Epigenetic reprogramming in mammals. *Hum Mol Genet*, **14 Spec No 1**, R47-58.

O'Carroll, D., Scherthan, H., Peters, A.H., Opravil, S., Haynes, A.R., Laible, G., Rea, S., Schmid, M., Lebersorger, A., Jerratsch, M., Sattler, L., Mattei, M.G., Denny, P., Brown, S.D., Schweizer, D. and Jenuwein, T. (2000) Isolation and characterization of Suv39h2, a second histone H3 methyltransferase gene that displays testis-specific expression. *Mol Cell Biol*, **20**, 9423-9433.

Ogryzko, V.V., Schiltz, R.L., Russanova, V., Howard, B.H. and Nakatani, Y. (1996) The transcriptional coactivators p300 and CBP are histone acetyltransferases. *Cell*, **87**, 953-959.

Orrenius, S., Nicotera, P. and Zhivotovsky, B. Cell death mechanisms and their implications in toxicology. *Toxicol Sci*, **119**, 3-19.

Orrenius, S., Zhivotovsky, B. and Nicotera, P. (2003) Regulation of cell death: the calcium-apoptosis link. *Nat Rev Mol Cell Biol*, **4**, 552-565.

Paik, W.K. and Kim, S. (1973) Enzymatic demethylation of calf thymus histones. *Biochem Biophys Res Commun*, **51**, 781-788.

Pfeifer, G.P., Drouin, R., Riggs, A.D. and Holmquist, G.P. (1991) In vivo mapping of a DNA adduct at nucleotide resolution: detection of pyrimidine (6-4) pyrimidone photoproducts by ligation-mediated polymerase chain reaction. *Proc Natl Acad Sci U S A*, **88**, 1374-1378.

Rabinowicz, P.D., Palmer, L.E., May, B.P., Hemann, M.T., Lowe, S.W., McCombie, W.R. and Martienssen, R.A. (2003) Genes and transposons are differentially methylated in plants, but not in mammals. *Genome Res*, **13**, 2658-2664.

Rea, S., Eisenhaber, F., O'Carroll, D., Strahl, B.D., Sun, Z.W., Schmid, M., Opravil, S., Mechtler, K., Ponting, C.P., Allis, C.D. and Jenuwein, T. (2000) Regulation of chromatin structure by site-specific histone H3 methyltransferases. *Nature*, **406**, 593-599.

Richards, E.J. and Elgin, S.C. (2002) Epigenetic codes for heterochromatin formation and silencing: rounding up the usual suspects. *Cell*, **108**, 489-500.

Richards, E.J. and Elgin, S.C. (2002) Epigenetic codes for heterochromatin formation and silencing: rounding up the usual suspects. *Cell*, **108**, 489-500.

C. Russmann, M. T., A. Fix, C. Naumer, T. Herrmann, J., and Schmitt, J. S., R. Beigang, and M. Beato. (1997). Two wavelength femtosecond laser induced DNA-protein crosslinking. *Nucleic Acids Res* **25**.

-
- Sage, E. (1993) Distribution and repair of photolesions in DNA: genetic consequences and the role of sequence context. *Photochem Photobiol*, **57**, 163-174.
- Schieferstein, U. and Thoma, F. (1996) Modulation of cyclobutane pyrimidine dimer formation in a positioned nucleosome containing poly(dA.dT) tracts. *Biochemistry*, **35**, 7705-7714.
- Solomon, M.J., Larsen, P.L. and Varshavsky, A. (1988) Mapping protein-DNA interactions in vivo with formaldehyde: evidence that histone H4 is retained on a highly transcribed gene. *Cell*, **53**, 937-947.
- Solomon, M.J. and Varshavsky, A. (1985) Formaldehyde-mediated DNA-protein crosslinking: a probe for in vivo chromatin structures. *Proc Natl Acad Sci U S A*, **82**, 6470-6474.
- Souto, J.A., Benedetti, R., Otto, K., Miceli, M., Alvarez, R., Altucci, L. and de Lera, A.R. New anacardic acid-inspired benzamides: histone lysine acetyltransferase activators. *ChemMedChem*, **5**, 1530-1540.
- Stec, I., Wright, T.J., van Ommen, G.J., de Boer, P.A., van Haeringen, A., Moorman, A.F., Altherr, M.R. and den Dunnen, J.T. (1998) WHSC1, a 90 kb SET domain-containing gene, expressed in early development and homologous to a Drosophila dysmorphia gene maps in the Wolf-Hirschhorn syndrome critical region and is fused to IgH in t(4;14) multiple myeloma. *Hum Mol Genet*, **7**, 1071-1082.
- Strahl, B.D. and Allis, C.D. (2000) The language of covalent histone modifications. *Nature*, **403**, 41-45.
- Strahl, B.D., Briggs, S.D., Brame, C.J., Caldwell, J.A., Koh, S.S., Ma, H., Cook, R.G., Shabanowitz, J., Hunt, D.F., Stallcup, M.R. and Allis, C.D. (2001) Methylation of histone H4 at arginine 3 occurs in vivo and is mediated by the nuclear receptor coactivator PRMT1. *Curr Biol*, **11**, 996-1000.
- Tachibana, M., Sugimoto, K., Fukushima, T. and Shinkai, Y. (2001) Set domain-containing protein, G9a, is a novel lysine-preferring mammalian histone methyltransferase with hyperactivity and specific selectivity to lysines 9 and 27 of histone H3. *J Biol Chem*, **276**, 25309-25317.
- Tang, M.S., Htun, H., Cheng, Y. and Dahlberg, J.E. (1991) Suppression of cyclobutane and mean value of 6-4 dipyrimidines formation in triple-stranded H-DNA. *Biochemistry*, **30**, 7021-7026.
- Tornaletti, S. and Pfeifer, G.P. (1995) UV light as a footprinting agent: modulation of UV-induced DNA damage by transcription factors bound at the promoters of three human genes. *J Mol Biol*, **249**, 714-728.
- Tse, C., Georgieva, E.I., Ruiz-Garcia, A.B., Sendra, R. and Hansen, J.C. (1998) Gcn5p, a transcription-related histone acetyltransferase, acetylates nucleosomes and folded nucleosomal arrays in the absence of other protein subunits. *J Biol Chem*, **273**, 32388-32392.

- Tycko, B. (2000) Epigenetic gene silencing in cancer. *J Clin Invest*, **105**, 401-407.
- Usachenko, S.I., Bavykin, S.G., Gavin, I.M. and Bradbury, E.M. (1994) Rearrangement of the histone H2A C-terminal domain in the nucleosome. *Proc Natl Acad Sci U S A*, **91**, 6845-6849.
- Verdin, E., Dequiedt, F. and Kasler, H.G. (2003) Class II histone deacetylases: versatile regulators. *Trends Genet*, **19**, 286-293.
- Vettese-Dadey, M., Grant, P.A., Hebbes, T.R., Crane-Robinson, C., Allis, C.D. and Workman, J.L. (1996) Acetylation of histone H4 plays a primary role in enhancing transcription factor binding to nucleosomal DNA in vitro. *Embo J*, **15**, 2508-2518.
- Waltregny, D., De Leval, L., Glenisson, W., Ly Tran, S., North, B.J., Bellahcene, A., Weidle, U., Verdin, E. and Castronovo, V. (2004) Expression of histone deacetylase 8, a class I histone deacetylase, is restricted to cells showing smooth muscle differentiation in normal human tissues. *Am J Pathol*, **165**, 553-564.
- Waltregny, D., North, B., Van Mellaert, F., de Leval, J., Verdin, E. and Castronovo, V. (2004) Screening of histone deacetylases (HDAC) expression in human prostate cancer reveals distinct class I HDAC profiles between epithelial and stromal cells. *Eur J Histochem*, **48**, 273-290.
- Wang, H., Huang, Z.Q., Xia, L., Feng, Q., Erdjument-Bromage, H., Strahl, B.D., Briggs, S.D., Allis, C.D., Wong, J., Tempst, P. and Zhang, Y. (2001) Methylation of histone H4 at arginine 3 facilitating transcriptional activation by nuclear hormone receptor. *Science*, **293**, 853-857.
- Wang, X., Moore, S.C., Laszckzak, M. and Ausio, J. (2000) Acetylation increases the alpha-helical content of the histone tails of the nucleosome. *J Biol Chem*, **275**, 35013-35020.
- Yang, L., Xia, L., Wu, D.Y., Wang, H., Chansky, H.A., Schubach, W.H., Hickstein, D.D. and Zhang, Y. (2002) Molecular cloning of ESET, a novel histone H3-specific methyltransferase that interacts with ERG transcription factor. *Oncogene*, **21**, 148-152.
- Yoo, C.B. and Jones, P.A. (2006) Epigenetic therapy of cancer: past, present and future. *Nat Rev Drug Discov*, **5**, 37-50.
- Zhang, L., Zhang, K., Prandl, R. and Schoffl, F. (2004) Detecting DNA-binding of proteins in vivo by UV-crosslinking and immunoprecipitation. *Biochem Biophys Res Commun*, **322**, 705-711.
- Zhang, Y. and Reinberg, D. (2001) Transcription regulation by histone methylation: interplay between different covalent modifications of the core histone tails. *Genes Dev*, **15**, 2343-2360.

Supplementary Tables

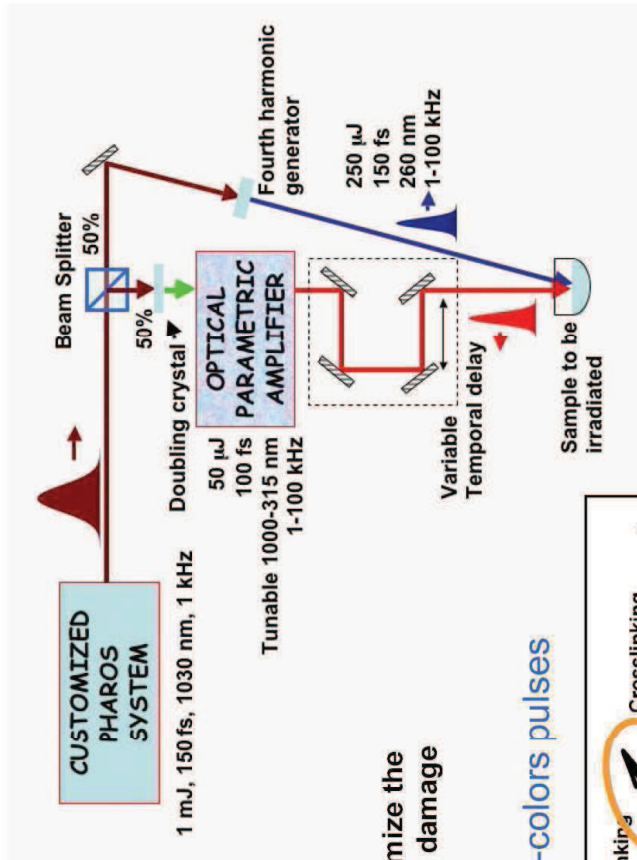
UV LASER FEATURES:

- Pulse duration <120 fs centered around 266 nm
- Excellent beam quality
- Average power 0. 4W (@ 10 kHz, 266 nm)
- Repetition rate of 1 Hz -350 kHz
- Pulse energy 150 μ J @ 2 kHz
- Forthcoming laser system (beginning 2010) with tuneable wavelength. Enable for two color experiments

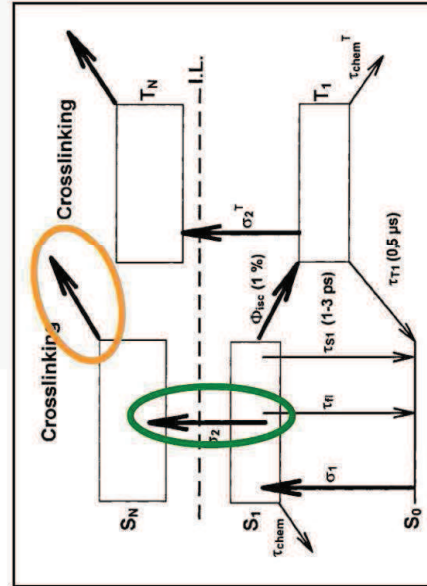
Minimize the DNA damage



.....two-colors pulses



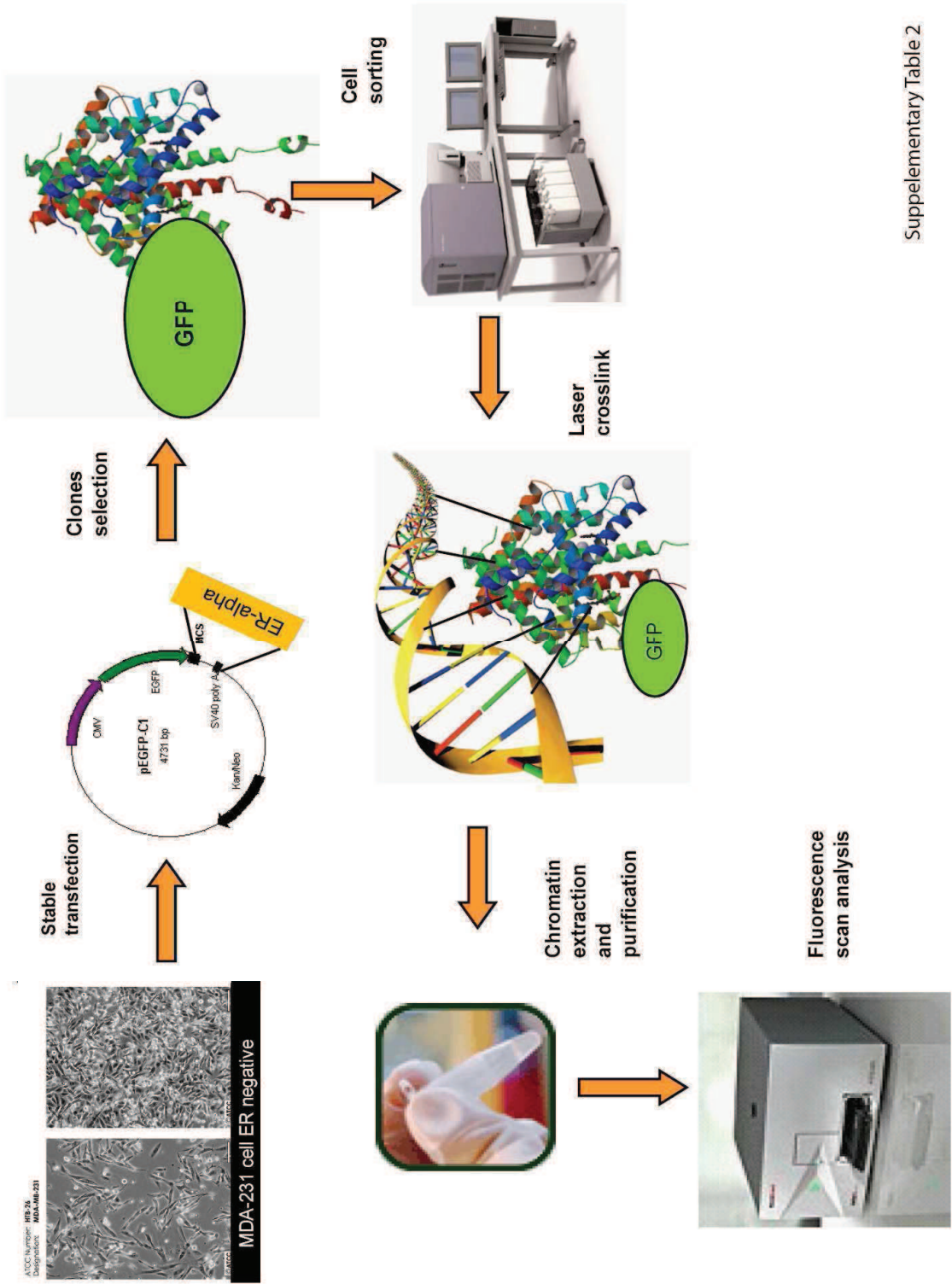
Electronic transition mediated by UV (260 nm) laser light



Crosslink obtained with blue (visible) laser light

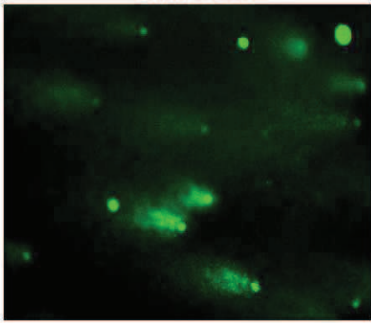
Supplementary Table 1

EXPERIMENTAL PROTOCOL:

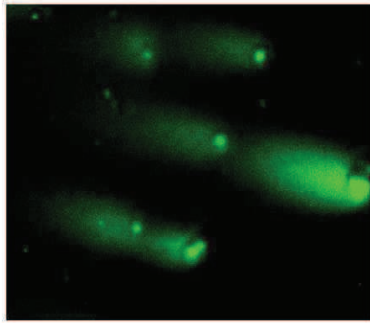


Supplementary Table 2

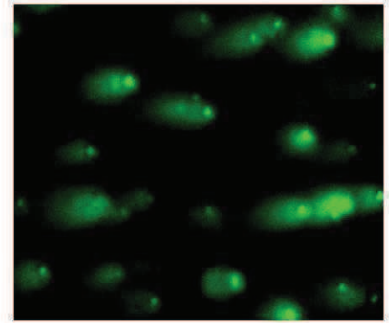
2Khz 90uJ



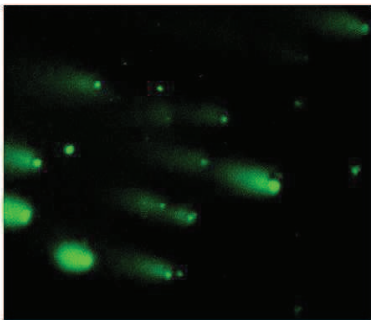
2Khz 60uJ



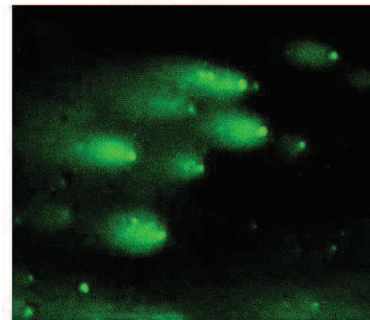
2Khz 30uJ



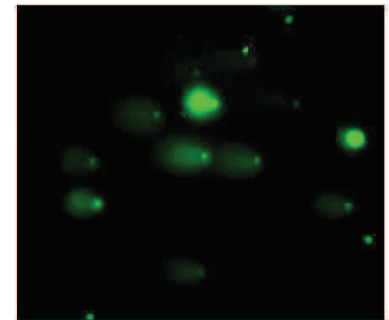
600Hz 100uJ



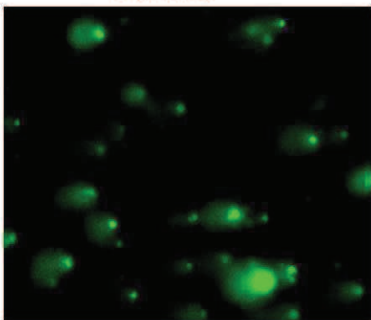
400Hz 150uJ



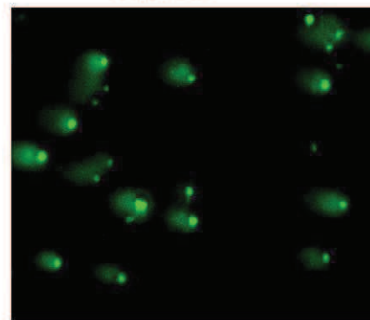
480Hz 125uJ



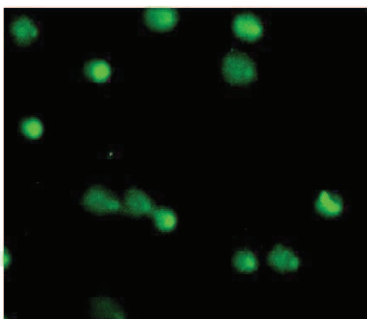
2Khz 7uJ



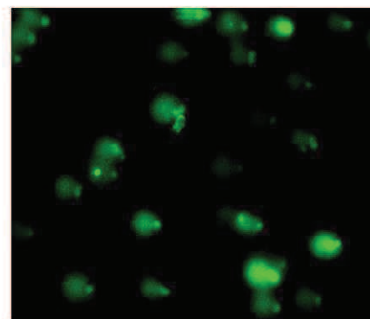
7Khz 7uJ



2Khz 7uJ 300nm



7Khz 7uJ 300nm



Supplementary Table 3

Publications

PUBLICATIONS:

- C. Altucci, A. Nebbioso, R. Benedetti, R. Esposito, V. Carafa, M. Conte, M. Micciarelli, L. Altucci, and R. Veletta (2011). Crosslink between proteins and nucleic acid induced by femtosecond UV laser pulses in living cells. Accepted by Laser Phys Lett
- Bontempo Paola, Doto Antonella, Benedetti Rosaria et al, Altucci Lucia (in press) Psidium guajava L. anticancer effects: induction of apoptosis and differentiation. Cell Proliferation, Manuscript ID: Cellprol-0963-11.R1
- Ciro Milite, Sabrina Castellano, Rosaria Benedetti, Alessandra Tosco, Carmen Ciliberti, Caterina Vicidomini, Ludovic Bouilly, Gianluigi Franci, Lucia Altucci, Antonello Mai, Gianluca Sbardella (2011). Modulation of the activity of histone acetyltransferases by long chain alkylidenemalonates (LoCAMs). Bioorganic & Medicinal Chemistry 19 (2011) 3690–3701
- Jos A. Souto, Rosaria Benedetti, Katharina Otto, Marco Miceli, Rosana Ivarez, Lucia Altucci, and Angel R. de Lera (2010). New Anacardic Acid-Inspired Benzamides: Histone Lysine Acetyltransferase Activators. ChemMedChem 2010, 5, 1530 – 1540
- Paola Bontempo, Luigi Mita, Rosaria Benedetti et al, Lucia Altucci (2009). Molecular analysis of the apoptotic effects of BPA in acute myeloid leukemia cells. Journal of Translational Medicine 2009, 7:48
- José García, Gianluigi Franci, Rosaria Benedetti, Angela Nebbioso, Fátima Rodríguez-Barrios, Hinrich Gronemeyer, Lucia Altucci, Angel R. de Lera (2011). Epigenetic profiling of the antitumor natural product psammaphin A and its analogues. Bioorganic & Medicinal Chemistry 19 (2011) 3637–3649

INTERNATIONAL COURSES AND CONFERENCES:

Selected speaker at the International Workshop "Chromatin remodeling and human disease" Rome, Regina Elena Institute, 3-4/12/2009

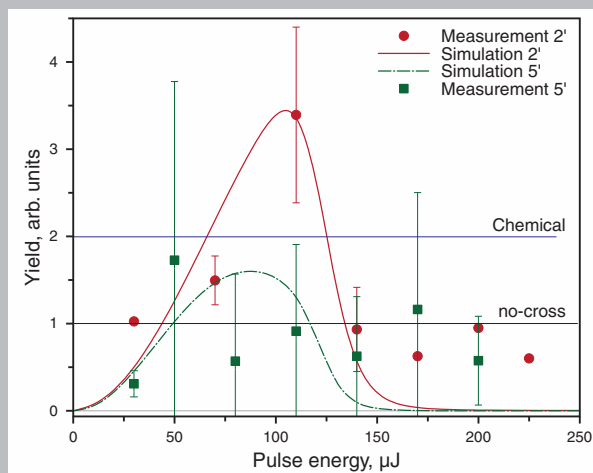
Practical course and conference "Concepts and Methods in Programmed Cell Death", ECDO Organization (European Cell Death Organization), in Belgium, Ghent 1-4/9/2010

Practical course and conference "Bioinformatics and High Throughput Sequencing" – 2011, Pasteur Institute, Paris 22/3/2011

RESEARCH ACTIVITY IN OTHER LABORATORIES:

The research activity was performed in collaboration with the Laboratory of Prof. Lucia Altucci, General Pathology Department, SUN, Naples.

Abstract: We investigate the interactions between proteins and DNA in solutions of living cells, triggered by UV, 200-fs laser pulses. DNA-protein crosslinking is obtained with two different techniques: conventional chemical or laser-induced. Our results evidence a nonlinear response of the cells to the laser irradiation in the investigated intensity range. The laser induced crosslink efficiency can reach a value approximately twice higher than that obtained with ordinary chemical methods. The experimental results are very well reproduced by a simple phenomenological model based on the interplay between two-photon absorption by DNA bases and cell damage induced by high intensity laser pulse.



Measured (experimental points)/calculated (lines) DNA-protein crosslinking yield in human U937 acute myeloid leukemia cells versus the laser pulse energy for 2' (circle) and 5' (squares) irradiation times

© 2011 by Astro Ltd.

Published exclusively by WILEY-VCH Verlag GmbH & Co. KGaA

Nonlinear protein – nucleic acid crosslinking induced by femtosecond UV laser pulses in living cells

C. Altucci,^{1,*} A. Nebbioso,² R. Benedetti,¹ R. Esposito,¹ V. Carafa,² M. Conte,² M. Micciarelli,¹ L. Altucci,^{2,3} and R. Velotta¹

¹ CNISM and Dipartimento di Scienze Fisiche, Università di Napoli "Federico II", Napoli, Italy

² Dipartimento di Patologia Generale, Seconda Università di Napoli, Napoli, Italy

³ IGB-CNR, Napoli, Italy

Received: 24 October 2011, Revised: 3 November 2011, Accepted: 6 November 2011

Published online: xx xxxxxx 2011

Key words: nonlinear optics; bio-polymers; femtosecond probing of biological molecules

1. Introduction

Femtosecond ultraintense laser pulses have been widely used so far micro- and even precise nano-machining of biological materials [1–5] and imaging of tissues for diagnostics purposes [6,7]. In this letter we focus on a different type of application of femtosecond laser pulses to bio-materials. In fact, we exploit the possibility of these pulses to efficiently trigger bio-molecule dynamics and, in a near-

future prospect, to monitor the system response with high temporal resolution.

Establishing a stable covalent bond between proteins and nucleic acids, usually referred to as crosslinking [8] in molecular biology, affords access to study otherwise transient interactions between bio-molecules, what is a crucial task for all bio-sciences. At the same time, it is possible this way investigating the interaction of complex systems with femtosecond, intense laser pulses, which repre-

* Corresponding author: e-mail: carlo.altucci@unina.it

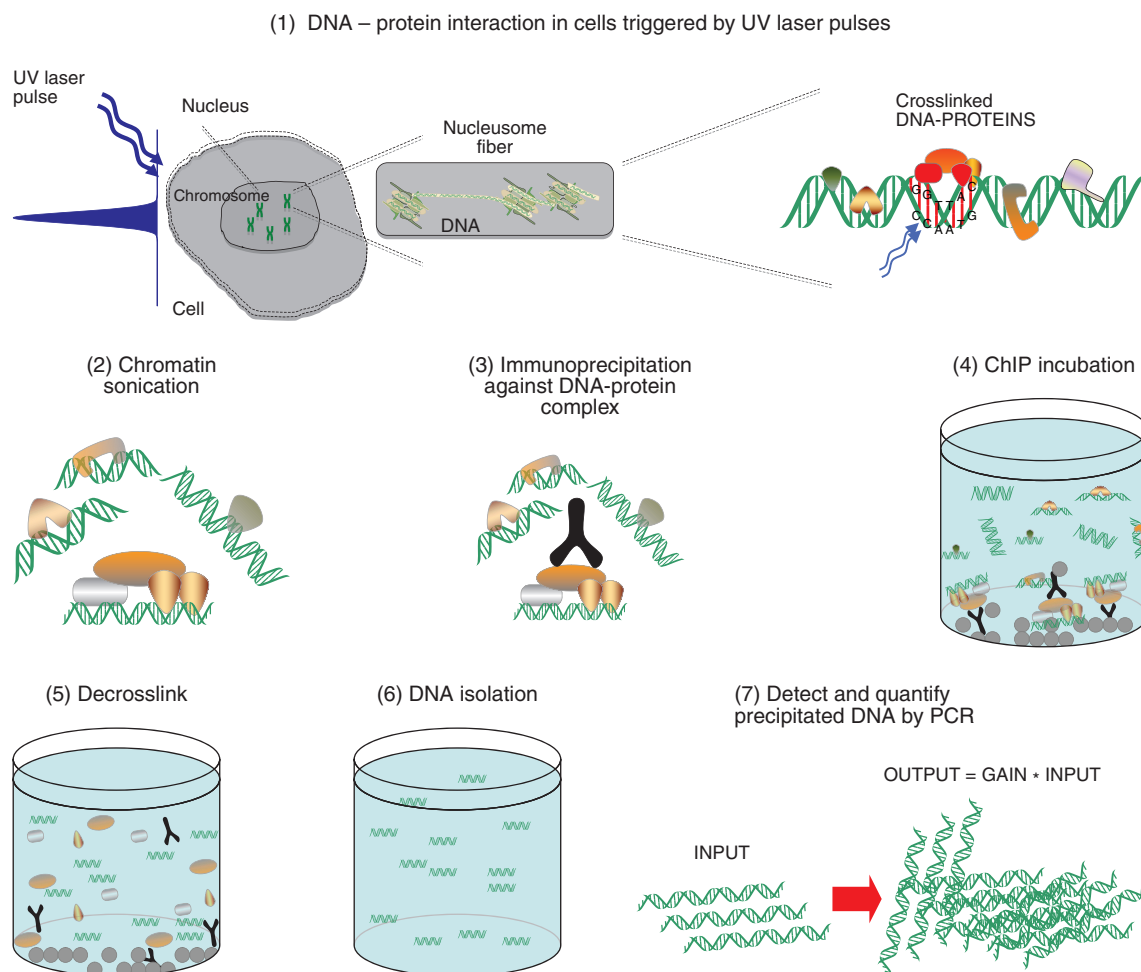


Figure 1 (online color at www.lphys.org) Schematic layout of the experiment. In (1) solutions containing living cells are irradiated by fs-UV laser pulses. This causes the formation of a covalent bond between an excited DNA base and a protein nearby. The samples are, then, processed by ChIP protocol [26,27] and qPCR [28] to measure the amount of a specific DNA region, the TRAIL promoter, bound to a specific protein, the H3K4me3 Histone [29]. (2)–(6) Scheme of the Chromatin Immunoprecipitation (ChIP) protocol consisting in five serial phases before accessing the final qPCR (7) for detection and quantification. In (2) cells are opened and DNA is sheared, in (3) the antibody of interest, which selectively recognizes only H3K4me3, is added. The last three phases consist in an immunoprecipitation (4) to isolate the protein of interest and, consequently, the crosslinked DNA fragments. A reverse crosslink takes place in (5) and (6) to purify and isolate the DNA fragments from the protein complexes. In (7), by means of qPCR, the appropriate DNA fragments are hugely amplified in number so as to quantify the amount of TRAIL promoter DNA region linked to the H3K4me3 protein

sents a fascinating challenge for femto-chemistry and nonlinear physics. Crosslinking with fs-UV lasers has been presented in the literature as a revolutionary technique to increase the otherwise low process yield of conventional methods based on chemical catalysts [9], conventional UV sources [10], or longer UV pulses [11,12].

It is known that crosslinking induced in cells by ultra-short laser pulses has a twofold advantage over conventional methods: (i) it binds only species that are in proximity (“zero length” covalent bond) of the absorbed photons rather than favoring unspecific bonds amongst many possible species in the cell and (ii) it should only operate until

the radiation is incident on the sample, thus paving the way for time-resolved studies of transient interactions. Moreover, when combined with biochemical techniques such as chromatin immunoprecipitation (ChIP) to analyze the produced bonds, the UV laser method will make feasible the characterization of the dynamics of the transcription factors bindings on chromatin in living cells, thus overcoming the technical limitations of the current ChIP technology [10,13,14].

One of the essential questions about the interaction of the UV laser light with living cells is the role played by the laser intensity. In fact, while the advantages gener-

ally offered by pulsed lasers over conventional radiation sources to photo-induce crosslink are widely recognized, it is still unclear if the photon absorption by DNA bases is a single or rather two photon process. Past experiments carried out on cellular fractions or *in vitro* purified DNA-fragment/protein reported linear [15–18] as well as non-linear dependence of cross-link yield on the laser intensity [11,12,18–22], suggesting that the discrepancies may result from the possible role played by the particular system under study. Thereby, this strongly limits the scope of *in vitro* experiments and pushes for experiments on living systems like cells.

Here we report on the femtosecond laser irradiation of human cells demonstrating the occurrence of DNA-protein crosslinking in their most native state. Our results match well with the two-photon absorption, thus corroborating the mechanism based on the radical formation proposed in [23]. Since the cross-link is demonstrated in *ex vivo* system (e.g. living cells), we expect that such a finding is of rather general validity. To explain our results we have adopted a simple, phenomenological model to describe the excitation process finding a fair agreement with the experimental results.

2. Experiment and modeling

The scheme of our experiment, from the initial excitation induced by laser pulses to the final measurement of the amount crosslinked material, is summarized in Fig. 1, in its seven steps. A solution of U937 human acute myeloid leukemia cells (see supplemental material [24] for details) was irradiated with the fourth harmonic (220 fs, 263 nm) of a Twinkle laser source operating at a repetition rate of 33 Hz [25]. Various irradiation times and pulse energies have been tested. For all experiments the cell concentration in the sample was 3.75×10^8 cells/ml whereas irradiations took place at room temperature (see supplemental material [24]). Shining a fs-UV-laser pulse onto the target can cause two-photon absorption by the DNA bases followed by the formation of a covalent bond with a protein lying in the proximity of the excited base (1). Successively, as shown in the (2)–(7) step sequence of Fig. 1, samples were treated by a ChIP protocol [26,27]. It was, then, possible to isolate and measure, by quantitative polymerase chain reaction (qPCR) (see [28] for a review), the amount of a specific DNA region, named TRAIL-gene-promoter, linked to a specific nuclear protein, named H3K4me3 [29]. In step (2) living cells are broken and the DNA is sheared, whereas in step (3) an antibody is added to selectively recognize only those DNA fragments cross-linked with the protein of interest (H3K4me3), thus enabling to fish them on. During an incubation time (Fig. 1, step (4)) the immunoprecipitation protocol is carried out, whereas in steps (5) and (6) selected DNA fragments are inversely cross-linked and washed by removing the protein-antibody complexes. Finally, in step (7) the appropriate DNA fragments are amplified and quantified by qPCR.

In order to analyze the obtained results we have developed a simple phenomenological model for the response of our system to the pulsed UV-irradiation, based on the following assumptions. i) Only DNA-bases of the cell chromatin get excited upon irradiation, ii) the dominant excitation is initiated by two-photon absorption as reported for ps pulses in [23,11], and iii) damage to the cells caused by irradiation with intense UV laser pulses occurs at relatively high peak intensities, larger than 2 GW/cm^2 , in agreement with a typical threshold-like behavior with the pulse energy [30].

As long as the first hypothesis is concerned, it is well known that aromatic amino-acids, tryptophan, phenylalanine, and tyrosine, which are abundant also in nuclear proteins, absorbs at 260 nm. Thus, in principle, UV light could also trigger crosslinking by first exciting proteins rather than DNA. Nevertheless, the static UV ($\approx 260 \text{ nm}$) absorption spectra of bases and aromatic amino-acids show much stronger absorption of bases compared to amino-acids. The influence of solvent and intra-cellular water-like liquid has also been discarded in view of the negligible water non-linear absorption at 260 nm at the used intensities [31], the linear absorption being very small as well in this UV window. The bi-photon excitation mechanism based on radical cation formation has been invoked in [23,11] and relies on the two-photon absorption by the same base. The two photons can also be absorbed by two different bases of the DNA double strand, separated by not more than two-three bases [32]. In this case, the decay channel of the system is governed by base-stacking conformation and the path followed by stacked bases can strongly differ from that of unstacked ones. Although our results are in agreement with two photon absorption mechanism, we are not able to discriminate the actual microscopic absorption mechanism.

Finally, by relying on the above hypotheses, it is easy to work out the expression of the crosslinking process yield, Y , as a function of the two macroscopic knobs of our experiment, i.e. the pulse energy, E_{pulse} , and the number of laser shots, N_{shot} , per irradiation. For the sake of simplicity we will refer in the following to E_{pulse} although the relevant physical quantity turns out to be the laser pulse intensity.

If $\Pi(E_{pulse})$ is the probability that a DNA base is led to double excited state by two UV photon absorption, and $D(E_{pulse})$ is the probability that a crosslinked specie survives after the irradiation of a single pulse (damage function), the overall yield, Y , after N_{shot} is:

$$Y(E_{pulse}, N_{shot}) \propto \Pi D^{N_{shot}-1} + \Pi(1 - \Pi)D^{N_{shot}-2} + \dots, \quad (1)$$

where the sum is over N_{shot} terms each of them containing a polynomial in Π whose coefficients form the Pascal triangle. The sum in Eq. (1) can be easily carried out to give:

$$Y(E_{pulse}, N_{shot}) = \dots \quad (2)$$

$$k\Pi(E_{pulse})D^{N_{shot}-1}(E_{pulse})\frac{1-\xi(E_{pulse})^{N_{shot}}}{1-\xi(E_{pulse})},$$

where

$$\xi(E_{pulse}) = \frac{1-\Pi(E_{pulse})}{D(E_{pulse})}$$

and k is an instrumental constant.

If σ_1 and σ_2 are the cross sections for the first and the second photon absorption respectively, and p is the probability the excitation leads to a covalent DNA-protein bond, $\Pi(E_{pulse})$ can be written as:

$$\Pi(E_{pulse}) = p\sigma_1\sigma_2\frac{E_{pulse}^2}{E_{photon}^2A^2}, \quad (3)$$

$E_{photon} = 4.5$ eV being the single photon energy and A the laser spot size onto the sample, which in our experiment has been measured to be 0.25 cm².

The damage function $D(E_{pulse})$ has been chosen so as to reproduce the above mentioned threshold-like behavior of the crosslinked cells damage with the pulse energy [21]:

$$D(E_{pulse}) = \frac{1}{2}\left[1 - \text{Erf}\left(\frac{E_{pulse} - E_{th}}{\Delta E}\right)\right]. \quad (4)$$

In Eq. (4) E_{th} stands for the energy threshold and ΔE for the slope of the damage when the energy increases. It is worth stressing that we have not accounted for possible damage to non-crosslinked cells. Such an assumption has been corroborated by checking irradiated non-crosslinked cells by means of the fluorescence activated cell sorting methodology and finding out that cell-damage is negligible in our conditions.

We have used Eq. (2) to best-fit our measurements which report the crosslink yield versus E_{pulse} for 2 and 5 minutes irradiations, as shown in Fig. 2. The best-fit parameter values turned out to be $p\sigma_1\sigma_2 = 4.4 \times 10^{-34}$ cm⁴, $E_{th} = 185$ μ J, and $\Delta E = 30$ μ J. The estimation of the product $\sigma_1\sigma_2$ depends on the particular macromolecule under consideration. For instance, the absorption cross-section of liquid aqueous solution of thymine at the wavelength of 282 nm for the $S_0 \rightarrow S_1$ transition triggered by fs laser pulses is $\sigma_1 \approx 3 - 10 \times 10^{-17}$ cm² [33], whereas the absorption cross-section of a uridine molecule from the first excited singlet state $S_1 \rightarrow S_2$ at 266 nm is $\sigma_2 \approx 10^{-15}$ cm² [23,34]. These values would provide $p \approx 0.1$ when the two-photon absorption involves two different bases each of them making the $S_0 \rightarrow S_1$ transition, and $p \approx 0.01$ for the mechanism involving one single base making the $S_0 \rightarrow S_1 \rightarrow S_2$ transition.

$E_{th} = 185$ μ J, and $\Delta E = 30$ μ J are realistic values in the damage dynamics of tissues due to irradiation with intense UV laser pulses [30]. In particular, $E_{th} = 185$ μ J leads to a threshold intensity of ≈ 3 GW/cm² for crosslinked cell damage in good agreement with the

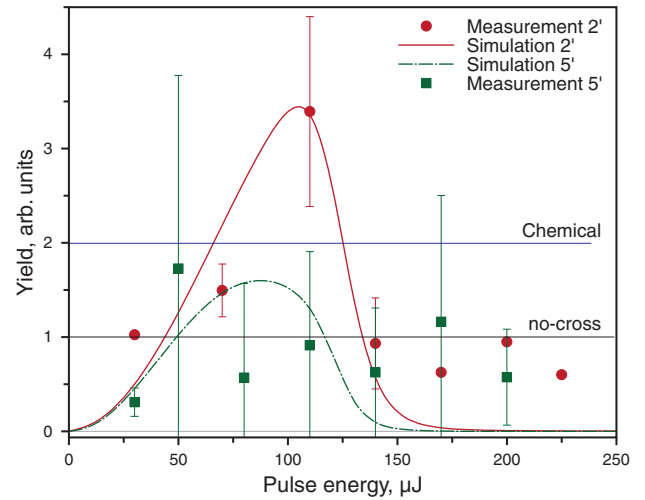


Figure 2 (online color at www.lphys.org) Measured (experimental points)/calculated (lines) DNA-protein crosslinking yield in human U937 acute myeloid leukemia cells versus the laser pulse energy for 2' (circle) and 5' (squares) irradiation times. The blue and black horizontal lines represent the yield values obtained with ordinary chemical methods and measured in non-irradiated cells, respectively

value reported for cell damage in Chinese hamster ovary by fs-345-nm laser pulses [35].

The behavior of the crosslinking yield versus the laser pulse energy in Fig. 2 clearly demonstrates the nonlinear response of the system to laser pulse irradiation. The yield increases quadratically up to a maximum value, after which it quickly drops off due to cross-linked cell damage. The longer irradiation time results in a smaller yield due to damage accumulation.

The maximum value falls at about 110 μ J for 2' irradiation, whereas it shifts to lower pulse energies (50 μ J) for 5' irradiation, again due to higher damage. The fair agreement between simulations and measurement is noticeable in view of the high intrinsic fluctuations of the extremely complex system under investigation. The error bars result from the root mean square of the values measured in five experimental runs carried out at different times with different samples of the same cell line. Thus, we can assess that our analysis is reliable even though only few experimental points are above the no-cross level, the latter being the amount of crosslink yield found in non-irradiated cells. This value is about half the yield usually obtained with ordinary chemical methods, which amount to $\approx 1 - 3\%$ [8]. It is remarkable that the maximum yield obtained in our experiment by inducing crosslink with UV fs-pulses is about twice as high as the value achieved with chemical methods. Thus, not only ultrashort UV pulses produces crosslink in time interval much shorter than those required by chemical methods, but even the yield can be definitely

larger than that obtained with the conventional methods currently used.

This is a striking finding which could be even improved paving the way to detect and study new interactions in molecular biology, which are too weak to be detected with standard techniques.

It worth stressing, however, that our model is far from being a detailed description of the crosslink mechanism in living cells from a microscopic prospect. Although we claim the fundamental role is played by the two photon absorption, we cannot state whether the absorption is localized in a single DNA base, as suggested in [11,12,23], or there is a contribution from a collective excitation involving two bases, rather close to each other in the double strand DNA, as suggested in [32] and theoretically predicted in [36]. Even the mechanism involving two singly-excited bases lying in the triplet T_1 state, next to each other, like in the bi-molecular triplet-triplet annihilation [37] is compatible with our results.

We point out that our model reaches three important goals:

1. it reproduces very well the response of our complex system to laser pulse irradiation in a number of cases,
2. it sheds light on the investigated crosslink mechanism, providing some explanation for the nonlinear behavior, still being of general validity,
3. it relates the measurable DNA-protein crosslink yield of a complex system such as a human cell directly to macroscopic degrees of freedom, such as E_{pulse} and N_{shot} , which are controlled in the experiment.

Hence, after testing the reliability of the model by fitting the measurements, we have looked for the best possible irradiation conditions within the $E_{pulse} - N_{shot}$ plane. The result is shown as a contour plot in Fig. 3.

We notice that the maximum crosslink efficiency is expected at $N_{shot} \approx 1000$ and $E_{pulse} \approx 120 \mu\text{J}$. This corresponds to about half a minute irradiation time and would lead to yield enhancement of a factor of 2.5 over the result achieved via the chemical method. Of course, the shorter the irradiation time the smaller the induced damage in the crosslinked cells.

3. Conclusion

In summary, we have experimentally demonstrated that living human cells non-linearly respond to irradiation with intense fs-UV-laser pulses. Amongst the phenomena triggered by such pulses a highly efficient DNA-protein occurs, which reaches yields twice (or even more) higher than those obtained with ordinary alternative methods. This observation provides an answer to the fundamental scientific question, debated over the past decade, whether the response of complex bio-molecules such as DNA and

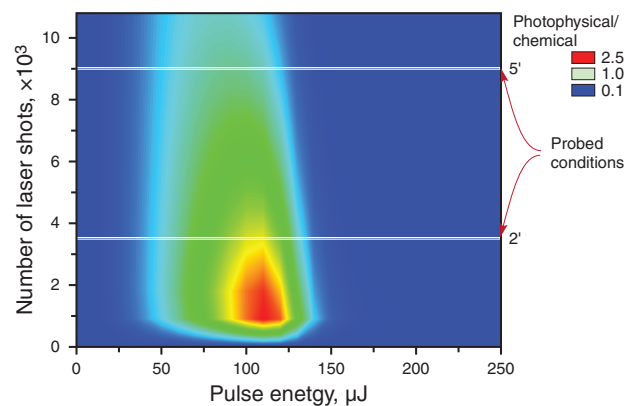


Figure 3 (online color at www.lphys.org) Map of the calculated ratio of photophysical/chemical yield for DNA-protein crosslink in living cells, as a function of the pulse energy and the number of laser shots. The white horizontal lines refer to the experienced conditions of the experiment, corresponding to 2' and 5' irradiations, respectively

proteins in living cells is linear or non-linear. Our experimental results are well reproduced by a simple phenomenological model based on the interplay between non-linear UV-absorption by DNA and cell damage induced beyond a typical pulse energy threshold. Our findings have a twofold importance: on the one hand they shed light on the physical behavior of highly complicated and interesting bio-systems, such as DNA and proteins, in a physical context typical of ultrashort non-linear dynamics driven by fs laser pulses; on the other hand they pave the way for a new technique aimed to establish DNA-protein crosslink in living cells, which promises to have a huge impact in molecular biology and bio-sciences. Such an approach can replace ordinary methods to study the interaction between DNA and proteins, due to its very high efficiency and general applicability. Not least, the short irradiation time can allow one to study the so-called transient interactions occurring on a short time scale and generally undetectable with conventional techniques.

Acknowledgements This work has been supported by the European Community (ATLAS contract No. 221952). A.N., R.B., and M.R. are fellows of the ATLAS Consortium. V.C. is fellow of the APOSYS Consortium (contract No. 200767). C.A. and R.V. acknowledge Sandro De Silvestri for valuable discussions.

References

- [1] X. Hu, B. Qian, P. Zhang, X. Wang, L. Su, J. Qiu, and C. Zhu, *Laser Phys. Lett.* **5**, 394 (2008).
- [2] R.F.Z. Lizarelli, M.M. Costa, E. Carvalho-Filho, F.D. Nunes, and V.S. Bagnato, *Laser Phys. Lett.* **5**, 63 (2008).
- [3] V.K. Pustovalov, A.S. Smetannikov, and V.P. Zharov, *Laser Phys. Lett.* **5**, 775 (2008).

- [4] A.A. Alekhin, A.A. Ionin, S.E. Kozhushko, I.M. Kourylyova, S.I. Kudryashov, K.K. Kuz'min, V.G. Likhvansteva, M.V. Samoylov, L.V. Seleznev, D.V. Sinitsyn, and S.D. Zakharov, *Laser Phys. Lett.* **7**, 463 (2010).
- [5] A.Z. Freitas, L.R. Freschi, R.E. Samad, D.M. Zezell, S.C. Gouw-Soares, and N.D. Vieira, Jr., *Laser Phys. Lett.* **7**, 236 (2010).
- [6] H. Ullah, M. Atif, S. Firdous, M.S. Mehmood, M. Ikram, C. Kurachi, C. Grecco, G. Nicolodelli, and V.S. Bagnato, *Laser Phys. Lett.* **7**, 889 (2010).
- [7] D. Chorvat, Jr. and A. Chorvatova, *Laser Phys. Lett.* **6**, 175 (2009).
- [8] M.J. Solomon and A. Varshavsky, *Proc. Natl. Acad. Sci. USA* **82**, 6470 (1985).
- [9] M.J. Solomon, P.L. Larsen, and A. Varshavsky, *Cell* **53**, 937 (1988).
- [10] L. Zhang, K. Zhang, R. Prändl, and F. Schöffl, *Biochem. Biophys. Res. Commun.* **322**, 705 (2004).
- [11] C. Russmann, M. Truss, A. Fix, C. Naumer, T. Herrmann, J. Schmitt, J. Stollhof, R. Beigang, and M. Beato, *Nucl. Acids Res.* **25**, 2478 (1997).
- [12] Ch. Russmann, M. Beato, J. Stollhof, C. Weiss, and R. Beigang, *Nucl. Acids Res.* **26**, 3967 (1998).
- [13] D.S. Gilmour and J.T. Lis, *Mol. Cell. Biol.* **5**, 2009 (1985).
- [14] D.S. Gilmour and J.T. Lis, *Mol. Cell. Biol.* **6**, 3984 (1986).
- [15] C.A. Harrison, D.H. Turner, and D.C. Hinkle, *Nucl. Acids Res.* **10**, 2399 (1982).
- [16] J.W. Hockensmith, W.L. Kubasek, W.R. Vorachek, and P.H. von Hippel, *J. Biol. Chem.* **261**, 3512 (1986).
- [17] J.W. Hockensmith, W.L. Kubasek, W.R. Vorachek, E.M. Evertsz, and P.H. von Hippel, *Methods Enzymol.* **208**, 211 (1990).
- [18] T. Shapkina, S. Lappi, S. Franzen, and P. Wollenzien, *Nucl. Acid Res.* **32**, 1518 (2004).
- [19] D. Angelov, M. Charra, C.W. Müller, J. Cadet, and S. Dimitrov, *Photochem. Photobiol.* **77**, 592 (2003).
- [20] D. Angelov, V.Yu. Stefanovsky, S.I. Dimitrov, V.R. Rusanova, E. Keskinova, and I.G. Pashev, *Nucl. Acids Res.* **16**, 4525 (1988).
- [21] E.I. Budowsky, M.S. Axentyeva, G.G. Abdurashidova, N.A. Simukova, and L.B. Rubin, *Eur. J. Biochem.* **159**, 95 (1986).
- [22] E.N. Dobrov, Z.Kh. Arbieva, E.K. Timofeeva, R.O. Esenaliev, A.A. Oraevsky, and D.N. Nikogosyan, *Photochem. Photobiol.* **49**, 595 (1989).
- [23] D.N. Nikogosyan, *Int. J. Radiat. Biol.* **57**, 233 (1990).
- [24] Supplemental material.
- [25] A. Dubietis, G. Valiulis, R. Danielius, and A. Piskarskas, *Pure Appl. Opt.* **7**, 271 (1998).
- [26] M. Vermeulen, H.C. Eberl, F. Matarese, H. Marks, S. Denisov, F. Butter, K.K. Lee, J.V. Olsen, A.A. Hyman, H.G. Stunnenberg, and M. Mann, *Cell* **142**, 967 (2010).
- [27] S. Denisov, M. van Driel, R. Voit, M. Hekkelman, T. Hulsen, N. Hernandez, I. Grummt, R. Wehrens, and H. Stunnenberg, *EMBO J.* **26**, 944 (2007).
- [28] M. Kubista, J.M. Andrade, M. Bengtsson, A. Forootan, J. Jonák, K. Lind, R. Sindelka, R. Sjöback, B. Sjögreen, L. Strömbom, A. Ståhlberg, and N. Zoric, *Mol. Aspects Med.* **27**, 95 (2006).
- [29] A. Nebbioso, N. Clarke, E. Voltz, E. Germain, C. Ambrosino, P. Bontempo, R. Alvarez, E.M. Schiavone, F. Ferrara, F. Bresciani, A. Weisz, A.R. de Lera, H. Gronemeyer, and L. Altucci, *Nat. Med.* **11**, 77 (2005).
- [30] S.H. Chung and E. Mazur, *J. Biophoton.* **2**, 557 (2009).
- [31] S. Lejnine, G. Durfee, M. Murnane, H.C. Kapteyn, V.L. Makarov, and J.P. Langmore, *Nucl. Acids Res.* **27**, 3676 (1999).
- [32] C.T. Middleton, K. de La Harpe, C. Su, Y.K. Law, C.E. Crespo-Hernández, and B. Kohler, *Annu. Rev. Phys. Chem.* **60**, 217 (2009).
- [33] A. Reuther, D.N. Nikogosyan, and A. Laubereau, *J. Phys. Chem.* **100**, 5570 (1996).
- [34] E.V. Khoroshilova and D.N. Nikogosyan, *J. Photochem. Photobiol. B* **5**, 413 (1990).
- [35] R. Le Harzic, I. Riemann, K. König, C. Wüllner, and C. Donitzky, *J. Appl. Phys.* **102**, 114701 (2007).
- [36] F. Santoro, V. Barone, and R. Improta, *Proc. Natl. Acad. Sci. USA* **104**, 9931 (2007).
- [37] S. Balushev, T. Miteva, V. Yakutkin, G. Nelles, A. Yasuda, and G. Wegner, *Phys. Rev. Lett.* **97**, 143903 (2006).



Psidium Guajava anticancer effects: induction of apoptosis and differentiation

Journal:	<i>Cell Proliferation</i>
Manuscript ID:	Cellprol-0946-11
Manuscript Type:	Original Manuscript
Date Submitted by the Author:	27-Jul-2011
Complete List of Authors:	Bontempo, Paola Doto, Antonella Miceli, Marco Mita, Luigi Benedetti, Rosaria nebbioso, angela veglione, manuela rigano, daniela Cioffi, Michele sica, vincenzo Molinari, Anna Maria Altucci, Lucia; SUN, Patologia generale
Keywords:	Psidium Guaiava, apoptosis, differentiation, cancer

1
2
3 *Psidium Guajava* anticancer effects: induction of apoptosis and differentiation
4
5
6
7

8 Paola Bontempo^{1,*}, Antonella Doto¹, Marco Miceli^{1,2}, Luigi Mita¹, Rosaria Benedetti^{1,3}, Angela
9
10 Nebbioso¹, Manuela Veglione¹, Daniela Rigano⁴, Michele Cioffi¹, Vincenzo Sica¹, Anna Maria
11
12 Molinari¹ and Lucia Altucci^{1,2,*}
13
14
15
16

17 ¹ Dipartimento di Patologia generale, Seconda Università degli Studi di Napoli, Vico L. de Crecchio
18
19 7, 80138, Napoli, IT; ² CNR-IGB, Via P. Castellino, 80100, Napoli, IT; ³ Dipartimento di Fisica,
20
21 Università degli Studi Federico II, Via Cinthia, 80100, Napoli, IT; ⁴ Dipartimento di Chimica delle
22
23 Sostanze Naturali, Università degli Studi di Napoli "Federico II", Via D. Montesano, 49, I-80131
24
25
26
27 Napoli, Italy
28
29
30
31
32
33

34 * To whom correspondence should be addressed.
35
36
37
38
39
40
41
42
43
44
45
46
47
48
49
50
51
52
53
54
55
56
57
58
59
60

Abstract

Objectives: Curative properties of medicinal plants such as *Psidium guajava* L. (Myrtaceae) have been often claimed by epidemiological studies on populations in which these fruits are consumed daily. However, a complete characterization of the active principles responsible for this capability has never been performed. We have characterized Guajava anticancer potential and identified the parts of the fruit involved in this anticancer action.

Material and methods: Cell cycle, apoptosis, differentiation analyses, morphological-stainings, western blots.

Results: We report that the Guajava acetonc extract exerts anti-cancer activities on hematological and solid cancers. Guajava extract anti-proliferative action is tightly bound to induction of apoptosis and differentiation. The use of *ex vivo* myeloid leukemia blasts corroborates that the Guajava extract is able to induce cell death. Guajava extract does not show anticancer effects on all the tested cancer cells indicating a selective activity against certain types of cancer models. The analyses of Guajava three different components, flesh, peel and seeds, identifies the flesh fraction as the relevant part for the induction of cell cycle arrest and apoptosis, whereas the peel component is responsible for differentiation. Guajava and the flesh-derived extract induces apoptosis accompanied by caspase activation and p16, p21, FASL, BAD and DR5 overexpression.

Conclusions: Our findings show that the Guajava extract is able to exert anti-cancer action *in vitro* and *ex vivo* supporting the hypothesis of pro-apoptotic regulation against cancer.

Introduction

The medicinal use of natural products - compounds that are derived from natural sources such as plants, animals and micro-organisms - precedes recorded human history probably by thousands of years. Only in the last decades natural products have taken on a role in drug discovery and development given that emerging sciences such as molecular biology and combinatorial chemistry appear to be able to satisfy the requests of the pharmaceutical industry. In concrete terms, the rational design of chemical compounds to target specific molecules often draws on what in nature already exists. Therefore improving and understanding the biological effects of many natural compounds represents a significant option for drug discovery in the field of biomedical sciences.

Natural compounds, particularly plant derivatives, are the subject of an increasing number of studies and growing interest is being directed to plants that are well known for their medicinal properties. Among these, *Psidium guajava* L. (Myrtaceae) has a long history of officinal and medical use in many tropical American and Southeast Asian populations (1). *Psidium guajava*, considered native in Mexico (2), is widespread throughout South America, Europe, Africa and Asia. Based on archaeological evidence it has been known and used widely in Peru since pre-Columbian times. It grows in all the tropical and subtropical areas of the world, adapts to different climatic conditions, although dry climates are preferred (3). The main traditional use known is as an anti-diarrheal. Other reported uses include treatment of gastroenteritis, dysentery, stomach ailments, and intestinal disorders due to pathogenic germs of the intestine (4). Its medicinal usage has been reported in indigenous systems of medicine in America more than elsewhere. *Psidium guajava* is a small tree which is 10 metres high with thin, smooth, patchy, peeling bark. Leaves are opposite, short-petiolate, the blade oval with prominent pinnate veins, 5–15 cm long. Flowers are somewhat showy, petals whitish up to 2 cm long, stamens numerous (3). Fruit are fleshy yellow globose to ovoid berry about 5 cm in diameter with an edible pink mesocarp containing numerous small, hard, white seeds. From a phyto-chemical point of view Guajava fruits contain many phenolic

1
2
3 compounds (such as gallic and ferulic acid), flavonoids (such as quercetin, kaempferol, guajaverin),
4
5 carotenoids, triterpenes, tannins and quinones. The heterogeneity of Guajava fruit constituents could
6
7 explain the immense potential of this plant in the treatment of conditions such as diarrhea (5),
8
9 gastroenteritis and rotavirus enteritis (6), wounds, acne, dental plaque, malaria, allergies, coughs,
10
11 diabetes, cardiovascular disorders, degenerative muscular diseases (7,8), inflammatory ailments
12
13 including rheumatism and menstrual pain, liver diseases etc (9) . Not surprisingly, Guajava also
14
15 exhibits antioxidant (10) and anti-inflammatory effects as oxidative injury underlies many of these
16
17 diseases (11). Recently, anticancer activity has been reported for Guajava and some other Myrtaceae
18
19 fruits (12,13) supported by epidemiological studies on populations in which these fruits are
20
21 consumed daily. However a deep analysis and a complete characterization of the active principles
22
23 responsible for this capability have never been performed.
24
25
26
27

28
29 Here, we have characterized the anticancer potential of Guajava and identified the parts of the fruit
30
31 involved in this anticancer action.
32
33
34
35

36 **Materials and methods**

37 *Plant material*

38
39
40 *Psidium guajava* L. (Myrtaceae) fruits were collected from Brazil. Identification was carried out by
41
42 Prof. Adriana Basile — Section of Plant Biology, Department of Biological Sciences, Federico II
43
44 University of Naples, IT.
45
46
47
48
49

50 *Method of extraction*

51
52
53 *P. guajava* fruits, fresh or after storage at -20° C, were treated with Triton X-100 0.8% water
54
55 solution to remove epiphytic hosts normally found on the surface. After extensive washings in TAP
56
57 buffer (Tris-HCl pH 7.0 50 mM, NaCl 180 mM, NP-40 0.15%, glycerol 10%, MgCl₂ 1.5 mM,
58
59 NaMO₄ 1 mM, NaF 0.5 mM with protease inhibitors (Sigma), 1 mM DTT and 0.2 mM PMSF) and
60

1
2
3 distilled water, the fruits were dried on filter paper. Four different acetonc extracts were then
4
5 prepared. For the first, 826 g of whole guava fruits were blended, freeze-dried and then extracted
6
7 for 3 days with acetone at room temperature (3×5 l). Following filtration, the solvent was
8
9 evaporated under reduced pressure and moderate temperature (35°C) to give a gum (48 g). The
10
11 same protocol was applied for the preparation of the other three extracts (peel, flesh and seed) after
12
13 isolating the different parts of the fruit (14). In brief, 364 g of fresh guava peel gave 6 g of dry
14
15 acetonc extract, 1,220 g of fresh guava flesh gave 50 g of dry acetonc extract and 31 g of seeds
16
17 gave 300 mg of dry acetonc extract. All four extracts were freeze-dried and successively assayed
18
19 for their anticancer potential.
20
21
22
23
24

25 *Cell lines, primary cells and culture conditions*

26

27
28 NB4 cells were provided by M. Lanotte. All other cell lines were purchased from ATCC and
29
30 routinely cultured. NB4 and U937 cells were grown at 37°C in air and 5% CO₂ in RPMI-1640
31
32 medium (GIBCO), supplemented with 10% heat-inactivated foetal bovine serum (FBS), 1% L-
33
34 glutamine, 1% ampicillin/streptomycin and 0.1% gentamicin. U2OS osteosarcoma cells were
35
36 grown at 37°C in air and 5% CO₂ in Dulbecco's Modified Eagle Medium (DMEM, GIBCO)
37
38 supplemented with 5% foetal bovine serum (FBS, GIBCO), 1% L-glutamine, 1%
39
40 ampicillin/streptomycin and 0.1% gentamicin. MDA-MB231 breast cancer cells were grown at
41
42 37°C in air and 5% CO₂ in Dulbecco's Modified Eagle Medium (DMEM, GIBCO) supplemented
43
44 with 5% foetal bovine serum (FBS, GIBCO), 1% L-glutamine, 1% ampicillin/streptomycin and
45
46 0.1% gentamicin. For the AML samples purifications and cultures were carried out as previously
47
48 described (15). This study was approved by the Ethical Committee of the Second University of
49
50 Naples. SAHA (kindly donated by Merck) and MS275 (Alexis) were resuspended in DMSO and
51
52 used at a final concentration of 5µM. All Trans Retinoic Acid (ATRA, Sigma) was resuspended in
53
54 100% ethanol and used at a final concentration of 1µM.
55
56
57
58
59
60

Cell cycle analysis

2.5×10⁵ cells were collected and resuspended in 500µl of a hypotonic buffer (0.1% Triton X-100, 0.1% sodium citrate, 50µg/ml propidium iodide (PI), RNase A). Cells were incubated in the dark for 30 min. Samples were acquired on a FACS-Calibur flow cytometer using Cell Quest software (Becton Dickinson) and analysed with standard procedures using Cell Quest software (Becton Dickinson) and the ModFit LT version 3 Software (Verity) as previously reported (16). All the experiments were performed in triplicate.

FACS analysis of apoptosis

Apoptosis was measured with Annexin V/PI double staining detection (Roche and Sigma–Aldrich respectively) as recommended by the suppliers; samples were analysed by FACS with Cell Quest software (Becton Dickinson) as previously reported (15,17). The apoptotic fraction was calculated by measuring Annexin V positive /PI negative cells. As second assays caspase 8, 9 and 7-3 detection (B-Bridge) was performed as recommended by suppliers and quantified by FACS (Becton Dickinson).

Granulocytic differentiation assay

Granulocytic differentiation was carried out as previously described (15,18). Briefly, NB4 cells were harvested and resuspended in 10µl phycoerythrine-conjugated CD11c (CD11c-PE) or 10µl FITC-conjugated CD14 (CD14- FITC) (Pharmingen). Control samples were treated with 10µl PE or FITC conjugated mouse IgG1, incubated for 30 min at 4°C in the dark, washed in PBS and resuspended in 500µl PBS containing PI (0.25µg/ml). Samples were analysed by FACS with Cell Quest software (Becton Dickinson). PI positive cells were excluded from the analysis.

Western blot analysis

1
2
3 Forty μg of total protein extracts were separated on a 15% polyacrylamide gel and blotted as
4
5 previously described (19). Western blots were performed for p21 (Transduction Laboratories,
6
7 dilution 1:500) and for p16 (Santa Cruz, dilution 1:500) and total ERKs (Santa Cruz, dilution
8
9 1:1000) were used to normalise for equal loading. For quantification of TRAIL protein, 100 μg of
10
11 total protein extracts were separated on a 10% polyacrylamide gel and blotted. Western blots were
12
13 performed for TRAIL (Abcam, dilution 1:200) and ERKs (Santa Cruz, dilution 1:1000) was used
14
15 to normalise for equal loading. The same protocol was applied for DR5 (Millipore, dilution 1:1000).
16
17 To determine FLIP levels, 35 μg of total protein extracts were separated on a 12% polyacrylamide
18
19 gel and blotted. Western blots were performed for FLIP (Alexis, dilution 1:500) and total ERKs
20
21 (Santa Cruz, dilution 1:1000) were used to normalise for equal loading. To determine BAD levels
22
23 35 μg of total protein extracts were separated on a 12% polyacrylamide gel and blotted; the same
24
25 was done for FASL (ProSci, dilution 1:500). For both proteins total ERKs (Santa Cruz, dilution
26
27 1:1000) was used to normalise for equal loading.
28
29
30
31
32
33

34 *Morphology staining*

35
36
37 NB4 cells were spun onto glass slides with a cytospin centrifuge. Cell morphology was analysed
38
39 after May-Grunwald Giemsa stain (SIGMA).
40
41
42
43
44
45
46

47 **Results**

48 *Total acetonic Guajava fruit extract induces anticancer action in leukaemia NB4 cells*

49
50
51
52
53
54
55
56 That Guajava exerts anticancer action was initially confirmed by using the total acetonic Guajava
57
58 fruit extract at different concentrations for a time of 48 hours in NB4 promyelocytic leukaemia cells.
59
60

Trypan blue staining carried out in NB4 cells treated with the total acetonic Guajava fruit extract at

1
2
3 different concentrations indicated its strong anti-proliferative effect. Interestingly, the effect of
4 Guajava total acetonc extract is linear and dose dependent (Fig. 1a, b). That two different time-long
5 treatments (3 and 5 days) displayed the greatest effect in a dose-dependent manner in a
6 concentration range of 5-1.5 mg/mL strongly suggested that the inhibition of cellular growth might
7 be related to a 'bona fide' anti-proliferative dose-dependent effect rather than to drug toxicity. When
8 cell cycle effects were analysed, treatment with total acetonc Guajava extract (in the range of the
9 biological active dose) induced a G1 cell cycle block (Fig. 1c) of around 80% at concentrations of
10 1.5 mg/mL and 3 mg/mL.
11
12
13
14
15
16
17
18
19
20
21
22
23

24 *Total acetonc Guajava fruit extract exerts anticancer action by inducing apoptosis and*
25 *differentiation in cancer cells and primary leukaemia blasts.*
26
27
28
29
30
31

32 When apoptosis was measured upon treatment of NB4 cells with total acetonc Guajava extract, the
33 percentage of apoptotic cells increased during treatment and the effect was already measurable at
34 very low dose concentrations (around 0.4mg/ml) (Fig. 2a). When total acetonc Guajava fruit
35 extract was tested for 48 hours *ex vivo* in primary leukaemia blasts deriving from a patient affected
36 with acute myeloid leukaemia (AML) (AML #106), the induction of apoptosis was confirmed
37 indicating that not only leukaemia cell lines, but also primary AML cells respond to Guajava extract
38 treatment with apoptosis (Fig. 2b). As positive controls for induction of apoptosis two different
39 HDAC inhibitors (HDACis), SAHA and MS275 were used.
40
41
42
43
44
45
46
47
48
49

50 To establish whether Guajava fruit extract was also able to induce differentiation, the presence of
51 CD11c, a specific marker for granulocytic differentiation, was evaluated in NB4 cells after 48 hours
52 of treatment. CD11c expression increased even at a concentration of 0.75 mg/ml, and reached its
53 maximum level at a concentration of 1.5 mg/ml (Fig. 2c). Nevertheless, the differentiative effect
54 was lower than that of All Trans Retinoic Acid (ATRA), a well known anti-tumour and pro-
55 differentiative agent (17, 18,20). In full agreement with these data immunoistochemical staining
56
57
58
59
60

1
2
3 revealed that after 120 hours of treatment with Guajava total acetonc extract, NB4 cells assume the
4
5 characteristic granulocytic morphology as bilobate nuclei and granules presence, as shown in Fig.
6
7
8 2d. Interestingly, total acetonc Guajava extract exerted both an anti-proliferative effect and
9
10 induction of cell death in MDA-MB 231 breast cancer cells (Fig. 2e), thus suggesting its anticancer
11
12 activity in some solid cancer models as well.
13
14

17 *Guajava flesh extract is essential for cancer apoptotic action*

19
20
21
22 To better understand the biological action of Guajava extract, we fractioned the fruit parts aiming to
23
24 identify which component(s) (peel [skin], flesh [pulp] and seeds) are actively responsible for its
25
26 anti-cancer action. As shown in Fig. 3a, after the indicated treatments cell cycle progression was
27
28 mainly altered by the flesh component, whereas peel and seed components only marginally affected
29
30 cell cycle. Furthermore, the flesh component also proved to be mainly responsible for the induction
31
32 of apoptosis, at around 65% (Fig. 3b). That the peel extract affected apoptosis to a lesser extent
33
34 indicates a partial contribution of this component to cell death. When differentiation was measured
35
36 by CD11c detection, the peel components were shown to be as significant for CD11c expression as
37
38 the total extract. Morphology of NB4 cells upon May-Grunwald Giemsa staining after the indicated
39
40 treatments further confirmed these data (Fig. 3c, d). Thus, flesh components mainly influenced
41
42 apoptosis, whereas peel extract was responsible for differentiation.
43
44
45
46
47

48 In order to understand to what extent the apoptotic effects can apply to different cancer cell models,
49
50 we tested the total and component-specific Guajava extracts in breast, bone and leukaemia cancers.

51
52 As shown in Fig. 4a, both total acetonc Guajava extract and flesh extract exerted an anti-
53
54 proliferative effect and induced cell death in MDA-MB 231 breast cancer cells. Differently, U937
55
56 AML cells and U2OS osteosarcoma cells displayed neither cell cycle variations nor apoptosis at the
57
58 time and concentrations tested, suggesting that only some cancer models are sensitive to Guajava
59
60 treatment (Figure 4b, c).

Guajava flesh extract mediates caspase activation and apoptotic molecular events

To better understand the molecular events underlying Guajava-induced cell death, caspase assay (caspase 8, 9 and caspase 3/7) were performed. As shown in Fig. 5a, caspase 8 and 9 are mainly activated by flesh extracts, thus suggesting that cell death is due to apoptosis and that the flesh component is the active anticancer part of the fruit. To confirm this hypothesis and to evaluate which molecular players could be involved in the anticancer action of Guajava flesh extract on NB4 cells, the expression levels of different known key factors in cell cycle progression and apoptosis were analysed by Western blot analysis. As shown in figure 5b, after 48 hours of induction the total acetic Guajava, peel, flesh and seed extracts induced the expression of p21 and p16, known cell cycle inhibitors. Taken together these data indicate that the most active Guajava fraction is the flesh component, confirming the observation on cell cycle block (Figure 5b and 1c). Under similar experimental conditions, the expression levels of pro- and anti-apoptotic proteins were analysed. Interestingly, DR-5, FASL and BAD appear to be induced after treatment with the total Guajava and flesh extracts, validating the pro-apoptotic action of both. In particular, only treatment with flesh fraction led to a significant decrease of the protein FLIP-L (a strong inhibitor of caspase 8-mediated apoptosis), although the expression level of the protein FLIP-S remained unchanged. (Figure 5b).

Discussion

Plants have long served as a useful and natural source of therapeutic agents. It is generally recognized that the consumption of a variety of local herbs and vegetables significantly contributes to the improvement of human health, in terms of prevention and treatment of diseases.

Presently, in many developing countries, about 80% of available drugs derive from medicinal plants. Frequently in industrialized countries, the raw materials used to synthesize pure chemical derivatives have plant origin (12).

1
2
3 *Psidium guajava* L. belongs to the family of Myrtaceae (21). It is a tropical plant widely grown in
4
5
6 Taiwan, Hawaii, Thailand, the Philippines and Malaysia, where Guajava fruits, leaves, and bark
7
8 have been traditionally used as traditional herbal medicines and exhibit many therapeutic effects
9
10 including amebicide, analgesic, vermifuge, anti-malarial, anti-bacterial, colic-relief, anti-spasmodic,
11
12 astringent, anti-ulcerous, hypotensive, anti-inflammatory, anti-hyperglycemic and anti-diarrheal
13
14 properties as well as acting as a gastrotonic cough suppressant and combatting some psychic
15
16 diseases.
17

18
19
20 *Psidium guajava* anticancer activity has been thoroughly investigated in our study and data
21
22 concerning the active anticancer parts of the fruit and their constituents are presented here.
23

24
25 Guajava fruits are characterized by a low content of carbohydrates (13.2%), fats (0.53%), and
26
27 proteins (0.88%) and by a high water content (84.9%) (22). Food value per 100 g is: calories 36–50
28
29 kcal, moisture 77–86 g, crude fibre 2.8–5.5 g, ash 0.43–0.7 g, calcium 9.1–17 mg, phosphorus (23)
30
31 17.8–30 mg, iron 0.30–0.70 mg (24), vitamin A 200–400 I.U., thiamine 0.046 mg, riboflavin 0.03–
32
33 0.04 mg, niacin 0.6–1.068 mg, ascorbic acid 100 mg, vitamin B3 40 I.U. (23,25,26). Manganese is
34
35 also present in the plant in combination with phosphoric, oxalic and malic acids (27). Hexanal
36
37 (65.9%), γ -butyrolactone (7.6%), (E)-2-hexenal (7.4%), (E,E)-2,4-hexadienal (2.2%), (Z)-3-
38
39 hexenal (2%), (Z)-2-hexenal (1%), (Z)-3-hexenyl acetate (1.3%) and phenol (1.6%) were reported
40
41 from fresh white-flesh Guajava fruit oil. 3-caryophyllene (24.1%), nerolidol (17.3%), 3-
42
43 phenylpropyl acetate (5.3%) and caryophyllene oxide (5.1%) were isolated from essential oil
44
45 extracted from the fruits (28). Subsequently, the active aromatic constituents in pink Guajava fruit,
46
47 3-penten-2-ol and 2-butenyl acetate, were isolated (29). The fruit also contains glykosen 4.14%,
48
49 saccharose 1.62%, and protein 0.3% (30, 31, 4, 32). The main constituents are, however,
50
51 bioflavonoids. By analysing this list it is clear that *Psidium guajava* contains many substances
52
53 normally employed in cancer research. That the crude acetonc extract was able to induce cell cycle
54
55 arrest and cell death in NB4 cells confirmed our hypothesis that some of its components have
56
57 anticancer activity. When acetonc extracts were prepared from Guajava peel, flesh and seed parts
58
59
60

1
2
3 the active parts were shown to be peel and flesh, capable of inducing CD11c expression and
4
5 apoptosis in acute promyelocytic leukaemia cells respectively. The differential sensitivity shown by
6
7 different cancer models, such as breast cancer and osteosarcomas, suggests both some cell-
8
9 selectivity and a very low toxic effect of the extract.
10
11

12 This hypothesis was also confirmed by the evidence that cell death, occurring upon treatment, is
13
14 caspase mediated and able to activate both cell cycle and molecular death programs. That not only
15
16 caspase 8, but also FAS, DR-5 and BID were regulated mainly by the total and by the flesh extract
17
18 (Fig. 5) strongly suggests the involvement of death receptor-mediated pathways in regulation of
19
20 apoptosis. Though not fully understood, the abundance of flavonoids in the Guajava flesh extract
21
22 indicates that they may play a key role in the anticancer action of the fruit.
23
24
25

26 Taken together these data provide a new perspective for the analysis and use of natural products in
27
28 the treatment of human pathologies and indicate that plant components exert anticancer activities.
29
30

31 Given the need for new 'smart' anticancer drugs, the in-depth investigation of the properties of
32
33 natural products with minor side effects and targeted action may represent a new approach for the
34
35 future development of cancer-selective drugs.
36
37
38
39

40 **Acknowledgements**

41 This study was supported by EU ('Aposys' contract n° 200767), by AIRC (Associazione Italiana per
42
43 la Ricerca sul Cancro project n° 4625), by MIUR (PRIN n° 2007RZWFBZ_004). We acknowledge
44
45 Dr Catherine Fisher for the kind revising of the manuscript. The authors declare that they are not in
46
47
48
49
50
51
52
53
54
55
56
57
58
59
60
conflict of interests.

55 **Figure legends**

56
57
58 **Figure 1: Total acetonc Guajava fruit extract exerts antiproliferative action in leukemia NB4**
59 **cells.** (a) Proliferation curve by Trypan blue assay in NB4 cells at day 3 after treatment with
60 acetonc Guajava extract at the reported concentrations. (b) Proliferation curve by Trypan blue assay
in NB4 cells at day 5. Results represent the average of triplicates. (c) Cell cycle analysis of NB4

1
2
3
4
5
6
7
8
9
10
11
12
13
14
15
16
17
18
19
20
21
22
23
24
25
26
27
28
29
30
31
32
33
34
35
36
37
38
39
40
41
42
43
44
45
46
47
48
49
50
51
52
53
54
55
56
57
58
59
60

cells after treatment with selected crude Guajava extracts for a period of 24 hours in comparison with ATRA (*all trans retinoic acid*).

Figure 2. Total acetonetic Guajava fruit extract exerts anticancer and differentiative action. (a) Percentage of apoptotic cells after 24 hours of treatment with indicated crude Guajava extracts. (b) Apoptosis evaluation carried out by FACS analysis in AML patient ex vivo blasts after 24 hours of treatment with indicated dose of total Guajava extract. MS275 and SAHA were used as controls. (c) CD11c expression levels measured by FACS after 48 hours of treatment with the indicated amounts of Guajava extract in NB4 cells. Note that PI positive cells were excluded from the analysis. ATRA was used as positive pro-differentiative compound. (d) Morphological analysis of granulocytes induction after the treatment with Guajava extract at day 4 in comparison with ATRA induction

Figure 3. Flesh Guajava component is essential for apoptosis, peel for differentiation. (a) Cell cycle analysis in NB4 cells after stimulation with total Guajava extract and the fractioned parts of Guajava fruits for a period of 24 hours and at a concentration of 1.5 mg/ml. (b) Apoptosis carried out by FACS analysis after 24 hours of induction with the same total and fractioned Guajava extracts. (c) FACS evaluation of CD11c in NB4 cells. The data show the average of triplicates. ATRA was used as positive control. (d) Morphological analysis of granulocyte induction after treatment with fractioned Guajava parts at day 4. The data are compared with ATRA effect.

Figure 4. Guajava extract and flesh extract exerted anti-proliferative effect in different cancer cell model. (a) Morphological analysis of MDA-MB231 cells after treatment with total Guajava, peel, flesh and seed extracts at a concentration of 1.5mg/ml for a period of 4 days. (b) FACS cell cycle analysis in U937 and U2OS cells after induction with flesh and peel extracts for a period of 24 hours and at a concentration of 1.5 mg/mL. The data show the average of triplicates.

Figure 5. Flesh guajava extract mediates caspase activation and apoptotic molecular events. (a) FACS analysis of caspase 8, 3/7 and 9 in NB4 cells after 2 days of incubation with selected extracts at a concentration of 1.5mg/ml. Data represent the average of duplicates. (b) Western blot analysis of some proteins involved in cellular death. NB4 cells were treated with total Guajava, peel, flesh and seed extracts for a period of 24 hours and at a concentration of 1.5mg/ml. ERKs signal was used to normalize the loading cellular extracts.

References

- 1 Abreu, P. R.C., Almeida, M. C., Bernardo, R.M., Bernardo, L.C., Brito, L.C., Garcia, E.A.C., Fonseca, A.S. & Bernardo-Filho, M. (2006). Guava extract (*Psidium guajava*) alters the labelling of blood constituents with technetium-99m. *Journal of Zhejiang University SCIENCE B*, 7, 429-435.
- 2 Altucci, L., & Gronemeyer, H., (2001). The promise of retinoids to fight against cancer. *Nat Rev Cancer*, 1, 181-193.

- 1
2
3 3 Altucci, L., Rossin, A., Raffelsberger, W., Reitmair, A., Chomienne, C. & Gronemeyer, H. (2001).
4
5 Retinoic acid-induced apoptosis in leukemia cells is mediated by paracrine action of tumor-
6
7 selective death ligand TRAIL. *Nat Med*, **7**, 680-686.
8
9 4 Altucci, L., Wilhelm, E. & Gronemeyer, H. (2004). Leukemia: beneficial actions of retinoids
10
11 and rexinoids. *Int J Biochem Cell Biol*, **36**, 178-182.
12
13 5 Arima, H., & Danno, G. (2002). Isolation of antimicrobial compounds from guava (*Psidium*
14
15 *guajava L.*) and their structural elucidation. *Biosci Biotechnol Biochem*, **66**, 1727-1730.
16
17 6 Basile, A., Vuotto, M.L., Violante, U., Sorbo, S., Martone, G. & Castaldo-Cobianchi, R. (1997).
18
19 Antibacterial activity in *Actinidia chinensis*, *Feijoa sellowiana* and *Aberia caffra*. *Int J*
20
21 *Antimicrob Agents*, **8**, 199-203.
22
23 7 Belemtougri, R. G., Constantin, B., Cognard, C., Raymond, G. & Sawadogo, L. (2006). Effects
24
25 of two medicinal plants *Psidium guajava L.* (Myrtaceae) and *Diospyros mespiliformis L.*
26
27 (Ebenaceae) leaf extracts on rat skeletal muscle cells in primary culture. *Journal of Zhejiang*
28
29 *University SCIENCE B*, **7**, 56-63.
30
31 8 Birdi, T., Daswani, P., Brijesh, S., Tetali, P., Natu, A. & Antia, N.(2010). Newer insights into the
32
33 mechanism of action of *Psidium guajava L.* leaves in infectious diarrhoea. *BMC Complement*
34
35 *Altern Med*, **10**, 33.
36
37 9 Bontempo, P., Mita, L., Miceli, M., Doto, A., Nebbioso, A., De Bellis, F., Conte, M., Minichiello,
38
39 A., Manzo, F., Carafa, V., Basile, A., Rigano, D., Sorbo, S., Castaldo Cobianchi, R., Schiavone,
40
41 E.M., Ferrara, F., De Simone, M., Vietri, M., Cioffi, M., Sica, V., Bresciani, F., de Lera, A.R.,
42
43 Altucci, L. & Molinari, A.M. (2007). *Feijoa sellowiana* derived natural Flavone exerts anti-
44
45 cancer action displaying HDAC inhibitory activities. *Int J Biochem Cell Biol*, **39**, 1902-1914.
46
47 10 Chen, K. C., Peng, C. C., Chiu, W.T., Cheng, Y.T., Huang, G.T., Hsieh, C.L. & Peng, R.Y.
48
49 (2010). Action mechanism and signal pathways of *Psidium guajava L.* aqueous extract in killing
50
51 prostate cancer LNCaP cells. *Nutr Cancer*, **62**, 260-270.
52
53 11 Conway, P. (2002). Tree Medicine: A Comprehensive Guide to the Healing Power of Over 170
54
55 Trees. *Judy Piatkus (Publishers) Ltd*, 2173-2177.
56
57 12 Deguchi, Y., & Miyazaki, K.(2010). Anti-hyperglycemic and anti-hyperlipidemic effects of
58
59 guava leaf extract. *Nutr Metab (Lond)*, **7**, 9
60
61 13 De Luca, A., Baldi, A., Russo, P., Todisco, A., Altucci, L., Giardullo, N., Pasquale, L., Iaquinto,
62
63 S., D'Onofrio, V., Parodi, M.C., Paggi, M.G. & Iaquinto, G.(2003). Coexpression of Helicobacter

1
2
3
4
5
6
7
8
9
10
11
12
13
14
15
16
17
18
19
20
21
22
23
24
25
26
27
28
29
30
31
32
33
34
35
36
37
38
39
40
41
42
43
44
45
46
47
48
49
50
51
52
53
54
55
56
57
58
59
60

pylori's proteins CagA and HspB induces cell proliferation in AGS gastric epithelial cells, independently from the bacterial infection. *Cancer Res*, **63**, 6350-6356.

14 Dweck, A. C. (2001). A review of *Psidium guajava*. *Malayan Journal of Medical Science*, *8*, 27-30.

15 Fujita, T., Massaharu, K., Tamotsu, K., Kenji, Y., Kejichi, O. & Kiyoshi, S.(1985). Nutrient contents in fruit and leaves of guava and in leaves of Japanese persimmon. *Seikatsu Eisei* ,**29**, 206-209.

16 Gutierrez, R. M. P., Mitchell, S. & Solis, R.V.(2008). *Psidium guajava*: a review of its traditional uses, phytochemistry and pharmacology. *J. Ethnopharmacol*, **117**, 1-27.

17 Hernandez, D. F. (1971). Plants of the Philippines. *M&L Licudine Enterprises. First Printing. Philippines. University of the Philippines*, 678-680.

18 Hwang J.S., Yen Y.P., Chang M.C., & Liu C.Y. (2002). Extraction and identification of volatile components of guava fruits and their attraction to Oriental fruit fly, *Bactrocera dorsalis* (Hendel). *Plant Protection Bulletin*, **44**, 279-302.

19 Ieven, M., Vanden Berghe D. A., Mertens, F., Vlietinck, A. & Lammens, E.(1979). Screening of higher plants for biological activities. I. Antimicrobial activity. *Planta Med*, **36**, 311-321.

20 Iwu, M. M.(1993). Handbook of African Medicinal Plants *CRC Press*, 786-789.

21 Jordan, M. J., Margaria, C. A., Shaw, P.E. . & Goodner, K.L.(2003). Volatile components and aroma active compounds in aqueous essence and fresh pink guava fruit puree (*Psidium guajava* L.) by GC–MS and multidimensional GC/GC-O. *Journal of Agriculture and Food Chemistry*, **51**,1421-1426.

22 Mai, A., Massa, S., Rotili, D., Simeoni, S., Ragno, R., Botta, G., Nebbioso, A., Miceli, M., Altucci, L. & Brosch, G. (2006). Synthesis and biological properties of novel, uracil-containing histone deacetylase inhibitors. *J Med Chem*, **49**, 6046-6056.

23 Matsuzaki, K., Ishii, R., Kobiyama, K. & Kitanaka S.(2010). New benzophenone and quercetin galloyl glycosides from *Psidium guajava* L. *J Nat Med*, **64**, 252-256.

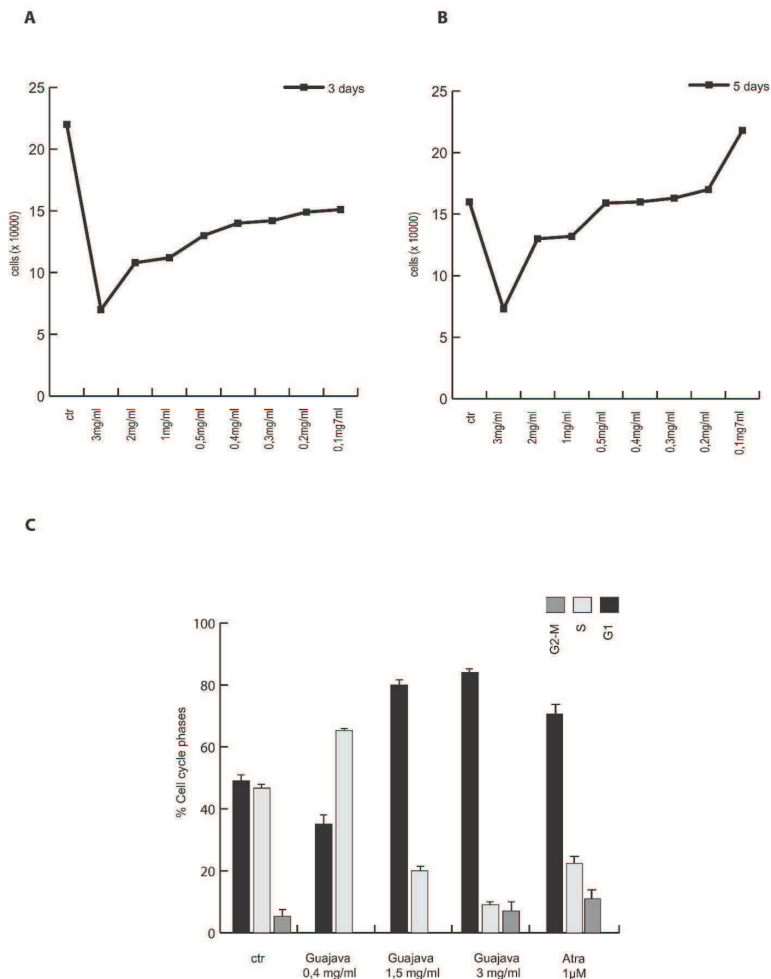
24 Medina, M. L. & Pagano, F. G. (2003). Characterization of *Psidium guajava* pulp “criolla roja. *Revista de la Facultad de Agronomía de La Universidad del Zulia*, (LUZ), **20**, 72-76.

25 Nadkarni, K. M. & Nadkarni A. K. (1999). Indian Materia Medica with Ayurvedic, Unani-Tibbi, Siddha, allopathic, homeopathic, naturopathic and home remedies. *Popular Prakashan Private Ltd, Bombay, India*, **1**, 142-149.

- 1
2
3 26 Nebbioso, A., Clarke, N., Voltz, E., Germain, E., Ambrosino, C., Bontempo, P., Alvarez, R.,
4 Schiavone, E.M., Ferrara, F., Bresciani, F., Weisz, A., de Lera, A.R., Gronemeyer, H. . &
5 Altucci, L.(2005). Tumor-selective action of HDAC inhibitors involves TRAIL induction in
6 acute myeloid leukemia cells. *Nat Med*, **11**, 77-84.
7
8
9
10
11 27 Nirmal, J., Babu, C. S., Harisudhan, & T. Ramanathan, M.(2008). Evaluation of behavioural and
12 antioxidant activity of *Cytisus scoparius Link* in rats exposed to chronic unpredictable mild
13 stress. *BMC Complement Altern Med*, **8**, 15.
14
15
16
17 28 Ogunlana, O. E. & Ogunlana, O. O. (2008). In vitro Assessment of the Free Radical
18 Scavenging Activity of *Psidium Guajava*. *Research Journal of Agriculture and Biological*
19 *Sciences*, **4**, 666-671.
20
21
22
23 29 Paniandy, J. C., Chane, M. J. & Pieribattesti, J.C.(2000). Chemical composition of the essential
24 oil and headspace solid-phase microextraction of the guava fruit (*Psidium guajava L.*). *Journal*
25 *of Essential Oil Research*, **12**, 153-158.
26
27
28
29 30 Rios, C. D., Salazar, C. R., Cardona, C., Victoria, K. & Torres, M. (1977). Guayaba. *Frutales*.
31 *Manual de Asistencia Tecnica* , **4**, 221-248.
32
33
34 31 Stone, B. (1970). The flora of Guam. *Micronesica*, **6**, 454-455.
35
36
37 32 Yusuf, S., Agunu, A., Katung, N.V. & Umana U.E.(2010). Ethanolic Leaf Extract of *Psidium*
38 *Guajava L. [Myrtaceae]* Protects the Stomach against Ischemia-Reperfusion Induced Gastric
39 Mucosal Injury. *Asian Journal of Medical Sciences*, **1**, 1-3.
40
41
42
43
44
45
46
47
48
49
50
51
52
53
54
55
56
57
58
59
60

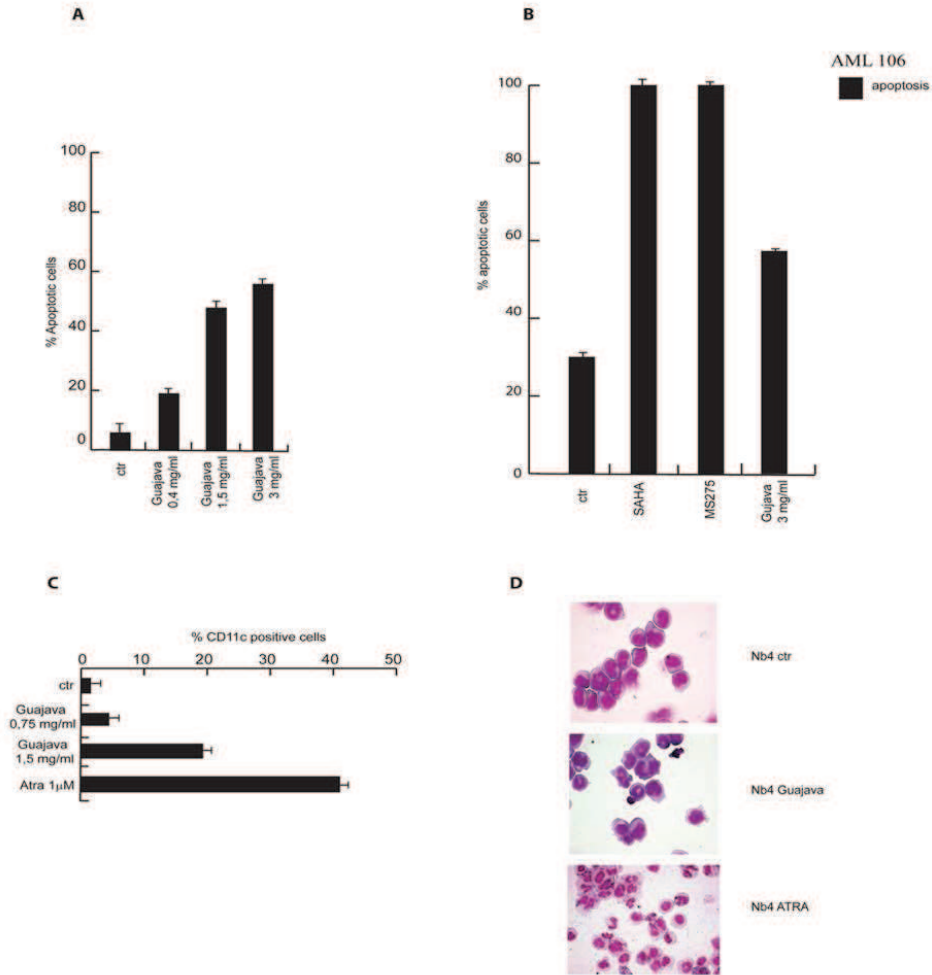
1
2
3
4
5
6
7
8
9
10
11
12
13
14
15
16
17
18
19
20
21
22
23
24
25
26
27
28
29
30
31
32
33
34
35
36
37
38
39
40
41
42
43
44
45
46
47
48
49
50
51
52
53
54
55
56
57
58
59
60

FIGURE 1



Total acetonc Guajava fruit extract exerts antiproliferative action in leukemia NB4 cells. (a) Proliferation curve by Trypan blue assay in NB4 cells at day 3 after treatment with acetonc Guajava extract at the reported concentrations. (b) Proliferation curve by Trypan blue assay in NB4 cells at day 5. Results represent the average of triplicates. (c) Cell cycle analysis of NB4 cells after treatment with selected crude Guajava extracts for a period of 24 hours in comparison with ATRA (all trans retinoic acid).
279x361mm (300 x 300 DPI)

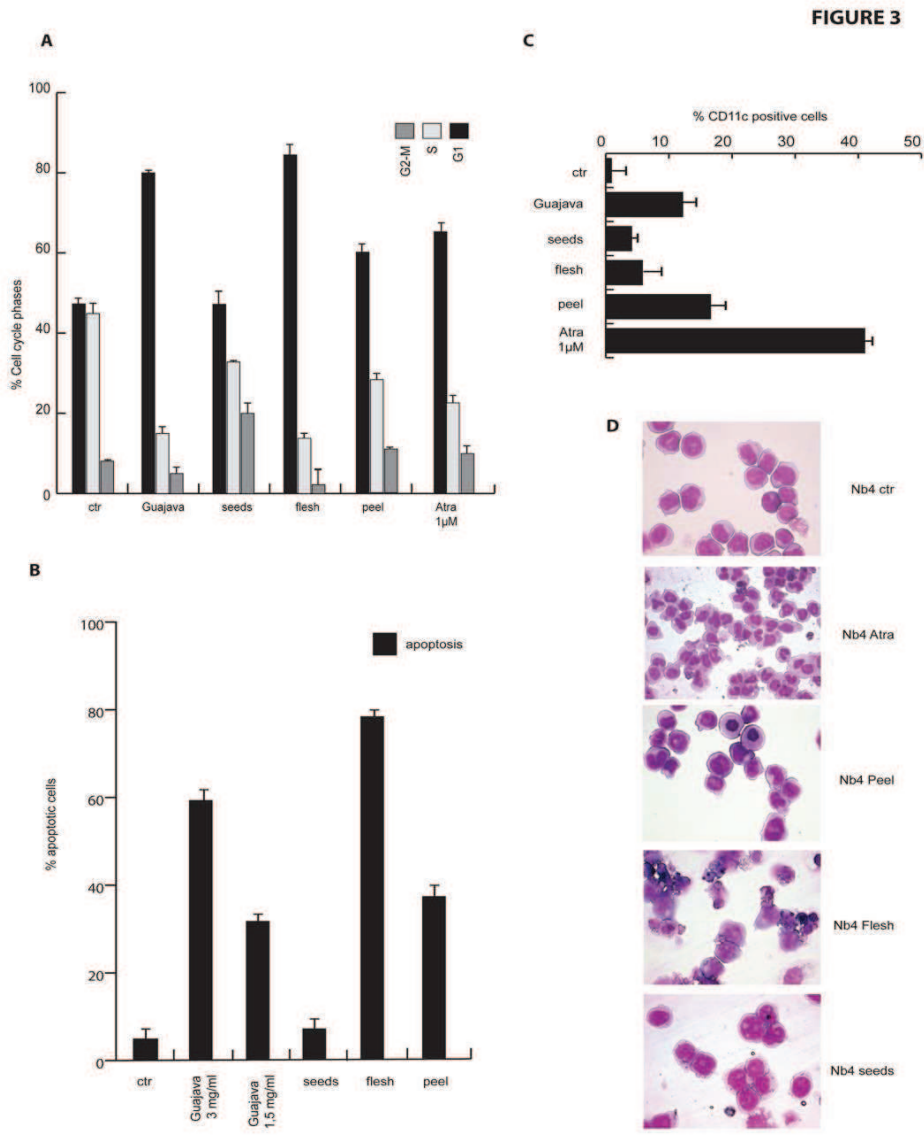
FIGURE 2



Total acetic Psidium Guajava fruit extract exerts anticancer and differentiative action. a, Percentage of apoptotic cells after 24 hours of treatment with indicated crude Guajava extracts; b, Apoptosis evaluation carried out by FACS analysis in AML patient ex vivo blasts after 24 hours of treatment with indicated dose of total Guajava extract. MS275 and SAHA were used as controls; c, CD11c expression levels measured by FACS after 48 hours of treatment with the indicated amounts of Guajava extract in NB4 cells. Note that PI positive cells were excluded from the analysis. ATRA was used as positive pro-differentiative compound; d, Morphological analysis of granulocytes induction after the treatment with Guajava extract at day 4 in comparison with ATRA induction.

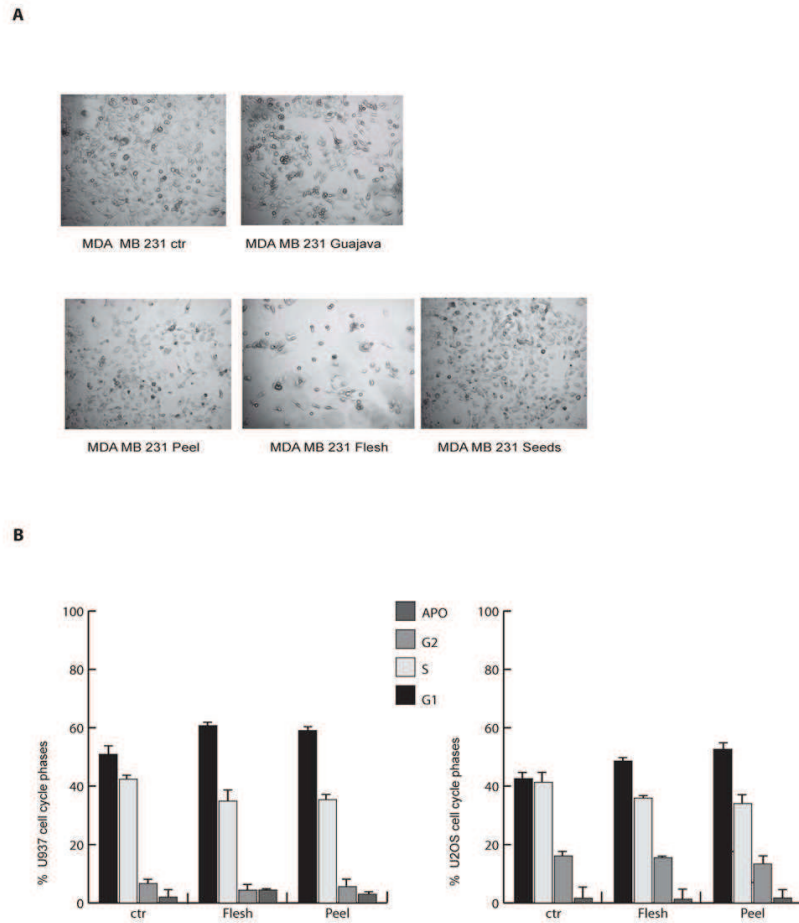
333x385mm (72 x 72 DPI)

1
2
3
4
5
6
7
8
9
10
11
12
13
14
15
16
17
18
19
20
21
22
23
24
25
26
27
28
29
30
31
32
33
34
35
36
37
38
39
40
41
42
43
44
45
46
47
48
49
50
51
52
53
54
55
56
57
58
59
60



Flesh Psidium Guajava component is essential for apoptosis, peel for differentiation. a, Cell cycle analysis in NB4 cells after stimulation with total Guajava extract and the fractioned parts of Guajava fruits for a period of 24 hours and at a concentration of 1.5 mg/ml; b, Apoptosis carried out by FACS analysis after 24 hours of induction with the same total and fractioned Guajava extracts; c, FACS evaluation of CD11c in NB4 cells. The data show the average of triplicates. ATRA was used as positive control; d, Morphological analysis of granulocyte induction after treatment with fractioned Guajava parts at day 4. The data are compared with ATRA effect.
388x463mm (72 x 72 DPI)

FIGURE 4

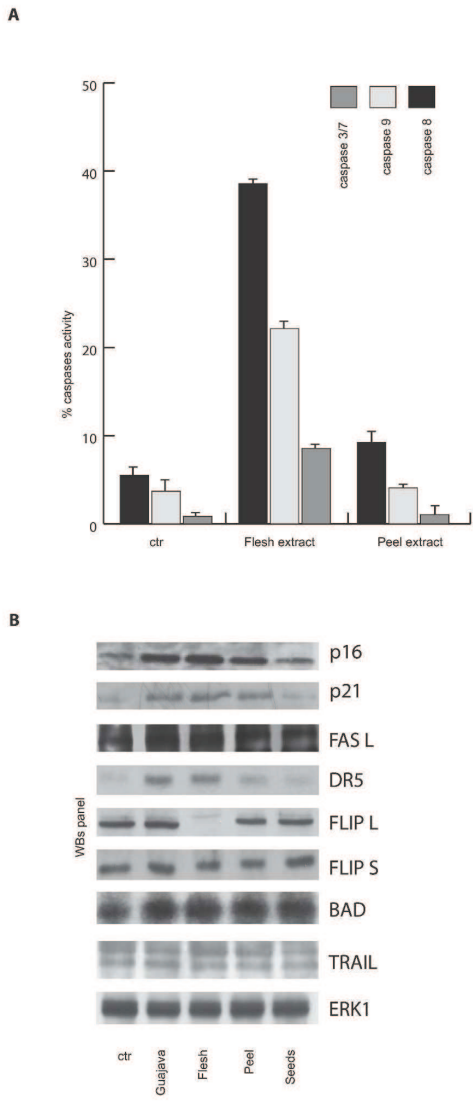


Psidium Guajava extract and flesh extract exerted anti-proliferative effect in different cancer cell model. a, Morphological analysis of MDA-MB231 cells after treatment with total Guajava, peel, flesh and seed extracts at a concentration of 1.5mg/ml for a period of 4 days; b, FACS cell cycle analysis in U937 and U2OS cells after induction with flesh and peel extracts for a period of 24 hours and at a concentration of 1.5 mg/ml. The data show the average of triplicates.

388x491mm (72 x 72 DPI)

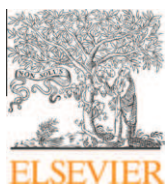
1
2
3
4
5
6
7
8
9
10
11
12
13
14
15
16
17
18
19
20
21
22
23
24
25
26
27
28
29
30
31
32
33
34
35
36
37
38
39
40
41
42
43
44
45
46
47
48
49
50
51
52
53
54
55
56
57
58
59
60

FIGURE 5



Flesh guajava extract mediates caspase activation and apoptotic molecular events. (a) FACS analysis of caspase 8, 3/7 and 9 in NB4 cells after 2 days of incubation with selected extracts at a concentration of 1.5mg/ml. Data represent the average of duplicates. (b) Western blot analysis of some proteins involved in cellular death. NB4 cells were treated with total Guajava, peel, flesh and seed extracts for a period of 24 hours and at a concentration of 1.5mg/ml. ERKs signal was used to normalize the loading cellular extracts.

279x361mm (300 x 300 DPI)



Contents lists available at ScienceDirect

Bioorganic & Medicinal Chemistry

journal homepage: www.elsevier.com/locate/bmc

Modulation of the activity of histone acetyltransferases by long chain alkylidenemalonates (LoCAMS)

Ciro Milite^a, Sabrina Castellano^a, Rosaria Benedetti^{b,c}, Alessandra Tosco^a, Carmen Ciliberti^a, Caterina Vicidomini^a, Ludovic Bouilly^a, Gianluigi Franci^{b,d}, Lucia Altucci^{b,d,*}, Antonello Mai^{e,*}, Gianluca Sbardella^{a,*}

^a Dipartimento di Scienze Farmaceutiche, Università degli Studi di Salerno, Via Ponte Don Melillo, 84084 Fisciano (SA), Italy

^b Dipartimento di Patologia Generale, Seconda Università degli Studi di Napoli, Vico L. De Crecchio 7, 80138 Napoli, Italy

^c Dipartimento di Fisica, Università di Napoli Federico II, Napoli, Italy

^d IGB-CNR, Via Pietro Castellino, 80100, Napoli, Italy

^e Dipartimento di Chimica e Tecnologie del Farmaco, Istituto Pasteur-Fondazione Cenci Bolognetti, 'Sapienza' Università di Roma, P.le A. Moro 5, 00185 Roma, Italy

ARTICLE INFO

Article history:

Received 19 November 2010

Revised 5 January 2011

Accepted 10 January 2011

Available online 14 January 2011

Keywords:

Histone acetyltransferases modulators

p300/CBP

PCAF activator

KAT

Epigenetics

ABSTRACT

A novel class of KAT modulators (long chain alkylidenemalonates, LoCAMS) has been identified. Variations of the alkyl chain length can change the activity profile from inhibition of both KAT3A/KAT2B (as derivative **2a**) to the peculiar profile of pentadecylidenemalonate **1b**, the first activator/inhibitor of histone acetyltransferases. Together with the powerful apoptotic effect (particularly notable if considering that anacardic acid and other KAT inhibitors are not cell permeable) appoint them as valuable biological tools to understand the mechanisms of lysine acetyltransferases.

© 2011 Elsevier Ltd. All rights reserved.

1. Introduction

Lysine acetylation is among the prominent posttranslational modifications in eukaryotic cells. Crosstalk between this and other identified posttranslational modifications^{1,2} such as methylation, ubiquitination, and phosphorylation give rise to a dense network which constitutes the histone code^{2–4} and is crucial in modulating chromatin-based transcriptional control and shaping inheritable epigenetic programs. First identified nearly 50 years ago,⁵ the acetylation state of histones within chromatin is correlated with gene regulation, with hypoacetylated histones being associated with transcriptionally repressed genes and hyperacetylated histones with transcriptionally active ones. Like histones, many non-histone proteins are subject to acetylation⁶ and a similar crosstalk (named 'protein modification code')^{3,7} with other posttranslational modifications is now known to occur in more than 80 transcription factors (i.e., p53),⁸ many other nuclear regulators (i.e., α -tubulin),⁹ and various cytoplasmic proteins.^{7,10} As a

result, lysine acetylation is not only crucial in the nucleus but also appears to be important for the regulation of different cytoplasmic processes, including cytoskeleton dynamics, energy metabolism, endocytosis, autophagy, and even signaling from the plasma membrane.^{11–13} In addition, reversible lysine acetylation may alter enzymatic activity to allow the cell to respond to environmental changes in metabolic demands and it has been proposed as an evolutionarily conserved mechanism for the regulation of cell functions.^{14–16}

Protein acetylation level is a consequence of the balance between the opposite activities of protein acetyltransferases (KATs)¹⁷ and deacetylases (KDACs),¹⁸ and its deregulation has been linked to several diseases,^{19,20} including cancer,^{21–29} inflammation^{30–33} and, probably, neurodegenerative diseases.^{34–38} Thus, lysine acetylation is a promising target for therapeutic development. As a matter of fact, a number of KDAC inhibitors are currently undergoing clinical evaluation for efficacy in the treatment of human tumours^{39,40} and two of them, suberoylanilide hydroxamic acid (SAHA, vorinostat),⁴¹ and romidepsin (FR901228, Istodax)⁴² were approved by the U.S. Food and Drug Administration (FDA) for the treatment of advanced cutaneous T-cell lymphoma.

On the contrary, KATs are less validated as chemotherapeutic targets. They can be organized into families based on primary-structure homology within the catalytic domain and similarities

* Corresponding authors. Tel.: +39 081 566 7569; fax: +39 081 450 169 (L.A.); tel.: +39 06 4991 3392; fax: +39 06 491 491 (A.M.); tel.: +39 089 96 9770; fax: +39 089 96 9602 (G.S.).

E-mail addresses: lucia.altucci@unina2.it (L. Altucci), antonello.mai@uniroma1.it (A. Mai), gsbardella@unisa.it (G. Sbardella).

in their biological function. Four of these families have been extensively studied: the Gcn5-related *N*-acetyltransferase (GNAT) family, the E1A-associated protein of 300 kDa (p300)/CREB-binding protein (CBP) family, the MYST family; and the regulation of Ty1 transposition gene product 109 (Rtt109) family.^{7,17,43–46} Several other KAT families have been identified, but they have been studied less extensively.^{6,14,17,47}

Misregulation of the activity of KAT enzymes has been linked to a broad set of diseases ranging from cancer to central nervous system pathologies. Yet, at least in cancer, their role cannot be simply generalized as they can function either as tumor suppressors or promoters depending on different tumor types and development stages.^{14,19} Therefore, cell-permeable, selective modulators of these enzymes could be invaluable tools for reverse chemical genetics studies^{48,49} and to assess the implication of KATs in several pathologies. Moreover, they can represent starting points for the design of novel epigenetic drugs.

Differently from KDAC proteins, just a few small molecule inhibitors of KATs have been reported to date (Fig. 1), with various degrees of selectivity and cell permeability. Peptide–CoA conjugates (Lys–CoA and H3–CoA-20) have been described as potent and selective bisubstrate inhibitors for KAT3B (p300) and KAT2B (PCAF), however the lack of cell permeability represents a drawback.^{34,50} A few natural products like anacardic acid,⁵¹ garcinol,⁵² curcumin,⁵³ plumbagin,⁵⁴ guttiferone A⁵⁵ as well as some analogues^{56–60} or semi-synthetic derivatives³² have also been reported as inhibitors of different classes of KATs. Isothiazolones were disclosed as cell-permeable and potent inhibitors of KAT2B, but their

chemical reactivity limits their specificity.^{61–64} Cell-permeable KAT2A (GCN5)-selective inhibitors like the γ -butyrolactone MB-3⁶⁵ and a few quinoline derivatives⁶⁶ were also reported. On the other side, only *N*-(4-chloro-3-trifluoromethyl-phenyl)-2-ethoxy-6-pentadecyl-benzamide (CTPB, Fig. 2)⁵¹ and nemorosone⁵⁵ were reported to selectively activate p300 HAT activity.

Recently we reported a unique activity profile for pentadecylid-enemalonate **1b** (Fig. 2), a simplified analogue of anacardic acid. This compound exhibits a good inhibitory activity against KAT3A/B (CBP/p300) and intriguingly, a significant increase of the acetylating activity of KAT2B.⁶⁷ This observation suggests that it is the first activator/inhibitor of histone acetyltransferases.

With the aim to derive structure–activity relationships, we decided to explore the effect on the biological activity of the length of the alkyl chain, the nature of the carbonyl function, the eventual presence of substituents, and the rigidity/flexibility of the scaffold (Fig. 3). Herein we thus report the synthesis of a number of analogues of compound **1b**, as well as the evaluation of their biological effects on the activity of KAT enzymes. In addition, the effects of tested compounds on cell cycle and apoptosis induction on U937 cells were also evaluated.

2. Chemistry

Most of the novel compounds were prepared by reacting a 1,3-dicarbonyl derivative with the proper electrophile. In fact, derivatives **1–3** were prepared, respectively, (Scheme 1) by Knoevenagel condensation of diethyl malonate or pentane-2,4-dione

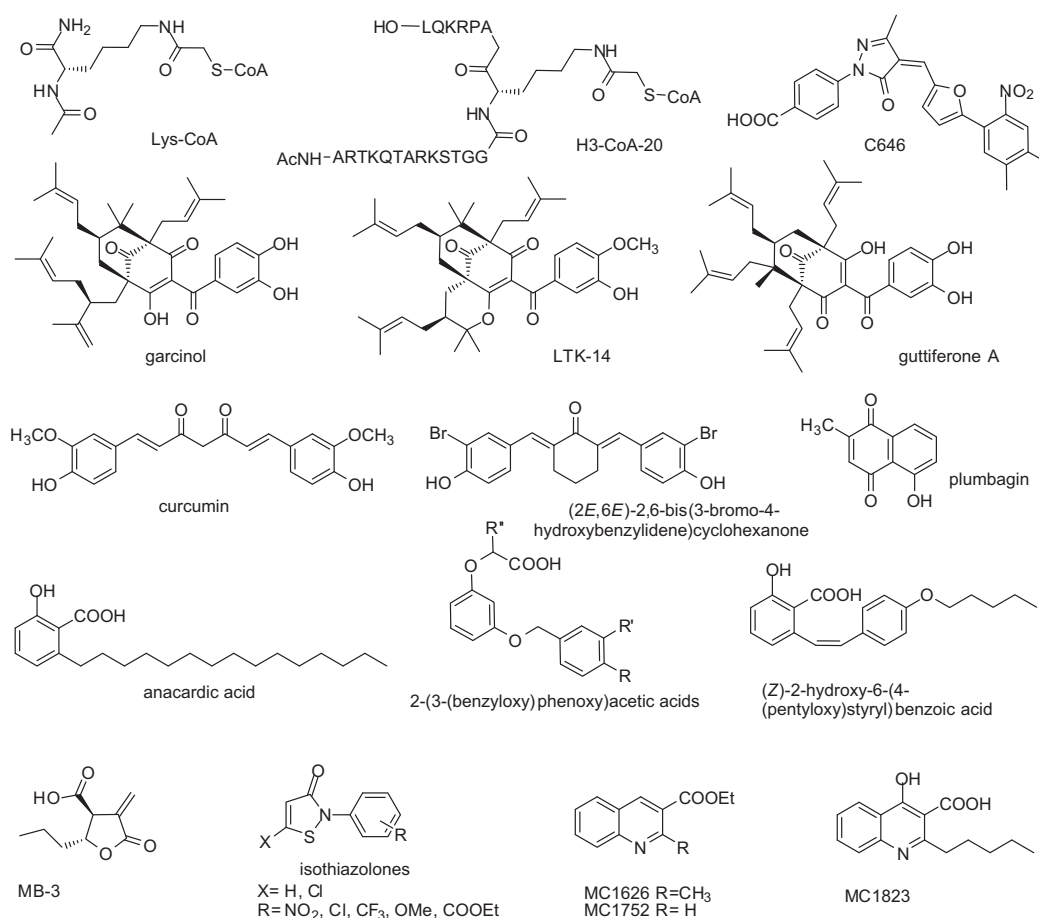


Figure 1. Known KAT inhibitors.

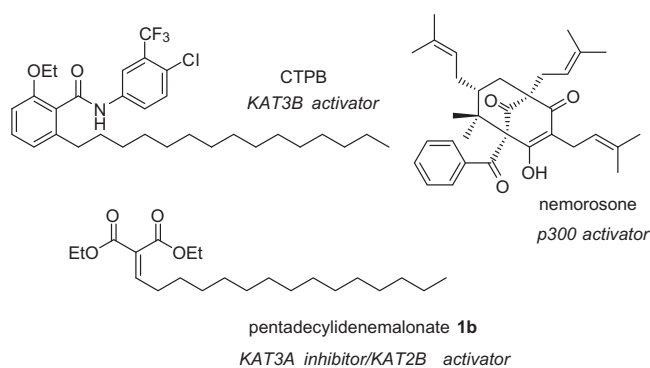


Figure 2. KAT activators.

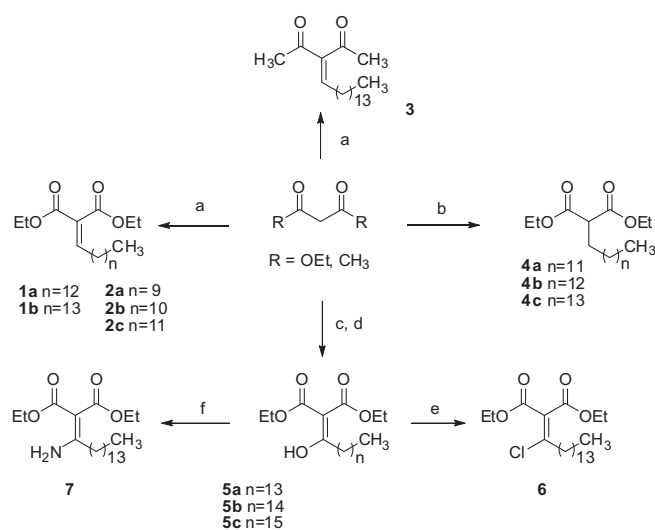
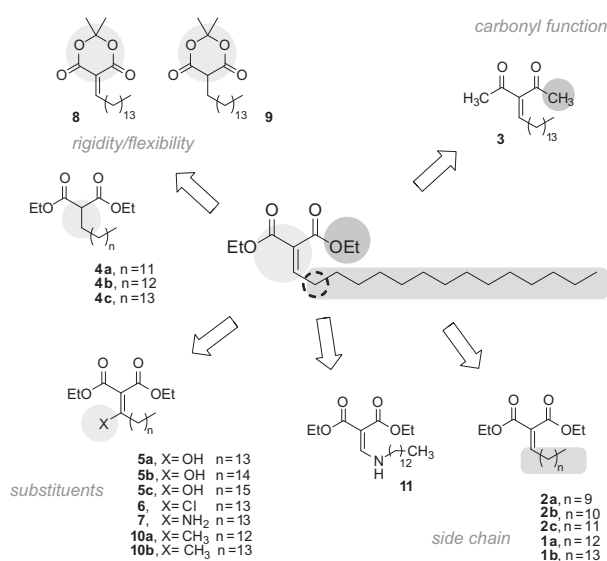
Scheme 1. Reagents and conditions: (a) alkyl aldehyde **12a–e**, acetic acid, piperidine, dichloromethane; (b) alkyl bromide, NaH, THF, 0 °C (100 min), rt (2 h) and 70 °C (15 h); (c) acylimidazolide, MgCl₂, Et₃N, acetonitrile, rt; (d) 13% HCl, rt; (e) POCl₃, TEA; (f) NH₄OAc, EtOH.

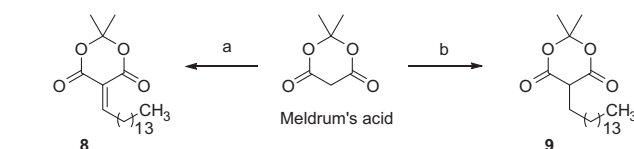
Figure 3. Compounds screened on U937 cells.

with aldehydes **12a–e**, commercially available or obtained from the corresponding alcohols by oxidation with 1,1,1-triacetoxy-1,1-dihydro-1,2-benziodoxol-3(1*H*)-one (Dess–Martin periodinane, DMP).^{67,68} The monoalkylation of diethyl malonate with the appropriate alkyl bromide in the presence of sodium hydride in dry THF⁶⁹ gave derivatives **4a–c**,^{69–71} while the acylation of the β-ketoester with tetradecanoyl, pentadecanoyl, or hexadecanoyl imidazolide in the presence of magnesium dichloride and triethylamine furnished derivatives **5a–c**.⁶⁷ The tetradecyl substituted compound **5a** was treated with phosphorus oxychloride or with ammonium acetate to obtain chloro-substituted or amino-substituted derivatives **6** and **7**, respectively (Scheme 1).

Similarly, when Meldrum's acid was used as 1,3-dicarbonyl compound in the Knoevenagel condensation or in the alkylation in the presence of sodium hydride, derivatives **8** and **9** were obtained, respectively (Scheme 2).

Alkan-2-ylidene malonates **10a,b** were obtained by reacting the corresponding alkan-2-ones with triethyl phosphonoacetate in the presence of sodium hydride in the Horner–Wadsworth–Emmons reaction conditions. The resulting mixture of *E* and *Z* α,β-unsaturated esters was then treated with lithium diisopropylamide and ethyl chloroformate to yield the desired derivatives (Scheme 3).

Finally, tridecylamino methylenemalonate **11** was obtained by refluxing diethyl ethoxymethylenemalonate with tridecylamine in anhydrous ethanol (Scheme 4).

Scheme 2. Reagents and conditions: (a) alkyl aldehyde **12b**, acetic acid, piperidine, dichloromethane; (b) alkyl bromide, NaH, THF, 0 °C (100 min), rt (2 h) and 70 °C (15 h).

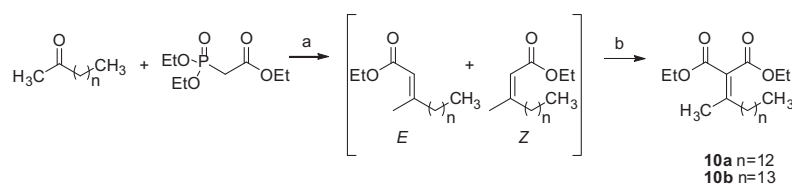
3. Biology

3.1. KAT3A and KAT2B inhibitory assays

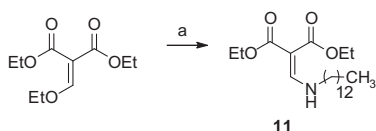
We previously reported that pentadecyldenemalonate **1b** possess a peculiar activity profile against acetyltransferases.⁶⁷ Thus, compounds **1–11** were tested for inhibition of the recombinant acetyltransferase enzymes KAT3A (CBP, Fig. 4A) and KAT2B (Fig. 4B), using anacardic acid (AA)⁵¹ as reference compound (at 50 μM). In agreement with what we previously reported, the inferior homologues of **1b** (with the exception of the tridecylidene derivative **2c** which resulted inactive) as well as the β-diketone **3** displayed a strong inhibition against recombinant KAT3A (in the range 79–83%), thereby being more powerful than AA when tested in the same conditions (62% of inhibition at 50 μM). Among the other derivatives, only **5a** exhibited a moderate enzyme inhibition (52%), the others being scarcely active (Fig. 4A). Similarly to **1b**, derivative **1a** induced an increase of the acetylating activity of KAT2B (Fig. 4B). A slight increase of the enzymatic activity was also detectable for compounds **5a** and **11** (characterized by the presence on the double bond of the lead scaffold of a OH and a NH group, respectively). All the other derivatives were inactive or displayed just a moderate inhibition, with the exception of the chloro-substituted malonate **6** which displayed a strong activating effect.

3.2. Western blot analyses

The effect of compounds **1–11** on the acetylation levels of histone (H3 terminal tails) or non-histone (α-tubulin) proteins was assessed in human leukemia U937 cell line (Fig. 5A), and in human



Scheme 3. Reagents and conditions: (a) NaH, THF, $-40\text{ }^{\circ}\text{C}$; (b) ClCOOEt, LDA, HMPA, THF, $-78\text{ }^{\circ}\text{C}$.



Scheme 4. Reagents and conditions: (a) tridecylamine, EtOH, reflux.

breast cancer MCF-7 cells (Fig. 5B), respectively. Cells were incubated with vehicle, tested compounds or with the reference compound suberoylanilide hydroxamic acid (SAHA, at $5\text{ }\mu\text{M}$), a well-known KDAC inhibitor⁴¹ able to increase histone H3 as well as the non-histone substrate α -tubulin acetylation levels. As shown by Western blot analysis (Fig. 5), the behavior of compound **1a** in these assays was quite similar to what we previously

observed with **1b**. In fact, both compounds produce an increase of the H3 acetylation level, similar (even if less pronounced) to the one induced by SAHA (Fig. 5A) but without affecting KDAC activity (not shown). Moreover, while SAHA exhibited a marked hyperacetylating effect on both substrates, compounds **1a** and **1b** produced no detectable effect⁷² on the acetylation level of the non-histone substrate α -tubulin (Fig. 5B). On the contrary, derivatives **2a** and **2b** and, to a lesser extent, derivative **3** induced a significant hypoacetylation of the H3 histone substrate in the same conditions (Fig. 5A). No effect was detectable on α -tubulin acetylation. The effects of all the other derivatives were comparable to control, with the exception of derivative **5b**, which induced a strong α -tubulin hyperacetylation at $15\text{ }\mu\text{M}$, and derivative **11**, which shows a weak but distinct dose-dependent hyperacetylation of the same substrate (Fig. 5B).

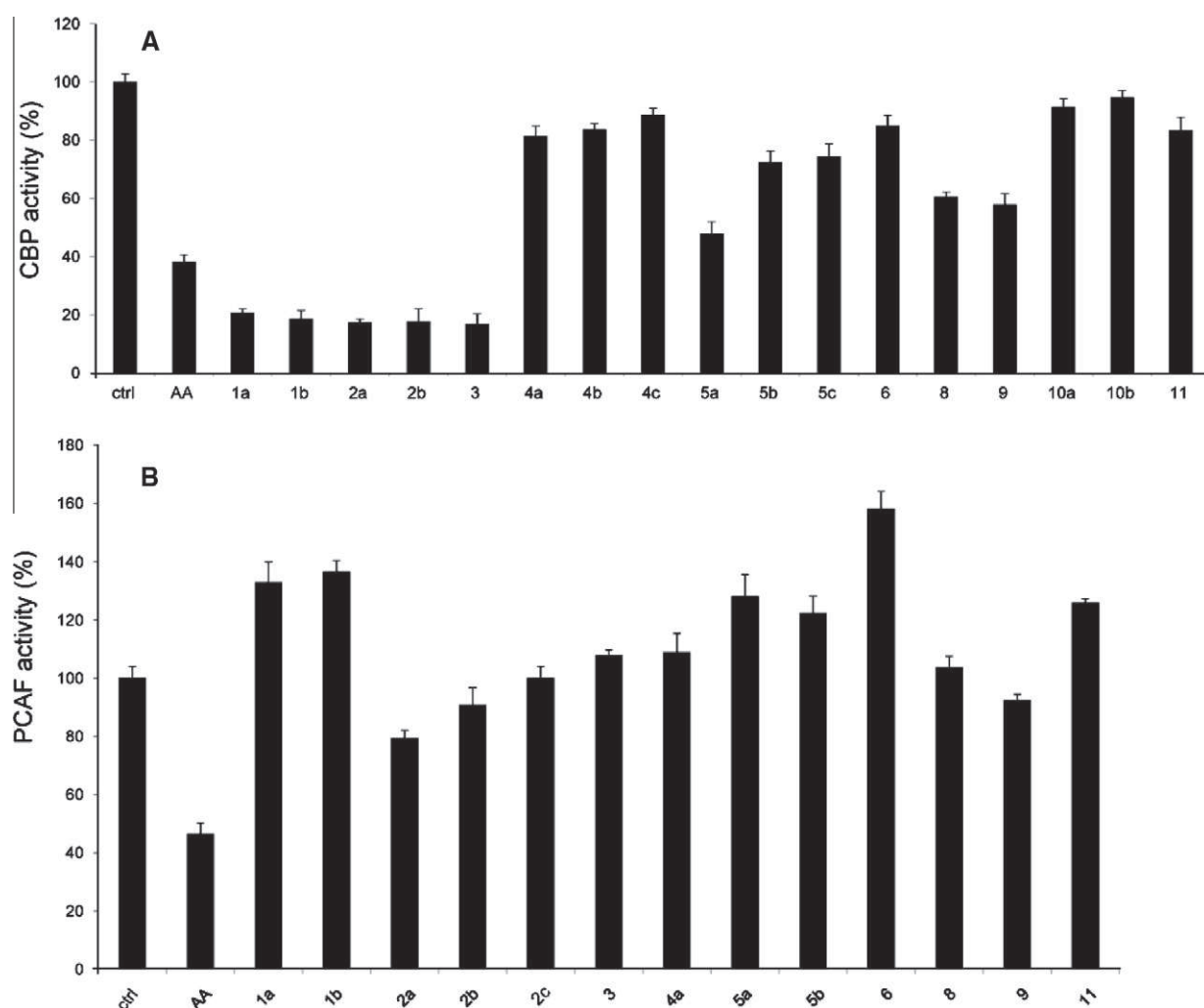


Figure 4. Enzymatic assay performed with $50\text{ }\mu\text{M}$ concentrations of compounds **1–11** on KAT3A (CBP, A) and KAT2B (PCAF, B). Anacardic acid (AA) was used as reference compound at $50\text{ }\mu\text{M}$ concentration.

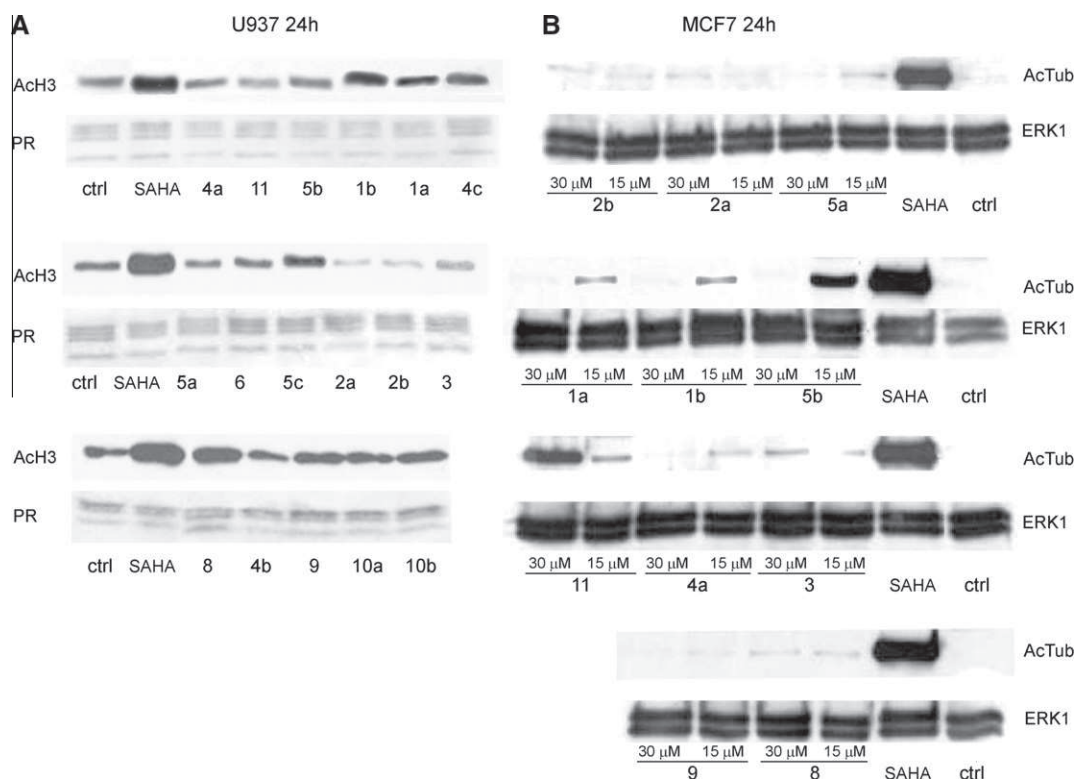


Figure 5. (A) Effects exerted by compounds **1–11** (50 μM) on H3 acetylation in histone extracts of U937 leukemia cells. (B) Effects exerted by compounds **1–11** (15 and 30 μM) on α -tubulin acetylation in MCF-7 breast cancer cells. Ponceau Red staining of histones (PR) and ERK1 (extracellular signal-regulated kinase-1) antibody were used, respectively, to check for equal loading. SAHA (5 μM) was used as reference compound.

3.3. In-cell evaluation. Effects on cell cycle and apoptosis induction on human leukemia U937 cell line

As cell permeability is a crucial issue for modulators of histone modifying enzymes,⁷³ all the derivatives were then screened for their effects on cell cycle, apoptosis induction, and granulocytic differentiation in the human leukemia U937 cell line, using anacardic acid (AA)⁵¹ as reference compound. After 30 h of treatment at 50 μM , compounds **1a,b** and **2a,b** were able to arrest the cell cycle in the S phase (Fig. 6A)⁷⁴ and, more importantly, displayed a strong apoptosis-inducing effect (51.8%, 94.4%, 25.4% and 60.2%, respectively; Fig. 6C). In the same conditions, the effects on cell cycle and apoptosis induction of derivative **3** were significantly lower, being barely detectable for all the other compounds, particularly when the experiment was repeated at lower concentration (25 μM , Fig. 6B and D). For the most active derivatives, **1a,b** and **2a,b**, a dose–response study was also performed. U937 cells were incubated for 30 h at 37 $^{\circ}\text{C}$ in the absence (control) or presence of increasing concentrations (5–200 μM) of tested compounds. Interestingly, again the length of the aliphatic side chain seems crucial for biological activity, similarly to what reported by Giannis for analogues of MB-3.⁶⁵

In fact, as shown in Figure 6E, compounds **1a** and **1b** displayed similar (42.90 μM and 44.91 μM , respectively) IC_{50} values (concentration inducing 50% apoptosis, calculated using GraphPad Prism 5.0 software, GraphPad Software Inc., San Diego, CA), whereas the shortening of the aliphatic chain (compounds **2a** and **2b**) resulted in a 2–3-fold lower activity. This outcomes are consistent with the effects exerted by tested compounds on the acetylation levels of histone and non-histone proteins. None of the tested compounds **1–11** showed any significant differentiating effect (see Supplementary data).

3.4. SPR-based binding assay

We previously reported that **1b** strongly inhibits (74% of inhibition at 50 μM) immunoprecipitated KAT3A/KAT3B from U937 cell nuclear extracts.⁶⁷ Thus, we resolved to ascertain if the long chain alkylidenemalonates (LoCAMs) **1–3**, the most active in cellular experiments, besides KAT3A could bind also to KAT3B. To this aim, we took advantage of a surface plasmon resonance-based binding assay as implemented with Biacore technology, recently set up and successfully employed by us to study kinetic and thermodynamic parameters of ligand–protein interactions between KAT3B and a series of polyisoprenylated benzophenone derivatives.⁵⁵ This assay allowed us to assess in real time how compounds associate and dissociate from the protein and provided detailed information on the interaction. Thus, human recombinant full-length KAT3B and KAT3B catalytic domain were immobilized on different flow cells of the biosensor chip and the five LoCAMs were injected at different concentrations (from 50–200 μM) over the protein surface; the binding of each compound was read out in real time as the change in mass at the sensor surface. After injection, running buffer was flowed over the surface and dissociation of the compounds from the surface was observed (Fig. 7). Noteworthy, three out of the five tested LoCAMs (compounds **2a**, **2b**, and **3**) interacted efficiently with the immobilized full-length protein, as shown by the concentration-dependent responses and the clearly evident exponential curves during both the association and dissociation phases, but not with the immobilized catalytic domain (see Supplementary data). This seems to suggest an interaction with a site different from the catalytic one. On the other hand, SPR experiments carried out on compounds **1a** and **1b** on both proteins also produced good sensorgrams, but showed very low and/or concentration-independent responses, thus suggesting negligible interactions of such molecules with p300. To evaluate possible

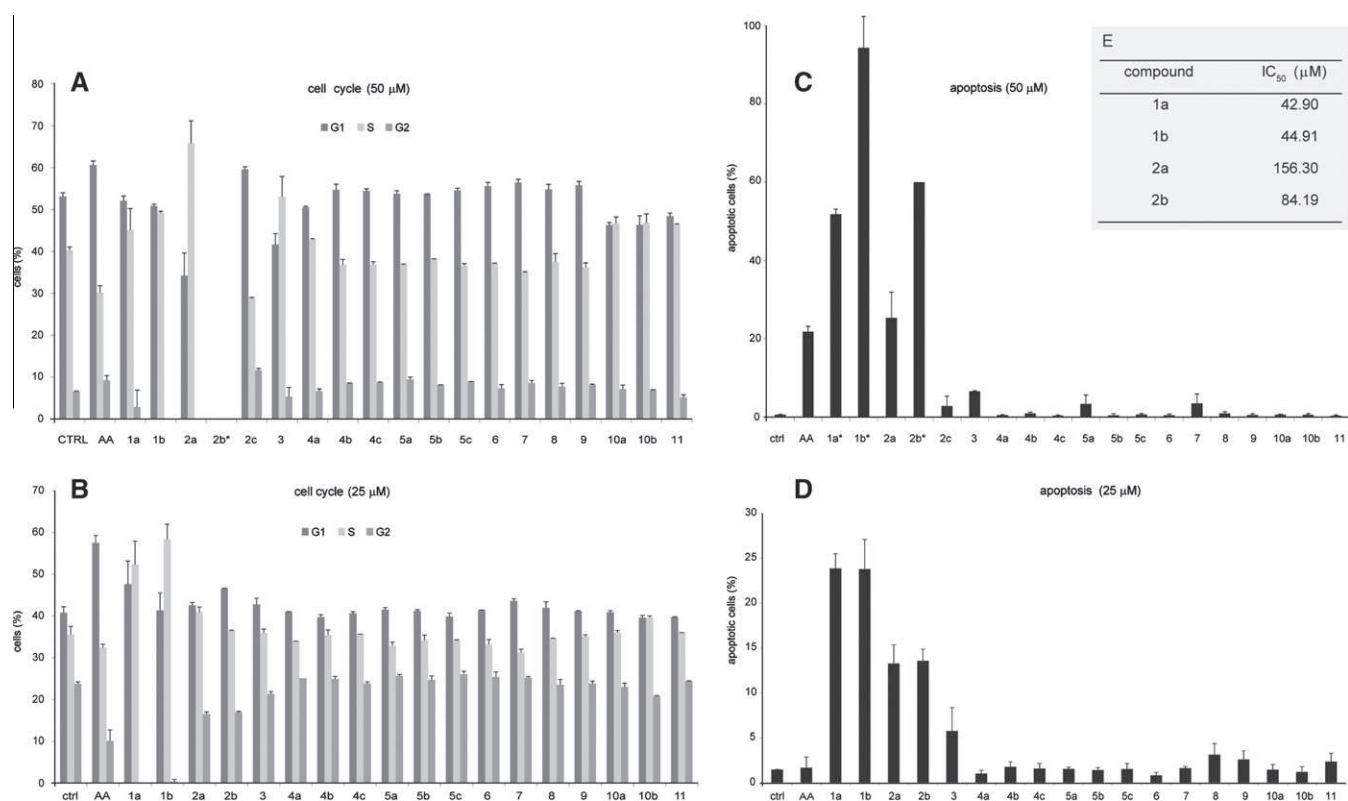


Figure 6. Cell cycle analysis (A and B) and analysis of apoptosis induction (C and D) in U937 cells by fluorescence-activated cell sorting (FACS). The U937 cells were treated with compounds **1–11** at 50 μM (top) or at 25 μM (bottom) for 30 h, then stained with propidium iodide and subjected to flow cytometric analysis to determine the cell distributions at each phase of the cell cycle (A and B) or double-stained with Annexin V/propidium iodide and subjected to flow cytometric analysis to determine apoptotic subpopulations (C and D). Caspase 3 was also detected and quantified (not shown). Anacardic acid (AA) was used as reference compound. Data are reported as mean \pm SD of three independent experiments. (E) IC₅₀ (concentration inducing 50% apoptosis) values for **1a,b** and **2a,b**, obtained from dose–response experiments in U937 cells with compounds tested at 5–200 μM .

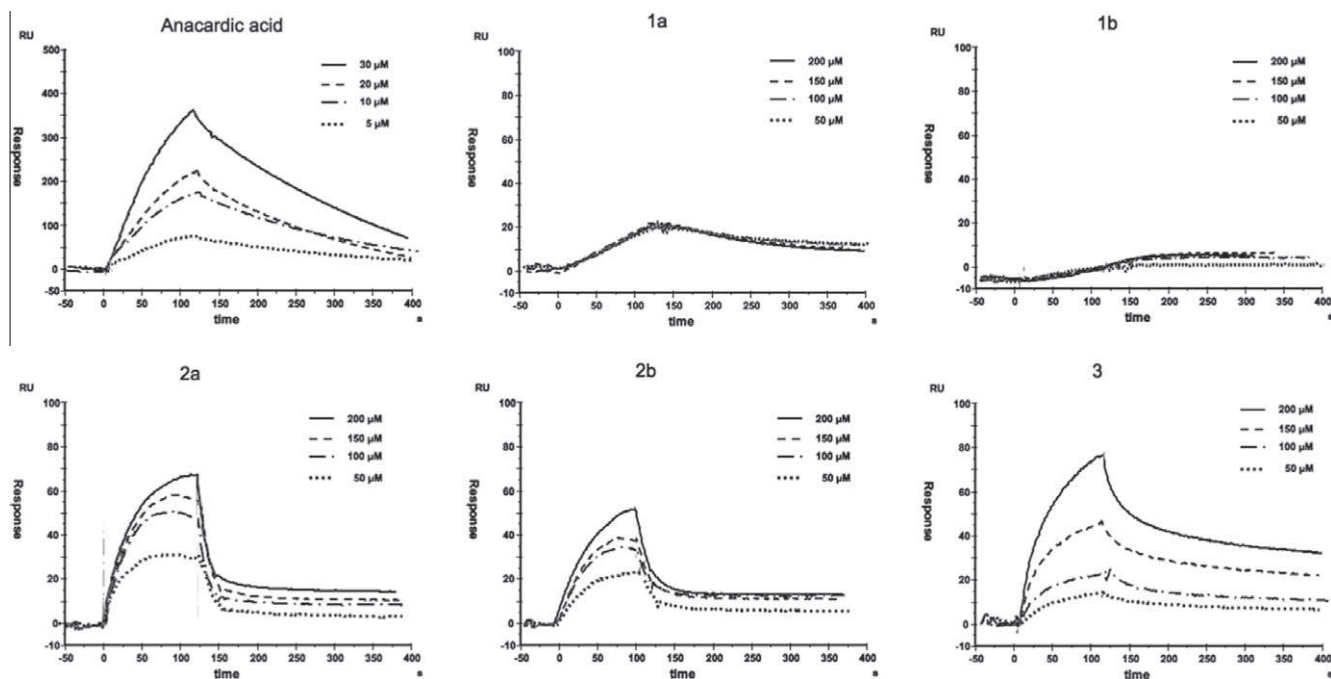


Figure 7. SPR interaction analysis of compounds **1–3** binding to immobilized KAT3B full length. SPR response data (sensorgrams). Each compound was injected at four different concentrations (50, 100, 150, and 200 μM).

unspecific bindings, compounds **1–3** were also injected on an immobilized bovine serum albumin (BSA), and no interaction was observed (data not shown).

The outcomes of SPR experiments were consistent with the results (see Supplementary data) of fluorescence-based assays, performed to evaluate the ability of compounds **1–3** to modulate

the acetyltransferase activity of KAT3B. As a matter of fact, all tested compounds showed negligible effects on KAT3B (both full-length and catalytic domain) biological activity.

3.5. Effect on the acetylation of specific lysine residues

We next examined the effects of compounds **1–3** on the acetylation of specific lysine residues of core histones H3 (K9, K14, K18, K56) and H4 (K5, K8, K16). Thus, U937 cells were incubated (for 24 h) with vehicle, compounds **1–3** (50 μ M) or with the reference compound SAHA (5 μ M), and the histone extracts were then immunoblotted with antibodies to specific histone acetylation sites (Fig. 8). This assay confirmed what we already observed that small differences in the length of the aliphatic side chain of LoCAM derivatives appear critical for biological activity. In fact, as shown in Figure 8, compounds **1b** and **2b** were able to induce hyperacetylation (in the case of **1b** similar to that exerted by SAHA) of specific H3 lysine residues (in particular H3K9 and H3K18) as well as the level of pan-acetylated H4, but while **1b** was comparable to control in all the other assays, dodecylidenemalonate **2b** inhibited the acetylation of all the other H3 and H4 lysines, with the exception of H4K8Ac.⁷⁵ On the contrary, derivatives **1a** and, even more evidently, **2a** exhibited a significant inhibition of the acetylation of almost any lysine residue explored, again with the sole exception of H4K8. Both derivatives **2a** and **2b** reduced the level of H4K5Ac and, more markedly, H4K16Ac. Tridecylidenemalonate **2c** and the diketone **3** showed inhibition (at a different extent,

according to the specific antibody used in the Western blots) against the acetylation of, respectively, H3K9/K18 and H3K9/K14, being practically inactive in all the other assays. None of the compounds tested exhibited a detectable effect the acetylation of H4K8.

4. Conclusion

In this article, we have described the synthesis of compounds **1–11** as analogues of pentadecylidenemalonate **1b**, recently reported by us as the first activator/inhibitor of histone acetyltransferases.⁶⁷ With the aim to identify the effects on the biological activity of structural modifications such as length of the alkyl chain, nature of the carbonyl function, occurrence of substituents, and rigidity/flexibility of the scaffold, we tested the capability of such derivatives to modulate the acetyltransferase activity of human recombinant KAT3A and KAT2B, and assayed their effects on the acetylation of both histone- (H3) and non-histone proteins (tubulin). Their effects on cell cycle, apoptosis induction, and granulocytic differentiation on U937 cells were also evaluated. In addition, we explored the binding capability of selected compounds to KAT3B, using both the full length protein and the catalytic domain in a SPR-based assay, and their effects on the acetylation of specific histonic lysine residues, by immunoblotting histone extracts with specific antibodies.

Taken together, the data resulting from biological assays showed that, in general, major modifications introduced in the

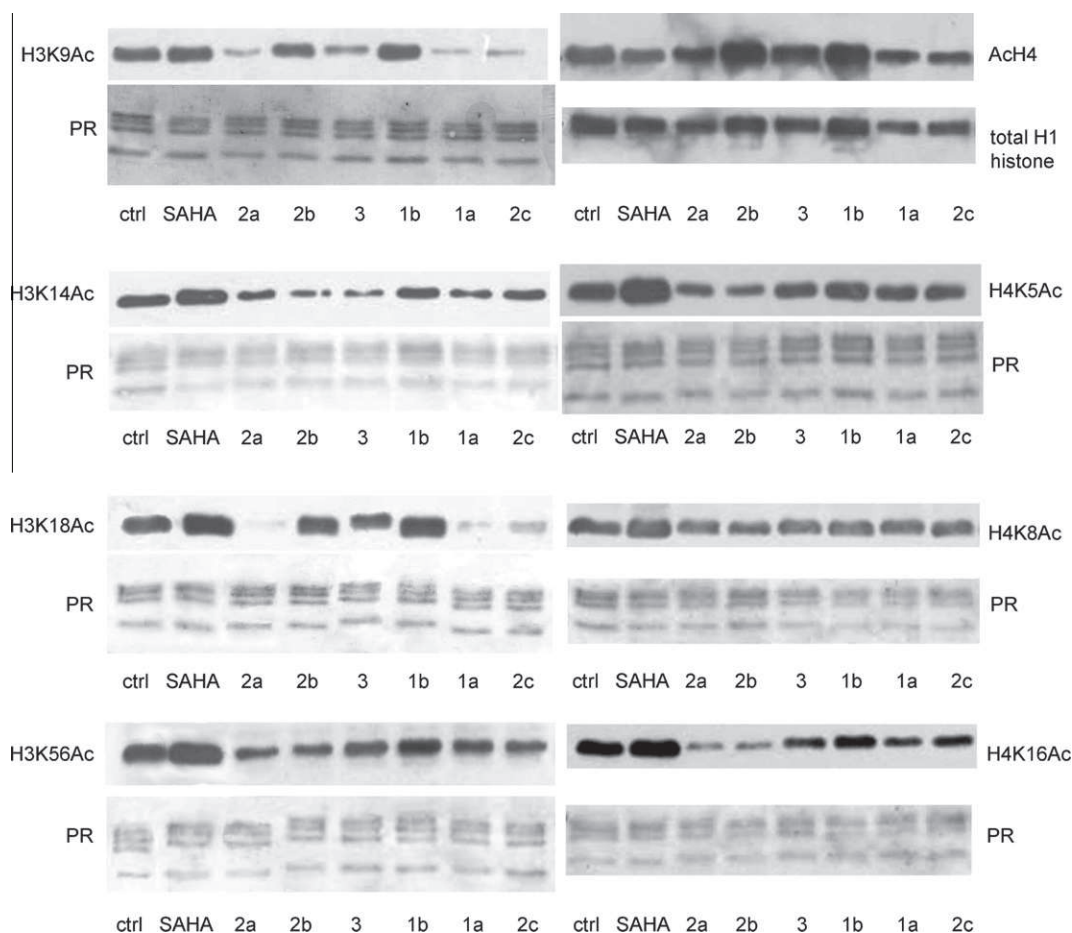


Figure 8. Western blot analyses performed with compounds **1–3** (50 μ M for 24 h) on the acetylation of specific lysine residues of histones H3 and H4 in histone extracts of U937 leukemia cells. Acetylation was detected by immunoblotting with antibodies to specific histone acetylation sites as indicated. Ponceau Red staining of histones (PR) or total H1 histone (in the case of pan-acH4) were used to check for equal loading. SAHA (5 μ M) was used as reference compound.

alkylidenemalonate scaffold were detrimental for the activity of the resulting compounds. In fact, only the variation of alkyl chain length (derivatives **1a** and **2a–c**) or the substitution of ester functions with keto groups (derivative **3**) yielded compounds displaying a strong inhibition against recombinant KAT3A (in the range 79–83%), thereby being more powerful than AA (62% of inhibition at 50 μM) in this assay. On the other hand, only compound **1a**, its inferior homologue, was comparable to **1b** in the activation of the enzymatic activity of KAT2B, whereas the shorter malonates **2a–c** were inactive or displayed just a moderate inhibition. Accordingly, western blot analyses showed that, similarly to **1b**, compound **1a** was able to induce hyperacetylation of H3 in U937 cells, without affecting tubulin acetylation (in MCF7 cells). On the contrary, derivatives **2a** and **2b** and, to a lesser extent, derivative **3** induced a significant hypoacetylation of the H3 histone substrate in the same conditions. The effects of tested compounds on cell cycle and apoptosis induction evidenced again that the shortening of the aliphatic chain (compounds **2a** and **2b**) resulted in a 2–3-fold lower activity, while compounds **1a** and **1b** displayed similar (42.90 μM and 44.91 μM , respectively) concentration inducing 50% apoptosis (IC_{50}) values. Interestingly, SPR-based assays showed that the long chain alkylidenemalonates (LoCAMs) **2a** and **2b** as well as the diketone **3** were able to interact with p300 full-length but not with the catalytic domain, whereas just negligible interactions were recorded for both **1a** and **1b**. It is noteworthy that Giannis and co-workers previously reported that the length of the aliphatic side chain seems crucial for biological activity of analogues of MB-3.⁶⁵ A few other derivatives exhibited various degrees of activity in one or both the enzymatic assays, but were practically inactive in cellular assays.

In summary, we have identified LoCAMs as a novel, interesting class of KAT modulators. Variations of the alkyl chain length can change their activity profile from KAT3A/KAT2B inhibitors (as derivative **2a**) to the peculiar profile of pentadecylidenemalonate **1b**, the first activator/inhibitor of histone acetyltransferases. Together with the powerful apoptotic effect (particularly notable if considering that anacardic acid and other KAT inhibitors are not cell permeable) appoint them as valuable biological tools to understand the mechanisms of lysine acetyltransferases. Further biological in vitro and in vivo studies are in progress to better characterize the observed properties of LoCAMs and to correlate the effects on the acetylation of specific lysine residues with the expression of particular genes. This may also prelude to a novel group of compounds for antineoplastic therapeutics.

5. Experimental section

5.1. Chemistry

All chemicals were purchased from Aldrich Chimica (Milan, Italy) or from Alfa Aesar GmbH (Karlsruhe, Germany) and were of the highest purity. All solvents were reagent grade and, when necessary, were purified and dried by standard methods. A sample of suberoylanilide hydroxamic acid (SAHA) for biological assays was prepared as previously reported by us.⁷⁶ All reactions requiring anhydrous conditions were conducted under a positive atmosphere of nitrogen in oven-dried glassware. Standard syringe techniques were used for anhydrous addition of liquids. Reactions were routinely monitored by TLC performed on aluminum-backed silica gel plates (Merck DC, Alufolien Kieselgel 60 F₂₅₄) with spots visualized by UV light ($\lambda = 254, 365 \text{ nm}$) or using a KMnO_4 alkaline solution. Concentration of solutions after reactions and extractions involved the use of a rotary evaporator operating at a reduced pressure of ~ 10 Torr. Organic solutions were dried over anhydrous sodium sulfate. Chromatographic separations were performed on silica gel (Silica Gel 60, 0.063–0.200 mm; Merck DC) columns.

Melting points were determined on a Gallenkamp melting point apparatus in open capillary tubes and are uncorrected. ^1H NMR spectra were recorded at 300 MHz on a Bruker Avance 300 spectrometer; chemical shifts are reported in δ (ppm) units relative to the internal reference tetramethylsilane (Me_4Si). Mass spectra were recorded on a Finnigan LCQ DECA TermoQuest (San Jose, CA, USA) mass spectrometer using an electrospray ion source (ESI-MS). Combustion analysis on target compounds was performed by our Analytical Laboratory at the University of Salerno. All compounds showed $\geq 98\%$ purity. When the elemental analysis is not included, crude compounds were used in the next step without further purification. As a rule, samples prepared for physical and biological studies were dried in high vacuum over P_2O_5 for 20 h at temperatures ranging from 25 to 110 $^\circ\text{C}$, depending on the sample melting point.

5.1.1. General procedure for the synthesis of aldehydes **12a,b**.

Example: tetradecanal (**12a**)^{67,77}

To a solution of commercial tetradecan-1-ol (0.72 g, 3.37 mmol) in DCM (20 mL) at 0 $^\circ\text{C}$ Dess–Martin periodinane (DMP) (1.53 g, 3.60 mmol) was added. After completion (45 min, TLC monitoring), the reaction crude was directly purified by column chromatography (silica gel, CHCl_3/n -hexane, 3:1) to afford the required aldehyde as a waxy white solid (187 mg, 98% yield). ^1H NMR (CDCl_3): δ 0.88 (t, 3H, CH_3), 1.26–1.29 (m, 20H, $10 \times \text{CH}_2$), 1.60–1.65 (m, 2H, CH_2), 2.40–2.50 (m, 2H, CH_2), 9.77 (t, 1H, H-1); MS (EI, 70 eV) m/z (%): 212.

Pentadecanal **12b**,⁷⁸ was obtained following the same procedure starting from commercial pentadecan-1-ol. ^1H NMR (CDCl_3): δ 0.86 (t, 3H, CH_3), 1.26–1.30 (m, 22H, $11 \times \text{CH}_2$), 1.59–1.64 (m, 2H, CH_2), 2.38–2.50 (m, 2H, CH_2), 9.87 (t, 1H, H-1); MS (EI, 70 eV) m/z (%): 226.

5.1.2. General procedure for the synthesis of derivatives **1–3**.

Example: diethyl 2-tetradecylidenemalonate (**1a**)⁶⁷

A stirred solution of the aldehyde **12a** (3.98 mmol) and diethyl malonate (4.38 mmol) in anhydrous methylene chloride (3 mL) was treated with piperidine (0.08 mmol) and acetic acid (0.08 mmol) at 0 $^\circ\text{C}$. After 45 min of stirring, a small amount of 3- \AA molecular sieves was added. Then the reaction mixture was stirred at room temperature for another 15 min (TLC monitoring), diluted with diethyl ether (50 mL), and washed with water (10 mL) until the aqueous phase was neutral. The collected aqueous phases were extracted with diethyl ether ($3 \times 10 \text{ mL}$). The combined ethereal phases were successively washed with saturated sodium hydrogen carbonate solution ($3 \times 10 \text{ mL}$) and brine ($3 \times 10 \text{ mL}$) and dried (Na_2SO_4). After removing the solvent, the crude was purified by column chromatography (SiO_2 , n -hexane/ AcOEt 8:2) to obtain compound **1a** as an oil, in a 83% yield. ^1H NMR (CDCl_3): δ 0.90 (t, 3H, CH_3), 1.27–1.36 (m, 26H, $10 \times \text{CH}_2$ and $2 \times \text{OCH}_2\text{CH}_3$, overlapped signals), 1.47–1.51 (m, 2H, $\text{CH}_2\text{CH}_2\text{C}=\text{C}$), 2.28–2.33 (m, 2H, $\text{CH}_2\text{C}=\text{C}$), 4.23–4.34 (dm, 4H, $2 \times \text{OCH}_2\text{CH}_3$, overlapped signals), 7.02 (t, 1H, CH); MS (EI, 70 eV) m/z (%): 354. Anal. Calcd for $\text{C}_{21}\text{H}_{38}\text{O}_4$ (354.52): C, 71.14; H, 10.80. Found: C, 71.07; H, 10.79.

Diethyl 2-pentadecylidenemalonate **1b**,⁶⁷ 2-undecylmalonate **2a**, 2-dodecylmalonate **2b**, and 2-tridecylmalonate **2c** were obtained following the same procedure starting, respectively, from pentadecanal (**12b**), undecanal, dodecanal (lauric aldehyde), and tridecanal. 3-pentadecylidenepentane-2,4-dione **3** was prepared following the same procedure starting from 2,4-pentanedione (acetylacetone) and pentadecanal **12b**.

Compound **1b**: oil (yield 86%); ^1H NMR (CDCl_3): δ 0.90 (t, 3H, CH_3), 1.27–1.36 (m, 28H, $11 \times \text{CH}_2$ and $2 \times \text{OCH}_2\text{CH}_3$, overlapped signals), 1.48–1.58 (m, 2H, $\text{CH}_2\text{CH}_2\text{C}=\text{C}$), 2.29–2.33 (m, 2H, $\text{CH}_2\text{C}=\text{C}$), 4.24–4.34 (dm, 4H, $2 \times \text{OCH}_2\text{CH}_3$, overlapped signals), 7.02 (t, 1H,

CH); MS (EI, 70 eV) m/z (%): 368. Anal. Calcd for $C_{22}H_{40}O_4$ (368.29): C, 71.70; H, 10.94. Found: C, 71.63; H, 10.93.

Compound **2a**: oil (yield 87%); 1H NMR ($CDCl_3$): δ 0.88 (t, 3H, CH_3), 1.25–1.35 (m, 20H, $7 \times CH_2$ and $2 \times OCH_2CH_3$, overlapped signals), 1.47 (m, 2H, $CH_2CH_2C=$), 2.27–2.30 (m, 2H, $CH_2C=$), 4.20–4.31 (dm, 4H, $2 \times OCH_2CH_3$, overlapped signals), 7.00 (t, 1H, CH); MS (EI, 70 eV) m/z (%): 312. Anal. Calcd for $C_{18}H_{32}O_4$ (312.23): C, 69.19; H, 10.32. Found: C, 69.01; H, 10.30.

Compound **2b**: oil (yield 85%); 1H NMR ($CDCl_3$): δ 0.88 (t, 3H, CH_3), 1.25–1.35 (m, 22H, $8 \times CH_2$ and $2 \times OCH_2CH_3$, overlapped signals), 1.47 (m, 2H, $CH_2CH_2C=$), 2.27–2.30 (m, 2H, $CH_2C=$), 4.22–4.31 (dm, 4H, $2 \times OCH_2CH_3$, overlapped signals), 7.00 (t, 1H, CH); MS (EI, 70 eV) m/z (%): 326. Anal. Calcd for $C_{19}H_{34}O_4$ (326.25): C, 69.90; H, 10.50. Found: C, 69.77; H, 10.48.

Compound **2c**: oil (yield 88%); 1H NMR ($CDCl_3$): δ 0.88 (t, 3H, CH_3), 1.25–1.35 (m, 24H, $9 \times CH_2$ and $2 \times OCH_2CH_3$, overlapped signals), 1.47 (m, 2H, $CH_2CH_2C=$), 2.25–2.32 (m, 2H, $CH_2C=$), 4.20–4.33 (dm, 4H, $2 \times OCH_2CH_3$, overlapped signals), 6.99 (t, 1H, CH); MS (EI, 70 eV) m/z (%): 340. Anal. Calcd for $C_{20}H_{36}O_4$ (340.26): C, 70.55; H, 10.66. Found: C, 70.41; H, 10.64.

Compound **3**: oil (yield 83%); 1H NMR ($CDCl_3$): δ 0.90 (t, 3H, CH_3), 1.26–1.38 (m, 22H, $11 \times CH_2$), 1.51 (m, 2H, $CH_2CH_2C=$), 2.23–2.28 (m, 2H, $CH_2C=$), 2.34 (s, 6H, $2 \times COCH_3$), 6.70 (t, 1H, CH); MS (EI, 70 eV) m/z (%): 308. Anal. Calcd for $C_{20}H_{36}O_2$ (308.27): C, 77.87; H, 11.76. Found: C, 77.69; H, 11.74.

5.1.3. General procedure for the synthesis of alkylmalonates **4a–c**

Diethyl 2-tridecylmalonate **4a**,⁷¹ tetradecylmalonate **4b**,⁶⁹ and pentadecylmalonate **4c**⁷⁰ were prepared as previously reported⁶⁹ from diethyl malonate and, respectively, tridecyl-, tetradecyl-, and pentadecylbromide.

Compound **4a**: oil (yield 75%); 1H NMR ($CDCl_3$): δ 0.88 (t, 3H, CH_3), 1.27–1.41 (m, 28H, $11 \times CH_2$ and $2 \times OCH_2CH_3$, overlapped signals), 1.75–1.80 (m, 2H, $-CH_2CH-$), 3.28–3.34 (t, 1H, $-CH_2CH-$), 4.12–4.18 (q, 4H, $2 \times OCH_2CH_3$); MS (EI, 70 eV) m/z (%): 342. Anal. Calcd for $C_{20}H_{38}O_4$ (342.28): C, 70.13; H, 11.18. Found: C, 70.06; H, 11.17.

Compound **4b**: oil (yield 71%); 1H NMR ($CDCl_3$): δ 0.88 (t, 3H, CH_3), 1.26–1.40 (m, 30H, $12 \times CH_2$ and $2 \times OCH_2CH_3$, overlapped signals), 1.76–1.81 (m, 2H, $-CH_2CH-$), 3.28–3.34 (t, 1H, $-CH_2CH-$), 4.12–4.18 (q, 4H, $2 \times OCH_2CH_3$); MS (EI, 70 eV) m/z (%): 356. Anal. Calcd for $C_{21}H_{40}O_4$ (356.29): C, 70.74; H, 11.31. Found: C, 70.58; H, 11.29.

Compound **4c**: oil (yield 72%); 1H NMR ($CDCl_3$): δ 0.89 (t, 3H, CH_3), 1.26–1.42 (m, 32H, $13 \times CH_2$ and $2 \times OCH_2CH_3$, overlapped signals), 1.76–1.81 (m, 2H, $-CH_2CH-$), 3.27–3.33 (t, 1H, $-CH_2CH-$), 4.13–4.19 (q, 4H, $2 \times OCH_2CH_3$); MS (EI, 70 eV) m/z (%): 370. Anal. Calcd for $C_{22}H_{42}O_4$ (370.31): C, 71.31; H, 11.42. Found: C, 71.15; H, 11.39.

5.1.4. General procedure for the synthesis of derivatives **5a–c**. Example: diethyl 2-(1-hydroxyhexadecylidene)malonate **5b**⁶⁷

Triethylamine (1.30 mL, 9.36 mmol) and magnesium chloride (0.71 g, 7.49 mmol) were added to a stirred solution of diethyl malonate (1.00 g, 6.24 mmol) in dry acetonitrile (20 mL) while cooling at 0 °C. The mixture was stirred at room temperature for 2 h. Then a previously prepared mixture of palmitic acid (1.60 g, 6.24 mmol) and *N,N'*-carbonyldiimidazole (1.11 g, 6.87 mmol) in dry acetonitrile (15 mL) was added, and the resulting slurry was stirred overnight. After completion (TLC monitoring, $SiO_2/CHCl_3$), the mixture was cautiously acidified with 13% HCl while keeping the temperature below 25 °C, and the resulting mixture was stirred for additional 15 min. The organic layer was separated and evaporated, and the residue was treated with ethyl acetate (20 mL). The aqueous layer was extracted with ethyl acetate (2×20 mL), and the organic phases were combined, washed with saturated sodium

bicarbonate solution (2×30 mL) and brine (3×30 mL), dried, and concentrated to give the crude diethyl 2-(1-hydroxyhexadecylidene)malonates which was purified by column chromatography (SiO_2 , $CHCl_3$) to obtain compound **5b** as a white solid (mp: 32–33 °C) in a 90% yield. 1H NMR ($CDCl_3$) δ 0.88 (t, 3H, CH_3), 1.29–1.34 (m, 30H, $12 \times CH_2$ and $2 \times OCH_2CH_3$, overlapped signals), 1.57–1.62 (m, 2H, $CH_2CH_2C(OH)=$), 2.40–2.45 (m, 1H, $CH_2CHH_A C(OH)=$), 2.58–2.63 (m, 1H, $CH_2CHH_B C(OH)=$), 4.21–4.30 (m, 4H, $2 \times OCH_2CH_3$), 13.41 (s, 1H, OH, exchangeable with D_2O). MS (EI, 70 eV) m/z (%): 398. Anal. Calcd for $C_{23}H_{42}O_5$ (398.30): C, 69.31; H, 10.62. Found: C, 69.18; H, 10.60.

Diethyl 2-(1-hydroxypentadecylidene)malonate **5a** and diethyl 2-(1-hydroxyheptadecylidene)malonates **5c** were obtained following the same procedure starting from diethyl malonates and, respectively, pentadecanoic acid and heptadecanoic (margaric) acid.

Compound **5a**: oil (yield 93%). 1H NMR ($CDCl_3$) δ 0.88 (t, 3H, CH_3), 1.28–1.33 (m, 28H, $11 \times CH_2$ and $2 \times OCH_2CH_3$, overlapped signals), 1.58–1.63 (m, 2H, $CH_2CH_2C(OH)=$), 2.40–2.45 (m, 1H, $CH_2CHH_A C(OH)=$), 2.58–2.63 (m, 1H, $CH_2CHH_B C(OH)=$), 4.21–4.30 (m, 4H, $2 \times OCH_2CH_3$), 13.41 (s, 1H, OH, exchangeable with D_2O). MS (EI, 70 eV) m/z (%): 384. Anal. Calcd for $C_{20}H_{40}O_5$ (384.29): C, 68.71; H, 10.48. Found: C, 68.56; H, 10.46.

Compound **5c**: oil (yield 91%). 1H NMR ($CDCl_3$) δ 0.89 (t, 3H, CH_3), 1.29–1.32 (m, 32H, $13 \times CH_2$ and $2 \times OCH_2CH_3$, overlapped signals), 1.57–1.62 (m, 2H, $CH_2CH_2C(OH)=$), 2.40–2.45 (m, 1H, $CH_2CHH_A C(OH)=$), 2.58–2.63 (m, 1H, $CH_2CHH_B C(OH)=$), 4.21–4.30 (m, 4H, $2 \times OCH_2CH_3$), 13.41 (s, 1H, OH, exchangeable with D_2O). MS (EI, 70 eV) m/z (%): 412. Anal. Calcd for $C_{24}H_{44}O_5$ (412.32): C, 69.86; H, 10.75. Found: C, 69.72; H, 10.73.

5.1.5. Preparation of diethyl 2-(1-chloropentadecylidene)malonate **6**

A solution of compound **5a** (2.16 g, 5.62 mmol) in phosphorus(V) oxychloride (4.79 g, 31.22 mmol) was cooled to 0 °C then treated with triethylamine (0.87 mL, 6.24 mmol) dropwise. The resulting mixture was stirred at room temperature overnight then heated to 80 °C for additional 4 h. After completion (TLC monitoring, SiO_2 , $CHCl_3/n$ -hexane 3:1), the mixture was evaporated and the brownish residue was treated with saturated sodium carbonate solution (30 mL) and extracted with petroleum ether (3×15 mL). The organic phases were combined, washed with saturated sodium bicarbonate solution (3×10 mL) and brine (3×30 mL), dried, and evaporated and the residue was purified by column chromatography (silica gel, $CHCl_3/n$ -hexane 1:1) to give the required ester **6** as a pale yellow oil (yield: 80%). MS (EI, 70 eV) m/z : 402 (100.0%), 404 (35.6%). 1H NMR ($CDCl_3$) δ 0.88 (t, 3H, CH_3), 1.26–1.34 (m, 28H, $11 \times CH_2$ and $2 \times OCH_2CH_3$, overlapped signals), 1.66 (m, 2H, $CH_2CH_2C=$), 2.89–2.94 (t, 2H, $CH_2C=$), 4.19–4.34 (m, 4H, $2 \times OCH_2CH_3$). Anal. Calcd for $C_{22}H_{39}ClO_4$ (402.25): C, 65.57; H, 9.75; Cl, 8.80. Found: C, 65.44; H, 9.73; Cl, 8.79.

5.1.6. Preparation of diethyl 2-(1-aminopentadecylidene)malonate **7**

A solution of compound **5a** (0.61 g, 1.59 mmol) in anhydrous ethanol (10 mL) was treated with ammonium acetate (1.23 g, 15.89 mmol) and the resulting mixture was stirred at room temperature for 2 h. After completion (TLC monitoring, SiO_2 , $CHCl_3/n$ -hexane 3:1), the mixture was evaporated and the residue was treated with saturated sodium bicarbonate solution (10 mL) and extracted with ethyl acetate (3×15 mL). The organic phases were combined, washed with brine (3×30 mL), dried, and evaporated to obtain the required aminoester **7** as a TLC pure pale yellow oil (yield: 95%). MS (EI, 70 eV) m/z : 383 (100.0%). 1H NMR ($CDCl_3$) δ 0.90 (t, 3H, CH_3), 1.29–1.34 (m, 28H, $11 \times CH_2$ and $2 \times OCH_2CH_3$, overlapped signals), 1.50–1.55 (m, 2H, $CH_2CH_2C(NH_2)=$),

2.20–2.25 (m, 1H, CH₂CHH_AC(NH₂)=), 2.38–2.43 (m, 1H, CH₂CHH_BC(NH₂)=), 4.21–4.30 (m, 4H, 2 × OCH₂CH₃), 8.51 (bs, 2H, NH₂, exchangeable with D₂O). Anal. Calcd for C₂₂H₄₁NO₄ (383.30): C, 68.89; H, 10.77; N, 3.65. Found: C, 68.74; H, 10.75; N, 3.64.

5.1.7. Preparation of 2,2-dimethyl-5-pentadecylidene-1,3-dioxane-4,6-dione **8**

Title compound was prepared following the same procedure described for derivatives **1–3**, starting from Meldrum's acid and pentadecanal **12b**, as an oil (yield 80%); ¹H NMR (CDCl₃): δ 0.88 (t, 3H, CH₃), 1.26 (m, 22H, 11 × CH₂), 1.57–1.62 (m, 2H, CH₂CH₂C=), 1.75 (s, 6H, 2 × CH₃), 2.91–2.96 (m, 2H, CH₂C=), 7.94 (t, 1H, CH); MS (EI, 70 eV) *m/z* (%): 352. Anal. Calcd for C₂₁H₃₆O₄ (352.26): C, 71.55; H, 10.29. Found: C, 71.44; H, 10.27.

5.1.8. Preparation of 2,2-dimethyl-5-pentadecyl-1,3-dioxane-4,6-dione **9**

Title compound was prepared following the same procedure⁶⁹ described for derivatives **4**, starting from Meldrum's acid and pentadecylbromide, as an oil (yield 75%); ¹H NMR (CDCl₃): δ 0.88 (t, 3H, CH₃), 1.26 (m, 24H, 12 × CH₂), 1.43 (m, 2H, CH₂CH₂CH–), 1.76–1.78 (ds, 6H, 2 × CH₃), 2.07–2.17 (m, 2H, CH₂CH–), 3.49 (t, 1H, CH); MS (EI, 70 eV) *m/z* (%): 354. Anal. Calcd for C₂₁H₃₈O₄ (354.28): C, 71.14; H, 10.80. Found: C, 70.98; H, 10.78.

5.1.9. General procedure for the preparation of alkan-2-ylidene malonates **10a,b**

To a stirred and cooled (–40 °C) suspension of pentane-washed NaH (1.3 equiv, 60% suspension in oil) in dry THF (10 mL) was added triethyl phosphonoacetate (1.3 equiv) in THF (10 mL). After 1 h at room temperature, the mixture was cooled again (–40 °C), then a solution of the proper ketone (1 equiv) in THF (10 mL) was added dropwise and the mixture stirred for 18 h at room temperature. After completion (TLC monitoring, SiO₂, CHCl₃/*n*-hexane 3:1), the mixture was cautiously diluted with saturated aqueous ammonium chloride (20 mL) and diethyl ether (40 mL), the organic layer separated and aqueous portion further extracted with ether (2 × 10 mL). The combined organic extract was then washed with water and brine and finally dried. Solvent removal followed by column chromatography of the residue (silica gel, CHCl₃/*n*-hexane 1:1) afforded the mixture of *E/Z* diastereomers in 90% yield. A solution of this mixture (1 equiv) in dry THF (8 mL) was stirred at –78 °C under nitrogen and a solution of lithium diisopropylamide (1.5 equiv) and HMPA (2 equiv) in dry THF (10 mL) was introduced dropwise. The resulting mixture was stirred at –78 °C for 2 h before ethyl chloroformate (1.2 equiv) was added. The reaction mixture was warmed to room temperature gradually and stirred for another 45 h. After completion (TLC monitoring, SiO₂, CHCl₃/*n*-hexane 1:1), ether (100 mL) was added, and the reaction mixture was washed with saturated aqueous NH₄Cl and brine. The organic layer was separated and the aqueous portion further extracted with ether (2 × 10 mL). The combined organic extract was then washed with water and brine and finally dried over Na₂SO₄. Solvent removal furnished the TLC pure malonates.

Compound **10a**: oil (yield 93%); ¹H NMR (CDCl₃): δ 0.89 (t, 3H, CH₃), 1.22–1.28 (m, 26H, 10 × CH₂ and 2 × OCH₂CH₃, overlapped signals), 1.46 (m, 2H, CH₂CH₂C=), 2.02 (s, 3H, CH₃C=), 2.26–2.31 (m, 2H, CH₂C=), 4.14–4.22 (m, 4H, 2 × OCH₂CH₃, overlapped signals); MS (EI, 70 eV) *m/z* (%): 368. Anal. Calcd for C₂₂H₄₀O₄ (368.29): C, 71.70; H, 10.94. Found: C, 71.63; H, 10.93.

Compound **10b**: oil (yield 92%); ¹H NMR (CDCl₃): δ 0.88 (t, 3H, CH₃), 1.21–1.30 (m, 28H, 11 × CH₂ and 2 × OCH₂CH₃, overlapped signals), 1.50 (m, 2H, CH₂CH₂C=), 2.05 (s, 3H, CH₃C=), 2.29–2.34 (m, 2H, CH₂C=), 4.18–4.26 (m, 4H, 2 × OCH₂CH₃, overlapped

signals); MS (EI, 70 eV) *m/z* (%): 382. Anal. Calcd for C₂₃H₄₂O₄ (382.31): C, 72.21; H, 11.07. Found: C, 72.06; H, 11.05.

5.1.10. Preparation of diethyl 2-((tridecylamino)methylene)-malonates **11**

A solution of diethyl ethoxymethylenemalonate (500 μL, 2.45 mmol) in dry ethanol (2 mL) was added to a stirred solution of tridecylamine (0.41 g, 2.00 mmol) in dry ethanol (8 mL) and the resulting mixture was refluxed overnight. After completion (TLC monitoring, SiO₂, CHCl₃/*n*-hexane 1:1), the solvent was removed under reduced pressure to obtain title compound as a TLC pure oil (yield 99%). ¹H NMR (CDCl₃): δ 0.88 (t, 3H, CH₃), 1.18–1.36 (m, 26H, 10 × CH₂ and 2 × OCH₂CH₃, overlapped signals), 1.57 (m, 2H, CH₂CH₂NH=), 3.28–3.27 (m, 2H, CH₂NH=), 4.14–4.27 (m, 4H, 2 × OCH₂CH₃, overlapped signals), 7.97–8.01 (d, 1H, CH), 9.22 (br m, 1H, NH); MS (EI, 70 eV) *m/z* (%): 369. Anal. Calcd for C₂₁H₃₉N₂O₄ (369.29): C, 68.25; H, 10.64; N, 3.79. Found: C, 68.11; H, 10.62; N, 3.78.

5.2. Biology

5.2.1. Cell culture

Human leukemia cell lines U937 was propagated in RPMI medium supplemented with 10% FBS (Foetal bovine serum; Hyclone) and antibiotics (100 U/mL penicillin, 100 μg/mL streptomycin and 250 ng/mL amphotericin-B). MCF7 cells were grown in the same condition but with D-MEM medium. Both cell lines were kept at the constant concentration of 200,000 cells per mL of culture medium, at the temperature of 37 °C and with 5% of CO₂.

5.2.2. Ligands and materials

Anacardic acid (Alexis) and SAHA⁷⁶ were dissolved in DMSO and used at 50 and 5 μM, respectively.

5.2.3. Expression and purification of KAT3B (p300)

His₆-tagged human p300 was expressed in Sf9 cells from a baculovirus-based plasmid (kind gift of Professor Alexandra Lusser and Professor James T. Kadonaga) and purified by affinity chromatography on Ni-NTA affinity resin (Qiagen) as described elsewhere.⁷⁹ Protein was eluted with buffer containing 250 mM imidazole, frozen in liquid nitrogen, and stored at –80 °C. p300 concentrations and purity were estimated by Bradford protein assays (Bio-Rad) and by comparison to BSA standards on SDS gels stained with Coomassie Brilliant Blue G-250.

5.2.4. Human recombinant KAT3A (CBP) assay

The recombinant CBP was prepared in *Escherichia coli* BL21 and purified by affinity chromatography. Recombinant CBP fraction corresponded to amino acids 1098–1877. CBP was incubated in HAT buffer (50 mM Tris–HCl pH 8.0, 10% glycerol, 0.1 mM EDTA, 1 mM DTT) with 10 μg of histone H4 peptide (corresponding to amino acids 2–24) and 20 μM acetyl-CoA containing 0.5 μCi/mL [³H]-acetyl-CoA in the presence of tested compounds at selected concentrations. After 2 h at 37 °C, 5 μL of samples were spotted onto Whatman P81 paper (in triplicate). The paper squares were washed three times in 5% TCA and once in 100% acetone and then placed into scintillation vials containing scintillation fluid to allow the DPM reading. The DPM of enzyme samples was compared to DPM of negative control. Data have been expressed as percentage.

5.2.5. KAT2B (PCAF) assays

PCAF radioactive assay was performed according to general indications provided by UPSTATE radioactive KIT. Human PCAF (200 ng) was incubated in KAT buffer (Upstate) with 10 μg of histone H4 peptide substrate (corresponding to amino acids 2–24) and 20 μM acetyl-CoA containing 0.5 μCi/mL [³H] acetyl-CoA.

The acetylation reaction was performed in a volume of 25 μL in the presence of testing compounds at the desired final concentration. After 2 h at 37 °C, 5 μL of samples were spotted onto chromatographic Whatman P81 paper (in triplicate). After a washing session (three times in 5% TCA and once in 100% acetone), the paper squares were placed into scintillation vials containing scintillation fluid to allow the DPM reading. The DPM of enzyme samples was compared to DPM of negative and positive control and reported as % of activity considering the untreated control as 100%.

5.2.6. Protein extraction protocol

MCF-7 and U937 cells were treated with reference compound or tested derivatives and harvested by centrifugation. After PBS wash, the samples were resuspended in a lysis buffer (50 mM Tris–HCl pH 7.4, 150 mM NaCl, 1% NP40, 10 mM sodium fluoride, 1 mM PMSF and protease inhibitor cocktail), and the lysis reaction was carried out for 15 min at 4 °C. The samples were centrifuged at 13,000 rpm for 30 min at 4 °C, and the proteins were quantified by the Bradford assay (Bio-Rad).

5.2.7. Histone extraction protocol

Cells were harvested and washed twice with ice-cold PBS and lysed in Triton Extraction Buffer (TEB: PBS containing 0.5% Triton X 100 (v/v), 2 mM phenylmethylsulfonyl fluoride (PMSF), 0.02% (w/v) NaN_3) at a cellular density of 10^7 cells per mL for 10 min on ice, with gentle stirring. After a brief centrifugation at 2000 rpm at 4 °C, the supernatant was removed and the pellet was washed in half the volume of TEB and centrifuged as before. The pellet was resuspended in 0.2 M HCl at a cell density of 4×10^7 cells per mL and acid extraction was left to proceed overnight at 4 °C on a rolling table. Next, the samples were centrifuged at 2000 rpm for 10 min at 4 °C, the supernatant was removed and its protein content was determined using the Bradford assay (Bio-Rad).

5.2.8. Western blot analyses

Western Blot analyses were performed according to standard procedures following suggestions of antibody suppliers. For α -tubulin, an amount of 30 μg for MCF-7 cells of total protein extracts was separated on 10% polyacrylamide gels and blotted.⁸⁰ For the histone H3 and H4 acetylations in U937 and MCF7 cells, 10 μg of histone extract was separated on 15% polyacrylamide gels and blotted.⁸⁰ The blotted nitrocellulose was washed twice with water and then blocked in freshly prepared PBS, containing 5% nonfat dry milk (PBS-MLK) for one hour at room temperature with constant agitation. The nitrocellulose was incubated with 1:1000 dilution of anti acetylated α -tubulin (Sigma), pan-acetylated histone H3 (Upstate), H3K9ac (Abcam), H3K14ac (Abcam), H3K18ac (Abcam), H3K56ac (Abcam), H4K5ac (Abcam), H4K8ac (Abcam), H4K16ac (Abcam), and pan-acetylated H4 (Abcam). ERK-1 (extracellular signal-regulated kinase-1, Santa Cruz) antibody, Ponceau Red (Sigma) staining, and histone H1 (Abcam) were used, respectively, to normalize for equal loading.

5.2.8.1. Cell cycle analysis. The 2.5×10^5 cells were collected and resuspended in 500 μL of an hypotonic buffer (0.1% Triton X-100, 0.1% sodium citrate, 50 $\mu\text{g}/\text{mL}$ propidium iodide, RNase A). Cells were incubated in the dark for 30 min. Samples were acquired on a FACS-Calibur flow cytometer using the Cell Quest software (Becton Dickinson) and analyzed with standard procedures using the Cell Quest software (Becton Dickinson) and the ModFit LT version 3 software (Verity). All the experiments were performed three times.

5.2.8.2. FACS analysis of apoptosis. Apoptosis was measured with Annexin V/propidium iodide double-staining detection

(Roche and Sigma–Aldrich, respectively), as recommended by the suppliers. Samples were analyzed by FACS with Cell Quest technology (Becton Dickinson). As second assays, the caspase 3 detection (B-Bridge) was performed and quantified by FACS (data not shown, Becton Dickinson).

5.2.8.3. Kinetic study of the interaction with KAT3B. SPR analyses were performed on a Biacore 3000 optical biosensor equipped with research-grade CM5 sensor chips (Biacore AB).⁸¹ Using this platform, two separate KAT3B (p300, both the full length protein and its KAT domain) surfaces, one BSA surface and one unmodified reference surface were prepared for simultaneous analyses. Proteins (30 $\mu\text{g}/\text{mL}^{-1}$ in 10 mM sodium acetate, pH 4.0) were immobilized on individual flow cells of the sensor chip at a flow rate of 10 $\text{mL}/\text{min}^{-1}$ by using standard amine-coupling protocols⁸² to obtain densities of 8–14 kRU. Compounds **1–3** were dissolved in DMSO (100%) to obtain 50 mM solutions, and diluted in HBS (10 mM Hepes pH 7.4, 0.15 M NaCl, 0.005% NP40) with a final DMSO concentration of 0.5%. Binding experiments were performed at 25 °C, by using a flow rate of 30 $\mu\text{L}/\text{min}^{-1}$, with 120 s monitoring of association and 400 s monitoring of dissociation. Regeneration of the surfaces was performed, when necessary, by a 10 s injection of 5 mM NaOH.

Acknowledgments

This work was partially supported by grants from Ministero dell'Università e della Ricerca Scientifica e Tecnologica–PRIN 2008, (S.C.), Fondazione Roma (A.M.), and Università di Salerno, Italy (G.S.). L.A. is supported by AIRC and 'ATLAS' HEALTH-F4-2009-221952.

We are grateful to Professor Alexandra Lusser and Professor James T. Kadonaga for the kind gift of p300 baculovirus expression construct.

Supplementary data

Supplementary data (experimental procedures for determination of granulocytic differentiation, KDAC assay, fluorescent KAT3B assay and additional graphs) associated with this article can be found, in the online version, at doi:10.1016/j.bmc.2011.01.013.

References and notes

- Kouzarides, T. *Cell* **2007**, *128*, 693.
- Berger, S. L. *Nature* **2007**, *447*, 407.
- Ruthenburg, A. J.; Li, H.; Patel, D. J.; Allis, C. D. *Nat. Rev. Mol. Cell Biol.* **2007**, *8*, 983.
- Strahl, B. D.; Allis, C. D. *Nature* **2000**, *403*, 41.
- Allfrey, V. G.; Faulkner, R.; Mirsky, A. E. *Proc. Natl. Acad. Sci. U.S.A.* **1964**, *51*, 786.
- Roth, S. Y.; Denu, J. M.; Allis, C. D. *Annu. Rev. Biochem.* **2001**, *70*, 81.
- Yang, X.-J.; Seto, E. *Mol. Cell* **2008**, *31*, 449.
- Liu, Y.; Colosimo, A. L.; Yang, X.-J.; Liao, D. *Mol. Cell. Biol.* **2000**, *20*, 5540.
- Hubbert, C.; Guardiola, A.; Shao, R.; Kawaguchi, Y.; Ito, A.; Nixon, A.; Yoshida, M.; Wang, X.-F.; Yao, T.-P. *Nature* **2002**, *417*, 455.
- Glozak, M. A.; Sengupta, N.; Zhang, X.; Seto, E. *Gene* **2005**, *363*, 15.
- Matthias, P.; Yoshida, M.; Khochbin, S. *Cell Cycle* **2008**, *7*, 7.
- Yang, X.-J.; Seto, E. *Nat. Rev. Mol. Cell Biol.* **2008**, *9*, 206.
- Arif, M.; Selvi, B. R.; Kundu, T. K. *ChemBioChem* **2010**, *11*, 1501.
- von Wantoch Rekowski, M.; Giannis, A. *Biochim. Biophys. Acta, Gene Regul. Mech.* **2010**, *1799*, 760.
- Zhao, S.; Xu, W.; Jiang, W.; Yu, W.; Lin, Y.; Zhang, T.; Yao, J.; Zhou, L.; Zeng, Y.; Li, H.; Li, Y.; Shi, J.; An, W.; Hancock, S. M.; He, F.; Qin, L.; Chin, J.; Yang, P.; Chen, X.; Lei, Q.; Xiong, Y.; Guan, K.-L. *Science* **2010**, *327*, 1000.
- Wang, Q.; Zhang, Y.; Yang, C.; Xiong, H.; Lin, Y.; Yao, J.; Li, H.; Xie, L.; Zhao, W.; Yao, Y.; Ning, Z.-B.; Zeng, R.; Xiong, Y.; Guan, K.-L.; Zhao, S.; Zhao, G.-P. *Science* **2010**, *327*, 1004.
- Allis, C. D.; Berger, S. L.; Cote, J.; Dent, S.; Jenuwien, T.; Kouzarides, T.; Pillus, L.; Reinberg, D.; Shi, Y.; Shiekhhattar, R.; Shilatifard, A.; Workman, J.; Zhang, Y. *Cell* **2007**, *131*, 633.

18. Lysine acetylation was initially identified in histones, so many KATs and KDACS are often referred to as histone acetyltransferases (HATs) and deacetylases (HDACs), respectively.
19. Dekker, F. J.; Haisma, H. J. *Drug Discovery Today* **2009**, *14*, 942.
20. Manzo, F.; Tambaro, F. P.; Mai, A.; Altucci, L. *Expert Opin. Ther. Pat.* **2009**, *19*, 761.
21. Howe, L.; Auston, D.; Grant, P.; John, S.; Cook, R. G.; Workman, J. L.; Pillus, L. *Genes Dev.* **2001**, *15*, 3144.
22. Gayther, S. A.; Batley, S. J.; Linger, L.; Bannister, A.; Thorpe, K.; Chin, S.-F.; Daigo, Y.; Russell, P.; Wilson, A.; Sowter, H. M.; Delhanty, J. D. A.; Ponder, B. A. J.; Kouzarides, T.; Caldas, C. *Nat. Genet.* **2000**, *24*, 300.
23. Bandyopadhyay, D.; Okan, N. A.; Bales, E.; Nascimento, L.; Cole, P. A.; Medrano, E. E. *Cancer Res.* **2002**, *62*, 6231.
24. Giordano, A.; Avantiaggiati, M. L. *J. Cell. Physiol.* **1999**, *181*, 218.
25. Pfister, S.; Rea, S.; Taipale, M.; Mendrzyk, F.; Straub, B.; Ittrich, C.; Thuerigen, O.; Sinn, H. P.; Akhtar, A.; Lichter, P. *Int. J. Cancer* **2008**, *122*, 1207.
26. Katsumoto, T.; Yoshida, N.; Kitabayashi, I. *Cancer Sci.* **2008**, *99*, 1523.
27. Iyer, N. G.; Xian, J.; Chin, S. F.; Bannister, A. J.; Daigo, Y.; Aparicio, S.; Kouzarides, T.; Caldas, C. *Oncogene* **2007**, *26*, 21.
28. Kitabayashi, I.; Aikawa, Y.; Yokoyama, A.; Hosoda, F.; Nagai, M.; Kakazu, N.; Abe, T.; Ohki, M. *Leukemia* **2001**, *15*, 89.
29. Ait-Si-Ali, S.; Poleskaya, A.; Filleur, S.; Ferreira, R.; Duquet, A.; Robin, P.; Vervish, A.; Trouche, D.; Cabon, F.; Harel-Bellan, A. *Oncogene* **2000**, *19*, 2430.
30. Adcock, I. M.; Tsaprouni, L.; Bhavsar, P.; Ito, K. *Curr. Opin. Immunol.* **2007**, *19*, 694.
31. Yang, X. J. *Nucleic Acids Res.* **2004**, *32*, 959.
32. Mantelingu, K.; Reddy, B. A. A.; Swaminathan, V.; Kishore, A. H.; Siddappa, N. B.; Kumar, G. V. P.; Nagashankar, G.; Natash, N.; Roy, S.; Sathale, P. P.; Ranga, U.; Narayana, C.; Kundu, T. K. *Chem. Biol.* **2007**, *14*, 645.
33. Barnes, P. J.; Adcock, I. M.; Ito, K. *Eur. Resp. J.* **2005**, *25*, 552.
34. Lau, O. D.; Kundu, T. K.; Soccio, R. E.; Ait-Si-Ali, S.; Khalil, E. M.; Vassilev, A.; Wolfe, A. P.; Nakatani, Y.; Roeder, R. G.; Cole, P. A. *Mol. Cell* **2000**, *5*, 589.
35. Saha, R. N.; Pahan, K. *Cell Death Differ.* **2005**, *13*, 539.
36. Rouaux, C.; Jokic, N.; Mbebi, C.; Boutillier, S.; Loeffler, J.-P.; Boutillier, A.-L. *EMBO J.* **2003**, *22*, 6537.
37. Barrett, R. M.; Wood, M. A. *Learn. Memory* **2008**, *15*, 460.
38. Maurice, T.; Duclot, F.; Meunier, J.; Naert, G.; Givalois, L.; Meffre, J.; Celerier, A.; Jacquet, C.; Copois, V.; Mechti, N.; Ozato, K.; Gongora, C. *Neuropsychopharmacology* **2007**, *33*, 1584.
39. Mai, A.; Massa, S.; Rotili, D.; Cerbara, I.; Valente, S.; Pezzi, R.; Simeoni, S.; Ragno, R. *Med. Res. Rev.* **2005**, *25*, 261.
40. Minucci, S.; Pelicci, P. G. *Nat. Rev. Cancer* **2006**, *6*, 38.
41. Richon, V. M.; Emiliani, S.; Verdin, E.; Webb, Y.; Breslow, R.; Rifkind, R. A.; Marks, P. A. *Proc. Natl. Acad. Sci. U.S.A.* **1998**, *95*, 3003.
42. Nakajima, H.; Kim, Y. B.; Terano, H.; Yoshida, M.; Horinouchi, S. *Exp. Cell. Res.* **1998**, *241*, 126.
43. Nagy, Z.; Tora, L. *Oncogene* **2007**, *26*, 5341.
44. Marmorstein, R.; Trievel, R. C. *Biochim. Biophys. Acta, Gene Regul. Mech.* **2009**, *1789*, 58.
45. Lee, K. K.; Workman, J. L. *Nat. Rev. Mol. Cell Biol.* **2007**, *8*, 284.
46. Hodawadekar, S. C.; Marmorstein, R. *Oncogene* **2007**, *26*, 5528.
47. Brownell, J. E.; Zhou, J.; Ranalli, T.; Kobayashi, R.; Edmondson, D. G.; Roth, S. Y.; Allis, C. D. *Cell* **1996**, *84*, 843.
48. Stockwell, B. R. *Nat. Rev. Genet.* **2000**, *1*, 116.
49. Bowers, E. M.; Yan, G.; Mukherjee, C.; Orry, A.; Wang, L.; Holbert, M. A.; Crump, N. T.; Hazzalin, C. A.; Liszczak, G.; Yuan, H.; Larocca, C.; Saldanha, S. A.; Abagyan, R.; Sun, Y.; Meyers, D. J.; Marmorstein, R.; Mahadevan, L. C.; Alani, R. M.; Cole, P. A. *Chem. Biol.* **2010**, *17*, 471.
50. Cebrat, M.; Kim, C. M.; Thompson, P. R.; Daugherty, M.; Cole, P. A. *Bioorg. Med. Chem.* **2003**, *11*, 3307.
51. Balasubramanyam, K.; Swaminathan, V.; Ranganathan, A.; Kundu, T. K. *J. Biol. Chem.* **2003**, *278*, 19134.
52. Balasubramanyam, K.; Altaf, M.; Varier, R. A.; Swaminathan, V.; Ravindran, A.; Sathale, P. P.; Kundu, T. K. *J. Biol. Chem.* **2004**, *279*, 33716.
53. Balasubramanyam, K.; Varier, R. A.; Altaf, M.; Swaminathan, V.; Siddappa, N. B.; Ranga, U.; Kundu, T. K. *J. Biol. Chem.* **2004**, *279*, 51163.
54. Ravindra, K. C.; Selvi, B. R.; Arif, M.; Reddy, B. A. A.; Thanuja, G. R.; Agrawal, S.; Pradhan, S. K.; Nagashayana, N.; Dasgupta, D.; Kundu, T. K. *J. Biol. Chem.* **2009**, *284*, 24453.
55. Dal Piaz, F.; Tosco, A.; Eletto, D.; Piccinelli, A. L.; Moltedo, O.; Franceschelli, S.; Sbardella, G.; Remondelli, P.; Rastrelli, L.; Vesci, L.; Pisano, C.; De Tommasi, N. *ChemBioChem* **2010**, *11*, 818.
56. Eliseeva, E. D.; Valkov, V.; Jung, M. O. *Mol. Cancer Ther.* **2007**, *6*, 2391.
57. Ghizzoni, M.; Boltjes, A.; Graaf, C. D.; Haisma, H. J.; Dekker, F. J. *Bioorg. Med. Chem.* **2010**, *18*, 5826.
58. Souto, J. A.; Conte, M.; Álvarez, R.; Nebbioso, A.; Carafa, V.; Altucci, L.; de Lera, A. R. *ChemMedChem* **2008**, *3*, 1435.
59. Costi, R.; Di Santo, R.; Artico, M.; Miele, G.; Valentini, P.; Novellino, E.; Cereseto, A. *J. Med. Chem.* **2007**, *50*, 1973.
60. Mai, A.; Cheng, D.; Bedford, M. T.; Valente, S.; Nebbioso, A.; Perrone, A.; Brosch, G.; Sbardella, G.; De Bellis, F.; Miceli, M.; Altucci, L. *J. Med. Chem.* **2008**, *51*, 2279.
61. Dekker, F. J.; Ghizzoni, M.; van der Meer, N.; Wisastra, R.; Haisma, H. J. *Bioorg. Med. Chem.* **2009**, *17*, 460.
62. Ghizzoni, M.; Haisma, H. J.; Dekker, F. J. *Eur. J. Med. Chem.* **2009**, *44*, 4855.
63. Gorsuch, S.; Bavetsias, V.; Rowlands, M. G.; Aherne, G. W.; Workman, P.; Jarman, M.; McDonald, E. *Bioorg. Med. Chem.* **2009**, *17*, 467.
64. Stimson, L.; Rowlands, M. G.; Newbatt, Y. M.; Smith, N. F.; Raynaud, F. I.; Rogers, P.; Bavetsias, V.; Gorsuch, S.; Jarman, M.; Bannister, A.; Kouzarides, T.; McDonald, E.; Workman, P.; Aherne, G. W. *Mol. Cancer Ther.* **2005**, *4*, 1521.
65. Biel, M.; Kretsovali, A.; Karatzali, E.; Papamatheakis, J.; Giannis, A. *Angew. Chem., Int. Ed.* **2004**, *43*, 3974.
66. Mai, A.; Rotili, D.; Tarantino, D.; Ornaghi, P.; Tosi, F.; Vicidomini, C.; Sbardella, G.; Nebbioso, A.; Miceli, M.; Altucci, L.; Filetici, P. *J. Med. Chem.* **2006**, *49*, 6897.
67. Sbardella, G.; Castellano, S.; Vicidomini, C.; Rotili, D.; Nebbioso, A.; Miceli, M.; Altucci, L.; Mai, A. *Bioorg. Med. Chem. Lett.* **2008**, *18*, 2788.
68. Dess, D. B.; Martin, J. C. *J. Am. Chem. Soc.* **1991**, *113*, 7277.
69. Haldar, J.; Kondaiah, P.; Bhattacharya, S. *J. Med. Chem.* **2005**, *48*, 3823.
70. Ahlquist, L.; Asselineau, C.; Asselineau, J.; Stallberg-Stenhagen, S.; Stenhagen, E. *Ark. Kemi* **1958**, *31*, 543.
71. Comeau, D.; Lai, R.; Charlot, C.; Ucciani, E. *Bull. Soc. Chim. Fr.* **1972**, 4163.
72. Actually, as noticeable in Figure 5B, a slight acetylation was observed for both compounds at 15 μ M concentration. Yet, it was completely undetectable at 30 μ M.
73. Varier, R. A.; Swaminathan, V.; Balasubramanyam, K.; Kundu, T. K. *Biochem. Pharmacol.* **2004**, *68*, 1215.
74. In these conditions, compound **2b** caused excessive cell death.
75. In Figure 8 as well as in the text we used the 'Brno nomenclature' to indicate specific acetylation sites. See also: Turner, B. M. *Nat. Struct. Mol. Biol.* **2005**, *12*, 110.
76. Mai, A.; Esposito, M.; Sbardella, G.; Massa, S. *Org. Prep. Proced. Int.* **2001**, *33*, 391.
77. Chang, Y.-H.; Uang, B.-J.; Wu, C.-M.; Yu, T.-H. *Synthesis* **1990**, *1990*, 1033.
78. Sorg, G.; Mengel, A.; Jung, G.; Rademann, J. *Angew. Chem., Int. Ed.* **2001**, *40*, 4395.
79. Kraus, W. L.; Kadonaga, J. T. *Genes Dev.* **1998**, *12*, 331.
80. Nebbioso, A.; Clarke, N.; Voltz, E.; Germain, E.; Ambrosino, C.; Bontempo, P.; Alvarez, R.; Schiavone, E. M.; Ferrara, F.; Bresciani, F.; Weisz, A.; de Lera, A. R.; Gronemeyer, H.; Altucci, L. *Nat. Med.* **2005**, *11*, 77.
81. Cooper, M. *Anal. Bioanal. Chem.* **2003**, *377*, 834.
82. Johnsson, B.; Löfås, S.; Lindquist, G. *Anal. Biochem.* **1991**, *198*, 268.

New Anacardic Acid-Inspired Benzamides: Histone Lysine Acetyltransferase Activators

José A. Souto,^[a] Rosaria Benedetti,^[b, d, e] Katharina Otto,^[a] Marco Miceli,^[b] Rosana Álvarez,^{*[a]} Lucia Altucci,^{*[b, c]} and Angel R. de Lera^{*[a]}

A series of *N*-(4-cyano-3-trifluoromethyl-phenyl)-2-ethoxy-6-alkyl (and alkenyl) benzamides related to the anacardic acid derivative CTPB have been prepared from 2,6-dihydroxybenzoic acid with a Suzuki coupling and addition of the anion of 4-cyano-3-trifluoromethylphenylamine to a benzodioxinone as the key steps. In U937 cells, these analogues, in particular **7c**,

7d, **7f** and **7j**, induced cell-cycle arrest in the G1 phase, caused apoptosis in about 20% of the cells, and increased the acetylation levels of H3. These activities correlate with the enzymatic activation of histone lysine acetyltransferases (KATs): CBP and PCAF.

Introduction

Data accumulated over the past decade clearly link cancer onset and tumour progression to the deregulation of the enzymatic machinery responsible for epigenetic modifications of both DNA and histone tails within the nucleosomes—the basic units of chromatin.^[1–5] The “epigenetic marks” on chromatin include methylation of DNA at CpG islands, as well as a variety of covalent modifications (notably methylation, acetylation, ADP-ribosylation, phosphorylation, sumoylation and ubiquitylation) of basic amino acid residues located primarily at the tails of histones H3 and H4.^[6] These alterations become docking sites for additional proteins that trigger the assembly of supramolecular structures,^[7,8] which among other cellular processes regulate chromatin remodelling, cell cycle, splicing, nuclear transport and actin nucleation.^[9–11] The reversible nature of most of the epigenetic modifications^[12] has been exploited for the development of novel approaches to cancer^[11,13–15] and therapies for other diseases as well.^[16]

Histone lysine acetyltransferases¹ (KATs)^[17,18] are responsible for the transfer of acetyl groups to lysine residues, whereas histone deacetylases (HDACs) catalyse the reversal of this covalent modification and remove acetyl substituents. Acetylation (but not methylation) weakens the interactions of histone tails with the negatively charged phosphate groups of DNA in the nucleosome, converting the nontranscribed heterochromatin to the more open euchromatin state, which is now accessible to the transcriptional machinery.^[19]

KATs have been recently grouped into seven families^[17,18] although only four of them have intrinsic KAT activities:^[20] Gcn5 and PCAF, which are related to the yeast KAT; the cyclic adenosine monophosphate response element-binding protein (CREB) binding protein (CBP) and p300, which act as coactivators for a

number of transcription factor complexes;^[21] TAF250, which is part of the basic transcription complex TFIID that binds to the TATA box; and finally SRC-1 and ACTR, which are coactivators for the ligand-activated nuclear receptors, and their KAT activities are controversial.^[21–23]

Although all KAT enzymes require acetyl-CoA as a cofactor, the precise mechanism of acetyl transfer to the lysine residue by the KAT enzyme^[20,24] might vary with isoform. A ternary complex, a “ping-pong” and a “hit and run” mechanism have been proposed.^[16] Regardless of the mechanistic details, dysfunction of acetyltransferase enzymatic activity has been associated to several diseases, including cancer, Huntington’s disease, inflammatory disease, diabetes mellitus and AIDS.^[17] Restoring the balance between acetylation and deacetylation via small-molecule modulation might correct aberrant cell growth and differentiation.^[25] In fact, inhibitors of HDACs display anticancer actions,^[4,26,27] and two drugs—SAHA (also known as vorinostat or Zolinza[®]) and FK228 (also known as romidepsin or Istodax[®])—are in the clinic for the treatment of cutaneous

[a] Dr. J. A. Souto, K. Otto, Prof. Dr. R. Álvarez, Prof. Dr. A. R. de Lera
Departamento de Química Orgánica, Facultad de Química, Universidade de Vigo, Campus As Lagoas-Marcosende, 36310 Vigo (Spain)
Fax: (+34) 986-811-940
E-mail: rar@uvigo.es
qolera@uvigo.es

[b] R. Benedetti, M. Miceli, Prof. Dr. L. Altucci
Dipartimento di Patologia Generale, Seconda Università degli Studi di Napoli, Vico L. de Crecchio 7 80138 Napoli (Italy)
Fax: (+39) 081-450-169
E-mail: lucia.altucci@unina2.it

[c] Prof. Dr. L. Altucci
IGB-CNR, Via Pietro Castellino, 80100 Napoli (Italy)

[d] R. Benedetti
Dipartimento di Fisica, Università di Napoli Federico II, Napoli (Italy)

[e] R. Benedetti
Dipartimento di Chimica Organica e Biochimica, Università di Napoli Federico II, Napoli (Italy)

¹ Traditionally histone acetyltransferases were abbreviated as HATs, however, to reflect their general activity beyond that on histone, the preferred abbreviation for lysine (K) acetyltransferases is now KATs. Further details on this change in nomenclature are given in Reference [17].

T-cell lymphomas. Modulators of KATs (inhibitors or activators) also have the potential to become new generation therapeutics.^[16]

KAT modulators of different structural classes, both of natural and synthetic origin, have been described in the literature (Figure 1).^[16] Bisubstrate analogues, such as LysCoA (**1**) and H3-CoA-20 (**2**) act as inhibitors of p300 and PCAF/MYST Esa1/Tip60, respectively.^[28] Inhibitors discovered by virtual ligand

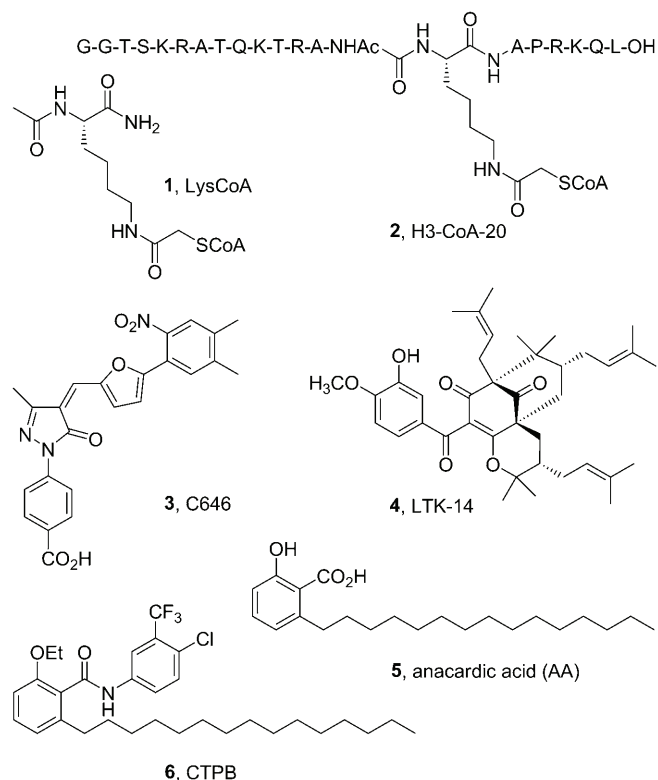


Figure 1. Selected histone acetyltransferase modulators.

screening or rational drug design include isothiazolones, alkylidenemalonates, thiazol-2-yl hydrazones, quinolines, the curcuminoid multiple epigenetic ligands, or the methylenebutyrolactone MB-3, among others.^[16] Recently, C646 (**3**) was described as a selective, linear, competitive inhibitor of p300 (86% inhibition of p300 at 10 μM compared with 10% inhibition for six other KATs) versus acetyl-CoA with a K_i value of 400 nM.^[29] It is the most potent KAT inhibitor reported, about 12-fold more potent than LTK14 (**4**),^[30] a synthetic phloroglucinol structurally related to garcinol.^[31]

6-Pentadecylsalicylic acid (anacardic acid, AA; **5**), the main component of the cashew nut-shell oil, was the first in vitro noncompetitive inhibitor of both p300 and PCAF reported (IC_{50} = 8.5 and 0.5 μM , respectively).^[32] It also inhibits the KAT activity of recombinant pGcn5 from *Plasmodium falciparum*.^[33] Synthetic modifications of anacardic acid **1** have yielded compounds with contrasting epigenetic profiles. In particular, CTPB (*N*-(4-chloro-3-trifluoromethyl-phenyl)-2-ethoxy-6-pentadecyl-

benzamide) **6** was reported as a potent activator of p300/CBP, and moreover, devoid of HDAC inhibitory activity.^[32,34] However, the related benzamides **7a,b** (Figure 2) with a shorter saturated side chain were characterised as p300 inhibitors with a profile similar to the parent **5**.^[35] A series of novel derivatives of CTPB, most notably 4-pyridylamides (**8a,b**; Figure 2) were shown to inhibit p300/CBP in the micromolar range.^[36]

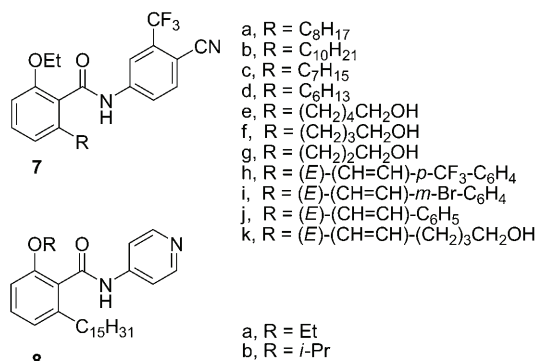


Figure 2. Anacardic acid-inspired amides.

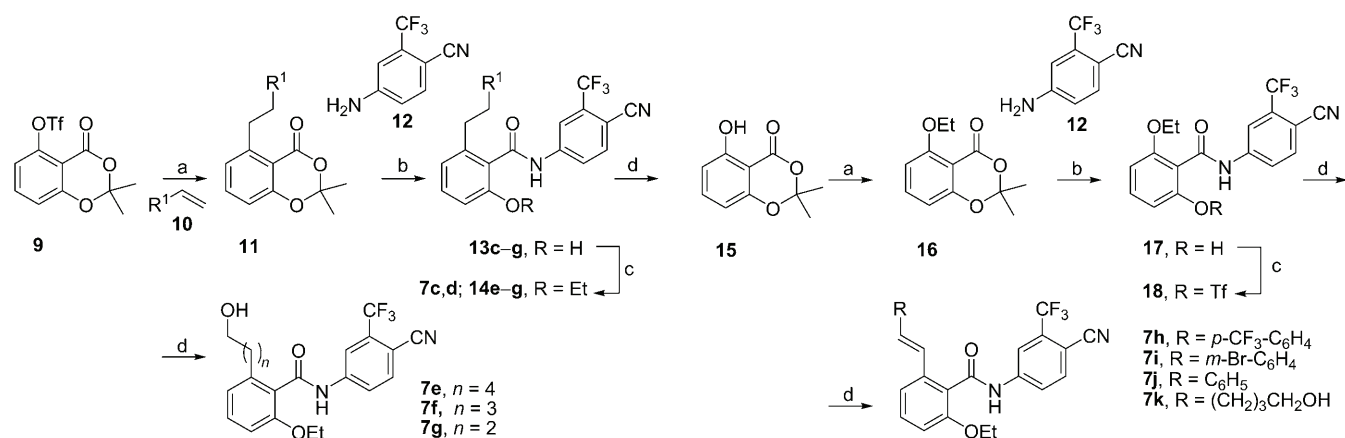
Since the strongest KAT inhibitors (**7a**, with an octyl group being the most potent) had the shortest hydrophobic alkyl chains of the series of CTPB analogues,^[35] we decided to further reduce the size of the chain and incorporate terminal polar and/or unsaturated groups in the same position of the C6-salicylic amide substituent, while preserving the ethoxy^[32] and the 4-cyano-3-trifluoromethylbenzamide functionalities.^[32,35]

Results and Discussion

Synthesis

Following the synthetic approach to the CTPB analogues that uses a Suzuki cross-coupling reaction^[37] between an aryl triflate and different trialkylboranes,^[38] known triflate **9**^[39,35] containing a 1,3-benzodioxinone group^[40–42] was coupled to the trialkylborane obtained by hydroboration of the terminal alkene with 9-BBN in the presence of PdCl₂(dppf), MeONa and KBr.^[42] Five alkenes (1-heptene, **10c**; 1-hexene, **10d**; 4-penten-1-ol, **10e**; 3-buten-1-ol, **10f**; 2-propen-1-ol, **10g**) were selected as precursors of the organoboranes. The combined yields for the hydroboration/coupling step ranged from 39 to 66%.

The acyl transfer/dioxinone deprotection step required the treatment of the corresponding aniline **12** with *n*BuLi in DMPU and heating with **11** at 80 °C, as reported for ester formation starting from similar substrates.^[43] Formation of the ethyl ether from salicylamides **13** provided the final benzamides **7c,d** and the protected primary alcohols **14e–g**, which were deprotected to afford **7e–g** upon treatment with tetra-*n*-butylammonium fluoride (TBAF) in THF (Scheme 1; Table 1).



Scheme 1. Reagents and conditions: a) **10 c–g**, 9-BBN, MeONa, PdCl₂(dppf), KBr, 70 °C, THF; b) Aniline **12**, *n*BuLi, DMPU, 80 °C, 2 h; c) Et₃SO₄, K₂CO₃, acetone; d) TBAF, THF. The yield for each step is given in Table 1.

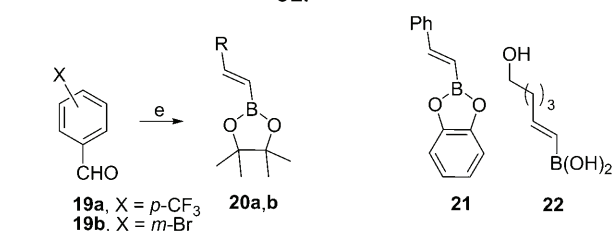
R ¹	Step a		Step b		Step c		Step d	
	P	[%]	P	[%]	P	[%]	P	[%]
C ₅ H ₁₁	11 c	39	13 c	76	7 c	76	–	–
C ₄ H ₉	11 d	41	13 d	65	7 d	46	–	–
(CH ₂) ₂ CH ₂ OTBS	11 e	32	13 e	35	–	–	7 e	61 ^[b]
CH ₂ CH ₂ OTBS	11 f	66	13 f	50	–	–	7 f	51 ^[b]
CH ₂ OTBS	11 g	32	13 g	37	–	–	7 g	97 ^[b]

[a] The product (P) and associated yield (%) is given for each step. R¹ introduced using compounds **10** (see Scheme 1). [b] Combined yield for steps c and d.

A reversal of the strategic key steps is also possible, and this strategy was employed for the synthesis of the C6-unsaturated salicylamides **7 h–k**. The 1,3-benzodioxinone **15** derived from 2,6-dihydroxybenzoic acid^[40–42] (the precursor to triflate **9**) was converted into the ethyl ether **16** as described above (91% yield). Addition of the anion derived from aniline **12** to **16** effected the acyl transfer/deprotection^[43] in 88% yield. Triflate **18** was obtained in 87% yield upon treating **17** with trifluoroacetic anhydride (TFAA) in pyridine at 25 °C (Scheme 2).

The alkenylboron reagents required for the completion of the series of C6-unsaturated salicylamides were acquired following complementary methods. (*E*)-Alkenyl boronates **20 a,b** were obtained in high yield and excellent stereoselectivity from commercially available benzaldehydes **19 a,b** using the Takai–Utimoto condensation reaction,^[44] after activation of 2-(dichloromethyl)pinacolboronate with chromium(II) in the presence of lithium iodide.^[45] Two previously described alkenylboron reagents **21**^[46] and **22**^[47] were obtained by the hydroboration of the precursor alkynes and hydrolysis for **22**.

The Suzuki coupling of triflate **18** and organoboranes **20–22** was complete after about 15 min in concentrated solutions (0.2 M) using microwave irradiation.^[48,49] Unfortunately, the instability of pinacolboronates **20** under the reaction conditions decreased the yield of the corresponding products **7 h** and **7 i**.



Scheme 2. Reagents and conditions: a) EtI, K₂CO₃, acetone, 25 °C, 12 h, 91%; b) **12**, *n*BuLi, DMPU, 80 °C, 2 h, 88%; c) TFAA, pyridine, 25 °C, 87%; d) **20 a,b**, **21** or **22**, Pd(PPh₃)₄, K₂CO₃, dioxane, microwave, 85 °C, 15 min (**7 h**, 43%; **7 i**, 27%; **7 j**, 80%; **7 k**, 92%); e) 2-(Dichloromethyl)pinacolboronate, CrCl₂, Lil, THF, 25 °C, 16 h (**20 a**, 81%; **20 b**, 91%).

Biological evaluation

To evaluate whether these novel CTPB-inspired benzamides are able to have an effect on KAT activity, we tested the compounds in enzymatic and whole-cell assays. In particular, cell-based assays were performed in U937 leukaemia cells to determine the antiproliferative potential and the ability of the synthetic compounds to alter the cell cycle. Compared with the vehicle-treated cells (negative control) and to the cells treated with the pan-HDAC inhibitor SAHA, used as a positive control for its known actions on cell cycle and apoptosis,^[50] at 5 μM the test compounds did not significantly alter the cell cycle. In contrast to SAHA, which accumulates the cell population in the S phase after 24 h of treatment, at the same concentration the synthetic salicylamides showed only a modest effect (~10% increase of U937 cells in the S phase; Figure 3a). However, after 24 h of induction, compounds **7 c–e** and **7 k** at 50 μM induced a time-dependent accumulation of U937 cells in the G1 phase that reached 70% (Figure 3b), doubling the effect of the controls SAHA and AA (**5**). The parent compound CTPB (**6**) had no effect on the cell cycle at the tested concentrations of 5 and 50 μM. The failure of **5** to influence the cell cycle regardless of its concentration (see Figure 3a and 3b) is consistent with reports on its inability to pass through the cell membrane.^[51] In contrast, some of the salicylamides altered the cell cycle, entering cells most likely due to the presence of functionalities that provide greater membrane permeability. In addition, the series of compounds induced a ~20% apoptosis in U937 cells (Figure 3).

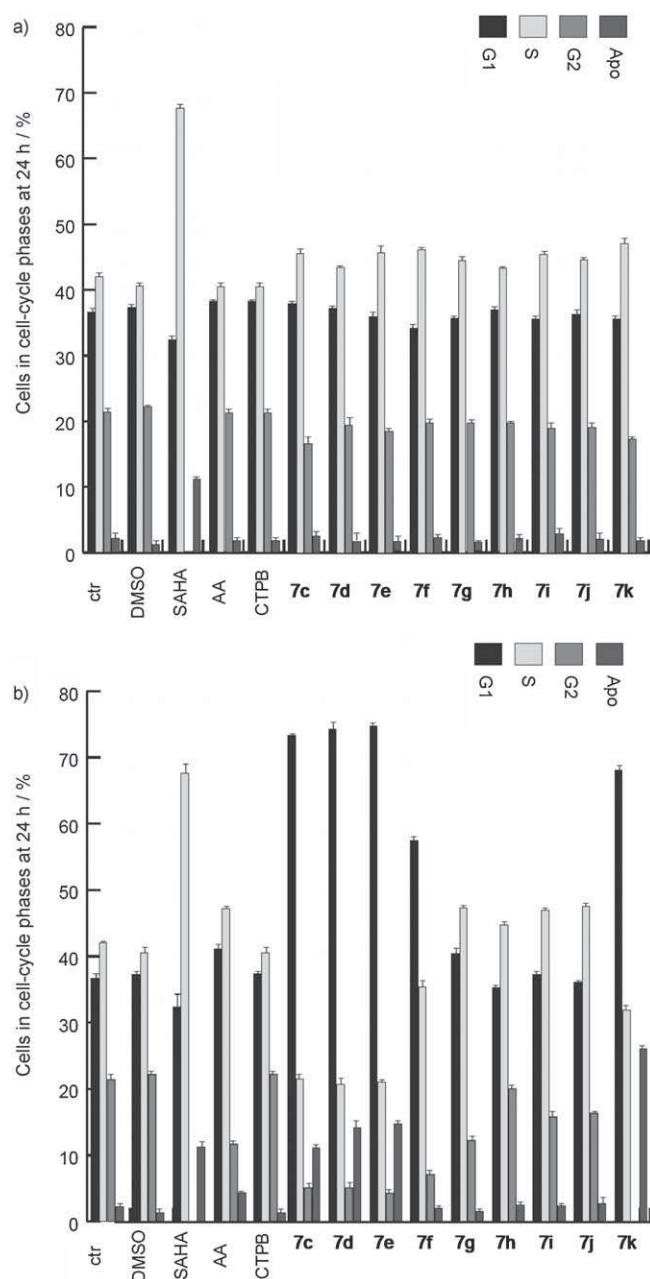


Figure 3. a) Cell-cycle analysis of U937 cells treated with the indicated compounds at 5 μM for 24 h. b) Cell-cycle analysis of U937 cells treated with the indicated compounds at 50 μM for 24 h. Cell-cycle phases (G1, S and S2) and apoptosis (Apo) are shown. The data represent the mean of three independent experiments.

To confirm the general involvement of these CTPB analogues in the modulation of KAT activity; we analysed the acetylation status of the representative histone protein H3, which is dependent upon the opposing activities of HDAC and KAT enzymes (Figure 4a). The activities of these AA-derived benzamides were compared to those of AA (50 μM), CTPB (50 μM), and the HDAC inhibitors SAHA (5 μM) and MS-275 (5 μM). The inhibition of HDACs is demonstrated by an increase in the global level of acetyl groups on H3 lysine tails after treatment of U937 cells for 24 h (Figure 4a), in comparison to the control experiments using SAHA and MS-275. Despite the reported

low cell permeability, CTPB **6** is able to induce an increase in the acetylation of H3 lysine tails due to its action on KAT enzymes (Figure 4a). Interestingly, a similar effect was observed with most of the salicylamides at 50 μM (Figure 4a). This effect can most likely be ascribed to the increase of KAT activity and the up-regulation of the acetylation reaction. Compounds **7c**, **7e**, **7f** and **7k**, which showed induction of KAT activity, also caused significant cell-cycle arrest in the G1 phase (see Figure 3a and 3b, and Figure 4a). The insensitivity of the intracellular acetylation status to the presence of AA, as deduced from Western blot analysis, further confirms its well-known inability to enter the cells.

To evaluate the effective induction of KAT activity, two enzymatic assays were performed: a PCAF and a CBP radioactive assay. Figure 4 shows the correlation between the enzymatic and whole-cell assay results. The CTPB analogues, in particular **7e**, **7f**, **7h**, **7k**, enhanced the CBP acetyltransferase activity by 30–40% relative to the control (Figure 4b). In our previous report, we determined that benzamides **7a** and **7b**, with an *n*-octyl and *n*-decyl chains at C6, respectively, behaved as modest inhibitors of p300. Indeed, the shorter homologue **7c** is a rather weak inhibitor of CBP, but the *n*-hexyl derivative **7d** is inactive, thus signalling the lower limit for modifications at that position with saturated groups.^[35]

Likewise, all the compounds in the series induced activation of PCAF in the radioactive enzymatic assay. Indeed these compounds enhanced the PCAF activity by at least 150%, and in particular **7e**, **7f**, **7g** and **7k** induced a 200–250-fold activation relative to the control (Figure 4c). In both assays, AA behaves as a very potent enzymatic inhibitor,^[32,51] whereas benzamide CTPB **6** is a selective activator of p300/CBP (Figure 4b, 4c and 4d) as previously described.^[32,34] On the contrary, benzamides **7** activate KATs and, moreover, exhibit a preference for the PCAF family. These experiments confirm that the analogues are able to modulate the acetylation balance inside the cell by the direct activation of KAT enzymes.

Conclusions

The development of chemical probes and modulators of KATs has provided valuable insights into the catalytic features of this enzyme class and revealed their roles in various cellular pathways.^[16] The great majority of these modulators are KAT inhibitors with various degrees of potency, selectivity and cell permeability. As far as we know, only the AA-derived benzamide CTPB is an activator of the p300/CBP KAT. However, no drugs have been described that selectively distinguish between the subtypes p300 and CBP or PCAF and GCN5. As a follow-up of our previous studies on the activities of AA-derived CTPB analogues,^[35] we have designed and synthesised a new series of compounds, which carry polar terminal groups to improve the permeability and enhance their activity. From the analysis of the biological readouts, we conclude that these amides act specifically on KAT enzymes both in enzymatic and whole-cell assays. The increase in KAT activity was ~30% for CBP and ~200% for PCAF when the compounds, in particular those with a primary alcohol on the side chain **7e** and **7k**,

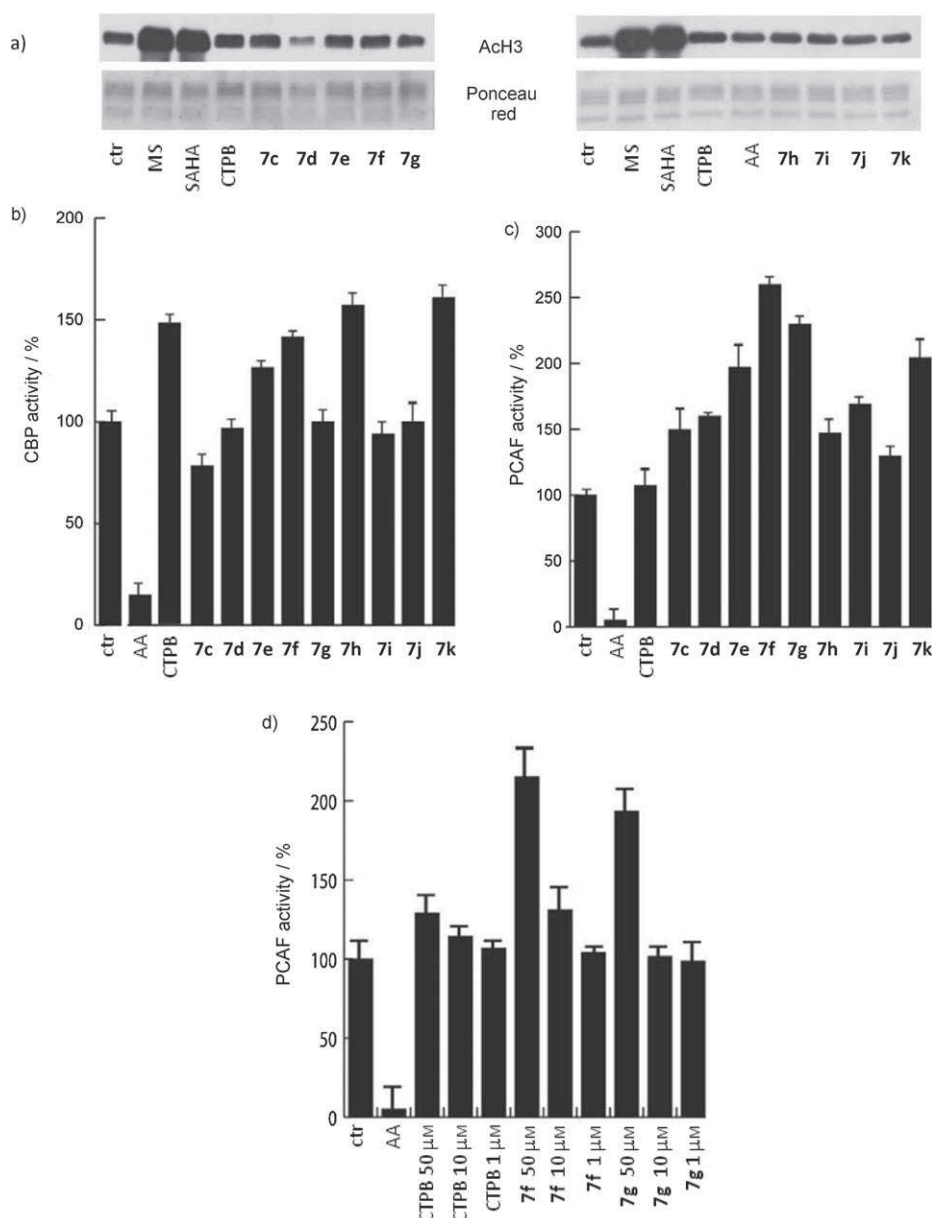


Figure 4. a) Western Blot analysis of histone H3 acetylation carried out in U937 cells after 24 h induction with compounds at 50 μM . b) CBP radioactive assay performed with 1 μg of recombinant CBP enzyme. The compounds were tested at 50 μM and the CBP activity (%) was compared in each case to anacardic acid (AA; 5) and CTPB (6) at the same concentration. c) PCAF radioactive assay performed with 200 ng of recombinant PCAF enzyme. The compounds were tested at 50 μM and the inhibition value was reported as a percentage of residual activity in comparison to the control, to anacardic acid (AA; 5) and to CTPB (6). The data represent the mean of three independent experiments. d) PCAF dose-response assay with the selected compounds (5 and 6 as reference compounds) at three different concentrations (50 μM , 10 μM and 1 μM).

were used at 50 μM . At the same concentration they also showed cell-cycle arrest in the G1 phase and a strong induction of acetylation of H3 tails.

From the limited number of CTPB-related compounds reported,^[32,34–36] the modifications at the C6-position have proved most informative:

- 1) Shorter saturated side chain benzamides **7a, 7b** (Figure 2) revert the modulatory profile of the parent CTPB (**6**)^[32,34] and behave as p300 inhibitors similar to anacardic acid (**5**).^[35]

- 2) Further reduction in the size of the alkyl chain (**7c, 7d**) was inconsequential, thus demonstrating a lower limit for modifications at that position.

- 3) The incorporation of hydroxy groups at the terminus of the C6-group (**7e, 7f, 7g, 7k**) modified the KAT inhibitory activities of the alkylbenzamide analogues **7a, 7b** and provided activators of both p300 and PCAF (Figure 4).

- 4) In contrast to CTPB (**6**), these compounds (most notably **7f** and **7g**) exhibit a preference for the activation of PCAF over p300, thus modifying the selectivity of parent **6**.

An examination of the biological results indicates the lack of a linear correlation between the enzymatic and whole-cell data for every compound. In fact, some of the CTPB analogues show a strong G1 phase blockade but not a direct activation of PCAF and/or CBP. The existence of ancillary mechanisms and additive pathways by which the balance of acetylated/deacetylated histones within a cell is maintained, in addition to the chemical structure of the compound itself, might partially explain some of the differences.

Given that the compounds showing a well-defined KAT activation profile (**7e, 7f, 7g, 7k**) act at a quite high concentration (50 μM), additional chemical modifications of the general scaffold might provide more potent activators that could

become valuable tools for understanding the correlation between the acetylation status of histones and nonhistone proteins, and transcriptional activation.

Experimental Section

Chemistry

General Procedures: Solvents were dried according to published methods and distilled before use. All other reagents were commer-

cial compounds of the highest purity available. All reactions were carried out under argon atmosphere, and those not involving aqueous reagents were carried out in oven-dried glassware. Analytical thin-layer chromatography (TLC) was performed on aluminium plates with Merck kieselgel 60 F₂₅₄ and visualised by UV irradiation (254 nm) or by staining with solution of phosphomolibdic acid. Flash column chromatography was carried out using Merck kieselgel 60 (230–400 mesh) under pressure. UV/VIS spectra were recorded on a Cary 100 bio-spectrophotometer. Infrared (IR) spectra were obtained on a JASCO FTIR 4200 spectrophotometer from a thin film deposited onto a NaCl glass. Mass Spectra (MS) were obtained on a Hewlett-Packard HP59970 instrument operating at 70 eV by electron ionisation. High-resolution mass spectra (HRMS) were taken either on a VG Autospec instrument, a Micromass GC-TOF or a Bruker FT-MS apex-Qe. ¹H NMR spectra were recorded in CDCl₃ and (CD₃)₂CO at room temperature on a Bruker AMX-400 spectrometer at 400 MHz with residual protic solvent as the internal reference (CDCl₃, δ_H = 7.26 ppm; (CD₃)₂CO, δ_H = 2.05 ppm); chemical shifts (δ) are given in parts per million (ppm), and coupling constants (*J*) are given in Hertz (Hz). The proton spectra are reported as follows: δ (multiplicity, coupling constant *J*, number of protons). ¹³C NMR spectra were recorded in CDCl₃ and (CD₃)₂CO at room temperature on the same spectrometer at 100 MHz, with the central peak of CDCl₃ (δ_C = 77.0 ppm) or (CD₃)₂CO (δ_C = 30.8 ppm) as the internal reference. Although DEPT 135 was used to aid the assignment of signals in the ¹³C NMR spectra, the multiplicity is only shown for fluorine-carbon bonds, with the *J*_{C-F} values measured.

2,2-Dimethyl-5-heptyl-4H-1,3-benzodioxin-4-one (11c): *General procedure for the alkyl Suzuki coupling reaction (Method A).* A solution of **10c** (0.09 mL, 0.65 mmol) in THF (0.6 mL) was treated with 9-BBN (1.3 mL, 0.5 M in THF, 0.65 mmol) and the reaction was stirred at 25 °C for 24 h. The mixture was transferred to a flask containing MeONa (0.035 g, 0.65 mmol) and the solution was stirred for 2 h. A mixture of dichloro-1,1'-bis-(diphenylphosphino)ferrocene palladium (0.006 g, 0.018 mmol), KBr (0.087 g, 0.728 mmol) and **9** (0.2 g, 0.61 mmol) in THF (4 mL) was added and the mixture was stirred at 70 °C for 4 h. Hexane (1 mL), aq NaOH (1 mL, 2 M) and H₂O₂ (1 mL, 30% w/w) were then added and the mixture was stirred at 25 °C. The aqueous layer was extracted with Et₂O (×3) and the combined organic layers were washed with a saturated aq NaHCO₃ (×3) and dried (Na₂SO₄), and the solvent was evaporated. The residue was purified by column chromatography (90:10, hexane/EtOAc) to afford **11c** as a yellow oil (70 mg, 39%); ¹H NMR (400 MHz, CDCl₃): δ = 7.37 (t, *J* = 7.9 Hz, 1H), 6.91 (d, *J* = 7.6 Hz, 1H), 6.78 (d, *J* = 8.2 Hz, 1H), 3.07 (t, *J* = 7.7 Hz, 2H), 1.67 (s, 6H, 2CH₃), 1.6–1.5 (m, 2H), 1.5–1.2 (m, 8H), 0.85 ppm (t, *J* = 6.5 Hz, 3H); ¹³C NMR (100 MHz, CDCl₃): δ = 160.2, 157.1, 148.5, 135.0, 125.1, 115.0, 112.1, 104.9, 34.4, 31.8, 31.2, 29.6, 29.1, 25.6 (2C), 22.6, 14.1 ppm; IR (NaCl): ν̄ = 2998 (w, C–H), 2954 (m, C–H), 2926 (s, C–H), 2856 (m, C–H), 1738 (s, C=O), 1605 (m, C=C), 1582 cm⁻¹ (C=C); MS (ESI+): *m/z* (%): 276 [M]⁺ (7), 219 (12), 218 (100), 176 (14), 162 (38), 161 (20), 148 (13), 147 (43), 134 (77), 133 (11), 105 (34), 91 (11), 77 (11); HRMS (ESI+): *m/z* [M]⁺ calcd for C₁₇H₂₄O₃: 276.1725, found: 276.1733.

N-(4-Cyano-3-trifluoromethylphenyl)-6-heptyl-2-hydroxybenzamide (13c): *General procedure for the amidation of dioxinones.* A cooled (0 °C) solution of **12** (0.4 g, 2.15 mmol) and 1,3-dimethyl-3,4,5,6-tetrahydro-2(1H)-pyrimidinone (DMPU; 0.38 mL, 3.14 mmol) in THF (8.3 mL) at 0 °C was treated with *n*BuLi (1.5 mL, 1.40 M in hexane, 2.15 mmol). After stirring for 30 min at 25 °C a solution of **11c** (0.12 g, 0.43 mmol) in THF (8.3 mL) was added and the reaction was stirred at 80 °C for 2 h. Water was added, the layers were

separated and the aqueous layer was extracted with EtOAc (×3). The combined organic layers were washed with 10% aq HCl (×1), water (×2) and brine (×1), dried (Na₂SO₄) and the solvent was evaporated. The residue was purified by column chromatography (85:15, hexane/EtOAc) to afford **13c** as a yellow oil (133 mg, 76%); mp: 147 °C (hexane/acetone); ¹H NMR (400 MHz, (CD₃)₂CO): δ = 10.08 (s, 1H), 8.83 (s, 1H), 8.54 (s, 1H), 8.30 (d, *J* = 8.4 Hz, 1H), 8.07 (d, *J* = 8.4 Hz, 1H), 7.21 (t, *J* = 7.9 Hz, 1H), 6.82 (d, *J* = 7.6 Hz, 1H), 6.81 (d, *J* = 8.2 Hz, 1H), 2.68 (t, *J* = 8.2 Hz, 2H), 1.7–1.5 (m, 2H), 1.3–1.2 (m, 8H), 0.82 ppm (t, *J* = 6.4 Hz, 3H); ¹³C NMR (100 MHz, (CD₃)₂CO): δ = 167.3, 154.0, 144.0, 142.0, 136.3, 132.7 (²*J*_{C-F} = 32.1 Hz), 130.4, 124.6, 122.7 (¹*J*_{C-F} = 273.1 Hz), 121.9, 120.7, 116.7 (³*J*_{C-F} = 5.6 Hz), 115.5, 113.3, 102.8, 32.9, 31.5, 31.3, 29.2, 28.8, 22.4, 13.4 ppm; IR (NaCl): ν̄ = 3600–3000 (br, N–H and O–H), 2929 (m, C–H), 2855 (m, C–H), 1651 (m, C=O), 1588 (s, C=C), 1535 (s, C=C), 1426 (s), 1188 cm⁻¹ (s); MS (ESI+): *m/z* (%): 404 [M]⁺ (8), 273 (11), 220 (15), 219 (100), 218 (21), 186 (37), 134 (20), 108 (21), 107 (24); HRMS (ESI+): *m/z* [M]⁺ calcd for C₂₂H₂₃F₃N₂O₂: 404.1712, found: 404.1731; Anal. calcd for C₂₂H₂₃F₃N₂O₂: C, 65.34; H, 5.73; found: C, 64.79; H, 5.74.

N-(4-Cyano-3-trifluoromethylphenyl)-2-ethoxy-6-heptylbenzamide (7c): *General procedure for the alkylation of phenols.* A solution of **13c** (0.1 g, 0.25 mmol) in acetone (10 mL) was treated sequentially with K₂CO₃ (0.085 g, 0.617 mmol) and Et₂SO₄ (0.071 mL, 0.54 mmol). After stirring for 3 h, saturated aq NH₄Cl was added (1.5 mL) and the aqueous layer was extracted with Et₂O (×3). The combined organic layers were washed with brine (×2), dried (Na₂SO₄) and the solvent was evaporated. The residue was purified by column chromatography (90:10, hexane/EtOAc) to afford **7c** as a white solid (82 mg, 76%); mp: 80 °C (hexane/EtOAc); ¹H NMR (400 MHz, (CD₃)₂CO): δ = 10.04 (s, 1H), 8.51 (s, 1H), 8.26 (d, *J* = 8.5 Hz, 1H), 8.06 (d, *J* = 8.5 Hz, 1H), 7.32 (dd, *J* = 8.3, 7.6 Hz, 1H), 6.90 (d, *J* = 8.3 Hz, 1H), 6.89 (d, *J* = 7.6 Hz, 1H), 4.07 (q, *J* = 6.9 Hz, 2H), 2.66 (t, *J* = 7.7 Hz, 2H), 1.7–1.6 (m, 2H), 1.4–1.2 (m, 11H), 0.81 ppm (t, *J* = 6.8 Hz, 3H); ¹³C NMR (100 MHz, (CD₃)₂CO): δ = 168.9, 157.6, 145.8, 143.8, 138.2, 134.7 (²*J*_{C-F} = 31.8 Hz), 132.3, 128.2, 124.7 (¹*J*_{C-F} = 272.7 Hz), 123.6, 123.5, 118.5 (³*J*_{C-F} = 5.7 Hz), 117.4, 111.5, 104.8, 65.9, 34.7 (2C), 33.4, 33.1, 31.4, 24.2, 16.0, 15.3 ppm; IR (NaCl): ν̄ = 3300–3100 (br, N–H), 2928 (s, C–H), 2856 (m, C–H), 1668 (m, C=O), 1587 (s, C=C), 1528 (s, C=C), 1326 (s), 1269 (s), 1179 (s), 1140 cm⁻¹ (s); MS (ESI+): *m/z* (%): 432 [M]⁺ (3), 248 (60), 247 (100), 147 (19), 145 (16), 135 (19), 133 (15), 107 (14), 105 (11); HRMS (ESI+): *m/z* [M]⁺ calcd for C₂₄H₂₇F₃N₂O₂: 432.2025, found: 432.2024; Anal. calcd for C₂₄H₂₇F₃N₂O₂: C, 66.65; H, 6.29; found: C, 66.81; H, 6.66.

2,2-Dimethyl-5-hexyl-4H-1,3-benzodioxin-4-one (11d): Following the general procedure described for the Suzuki cross coupling (Method A), the reaction of **9** (0.25 g, 0.07 mmol), **10d** (0.06, 0.65 mmol), 9-BBN (1.3 mL, 0.65 mmol), MeONa (0.04 g, 0.65 mmol), PdCl₂(dppf) (6 mg, 0.02 mmol) and KBr (0.09 g, 0.73 mmol) in THF (5.4 mL) afforded, after purification by column chromatography (90:10, hexane/EtOAc), **11d** as a colourless oil (71 mg, 41%); ¹H NMR (400 MHz, CDCl₃): δ = 7.40 (t, *J* = 7.9 Hz, 1H), 6.94 (d, *J* = 7.6 Hz, 1H), 6.80 (d, *J* = 8.2 Hz, 1H), 3.09 (t, *J* = 7.9 Hz, 2H), 1.70 (s, 6H, 2CH₃), 1.6–1.5 (m, 2H), 1.4–1.3 (m, 6H), 0.89 ppm (t, *J* = 6.2 Hz, 3H); ¹³C NMR (100 MHz, CDCl₃): δ = 160.2, 157.1, 148.5, 135.0, 125.0, 115.0, 112.0, 104.9, 34.3, 31.6, 31.1, 29.3, 25.6 (2C), 22.6, 14.0 ppm; IR (NaCl): ν̄ = 2998 (w, C–H), 2925 (s, C–H), 2855 (m, C–H), 1739 (s, C=O), 1605 (m, C=C), 1582 (m, C=C), 1312 (m), 1213 (m), 1042 cm⁻¹ (m); MS (ESI+): *m/z* (%): 262 [M]⁺ (8), 204 (100), 162 (32), 147 (22), 134 (57), 105 (25); HRMS (ESI+): *m/z* [M]⁺ calcd for C₁₆H₂₂O₃: 262.1569, found: 262.1572.

N-(4-Cyano-3-trifluoromethylphenyl)-6-hexyl-2-hydroxybenzamide (13 d): Following the general procedure described for amide formation, the reaction of **11 d** (0.06 g, 0.23 mmol), **12** (0.21 g, 1.15 mmol), *n*BuLi (0.82 mL, 1.40 M in hexane, 1.15 mmol) and DMPU (0.2 mL, 1.68 mmol) in THF (8.8 mL) afforded, after purification by column chromatography (80:20, hexane/EtOAc), **13 d** as a white solid (58 mg, 65%); mp: 161 °C (hexane/acetone); ¹H NMR (400 MHz, (CD₃)₂CO): δ = 10.07 (br, 1H), 8.54 (s, 1H), 8.29 (d, *J* = 8.4 Hz, 1H), 8.07 (d, *J* = 8.5 Hz, 1H), 7.21 (t, *J* = 7.9 Hz, 1H), 6.82 (d, *J* = 7.7 Hz, 1H), 6.81 (d, *J* = 8.1 Hz, 1H), 2.85 (br, 1H), 2.68 (t, *J* = 7.9 Hz, 2H), 1.7–1.6 (m, 2H), 1.4–1.3 (m, 2H), 1.3–1.2 (m, 4H), 0.82 ppm (t, *J* = 6.7 Hz, 3H); ¹³C NMR (100 MHz, (CD₃)₂CO): δ = 167.2, 154.0, 143.9, 142.0, 136.3, 132.7 (²*J*_{C-F} = 31.3 Hz), 130.4, 124.5, 123.0 (¹*J*_{C-F} = 273.0 Hz), 121.9, 120.7, 116.7 (³*J*_{C-F} = 5.7 Hz), 115.5, 113.3, 102.9, 32.9, 31.4, 31.2, 28.9, 22.2, 13.3 ppm; IR (NaCl): $\tilde{\nu}$ = 3600–3000 (br, N–H and O–H), 3020 (m, C–H), 2931 (m, C–H), 2857 (w, C–H), 1654 (m, C=O), 1588 (s, C=C), 1534 (s, C=C), 1426 (s), 1331 (s), 1217 cm⁻¹ (s); MS (ESI⁺): *m/z* [M]⁺ (7), 1212 (29), 205 (100), 186 (54), 108 (31), 107 (34), 77 (18); HRMS (ESI⁺): *m/z* [M]⁺ calcd for C₂₁H₂₁F₃N₂O₂: 390.1555, found: 390.1552.

N-(4-Cyano-3-trifluoromethylphenyl)-2-ethoxy-6-hexylbenzamide (7 d): Following the general procedure described for the alkylation of phenols, the reaction of **13 d** (0.03 g, 0.08 mmol), Et₂SO₄ (0.02 mL, 0.17 mmol) and K₂CO₃ (0.03 g, 0.19 mmol) in acetone (3.2 mL) afforded, after purification by column chromatography (90:10, hexane/EtOAc), **7 d** as a white solid (15 mg, 46%); mp: 109 °C (hexane/EtOAc); ¹H NMR (400 MHz, CDCl₃): δ = 8.1–8.0 (m, 3H), 7.81 (d, *J* = 8.2 Hz, 1H), 7.31 (t, *J* = 8.0 Hz, 1H), 6.89 (d, *J* = 7.7 Hz, 1H), 6.80 (d, *J* = 8.3 Hz, 1H), 4.08 (q, *J* = 6.9 Hz, 2H), 2.71 (t, *J* = 7.7 Hz, 2H), 1.6–1.5 (m, 2H), 1.4–1.2 (m, 9H), 0.85 ppm (t, *J* = 6.5 Hz, 3H); ¹³C NMR (100 MHz, CDCl₃): δ = 166.5, 155.5, 143.6, 142.4, 136.0, 134.1 (²*J*_{C-F} = 33.0 Hz), 131.2, 124.6, 122.6, 122.2 (¹*J*_{C-F} = 274.0 Hz), 121.7, 117.0 (³*J*_{C-F} = 4.8 Hz), 115.6, 109.7, 104.1, 64.5, 33.4, 31.6, 31.5, 29.2, 22.5, 14.8, 14.0 ppm; IR (NaCl): $\tilde{\nu}$ = 3500–3100 (br, N–H), 2929 (s, C–H), 2857 (m, C–H), 1668 (m, C=O), 1587 (s, C=C), 1528 (s, C=C), 1327 (s), 1179 (s), 1140 cm⁻¹ (s); MS (ESI⁺): *m/z* (%): 418 [M]⁺ (6), 234 (99), 233 (100), 205 (22), 147 (47), 145 (63), 135 (58), 134 (29), 133 (52), 107 (52), 105 (35), 91 (29), 77 (28); HRMS (ESI⁺): *m/z* [M]⁺ calcd for C₂₃H₂₅F₃N₂O₂: 418.1868, found: 418.1870; Anal. calcd for C₂₃H₂₅F₃N₂O₂: C, 66.02; H, 6.02; found: C, 66.21; H, 6.07.

2,2-Dimethyl-5-(tert-butyl)dimethylsilyloxybut-1-yl)-4H-1,3-benzodioxin-4-one (11 e): Following the general procedure described for the Suzuki cross coupling (Method A), the reaction of **9** (0.25 g, 0.07 mmol), **10 e** (0.13 g, 0.65 mmol), 9-BBN (1.3 mL, 0.5 M in THF, 0.65 mmol), MeONa (0.04 g, 0.65 mmol), PdCl₂(dppf) (6 mg, 0.02 mmol) and KBr (0.09 g, 0.73 mmol) in THF (5.4 mL) afforded, after purification by column chromatography (90:10, hexane/EtOAc), **11 e** as a colourless oil (80 mg, 32%); ¹H NMR (400 MHz, CDCl₃): δ = 7.40 (t, *J* = 7.9 Hz, 1H), 6.93 (d, *J* = 7.6 Hz, 1H), 6.81 (d, *J* = 8.2 Hz, 1H), 3.61 (t, *J* = 6.5 Hz, 2H), 3.09 (t, *J* = 7.7 Hz, 2H), 1.70 (s, 6H, 2CH₃), 1.6–1.4 (m, 6H), 0.89 (s, 9H, SiC(CH₃)₃), 0.04 ppm (s, 6H, 2SiCH₃); ¹³C NMR (100 MHz, CDCl₃): δ = 160.2, 157.1, 148.3, 135.1, 125.1, 115.1, 112.0, 104.9, 63.1, 34.3, 32.7, 30.9, 26.0 (3C), 25.8, 25.6 (2C), 18.4, –5.2 ppm (2C); IR (NaCl): $\tilde{\nu}$ = 2929 (m, C–H), 2857 (m, C–H), 1740 (s, C=O), 1606 (m, C=C), 1582 (s, C=C), 1476 cm⁻¹ (s, C=C); MS (ESI⁺): 401 [M+Na]⁺ (100), 379 [M+H]⁺ (76), 287 (9), 201 (20); HRMS (ESI⁺): *m/z* [M+H]⁺ calcd for C₂₁H₃₅O₄Si: 379.2299, found: 379.2300.

N-(4-Cyano-3-trifluoromethylphenyl)-6-(5-tert-butyl)dimethylsilyloxybut-1-yl)-2-hydroxybenzamide (13 e): Following the general procedure described for amide formation, the reaction of **11 e**

(0.08 g, 0.21 mmol), **12** (0.20 g, 1.05 mmol), *n*BuLi (0.75 mL, 1.40 M in hexane, 1.05 mmol) and DMPU (0.19 mL, 1.54 mmol) in THF (8.1 mL) afforded, after purification by column chromatography (80:20, hexane/EtOAc), **13 e** as a colourless oil (37 mg, 35%); ¹H NMR (400 MHz, (CD₃)₂CO): δ = 10.00 (br, 1H), 8.86 (s, 1H), 8.54 (s, 1H), 8.30 (d, *J* = 8.2 Hz, 1H), 8.07 (d, *J* = 8.3 Hz, 1H), 7.21 (t, *J* = 8.0 Hz, 1H), 6.82 (d, *J* = 7.6 Hz, 1H), 6.81 (d, *J* = 8.2 Hz, 1H), 3.59 (t, *J* = 6.2 Hz, 2H), 2.69 (t, *J* = 7.9 Hz, 2H), 1.7–1.4 (m, 6H), 0.86 (s, 9H, SiC(CH₃)₃), 0.01 ppm (s, 6H, 2SiCH₃); ¹³C NMR (100 MHz, (CD₃)₂CO): δ = 167.2, 154.1, 144.0, 141.9, 136.3, 132.8 (²*J*_{C-F} = 32.1 Hz), 130.4, 124.5, 122.8 (¹*J*_{C-F} = 273.0 Hz), 121.9, 120.7, 116.7 (³*J*_{C-F} = 4.9 Hz), 115.5, 113.3, 102.9, 62.5, 33.0, 32.4, 31.1, 25.5, 25.4 (3C), 17.9, –6.1 ppm (2C); IR (NaCl): $\tilde{\nu}$ = 3500–3000 (br, N–H and O–H), 2931 (s, C–H), 2858 (m, C–H), 1656 (m, C=O), 1588 (s, C=C), 1533 (s, C=C), 1426 (s), 1330 cm⁻¹ (s); MS (ESI⁺): 507 [M+H]⁺ (24), 371 (56), 197 (100); HRMS (ESI⁺): *m/z* [M+H]⁺ calcd for C₂₆H₃₄F₃N₂O₃Si: 507.2285, found: 507.2298.

N-(4-Cyano-3-trifluoromethylphenyl)-2-ethoxy-6-(5-hydroxypent-1-yl)benzamide (7 e): Following the general procedure described for the alkylation of phenols, the reaction of **13 e** (0.03 g, 0.05 mmol), Et₂SO₄ (0.02 mL, 0.12 mmol), K₂CO₃ (0.02 g, 0.13 mmol) in acetone (2.1 mL) afforded, after purification by column chromatography (90:10, hexane/EtOAc), a colourless oil (16 mg) that was used in the next step without further purification. *General procedure for the deprotection of silyl ethers.* A solution of the residue obtained above (0.02 g, 0.03 mmol) in THF (0.5 mL) at 0 °C was treated with TBAF (0.05 mL, 1 M in THF, 0.055 mmol) and stirred at RT for 5 h. The mixture was diluted with EtOAc and washed with saturated aq NaHCO₃ (×3). The aqueous layer was extracted with EtOAc (×3) and the combined organic layers were washed with brine (×3), dried (Na₂SO₄) and the solvent was evaporated. The residue was purified by column chromatography (50:50, hexane/EtOAc) to afford **7 e** as a colourless oil (8 mg, 61% combined yield); ¹H NMR (400 MHz, CDCl₃): δ = 8.27 (s, 1H), 8.06 (s, 1H), 8.04 (d, *J* = 8.1 Hz, 1H), 7.82 (d, *J* = 8.2 Hz, 1H), 7.32 (t, *J* = 8.0 Hz, 1H), 6.90 (d, *J* = 7.7 Hz, 1H), 6.81 (d, *J* = 8.3 Hz, 1H), 4.09 (q, *J* = 6.6 Hz, 2H), 3.60 (t, *J* = 6.3 Hz, 2H), 2.74 (t, *J* = 7.6 Hz, 2H), 1.7–1.4 ppm (m, 9H); ¹³C NMR (100 MHz, CDCl₃): δ = 166.6, 155.6, 143.0, 142.4, 136.0, 134.1 (²*J*_{C-F} = 33.0 Hz), 131.2, 124.8, 122.5, 122.2 (¹*J*_{C-F} = 273.1 Hz), 121.7, 117.1 (³*J*_{C-F} = 4.8 Hz), 115.6, 109.8, 104.1, 64.5, 62.7, 33.2, 32.3, 30.9, 25.4, 14.8 ppm; IR (NaCl): $\tilde{\nu}$ = 3500–3000 (br, N–H and O–H), 2932 (s, C–H), 2859 (m, C–H), 1679 (m, C=O), 1588 (s, C=C), 1529 (s, C=C), 1327 (s), 1138 cm⁻¹ (s); MS (ESI⁺): 443 [M+Na]⁺ (33), 421 [M+H]⁺ (100); HRMS (ESI⁺): *m/z* [M+H]⁺ calcd for C₂₂H₂₄F₃N₂O₃: 421.1734, found: 421.1736.

2,2-Dimethyl-5-(tert-butyl)dimethylsilyloxybut-1-yl)-4H-1,3-benzodioxin-4-one (11 f): Following the general procedure described for the Suzuki cross coupling (Method A), the reaction of **9** (0.25 g, 0.07 mmol), **10 f** (0.12 g, 0.65 mmol), 9-BBN (1.3 mL, 0.5 M in THF, 0.65 mmol), MeONa (0.04 g, 0.65 mmol), PdCl₂(dppf) (6 mg, 0.02 mmol) and KBr (0.09 g, 0.73 mmol) in THF (5.4 mL) afforded, after purification by column chromatography (90:10, hexane/EtOAc), **11 f** as a colourless oil (160 mg, 66%); ¹H NMR (400 MHz, CDCl₃): δ = 7.39 (t, *J* = 7.9 Hz, 1H), 6.93 (d, *J* = 7.6 Hz, 1H), 6.80 (d, *J* = 8.2 Hz, 1H), 3.63 (t, *J* = 5.8 Hz, 2H), 3.11 (t, *J* = 7.0 Hz, 2H), 1.69 (s, 6H, 2CH₃), 1.7–1.6 (m, 4H), 0.88 (s, 9H, SiC(CH₃)₃), 0.03 ppm (s, 6H, 2SiCH₃); ¹³C NMR (100 MHz, CDCl₃): δ = 160.2, 157.1, 148.1, 135.1, 125.1, 115.2, 112.1, 104.9, 63.1, 34.0, 32.7, 27.3, 26.0 (3C), 25.6 (2C), 18.3, –5.2 ppm (2C); IR (NaCl): $\tilde{\nu}$ = 2929 (s, C–H), 2857 (m, C–H), 1739 (s, C=O), 1605 (m, C=C), 1582 (m, C=C), 1312 (m), 1217 cm⁻¹ (m); MS (ESI⁺): 387 [M+Na]⁺ (42), 365 [M+H]⁺ (100);

HRMS (ESI+): m/z $[M+H]^+$ calcd for $C_{20}H_{33}O_4Si$: 365.2143, found: 365.2142.

N-(4-Cyano-3-(trifluoromethyl)phenyl)-6-(4-tert-butylidimethylsilyloxybut-1-yl)-2-hydroxybenzamide (13 f): Following the general procedure described for amide formation, the reaction of **11 f** (0.16 g, 0.44 mmol), **12** (0.41 g, 2.20 mmol), *n*BuLi (1.57 mL, 1.40 M in hexane, 2.20 mmol) and DMPU (0.39 mL, 3.20 mmol) in THF (17 mL) afforded, after purification by column chromatography (80:20, hexane/EtOAc), **13 f** as a colourless oil (109 mg, 50%); 1H NMR (400 MHz, $(CD_3)_2CO$): δ = 10.06 (br, 1H), 8.54 (s, 1H), 8.30 (d, J = 8.5 Hz, 1H), 8.06 (d, J = 8.6 Hz, 1H), 7.21 (t, J = 7.9 Hz, 1H), 6.82 (d, J = 7.6 Hz, 1H), 6.81 (d, J = 7.6 Hz, 1H), 3.61 (t, J = 6.3 Hz, 2H), 2.71 (t, J = 7.4 Hz, 2H), 1.7–1.4 (m, 4H), 0.84 (s, 9H, SiC(CH₃)₃), –0.01 ppm (s, 6H, 2SiCH₃); ^{13}C NMR (100 MHz, $(CD_3)_2CO$): δ = 167.3, 154.1, 144.0, 141.9, 136.3, 132.8 ($^2J_{C-F}$ = 32.1 Hz), 130.4, 124.6, 122.8 ($^1J_{C-F}$ = 273.0 Hz), 121.9, 120.6, 116.7 ($^3J_{C-F}$ = 4.1 Hz), 115.6, 113.4, 102.8, 62.5, 32.7, 32.5, 27.6, 25.4 (3C), 17.9, –6.1 ppm (2C); IR (NaCl): $\tilde{\nu}$ = 3500–3000 (br, N–H and O–H), 2953 (s, C–H), 2931 (s, C–H), 2857 (m, C–H), 1656 (m, C=O), 1588 (s, C=C), 1533 (s, C=C), 1426 (s), 1329 (s), 1187 cm^{-1} (m); MS (ESI+): 515 $[M+Na]^+$ (38), 493 $[M+H]^+$ (100); HRMS (ESI+): m/z $[M+H]^+$ calcd for $C_{25}H_{32}F_3N_2O_3Si$: 493.2129, found: 493.2128.

N-(4-Cyano-3-trifluoromethylphenyl)-2-ethoxy-6-(4-hydroxybut-1-yl)benzamide (7 f): Following the general procedure described for the alkylation of phenols, the reaction of **13 f** (0.08 g, 0.16 mmol), Et₂SO₄ (0.05 mL, 0.36 mmol), K₂CO₃ (0.06 g, 0.41 mmol) in acetone (6.5 mL) afforded, after purification by column chromatography (80:20, hexane/EtOAc), a colourless oil (67 mg) that was used in the next step without further purification. Following the general procedure described for the deprotection of silyl ethers, the reaction of the residue obtained above (67 mg, 0.129 mmol) and TBAF (0.19 mL, 1 M in THF, 0.19 mmol) in THF (2.2 mL) afforded, after purification by column chromatography (60:40, hexane/EtOAc), **7 f** as a colourless oil (27 mg, 51%); 1H NMR (400 MHz, $(CD_3)_2CO$): δ = 10.07 (br, 1H), 8.51 (s, 1H), 8.26 (d, J = 7.1 Hz, 1H), 8.07 (d, J = 8.5 Hz, 1H), 7.33 (t, J = 8.0 Hz, 1H), 6.92 (d, J = 7.4 Hz, 2H), 4.08 (q, J = 7.0 Hz, 2H), 3.50 (t, J = 6.0 Hz, 2H), 3.39 (t, J = 5.2 Hz, 1H), 2.70 (t, J = 7.8 Hz, 2H), 1.7–1.5 (m, 4H), 1.30 ppm (t, J = 6.9 Hz, 3H); ^{13}C NMR (100 MHz, $(CD_3)_2CO$): δ = 167.0, 155.8, 143.9, 141.7, 136.3, 132.8 ($^2J_{C-F}$ = 31.3 Hz), 130.4, 126.3, 122.7 ($^1J_{C-F}$ = 273.9 Hz), 121.9, 121.6, 116.7 ($^3J_{C-F}$ = 4.8 Hz), 115.5, 109.6, 102.9, 63.9, 61.3, 32.6, 32.5, 27.6, 14.1 ppm; IR (NaCl): $\tilde{\nu}$ = 3500–3000 (br, N–H and O–H), 2933 (m, C–H), 1678 (m, C=O), 1588 (s, C=C), 1529 (s, C=C), 1327 cm^{-1} (s); MS (ESI+): 429 $[M+Na]^+$ (23), 407 $[M+H]^+$ (100); HRMS (ESI+): m/z $[M+H]^+$ calcd for $C_{21}H_{22}F_3N_2O_3$: 407.1577, found: 407.1585.

2,2-Dimethyl-5-(3-tert-butylidimethylsilyloxyprop-1-yl)-4H-1,3-benzodioxin-4-one (11 g): Following the general procedure described for the Suzuki cross coupling (Method A), **9** (0.25 g, 0.07 mmol), **10 g** (0.11 g, 0.65 mmol), 9-BBN (1.3 mL, 0.5 M in THF, 0.65 mmol), MeONa (0.04 g, 0.65 mmol), PdCl₂(dppf) (6 mg, 0.02 mmol) and KBr (0.09 g, 0.73 mmol) in THF (5.4 mL) afforded, after purification by column chromatography (90:10, hexane/EtOAc), **11 g** as a colourless oil (74 mg, 32%); 1H NMR (400 MHz, CDCl₃): δ = 7.41 (t, J = 7.9 Hz, 1H), 6.96 (d, J = 7.6 Hz, 1H), 6.81 (d, J = 8.2 Hz, 1H), 3.69 (t, J = 6.4 Hz, 2H), 3.14 (t, J = 7.7 Hz, 2H), 1.84 (t, J = 6.6 Hz, 2H), 1.70 (s, 6H, 2CH₃), 0.91 (s, 9H, SiC(CH₃)₃), 0.07 ppm (s, 6H, 2SiCH₃); ^{13}C NMR (100 MHz, CDCl₃): δ = 160.2, 157.1, 147.8, 135.1, 125.2, 115.2, 112.1, 105.0, 62.8, 34.0, 30.7, 26.0 (3C), 25.6 (2C), 18.3, –5.3 ppm (2C); IR (NaCl): $\tilde{\nu}$ = 2952 (m, C–H), 2928 (m, C–H), 2887 (w, C–H), 2857 (m, C–H), 1739 (s, C=O), 1606 (m, C=C), 1582 (m, C=C), 1476 (s), 1313 (s), 1271 cm^{-1} (s); MS

(ESI+): 373 $[M+Na]^+$ (71), 351 $[M+H]^+$ (100); HRMS (ESI+): m/z $[M+H]^+$ calcd for $C_{19}H_{31}O_4Si$: 351.1986, found: 351.1989.

N-(4-Cyano-3-(trifluoromethyl)phenyl)-6-(3-tert-butylidimethylsilyloxyprop-1-yl)-2-hydroxybenzamide (13 g): Following the general procedure described for amide formation, the reaction of **11 g** (0.11 g, 0.17 mmol), **12** (0.16 g, 0.85 mmol), *n*BuLi (0.57 mL, 1.50 M in hexane, 0.85 mmol) and DMPU (0.15 mL, 1.24 mmol) in THF (6.5 mL) afforded, after purification by column chromatography (80:20, hexane/EtOAc), **13 g** as a colourless oil (30 mg, 37%); 1H NMR (400 MHz, $(CD_3)_2CO$): δ = 10.07 (br, 1H), 8.57 (s, 1H), 8.27 (d, J = 8.5 Hz, 1H), 8.06 (d, J = 8.5 Hz, 1H), 7.22 (t, J = 7.9 Hz, 1H), 6.9–6.8 (m, 2H), 3.65 (t, J = 6.1 Hz, 2H), 2.75 (t, J = 7.8 Hz, 2H), 1.9–1.8 (m, 2H), 0.83 (s, 9H, SiC(CH₃)₃), 0.00 ppm (s, 6H, 2SiCH₃); ^{13}C NMR (100 MHz, $(CD_3)_2CO$): δ = 167.2, 154.1, 144.0, 141.5, 136.2, 132.7 ($^2J_{C-F}$ = 34.5 Hz), 130.4, 124.7, 122.7 ($^1J_{C-F}$ = 272.5 Hz), 121.9, 120.7, 116.7 ($^3J_{C-F}$ = 5.6 Hz), 115.6, 113.3, 102.8, 62.3, 34.5, 29.5, 25.3 (3C), 17.8, –6.1 ppm (2C); IR (NaCl): $\tilde{\nu}$ = 3500–3000 (br, N–H and O–H), 2928 (m, C–H), 2858 (m, C–H), 1652 (m, C=O), 1588 (s, C=C), 1534 (s, C=C), 1427 (s), 1330 cm^{-1} (s); MS (ESI+): 501 $[M+Na]^+$ (100), 479 $[M+H]^+$ (14); HRMS (ESI+): m/z $[M+H]^+$ calcd for $C_{24}H_{30}F_3N_2O_3Si$: 479.1972, found: 479.1984.

N-(4-Cyano-3-trifluoromethylphenyl)-2-ethoxy-6-(3-hydroxyprop-1-yl)benzamide (7 g): Following the general procedure described for the alkylation of phenols, the reaction of **13 g** (0.03 g, 0.07 mmol), Et₂SO₄ (0.02 mL, 0.16 mmol) and K₂CO₃ (0.03 g, 0.18 mmol) in acetone (2.8 mL) afforded, after purification by column chromatography (80:20, hexane/EtOAc), a colourless oil (25 mg) that was used in the next step without further purification. Following the general procedure described for the deprotection of silyl ethers, the reaction of the residue obtained above (24 mg, 0.047 mmol) and TBAF (0.071 mL, 1 M in THF, 0.071 mmol) in THF (0.8 mL) afforded, after purification by column chromatography (60:40, hexane/EtOAc), **7 g** as a colourless oil (18 mg, 97%); 1H NMR (400 MHz, $(CD_3)_2CO$): δ = 10.08 (s, 1H), 8.49 (s, 1H), 8.25 (d, J = 8.4 Hz, 1H), 8.05 (d, J = 8.5 Hz, 1H), 7.33 (t, J = 8.0 Hz, 1H), 6.9–6.8 (m, 2H), 4.07 (q, J = 7.0 Hz, 2H), 3.6–3.5 (m, 2H), 2.74 (t, J = 8.5 Hz, 2H), 1.9–1.8 (m, 2H), 1.29 ppm (t, J = 6.9 Hz, 3H); ^{13}C NMR (100 MHz, $(CD_3)_2CO$): δ = 169.0, 157.7, 145.8, 143.3, 138.2, 134.7 ($^2J_{C-F}$ = 31.0 Hz), 132.4, 128.4, 125.1 ($^1J_{C-F}$ = 270.6 Hz), 123.9, 123.5, 118.7 ($^3J_{C-F}$ = 4.9 Hz), 117.4, 111.6, 104.8, 65.9, 62.7, 36.2, 31.1, 16.0 ppm; IR (NaCl): $\tilde{\nu}$ = 3500–3200 (br, N–H and O–H), 2928 (m, C–H), 1671 (m, C=O), 1589 (s, C=C), 1526 (s, C=C), 1327 (s), 1220 cm^{-1} (s); MS (ESI+): 415 $[M+Na]^+$ (100), 393 $[M+H]^+$ (65); HRMS (ESI+): m/z $[M+H]^+$ calcd for $C_{20}H_{20}F_3N_2O_3$: 393.1421, found: 393.1419.

5-Ethoxy-2,2-dimethyl-4H-1,3-benzodioxin-4-one (16): Following the general procedure described for the alkylation of phenols, the reaction of **15** (0.10 g, 0.51 mmol), K₂CO₃ (0.18 g, 1.28 mmol) and ethyl iodide (0.09 mL, 1.13 mmol) in acetone (16 mL), afforded, after purification by column chromatography (90:10, hexane/EtOAc), **16** as a white solid (0.106 g, 91%); mp: 101 °C (hexane/acetone); 1H NMR (400 MHz, CDCl₃): δ = 7.42 (t, J = 8.4 Hz, 1H), 6.62 (d, J = 8.4 Hz, 1H), 6.55 (d, J = 8.4 Hz, 1H), 4.19 (q, J = 6.8 Hz, 2H), 1.72 (s, 6H, 2CH₃), 1.53 ppm (t, J = 6.8 Hz, 3H); ^{13}C NMR (100 MHz, CDCl₃): δ = 160.7, 158.0, 157.6, 136.2, 108.8, 106.3, 105.0, 103.3, 64.8, 25.5 (2C), 14.4 ppm; IR (NaCl): $\tilde{\nu}$ = 2988 (w, C–H), 2938 (w, C–H), 2888 (w, C–H), 1736 (s, C=O), 1582 (m, C=C), 1461 (s), 1254 (s), 1081 cm^{-1} (s); MS (ESI+): 245 $[M+Na]^+$ (100), 223 $[M+H]^+$ (46); HRMS (ESI+): m/z $[M+Na]^+$ calcd for $C_{12}H_{14}NaO_4$: 245.0784; found: 245.0779; Anal. calcd for $C_{12}H_{14}O_4$: C, 64.85; H, 6.35; found: C, 64.76; H, 6.38.

N-(4-Cyano-3-trifluoromethylphenyl)-6-ethoxy-2-hydroxybenzamide (17): Following the general procedure described for amide formation, the reaction of **16** (0.34 g, 1.51 mmol), **12** (0.703 g, 3.78 mmol), *n*BuLi (3.10 mL, 1.22 M in hexane, 3.78 mmol) and DMPU (4.15 mL, 34.50 mmol) in THF (56 mL) afforded, after purification by column chromatography (60:10:30, hexane/EtOAc/CH₂Cl₂), **17** as a white solid (0.47 g, 88%); mp: 167 °C (hexane/acetone); ¹H NMR (400 MHz, (CD₃)₂CO): δ = 11.06 (s, 1H), 8.40 (s, 1H), 8.1–8.0 (m, 2H), 7.43 (t, *J* = 8.4 Hz, 1H), 6.67 (d, *J* = 8.4 Hz, 1H), 6.61 (dd, *J* = 8.4, 0.9 Hz, 1H), 4.38 (q, *J* = 7.0 Hz, 2H), 1.66 ppm (t, *J* = 7.0 Hz, 3H); ¹³C NMR (100 MHz, (CD₃)₂CO): δ = 171.3, 166.4, 160.0, 144.1, 138.1, 137.0, 134.7 (²*J*_{C-F} = 32.5 Hz), 125.6, 124.5 (¹*J*_{C-F} = 273.4 Hz), 120.2 (²*J*_{C-F} = 5.6 Hz), 117.2, 113.2, 106.0 (⁴*J*_{C-F} = 2.6 Hz), 105.7, 104.6, 67.8, 15.8 ppm; IR (NaCl): $\tilde{\nu}$ = 3600–3000 (br, N–H and O–H), 1648 (m, C=O), 1585 (s, C=C), 1544 (s, C=C), 1451 (m), 1430 (m), 1326 (s), 1234 (s), 1136 cm⁻¹ (s); MS (ESI⁺): 373 [M+Na]⁺ (20), 351 [M+H]⁺ (92), 209 (100); HRMS (ESI⁺): *m/z* [M+H]⁺ calcd for C₁₇H₁₄F₃N₂O₃: 351.0951; found 351.0965; Anal. calcd for C₁₇H₁₃F₃N₂O₃: C, 58.29; H, 3.74; found: C, 58.25; H, 3.76.

2-(4-Cyano-3-trifluoromethylphenylcarbamoyl)-3-ethoxyphenyl trifluoromethanesulfonate (18): Following the general procedure described for the synthesis of triflates, the reaction of **17** (0.15 g, 0.43 mmol) and trifluoromethanesulfonic anhydride (0.07 mL, 0.43 mmol) in pyridine (0.75 mL) afforded, after purification by column chromatography (70:30, hexane/EtOAc), **18** as a white solid (0.18 g, 87%); mp: 148 °C (hexane/EtOAc); ¹H NMR (400 MHz, CDCl₃): δ = 8.52 (s, 1H), 8.02 (d, *J* = 9.2 Hz, 1H), 7.96 (s, 1H), 7.79 (d, *J* = 8.4 Hz, 1H), 7.49 (t, *J* = 8.4 Hz, 1H), 7.03 (d, *J* = 8.8 Hz, 1H), 6.98 (d, *J* = 8.4 Hz, 1H), 4.19 (q, *J* = 7.2 Hz, 2H), 1.46 ppm (t, *J* = 7.2 Hz, 3H); ¹³C NMR (100 MHz, CDCl₃): δ = 161.0, 157.0, 147.6, 141.7, 136.0, 134.1 (²*J*_{C-F} = 33.2 Hz), 132.8, 122.2, 122.1 (¹*J*_{C-F} = 274.0 Hz), 118.6, 118.5 (¹*J*_{C-F} = 320.6 Hz), 117.3 (²*J*_{C-F} = 4.9 Hz), 115.5, 114.9, 112.5, 104.8, 65.7, 14.6 ppm; IR (NaCl): $\tilde{\nu}$ = 3286 (m, N–H), 2979 (w, C–H), 1650 (m, C=O), 1582 (s, C=C), 1545 (s, C=C), 1431 (s, C=C), 1322 cm⁻¹ (s); MS (ESI⁺): 505 [M+Na]⁺ (91), 483 [M+H]⁺ (100); HRMS (ESI⁺): *m/z* [M+H]⁺ calcd for C₁₈H₁₃F₆N₂O₅S: 483.0444; found: 483.0446; Anal. calcd for C₁₈H₁₂F₆N₂O₅S: C, 44.82; H, 2.51; found: C, 44.63; H, 1.98.

(E)-4,4,5,5-Tetramethyl-2-(4-trifluoromethylphenyl-vin-1-yl)-1,3,2-dioxaborolane (20a): General procedure for the Takai–Utimoto reaction. A suspension of CrCl₃ (2.76 g, 22.43 mmol) in THF (30 mL) was treated with **19a** (0.38 mL, 2.80 mmol) and 3-(dichloromethyl)-4,4,5,5-tetramethyl-1,3,2-dioxaborolane (1.18 g, 5.60 mmol) in THF (6 mL). Then Lil (1.50 g, 11.20 mmol) in THF (6 mL) was added and the suspension was stirred for 16 h at RT. The mixture was poured into water, extracted with EtOAc (×3), and the solvent was evaporated. The residue was purified by column chromatography (95:5, hexane/EtOAc) to afford **20a** as a white solid (0.68 g, 81%); mp: 60 °C (hexane/EtOAc); ¹H NMR (400 MHz, CDCl₃): δ = 7.6–7.5 (m, 4H), 7.39 (d, *J* = 18.4 Hz, 1H), 6.25 (d, *J* = 18.4 Hz, 1H), 1.28 ppm (s, 12H, 4CH₃); ¹³C NMR (100 MHz, CDCl₃): δ = 147.6, 140.8, 130.4 (²*J*_{C-F} = 32.5 Hz), 127.1 (2C), 125.5 (³*J*_{C-F} = 4.2 Hz, 2C), 124.1 (¹*J*_{C-F} = 274.7 Hz), 119.5, 83.5 (2C), 24.7 ppm (4C); IR (NaCl): $\tilde{\nu}$ = 2923 (s, C–H), 2853 (m, C–H), 1623 cm⁻¹ (w, C=C); MS (ESI⁺): 321 [M+Na]⁺ (72), 299 [M+H]⁺ (100), 279 (20); HRMS (ESI⁺): *m/z* [M+H]⁺ calcd for C₁₅H₁₉BF₃O₂: 299.1427; found: 299.1438; Anal. calcd for C₁₅H₁₈BF₃O₂: C, 60.43; H, 6.09; found: C, 60.49; H, 6.09.

(E)-4,4,5,5-Tetramethyl-2-(3-bromophenyl)ethen-1-yl-1,3,2-dioxaborolane (20b): Following the general procedure described for the Takai–Utimoto reaction, **19b** (0.33 mL, 2.80 mmol), 3-(dichloromethyl)-4,4,5,5-tetramethyl-1,3,2-dioxaborolane (1.18 g, 5.60 mmol), CrCl₃ (2.76 g, 22.43 mmol) and Lil (1.50 g, 11.20 mmol) in THF

(42 mL) afforded, after purification by column chromatography (95:5, hexane/EtOAc), **20b** as a yellow oil (0.78 g, 91%); ¹H NMR (400 MHz, CDCl₃): δ = 7.63 (t, *J* = 1.7 Hz, 1H), 7.42 (td, *J* = 8.0, 1.6 Hz, 2H), 7.32 (d, *J* = 18.4 Hz, 1H), 7.23 (t, *J* = 7.6 Hz, 1H), 6.18 (d, *J* = 18.4 Hz, 1H), 1.33 ppm (s, 12H); ¹³C NMR (100 MHz, CDCl₃): δ = 147.5, 139.5, 131.5, 129.9 (2C), 129.7, 125.4, 122.6, 83.3 (2C), 24.7 ppm (4C); MS (ESI⁺): 429 [M+Na]⁺ (23), 407 [M+H]⁺ (100); IR (NaCl): $\tilde{\nu}$ = 2979 (m, C–H), 1626 (m, C=O), 1563 (w, C=C), 1471 (w), 1345 (s), 1210 (m), 1145 cm⁻¹ (s); MS (ESI⁺): 333 [M+Na]⁺ (51), 331 [M+Na]⁺ (62), 311 [M+H]⁺ (100), 309 [M+H]⁺ (100); HRMS (ESI⁺): *m/z* [M+H]⁺ calcd for C₁₄H₁₉B⁷⁹BrO₂: 309.0659; found: 309.0667.

(E)-N-(4-Cyano-3-trifluoromethylphenyl)-2-ethoxy-6-phenylethen-1-yl benzamide (7j): General procedure for the Suzuki cross coupling (Method B). **21** (41.9 mg, 0.19 mmol), **18** (0.05 g, 0.11 mmol), Pd(PPh₃)₄ (6 mg, 5.2 μmol) and K₃PO₄ (0.04 g, 0.19 mmol) were suspended in dioxane (0.55 mL). The suspension was irradiated in a microwave reactor for 15 min at 100 °C (90 W). Benzene (1 mL), aq NaOH (100 μL, 3 M) and H₂O₂ (30%, 100 μL) were added and the mixture was stirred at RT for 1 h. Water was added and the aqueous layer was extracted with EtOAc (×3). The combined organic layers were dried (Na₂SO₄) and the solvent was evaporated. The residue was purified by column chromatography (-NH₂ silica gel; 90:10, hexane/EtOAc) to afford **7j** as a white solid (36.8 mg, 80%); mp: 182 °C (hexane/acetone); ¹H NMR (400 MHz, (CD₃)₂CO): δ = 10.16 (s, 1H), 8.50 (s, 1H), 8.29 (dd, *J* = 8.5, 1.4 Hz, 1H), 8.07 (d, *J* = 8.5 Hz, 1H), 7.6–7.4 (m, 4H), 7.4–7.2 (m, 5H), 7.03 (dd, *J* = 7.7, 1.3 Hz, 1H), 4.12 (q, *J* = 7.0 Hz, 2H), 1.31 ppm (t, *J* = 7.0 Hz, 3H); ¹³C NMR (100 MHz, (CD₃)₂CO): δ = 168.4, 158.0, 145.8, 139.0, 138.3, 138.2, 134.7 (²*J*_{C-F} = 34.6 Hz), 133.5, 132.6, 130.6 (2C), 129.9, 128.6 (2C), 127.7, 126.7, 124.6 (¹*J*_{C-F} = 272.0 Hz), 123.9, 119.3, 118.7 (³*J*_{C-F} = 5.6 Hz), 117.4, 113.1, 105.0, 66.1, 16.0 ppm; IR (NaCl): $\tilde{\nu}$ = 3292 (br, N–H), 2964 (s, C–H), 1668 (s, C=O), 1587 (s, C=C), 1530 (s, C=C), 1426 (m), 1260 (s), 1137 cm⁻¹ (s); MS (ESI⁺): 459 [M+Na]⁺ (38), 437 [M+H]⁺ (100), 391 (38); HRMS (ESI⁺): *m/z* [M+H]⁺ calcd for C₂₅H₂₀F₃N₂O₂: 437.1471; found: 437.1468.

(E)-N-(4-Cyano-3-trifluoromethylphenyl)-2-ethoxy-6-(4-trifluoromethylphenyl)ethen-1-yl benzamide (7h): Following the general procedure described for the Suzuki cross coupling (Method B), the reaction of **20a** (0.06 g, 0.19 mmol), **18** (0.05 g, 0.11 mmol), Pd(PPh₃)₄ (6 mg, 5.19 μmol) and K₃PO₄ (0.04 g, 0.19 mmol) in dioxane (0.55 mL) afforded, after purification by column chromatography (-NH₂ silica gel; 90:10→85:15, hexane/EtOAc), **7h** as a white solid (22.7 mg, 43%); mp: 180 °C (hexane/acetone); ¹H NMR (400 MHz, (CD₃)₂CO): δ = 10.19 (s, 1H), 8.50 (s, 1H), 8.28 (dd, *J* = 8.5, 1.0 Hz, 1H), 8.07 (d, *J* = 8.5 Hz, 1H), 7.71 (d, *J* = 8.4 Hz, 2H), 7.67 (d, *J* = 8.4 Hz, 2H), 7.5–7.4 (m, 3H), 7.36 (d, *J* = 16.3 Hz, 1H), 7.08 (d, *J* = 7.9 Hz, 1H), 4.13 (q, *J* = 7.0 Hz, 2H), 1.32 ppm (t, *J* = 7.0 Hz, 3H); ¹³C NMR (100 MHz, (CD₃)₂CO): δ = 168.2, 158.1, 145.7, 142.9, 138.3, 137.8, 134.7 (²*J*_{C-F} = 32.5 Hz), 132.8, 131.9, 130.7 (²*J*_{C-F} = 32.5 Hz), 129.7, 129.1 (2C), 127.9, 127.5 (³*J*_{C-F} = 3.9 Hz, 2C), 126.3 (¹*J*_{C-F} = 271.7 Hz), 124.6 (¹*J*_{C-F} = 273.8 Hz), 124.0, 119.6, 118.7 (³*J*_{C-F} = 4.9 Hz), 117.4, 113.8, 105.1, 66.2, 16.0 ppm; IR (NaCl): $\tilde{\nu}$ = 3500–3200 (br, N–H), 2963 (m, C–H), 2931 (m, C–H), 1666 (m, C=O), 1588 (s, C=C), 1531 (s, C=C), 1326 (s), 1121 cm⁻¹ (s); MS (ESI⁺): 527 [M+Na]⁺ (48), 505 [M+H]⁺ (71), 391 (100); HRMS (ESI⁺): *m/z* [M+H]⁺ calcd for C₂₆H₁₉F₆N₂O₂: 505.1345; found: 505.1343.

(E)-N-(4-Cyano-3-trifluoromethylphenyl)-2-ethoxy-6-(3-bromophenyl)ethen-1-yl benzamide (7i): Following the general procedure described for the Suzuki cross coupling (Method B), the reaction of **20b** (58.4 mg, 0.19 mmol), **18** (50 mg, 0.11 mmol), Pd(PPh₃)₄ (6 mg, 5.19 μmol) and K₃PO₄ (40.1 mg, 0.19 mmol) in dioxane

(0.55 mL) afforded, after purification by column chromatography (-NH₂ silica gel; 90:10→85:15, hexane/EtOAc), **7i** as a white solid (15 mg, 27%); mp: 144 °C (hexane/acetone); ¹H NMR (400 MHz, (CD₃)₂CO): δ = 10.17 (s, 1H), 8.49 (d, *J* = 1.6 Hz, 1H), 8.28 (dd, *J* = 8.4, 1.6 Hz, 1H), 8.07 (d, *J* = 8.6 Hz, 1H), 7.68 (t, *J* = 1.7 Hz, 1H), 7.52 (d, *J* = 7.8 Hz, 1H), 7.5–7.4 (m, 3H), 7.39 (d, *J* = 16.3 Hz, 1H), 7.30 (t, *J* = 7.9 Hz, 1H), 7.25 (d, *J* = 16.3 Hz, 1H), 7.06 (dd, *J* = 6.7, 2.4 Hz, 1H), 4.12 (q, *J* = 7.0 Hz, 2H), 1.31 ppm (t, *J* = 7.0 Hz, 3H); ¹³C NMR (100 MHz, (CD₃)₂CO): δ = 168.2, 158.0, 145.7, 141.5, 138.3, 138.0, 134.6 (²*J*_{C-F} = 31.2 Hz), 132.7, 132.6, 132.5, 131.9, 131.4, 128.6, 127.8, 127.3, 124.6 (¹*J*_{C-F} = 272.7 Hz), 124.3, 124.0, 119.6, 118.7 (³*J*_{C-F} = 4.9 Hz), 117.4, 113.6, 105.0, 66.1, 16.0 ppm; IR (NaCl): $\tilde{\nu}$ = 3500–3200 (br, N–H), 2980 (w, C–H), 2937 (w, C–H), 2891 (w), 1654 (s, C=O), 1584 (s, C=C), 1510 (s, C=C), 1424 (s), 1271 (s), 1178 (s), 1133 cm⁻¹ (s); MS (ESI⁺): 539 [M+Na]⁺ (28), 537 [M+Na]⁺ (28), 515 [M+H]⁺ (31), 515 [M+H]⁺ (31), 38 (100); HRMS (ESI⁺): *m/z* [M+H]⁺ calcd for C₂₅H₁₉BrF₃N₂O₂: 515.0577, found: 515.0585; Anal. calcd for C₂₅H₁₈BrF₃N₂O₂: C, 58.27; H, 3.52; found: C, 58.03; H, 3.62.

(E)-N-(4-Cyano-3-trifluoromethylphenyl)-2-ethoxy-6-(6-hydroxyhex-1-enyl)benzamide (7k): Following the general procedure described for the Suzuki cross coupling (Method B), the reaction of **22** (27.2 mg, 0.19 mmol), **18** (50 mg, 0.11 mmol), Pd(PPh₃)₄ (6 mg, 5.19 μmol) and K₃PO₄ (40.1 mg, 0.19 mmol) in dioxane (0.55 mL) afforded, after purification by column chromatography (-NH₂ silica gel; 90:10→55:45, hexane/EtOAc), **7k** as a colourless oil (43.5 mg, 92%); ¹H NMR (400 MHz, (CD₃)₂CO): δ = 10.09 (s, 1H), 8.50 (s, 1H), 8.25 (d, *J* = 8.5 Hz, 1H), 8.05 (d, *J* = 8.5 Hz, 1H), 7.34 (t, *J* = 8.1 Hz, 1H), 7.22 (d, *J* = 7.9 Hz, 1H), 6.94 (d, *J* = 8.2 Hz, 1H), 6.53 (d, *J* = 15.7 Hz, 1H), 6.32 (td, *J* = 15.6, 7.0 Hz, 1H), 4.08 (q, *J* = 6.9 Hz, 2H), 3.49 (q, *J* = 5.7 Hz, 2H), 3.4–3.3 (m, 1H), 2.18 (q, *J* = 6.6 Hz, 2H), 1.6–1.5 (m, 4H), 1.28 ppm (t, *J* = 6.9 Hz, 3H); ¹³C NMR (100 MHz, (CD₃)₂CO): δ = 168.6, 157.8, 145.8, 138.7, 138.2, 136.1, 134.6 (²*J*_{C-F} = 32.5 Hz), 132.3, 128.2, 127.1, 125.0 (¹*J*_{C-F} = 272.7 Hz), 123.8, 119.4, 118.6 (³*J*_{C-F} = 4.9 Hz), 117.4, 112.4, 104.8, 66.0, 63.1, 34.6, 34.1, 27.3, 16.0 ppm; IR (NaCl): $\tilde{\nu}$ = 3500–3200 (br, N–H and O–H), 2935 (m, C–H), 1675 (m, C=O), 1591 (s, C=C), 1532 (s, C=C), 1329 (s), 1266 (s), 1177 cm⁻¹ (s); MS (ESI⁺): 455 [M+Na]⁺ (61), 433 [M+H]⁺ (100); HRMS (ESI⁺): *m/z* [M]⁺ calcd for C₂₃H₂₄F₃N₂O₃: 433.1734, found: 433.1731.

Biology

Ligands and materials: SAHA (Merck; Rome, Italy), MS-275 (Bayer Schering AG; Berlin, Germany), and anacardic acid and CTPB (Alexis–Enzo Life Sciences; New York, USA) were dissolved in DMSO and used at 5 × 10⁻⁶ M. All other compounds described were dissolved in DMSO (Sigma–Aldrich; Milan, Italy) and used at 5 μM and 50 μM.

Cell Culture: Human U937 and HL60 leukaemia cell lines were propagated in RPMI medium supplemented with 10% fetal bovine serum (FBS; Hyclone, Milan, Italy) and antibiotics (100 U mL⁻¹ penicillin, 100 μg mL⁻¹ streptomycin and 250 ng mL⁻¹ amphotericin-B). Cells were kept at the constant concentration of 200 000 cells per mL of culture medium.

Cell Cycle Analysis: 2.5 × 10⁵ U937 cells were collected and resuspended in 500 μL of hypotonic buffer (0.1% Triton X-100, 0.1% sodium citrate, 50 μg mL⁻¹ propidium iodide, RNase A). Cells were incubated in the dark for 30 min. Data were acquired on a FACS-Calibur flow cytometer using the CellQuest software (Becton, Dickinson & Co.) and analysed with standard procedures also using CellQuest and the ModFit LT v3 software (Verity) as previously reported.^[27] Nuclear fragmentation (the so-called “sub-G1 DNA

peak”), monitored by FACS and analysed by CellQuest technology, was used as an indicator of apoptosis.

Histone Extraction Protocol: Cells were harvested and washed twice with ice-cold phosphate-buffered saline (PBS) and lysed in Triton extraction buffer (TEB; PBS containing 0.5% Triton X-100 (v/v), 2 mM phenylmethylsulfonyl fluoride (PMSF), 0.02% (w/v) NaN₃) at a cellular density of 10⁷ cells per mL for 10 min on ice, with gentle stirring. After brief centrifugation at 2000 rpm at 4 °C, the supernatant was removed and the pellet was washed in half the volume of TEB and centrifuged as before. The pellet was resuspended in 0.2 M HCl at a cell density of 4 × 10⁷ cells per mL, and acid extraction was left to proceed overnight at 4 °C on a rolling table. Next, the samples were centrifuged at 2000 rpm for 10 min at 4 °C, the supernatant was removed and the protein content was determined using the Bradford assay.

Western Blot analyses: Western Blot analyses were performed according to standard procedures following the suggestions of the antibody suppliers.

Determination of Histone H3 Specific Acetylation: For histone H3 acetylation in U937 cells, 5 μg of histone extract were separated on 15% polyacrylamide gels and blotted. Western blots were shown for pan-acetylated histone H3 (Upstate Biotechnology; Milan, Italy).

Human recombinant CBP assay: The recombinant cyclic adenosine monophosphate response element-binding protein (CREB) binding protein (CBP) was prepared in *E. coli* BL21 and purified by affinity chromatography. The recombinant CBP fraction corresponded to amino acids 1098–1877. CBP was incubated in KAT buffer x5 (250 mM TRIS base pH 8.0, 50% glycerol, 0.5 mM EDTA, 5 mM DTT) with 10 μg of histone H4 peptide (corresponding to amino acids 2–24) and 20 μM acetyl-CoA containing 0.5 μCi mL⁻¹ [³H]acetyl-CoA in the presence of inhibitors and putative KAT activators. After 2 h at 37 °C, 5 μL of samples were spotted onto Whatman P81 paper (in triplicate). The paper squares were washed in 5% TCA (x3) and 100% acetone (x1) and then placed into scintillation vials containing scintillation fluid to allow the disintegrations per minute (dpm) reading. The dpm value of enzyme samples was compared with the dpm value of negative and positive controls. Data have been expressed as the percentage of activity considering the control without treatment as 100%.

PCAF radioactive assay: 200 ng of human PCAF were incubated in KAT buffer (Upstate Biotechnology) with 10 μg of histone H4 peptide substrate (corresponding to amino acids 2–24) and 20 μM acetyl-CoA containing 0.5 μCi mL⁻¹ [³H]acetyl-CoA. The acetylation reaction was performed in a volume of 25 μL in the presence of test compounds at the desired final concentration. After 2 h at 37 °C, 5 μL of samples were spotted onto chromatographic Whatman P81 paper (in triplicate). After a washing session (3 × 5% TCA; 1 × 100% acetone), the paper squares were placed into scintillation vials containing scintillation fluid to allow the dpm reading. The dpm value of enzyme samples was compared to the dpm value of the negative and positive controls and reported as the percentage of activity considering the untreated control as 100%.

Acknowledgements

This work was partially supported by grants from the European Union (EPITRON, LSHC-CT2005-518417; ATLAS, 221952), AIRC, MICINN-Spain (SAF2007-63880-FEDER) and Xunta de Galicia-Spain (Inbiomed).

Keywords: anacardic acid · chromatin · histone acetylation · histone lysine acetyltransferases · salicylamides

- [1] E. Ballestar, M. Esteller, *Carcinogenesis* **2002**, *23*, 1103–1109.
- [2] P. M. Das, R. Singal, *J. Clin. Oncol.* **2004**, *22*, 4632–4642.
- [3] S. B. Baylin, J. E. Ohm, *Nat. Rev. Cancer* **2006**, *6*, 107–116.
- [4] S. Minucci, P. G. Pelicci, *Nat. Rev. Cancer* **2006**, *6*, 38–51.
- [5] R. J. Klose, Y. Zhang, *Nat. Rev. Mol. Cell Biol.* **2007**, *8*, 307–318.
- [6] T. Kouzarides, *Cell* **2007**, *128*, 693–705.
- [7] S. D. Taverna, H. Li, A. J. Ruthenburg, C. D. Allis, D. J. Patel, *Nat. Struct. Mol. Biol.* **2007**, *14*, 1025–1040.
- [8] J. A. Latham, S. Y. R. Dent, *Nat. Struct. Mol. Biol.* **2007**, *14*, 1017–1024.
- [9] C. Choudhary, C. Kumar, F. Gnäd, M. L. Nielsen, M. Rehman, T. C. Walther, J. V. Olsen, M. Mann, *Science* **2009**, *325*, 834–840.
- [10] B. Li, M. Carey, J. L. Workman, *Cell* **2007**, *128*, 707–719.
- [11] S. R. Bhaumik, E. Smith, A. Shilatifard, *Nat. Struct. Mol. Biol.* **2007**, *14*, 1008–1016.
- [12] M. Biel, V. Waschowski, A. Giannis, *Angew. Chem.* **2005**, *117*, 3248–3280; *Angew. Chem. Int. Ed.* **2005**, *44*, 3186–3216.
- [13] P. A. Jones, S. B. Baylin, *Cell* **2007**, *128*, 683–692.
- [14] A. G. Inche, N. B. La Thangue, *Drug Discovery Today* **2006**, *11*, 97–109.
- [15] C. B. Yoo, P. A. Jones, *Nat. Rev. Drug Discovery* **2006**, *5*, 37–50.
- [16] M. von Wantoch Rekowski, A. Giannis in *Epigenetic Targets in Drug Discovery*, (Eds.: W. Sippl, M. Jung), Wiley-VCH, Weinheim, **2009**, pp. 243–250.
- [17] C. D. Allis, S. L. Berger, J. Cote, S. Dent, T. Jenuwein, T. Kouzarides, L. Pillus, D. Reinberg, Y. Shi, R. Shiekhattar, A. Shilatifard, J. L. Workman, Y. Zhang, *Cell* **2007**, *131*, 633–636.
- [18] B. C. Smith, J. M. Denu, *Biochim. Biophys. Acta, Gene Regul. Mech.* **2009**, *1789*, 45–57.
- [19] M. D. Shahbazian, M. Grunstein, *Ann. Rev. Biochem.* **2007**, *76*, 75–100.
- [20] S. C. Hodawadekar, R. Marmorstein, *Oncogene* **2007**, *26*, 5528–5540.
- [21] A. J. Bannister, T. Kouzarides, *Nature* **1996**, *384*, 641–643.
- [22] V. V. Ogryzko, R. L. Schiltz, V. Russanova, B. H. Howard, Y. Nakatani, *Cell* **1996**, *87*, 953–959.
- [23] C. A. Mizzen, X. J. Yang, T. Kokubo, J. E. Brownell, A. J. Bannister, T. Owen-Hughes, J. Workman, L. Wang, S. L. Berger, T. Kouzarides, Y. Nakatani, C. D. Allis, *Cell* **1996**, *87*, 1261–1270.
- [24] X. Liu, L. Wang, K. Zhao, P. R. Thompson, Y. Hwang, R. Marmorstein, P. A. Cole, *Nature* **2008**, *451*, 846.
- [25] Z. Wang, C. Zang, K. Cui, D. E. Schones, A. Barski, W. Peng, K. Zhao, *Cell* **2009**, *138*, 1019–1031.
- [26] A. Insinga, S. Monestiroli, S. Ronzoni, V. Gelmetti, F. Marchesi, A. Viale, L. Altucci, C. Nervi, S. Minucci, P. G. Pelicci, *Nat. Med.* **2005**, *11*, 71–76.
- [27] A. Nebbioso, N. Clarke, E. Voltz, E. Germain, C. Ambrosino, P. Bontempo, R. Alvarez, E. M. Schiavone, F. Ferrara, F. Bresciani, A. Weisz, A. R. de Lera, H. Gronemeyer, L. Altucci, *Nat. Med.* **2005**, *11*, 77–84.
- [28] J. Wu, N. Xie, Z. Wu, Y. Zhang, Y. G. Zheng, *Bioorg. Med. Chem.* **2009**, *17*, 1381–1386.
- [29] E. M. Bowers, G. Yan, C. Mukherjee, A. Orry, L. Wang, M. A. Holbert, N. T. Crump, C. A. Hazzalin, G. Liszczak, H. Yuan, C. Larocca, S. A. Saldanha, R. Abagyan, Y. Sun, D. J. Meyers, R. Marmorstein, L. C. Mahadevan, R. M. Alani, P. A. Cole, *Chem. Biol.* **2010**, *17*, 471–482.
- [30] K. Mantelingu, B. A. A. Reddy, V. Swaminathan, A. H. Kishore, N. B. Siddappa, G. V. P. Kumar, G. Naganshankar, N. Natesh, S. Roy, P. P. Sadhale, U. Ranga, C. Narayana, T. K. Kundu, *Chem. Biol.* **2007**, *14*, 645–657.
- [31] K. Balasubramanyam, M. Altaf, R. A. Varier, V. Swaminathan, A. Ravindran, P. P. Sadhale, T. K. Kundu, *J. Biol. Chem.* **2004**, *279*, 33716–33726.
- [32] K. Balasubramanyam, V. Swaminathan, A. Ranganathan, T. K. Kundu, *J. Biol. Chem.* **2003**, *278*, 19134–19140.
- [33] L. Cui, J. Miao, T. Furuya, Q. Fan, X. Li, P. K. Rathod, X.-z. Su, L. Cui, *Eukaryotic Cell* **2008**, *7*, 1200–1210.
- [34] K. Mantelingu, A. H. Kishore, K. Balasubramanyam, G. V. P. Kumar, M. Altaf, S. N. Swamy, R. Selvi, C. Das, C. Narayana, K. S. Rangappa, T. K. Kundu, *J. Phys. Chem. B* **2007**, *111*, 4527–4534.
- [35] J. A. Souto, M. Conte, R. Alvarez, A. Nebbioso, V. Carafa, L. Altucci, A. R. de Lera, *ChemMedChem* **2008**, *3*, 1435–14426.
- [36] R. Costi, R. DiSanto, M. Artico, G. Miele, P. Valentini, E. Novellino, A. Cereseto, *J. Med. Chem.* **2007**, *50*, 1973–1977.
- [37] S. Kotha, K. Lahiri, D. Kashinath, *Tetrahedron* **2002**, *58*, 9633–9695.
- [38] N. Miyaura, T. Ishiyama, H. Sasaki, M. Sihikama, M. Sato, A. Suzuki, *J. Am. Chem. Soc.* **1989**, *111*, 314.
- [39] A. Hadfield, H. Schweitzer, M. P. Trova, K. Green, *Synth. Commun.* **1994**, *24*, 1025–1028.
- [40] R. G. Dushin, S. J. Danishefsky, *J. Am. Chem. Soc.* **1992**, *114*, 655–659.
- [41] J. H. P. Tyman, *Chem. Soc. Rev.* **1979**, *8*, 499–537.
- [42] A. Fürstner, I. Konetzki, *Tetrahedron* **1996**, *52*, 15071–15075.
- [43] G. A. Molander, F. Dehmel, *J. Am. Chem. Soc.* **2004**, *126*, 10313–10318.
- [44] T. Okazoe, K. Takai, K. Utimoto, *J. Am. Chem. Soc.* **1987**, *109*, 951–952.
- [45] A. Fürstner, *Chem. Rev.* **1999**, *99*, 991–1046.
- [46] H. C. Brown, S. K. Gupta, *J. Am. Chem. Soc.* **1972**, *94*, 4370–4371.
- [47] W. R. Roush, M. Kageyama, R. Riva, B. B. Brown, J. S. Warmus, K. J. Moriarty, *J. Org. Chem.* **1991**, *56*, 1192–1210.
- [48] K. Olofsson, M. Larhed in *Microwave-Assisted Organic Synthesis*, (Eds.: J. P. Tierney, P. Lidström), Blackwell Publishing Ltd., Oxford, **2005**, Chapter 2.
- [49] N. E. Leadbeater, M. Marco, *J. Org. Chem.* **2003**, *68*, 888–892.
- [50] N. Khan, M. Jeffers, S. Kumar, C. Hackett, F. Boldog, N. Khrantsov, X. Qian, E. Mills, S. C. Berghs, N. Carey, P. W. Finn, L. S. Collins, A. Tumber, J. W. Ritchie, P. B. Jensen, H. S. Lichtenstein, M. Sehested, *Biochem. J.* **2008**, *409*, 581–589.
- [51] E. D. Eliseeva, V. Valkov, M. Jung, M. O. Jung, *Mol. Cancer Ther.* **2007**, *6*, 2391–2398.

Received: April 15, 2010

Revised: June 30, 2010

Published online on August 3, 2010

Research

Open Access

Molecular analysis of the apoptotic effects of BPA in acute myeloid leukemia cells

Paola Bontempo^{1,2}, Luigi Mita^{1,2,3}, Antonella Doto¹, Marco Miceli¹, Angela Nebbioso¹, Ilaria Lepore¹, GianLuigi Franci¹, Roberta Menafra¹, Vincenzo Carafa¹, Mariarosaria Conte¹, Floriana De Bellis¹, Fabio Manzo¹, Vincenzo Di Cerbo¹, Rosaria Benedetti⁴, Loredana D'Amato¹, Maria Marino^{2,5}, Alessandro Bolli^{2,5}, Giovanna Del Pozzo^{2,6}, Nadia Diano^{2,3,6}, Marianna Portaccio^{2,3}, Gustavo D Mita^{3,4}, Maria Teresa Vietri¹, Michele Cioffi¹, Ernesto Nola¹, Carmela Dell'Aversana¹, Vincenzo Sica¹, Anna Maria Molinari¹ and Lucia Altucci*^{1,2}

Address: ¹Dipartimento di Patologia generale, Seconda Università di Napoli, Via L. De Crecchio 7 Napoli, Italy, ²Istituto Nazionale di Biostruttura e dei Biosistemi, Viale Medaglie d'Oro, 305, 00100 Roma, Italy, ³Dipartimento di Medicina sperimentale, Seconda Università di Napoli, Via De Crecchio, Napoli, Italy, ⁴Dipartimento di Fisica, Università di Napoli 'Federico II', Napoli, Italy, ⁵Dipartimento di Biologia, Università Roma Tre, Viale Guglielmo Marconi 446, 00146 Roma, Italy and ⁶Istituto di Genetica e Biofisica del CNR, Via P. Castellino 111, 80100 Napoli, Italy

Email: Paola Bontempo - paola.bontempo@unina2.it; Luigi Mita - luigi.mita@unina2.it; Antonella Doto - antonella.doto@unina2.it; Marco Miceli - marco.miceli@unina2.it; Angela Nebbioso - angela.nebbioso@unina2.it; Ilaria Lepore - ilaria.lepore@unina2.it; GianLuigi Franci - gianluigi.franci@unina2.it; Roberta Menafra - roberta.menafra@unina2.it; Vincenzo Carafa - vincenzo.carafa@unina2.it; Mariarosaria Conte - mariarosaria.conte@unina2.it; Floriana De Bellis - floriana.debellis@unina2.it; Fabio Manzo - fabio.manzo@unina2.it; Vincenzo Di Cerbo - vincenzo.dicerbo@unina2.it; Rosaria Benedetti - rosaria.benedetti@unina2.it; Loredana D'Amato - loredanadamato@yahoo.it; Maria Marino - m.marino@uniroma3.it; Alessandro Bolli - A.Bolli@uniroma3.it; Giovanna Del Pozzo - delpozzo@igb.cnr.it; Nadia Diano - diano@igb.cnr.it; Marianna Portaccio - portaccio@igb.cnr.it; Gustavo D Mita - mita@igb.cnr.it; Maria Teresa Vietri - mariateresa.vietri@unina2.it; Michele Cioffi - michele.cioffi@unina2.it; Ernesto Nola - ernesto.nola@unina2.it; Carmela Dell'Aversana - carmela.dellaversana@unina2.it; Vincenzo Sica - vincenzo.sica@unina2.it; Anna Maria Molinari - annamaria.molinari@unina2.it; Lucia Altucci* - lucia@altucci.com

* Corresponding author

Published: 18 June 2009

Received: 24 February 2009

Journal of Translational Medicine 2009, 7:48 doi:10.1186/1479-5876-7-48

Accepted: 18 June 2009

This article is available from: <http://www.translational-medicine.com/content/7/1/48>

© 2009 Bontempo et al; licensee BioMed Central Ltd.

This is an Open Access article distributed under the terms of the Creative Commons Attribution License (<http://creativecommons.org/licenses/by/2.0>), which permits unrestricted use, distribution, and reproduction in any medium, provided the original work is properly cited.

Abstract

Background: BPA (bisphenol A or 2,2-bis(4-hydroxy-phenyl)propane) is present in the manufacture of polycarbonate plastic and epoxy resins, which can be used in impact-resistant safety equipment and baby bottles, as protective coatings inside metal food containers, and as composites and sealants in dentistry. Recently, attention has focused on the estrogen-like and carcinogenic adverse effects of BPA. Thus, it is necessary to investigate the cytotoxicity and apoptosis-inducing activity of this compound.

Methods: Cell cycle, apoptosis and differentiation analyses; western blots.

Results: BPA is able to induce cell cycle arrest and apoptosis in three different acute myeloid leukemias. Although some granulocytic differentiation concomitantly occurred in NB4 cells upon BPA treatment, the major action was the induction of apoptosis. BPA mediated apoptosis was

caspase dependent and occurred by activation of extrinsic and intrinsic cell death pathways modulating both FAS and TRAIL and by inducing BAD phosphorylation in NB4 cells. Finally, also non genomic actions such as the early decrease of both ERK and AKT phosphorylation were induced by BPA thus indicating that a complex intersection of regulations occur for the apoptotic action of BPA.

Conclusion: BPA is able to induce apoptosis in leukemia cells via caspase activation and involvement of both intrinsic and extrinsic pathways of apoptosis.

Background

The Endocrine Disrupting Compounds are defined as "exogenous substances that cause adverse health effects in an intact organism, or its progeny, secondary to changes in endocrine function" (EEC, 1996). Their effects on humans, wildlife and the environment have been subject of high attention by the scientific community, since concerns were first raised about them by Colborn [1]. Recently, the potential of certain pesticides to act as EDCs has been confirmed. These include organometallic compounds, and many other organochlorine compounds that are also toxic and persistent [2,3], and many have been banned as a result [2]. Other pesticides such as organophosphates, carbamates, triazines and pyrethroids that are less persistent and less toxic than the organochlorines, were used to replace them, but many are now confirmed or suspected EDCs [4]. Conventional toxicological testing of pesticides can miss the potential of a substance to disrupt the endocrine system, especially at the low concentrations likely to be found in the environment. It is generally assumed that chemical substances will show a simple monotonic dose-response curve, but some ED pesticides have j-type dose-response curves [5], whereby the toxic effects decrease as the dose decreases, until at very low doses (often as low as parts per billion or even trillion) their effects increase [5]. Of the more than 2,000 high-production volume chemicals that are manufactured in or imported many are widely used in consumer products. Among the many chemicals is bisphenol A [BPA; 2,2-bis(4-hydroxyphenyl)propane]. BPA is used in the manufacture of polycarbonate plastic and epoxy resins, which can be used in impact-resistant safety equipment and baby bottles, as protective coatings inside metal food containers, and as composites and sealants in dentistry. Exposure to BPA is thought to result primarily from ingestion of food containing BPA [6,7]. At high doses, BPA demonstrates estrogen-like effects on uterine and prostate organ weights in experimental animals. At doses below the putative lowest observed adverse effect level, exposure to BPA has resulted in decreased sperm production, increased prostate gland volume, altered development and tissue organization of the mammary gland, altered vaginal morphology and estrous cycles, disruption of sexual differentiation in the brain, and accelerated growth and puberty [8-16]. BPA is of concern to environmental public health because of the

high potential for exposure of humans to these phenols and their demonstrated animal toxicity. Recently, attention has focused on the carcinogenic adverse effects of BPA. Thus, it is important to investigate the cytotoxicity and apoptosis-inducing activity of these compounds [17,18]. In the present manuscript, we decided to investigate the effects of different doses of BPA on acute myeloid leukemia models to understand the mechanism(s) of BPA action in systems not directly related to the endocrine system. We show indeed that BPA is able to induce apoptosis in leukemia cells by activation of the initiator caspases 8, 9 and the effector caspases 37. Moreover we show that many genomic and non-genomic players are influenced by the action of BPA and contribute to its adverse effects.

Methods

Cell lines

All cell lines have been obtained from ATCC and routinely cultured. NB4, U937, k562, and cells HL60, were grown at 37°C in air and 5% CO₂ in RPMI 1640 medium (GIBCO), supplemented with 10% heat-inactivated foetal bovine serum (FBS), 1% l-glutamine, 1% ampicillin/streptomycin and 0, 1% gentamicin. BPA (SIGMA) was resuspended in ethanol and at the final concentration of 1 µM. All *trans* retinoic acid (SIGMA) (RA) was resuspended in ethanol and at the final concentration of 1 µM. To understand the potential role of BPA leukemia cell lines were treated with different concentrations of BPA (10, 30, 60, 100 µM) for different times.

Cell cycle analysis

2.5 × 10⁵ cells were collected and resuspended in 500 µl of a hypotonic buffer (0.1% Triton X-100, 0.1% sodium citrate, 50 µg/ml propidium iodide (PI), RNase A). Cells were incubated in the dark for 30 min. Samples were acquired on a FACS Calibur flow cytometer using the Cell Quest software (Becton Dickinson) and analysed with standard procedures using the Cell Quest software (Becton Dickinson) and the ModFit LT version 3 Software (Verity) as previously reported [19]. All the experiments were performed in triplicate.

FACS analysis of apoptosis

Apoptosis was measured with Annexin V/PI double staining detection (Roche and Sigma-Aldrich, respectively) as

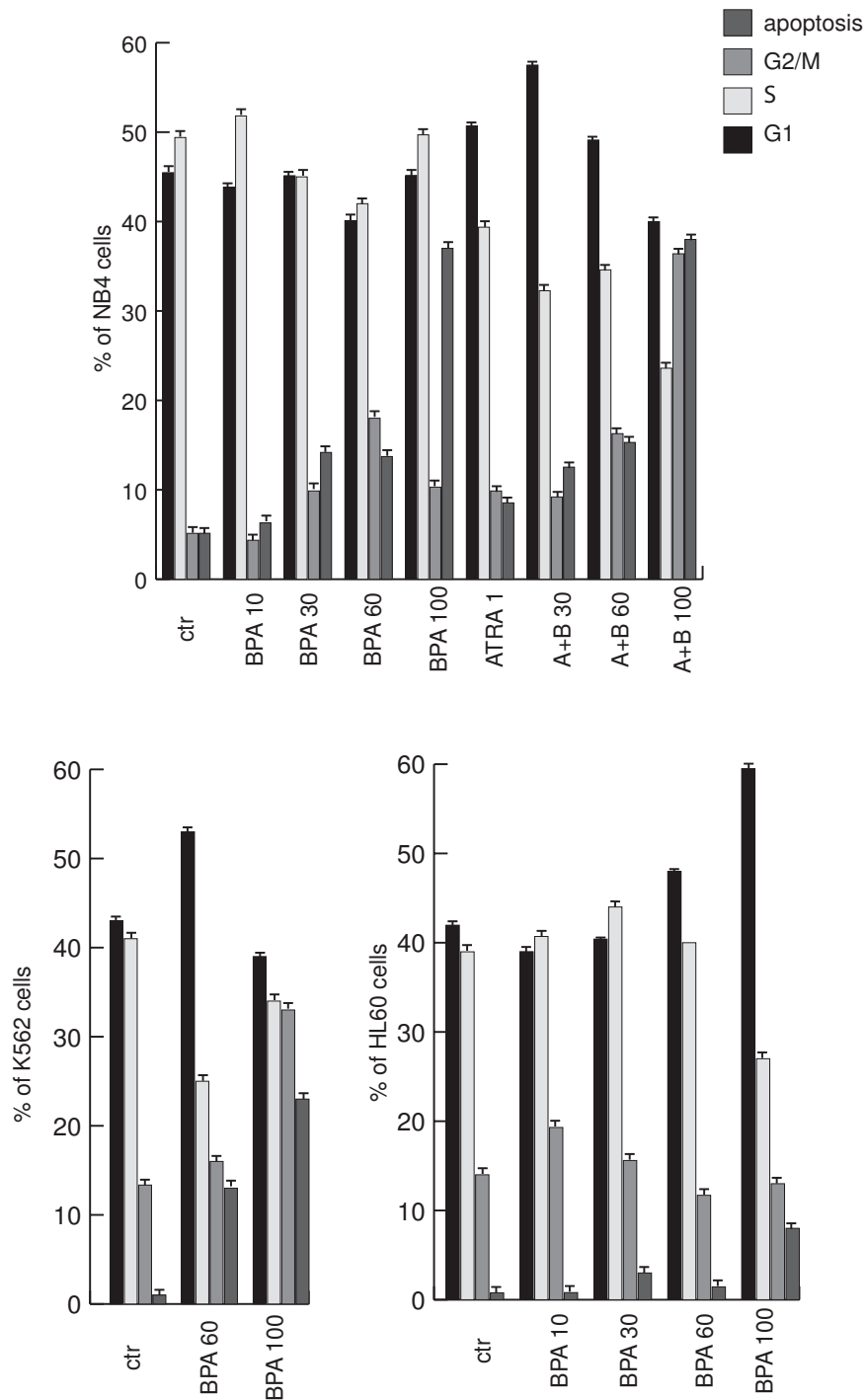


Figure 1
BPA induces dose dependent apoptosis and cell cycle block in acute myeloid leukemia cells. (A) Cell cycle and apoptosis in NB4 cells after treatment with 10,30,60 and 100 μ M BPA, ATRA (all-*trans*-retinoic acid) 1 μ M and the combination of ATRA 1 μ M and BPA, at the indicated concentrations for 48 hrs. (B) Cell cycle analysis and apoptosis in K562 cells after 48 hrs of treatment with 60 and 100 μ M BPA. (C) Cell cycle analysis and apoptosis in HL60 cells after treatment with 10, 30, 60 and 100 μ M BPA for 48 hrs.

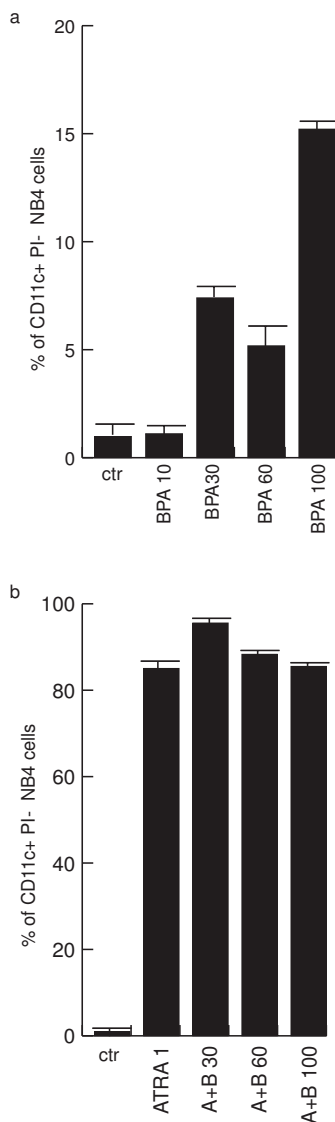


Figure 2
BPA induces dose dependent differentiation in NB4 cells. (A) CD11c expression levels measured by FACS after 48 h of treatment with 10,30,60 and 100 μM BPA. (B) CD11c expression levels after treatment with ATRA 1 μM or with the combination of ATRA 1 μM and BPA at the indicated concentrations for 48 hrs. Note that PI positive cells have been excluded from the analysis.

recommended by the suppliers; samples were analysed by FACS with Cell Quest technology (Becton Dickinson) as previously reported [20,21]. We measured as apoptotic fraction the Annexin V positive, PI negative cells. As second assays the caspase 8, 9 and 7, 3 detection (B-Bridge) was performed as recommended by suppliers and quantified by FACS (Becton Dickinson). NB4 cells were treated for 48 h with 10-60-100 μM BPA.

Granulocytic differentiation assay

Granulocytic differentiation was carried out as previously described [22]. Briefly, NB4 cells, treated for 48 h with 10-30-60-100 μM BPA, ATRA 1 μM or with ATRA 1 μM and BPA at the indicate prima concentrations, were harvested and resuspended in 10 μl phycoerythrine-conjugated CD11c (CD11c-PE) (Pharmingen). Control samples were incubated with 10 μl PE or FITC conjugated mouse IgG1, incubated for 30 min at 4 °C in the dark, washed in PBS and resuspended in 500 μl PBS containing PI (0.25 μg/ml). Samples were analysed by FACS with Cell Quest technology (Becton Dickinson). PI positive cells have been excluded from the analysis.

Western blot analyses

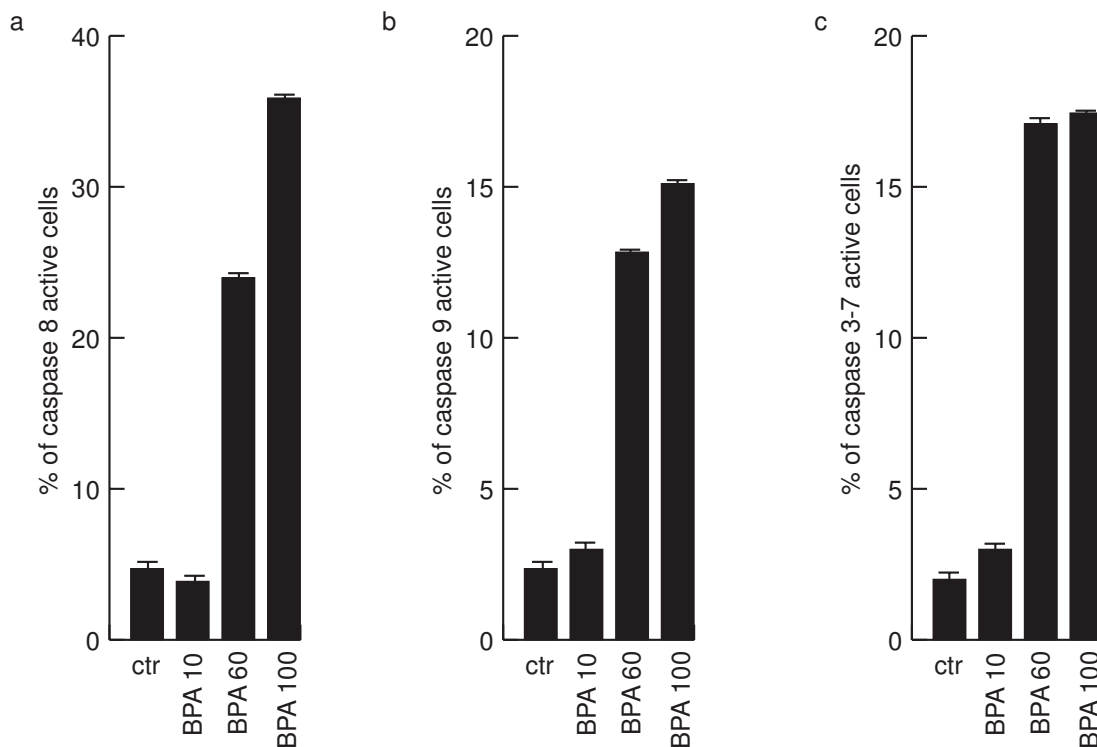
40 micrograms of total protein extracts were separated on a 15% polyacrylamide gel and blotted as previously described [23]. Western blots were shown for p21 (Transduction Laboratories, dilution 1:500), p27 c-19 (Santa Cruz sc-528 rabbit, dilution 1:500), p16 (Santa Cruz sc-468 rabbit, dilution 1:500). For determination of Rb, pRb, p53, ERalpha and cyclin D 35 μg of total protein extracts were separated on a polyacrylamide gel and blotted. Antibodies were: cyclin D (Zymed), pRb, p53, RB and ERalpha (Santa Cruz). Total ERKs (Santa Cruz) were used to normalise for equal loading. For quantification of TRAIL protein, 100 μg of total protein extracts were separated on a 10% polyacrylamide gel and blotted. Western blots were shown for TRAIL (Abcam Ab 16963-1). For determination of FAS, FLIP-L and FLIP-S, BAD, pBAD and BCL2, 35 μg of total protein extracts were separated on a 12% polyacrylamide gel and blotted. Antibodies used were: FAS (ProSci xw-7192, dilution 1:500), Flip (Alexis 804-429-C100, dilution 1:500), BAD (Cell signalling #9292, dilution 1:500), pBAD (p-Bad ser 136, #9295 cell signalling, dilution 1:500), Bcl2 (Bcl2 (Ab-1) Oncogene Science, dilution 1:500). Total ERKs were used to normalise for equal loading.

For determination of ERK2, pERK, Akt and pAkt, 35 μg of total protein extracts were separated on a 12% polyacrylamide gel and blotted. Antibodies used were: ERK2 (Santa Cruz sc-154, dilution 1:500), pERK (Santa Cruz sc-7383, dilution 1:200), pAkt (Cell signalling cod 9271, dilution 1:1000) and Akt (Cell signalling Akt cod 9272, dilution 1:1000). For quantification of histone H3 acetylation, 40 μg of total protein extracts were separated on a 15% polyacrylamide gel and blotted. Antibodies used were: acetylated histone H3 (Upstate cat. 06-599, dilution 1:500). Total ERKs were used to normalise for equal loading.

Results

BPA induces dose dependent apoptosis in acute myeloid leukemia cells

To understand the potential role of BPA in biological systems of leukemias we tested the action of BPA in three different acute myeloid leukemia models such as NB4,

**Figure 3**

BPA induces apoptosis via caspase activation in NB4 cells. Caspase 8, 9 and 37 assays have been carried out by FACS analysis in NB4 cells after 48 h of incubation with the indicated concentrations of BPA.

HL60 and K562 cells. As it is shown in Fig. 1, different concentrations of BPA are able to induce an increase of the sub-G1 peak in all the cell lines tested, HL60 being the most resistant one. In NB4 cells, a model from promyelocytic leukemia containing the fusion protein PML-RAR α and sensitive to retinoids, the highest concentration of BPA used induces around 38% of apoptosis after 48 hrs. This apoptosis is not synergistically modulated by the double treatment with 1 μ M Retinoic Acid (RA) as shown in Fig. 1A. Differently, cell cycle arrest seems to be affected by the double treatment, showing an increase of the G1 peak at low dose BPA (30 μ M) and an increase of the G2-M fraction of cells at the highest concentration of BPA (100 μ M). Differently, in the K562 cells, a model of AML derived from a CML containing the Philadelphia chromosome, the treatment with BPA showed an increase of cell death proportional to the dose increase of BPA, together with a G1 peak at the lower dose and a G2-M increase at the higher dose (Fig. 1B). Finally, HL60 cells showed an increase of apoptosis at the higher dose of BPA (100 μ M) in agreement with what reported previously [17]. This increase is directly proportional with the

enrichment in G1 phase of HL60 cells upon treatment with increasing doses of BPA (Fig. 1C).

BPA induces dose dependent differentiation in NB4 cells

That BPA was able to induce apoptosis and to influence the cell cycle of NB4 cells, prompted us to check its effects on granulocytic differentiation of these cells. As shown in Fig. 2A by FACS analyses, BPA is able to differentiate NB4 cells versus granulocytes in a dose dependent manner. However, the effect was weak if compared with the one of RA at the same time in the NB4 cells (Fig. 2B), thus showing that BPA preferentially activates apoptotic actions in respect to differentiative effects in these cells.

BPA induces apoptosis via caspase activation in NB4 cells

To better identify which apoptotic pathway is activated by BPA, we tested by FACS analyses the initiator and effector caspases activation in NB4 cells after 48 h treatment with BPA. As it is shown in Fig. 3, both caspase 8 (Fig. 3A) and 9 (Fig. 3B) are cleaved and active upon BPA treatment. Note that caspase 8 resulted more active, suggesting a prior activity of BPA on the extrinsic pathway of apoptosis

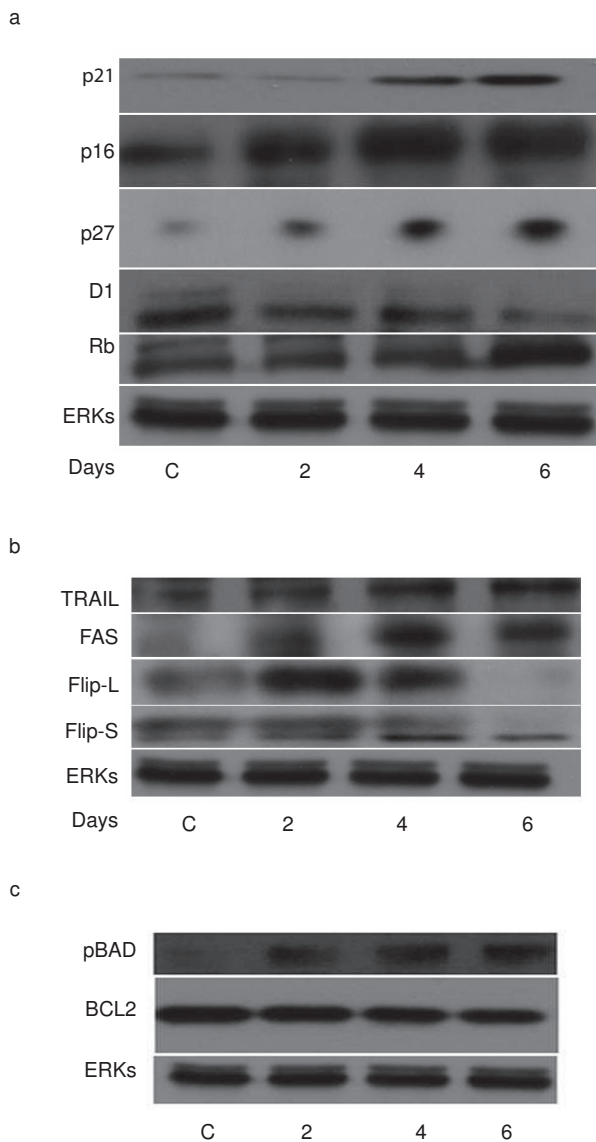


Figure 4
BPA induces modulation of cell cycle regulators and apoptotic players in NB4 cells. (A) Western blot analysis showing p21, p27, p16, cyclin D1 and RB expression levels in NB4 cells treated with 60 μM BPA for 2, 4 and 6 days. (B) Western blot analysis showing TRAIL, FAS, Flip-L and Flip-S expression levels in NB4 cells treated with 60 μM BPA for the indicated days. (C) Western blot analysis showing BCL2 and pBAD expression levels after treated with 60 μM BPA for the indicated days. Total ERKs expression levels account for equal loading.

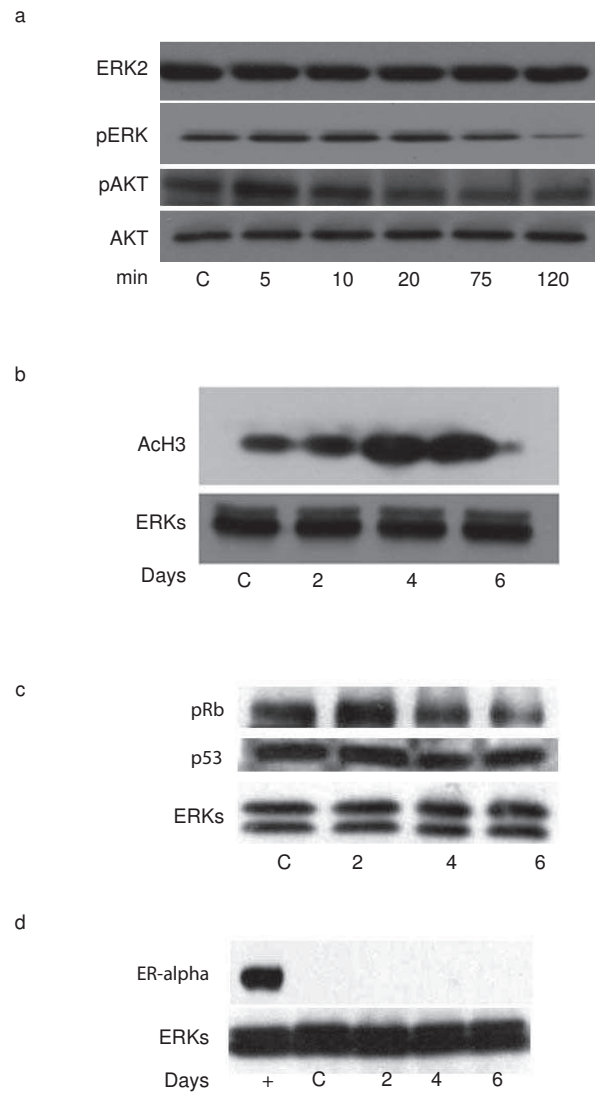


Figure 5
BPA induces modulation of ERK and AKT phosphorylation and increase of histone acetylation in NB4 cells. (A) Western blot analysis showing ERK and AKT phosphorylation in NB4 cells treated with 60 μM BPA at the times indicated times; (B) Western blot analysis of the acetylation levels of Histone H3 in NB4 cells treated for 2, 4 and 6 days with 60 μM BPA. ERKs expression levels account for equal loading); (C) Western blot analysis of the phosphorylation levels of Rb and p53 expression in NB4 cells treated for 2, 4 and 6 days with 60 μM BPA. ERKs expression levels account for equal loading); (D) Western blot analysis of the expression levels of ER alpha in NB4 cells treated for 2, 4 and 6 days with 60 μM BPA. As positive control for the ER alpha detection (indicated as +) 25 μg of MCF7 protein extracts have been used. ERKs expression levels account for equal loading.

at least as time scale. As expected, caspase 37, which are downstream of caspase 8 and 9, resulted activated by medium (60) and high doses (100) of BPA.

BPA induces modulation of cell cycle regulators and apoptotic players in NB4 cells

That BPA influenced both cell cycle progression and apoptosis of acute myeloid leukemias has been clarified by these results. To understand which molecular events underlie to these effects, we have tested its action on known cell cycle regulators in NB4 cells in a time dependent manner. As shown in Fig 4A, p21, p27 and p16 together with RB are up-regulated by BPA at the 60 μ M dose, whereas cyclin D1 which is known to modulate proliferation gets decreased. This scenario is reminiscent of a cell cycle block regulated at the molecular level. At the same time, checking for apoptotic key players we found that both FAS and TRAIL are up-regulated already at day 2 of treatment, while Flip-L is transiently up-regulated and then down-regulated, whereas Flip-S is down regulated (Fig. 4B). At the mitochondria cell death level, we could not find modulation of BCL2, but we could see increased phosphorylation of BAD (Fig. 4C) thus confirming that both pathways (extrinsic and intrinsic) gets activated by BPA in NB4 cells.

BPA induces modulation of ERK, AKT and Rb phosphorylation and increase of histone acetylation in NB4 cells

To better focus the activity of BPA in acute myeloid leukemia models, we decided to check whether BPA can also modulate non genomic actions. As shown in Fig. 5, BPA induce a decrease of ERK, Rb and AKT phosphorylation thus indicating that anti-proliferative actions occur by induction of non genomic pathways by 60 μ M of BPA in NB4 cells. Note that p53 expression levels stayed unchanged (Fig. 5c). In agreement with these findings, histone H3 acetylation is increased upon BPA treatment suggesting an effect (direct or indirect) on chromatin accessibility of BPA (Fig. 5B).

Discussion

The Endocrine Disrupting Compounds have been subject of high attention by the scientific community, since concerns have been raised about their actions and potential toxicities. Among the many chemicals, BPA is used in the assemble of polycarbonate plastic and epoxy resins, used in impact-resistant safety equipment and baby bottles, as protective coatings inside metal food containers, and as composite and sealant in dentistry. Exposure to BPA is thought to result primarily from ingestion of food containing BPA [6,7]. BPA is of concern to environmental public health because of its toxicity. At high doses, BPA demonstrates estrogen-like effects in experimental animals, but effects independent from its endocrine modu-

lating function have been poorly investigated. Thus, it is central to investigate the cyto-toxicity and apoptosis-inducing activities of BPA at the molecular level. The fact that BPA is able to induce effects on cell cycle and apoptosis in AML models indicates that BPA actions can go beyond the endocrine interference. This is also demonstrated by the fact that NB4 cells do not display detectable levels of ER alpha. Thus suggesting that effects of BPA in this cells are largely ER independent (Fig. 5d). This notion is a key point considering that BPA is industrially used and that its effects can cumulate. Although the properties seen on granulocytic differentiation are minor when compared to those of RA, the fact that BPA is used in equipments and baby bottles makes also these weak effects of significance. Even more interesting is the induction of cell death which is clearly specifically regulated at the molecular level. Indeed, the fact that three different cell lines respond with apoptosis to BPA treatment and that this effect seems to be dose dependent indicates that this is a general feature of BPA treatment and that this might be reproduced in many other cells. These evidences are exciting from several point of view: if from one side we might consider the induction of apoptosis as an interesting anti-cancer action, on the other side we have to keep in mind that these effects might also be elicited in normal cells in the different compartments of the human body and thus might contribute to the toxicity of BPA. The regulation of caspase-dependent pathways of apoptosis suggests a specific action on the extrinsic and intrinsic pathways of apoptosis which is confirmed by the clear induction of Fas and TRAIL and by Flip down regulation in NB4 cells. Even if our data would support a model in which the extrinsic pathway of apoptosis is more active, we do not exclude the importance of the mitochondria de-regulation of apoptosis which is indeed confirmed by caspase 9 activation and BAD phosphorylation. Considering that many clinical treatments target apoptosis at the present, our data suggest that the contact or the assumption of BPA might increase the effects of a on-going treatment in humans, apart, of course, having effects on its own. Finally, the fact that BPA decreases the activity of ERK and AKT well integrates with its anti-proliferative and apoptotic actions suggesting that the cross-talk of different molecular actions contribute to the cell cycle arrest and to the apoptosis in human biological systems. The hyperacetylating effect shown on histone H3 confirms the property of BPA to modulate the chromatin in a more accessible state thus corroborating the hypothesis that BPA contributes with a plethora of different effects to the induction of cell cycle arrest, weak differentiation and apoptosis in a specific and molecularly defined manner. If the hyperacetylation upon BPA treatment is a direct or indirect effect on chromatin, remains to be established. More characterized studies on BPA exposed population in healthy or unhealthy status will decipher in the future the real impact of these molecular actions.

Conclusion

Our data strongly indicate that BPA has molecular activities that go much beyond its ED function. These actions have been well focused as cell cycle arrest and apoptosis and the molecular pathways involved have been identified. This knowledge clearly shows that BPA effects have to be considered independently of its ED action and might help in the understanding of the adverse effects caused in humans.

Abbreviations

AKT: RAC-alpha serine/threonine-protein kinase; AML: Acute Myeloid Leukemia; ATRA: All Trans Retinoic Acid; BAD: Bcl2 Antagonist of cell Death, BCL2-associated death promoter; BCL2: B Cell Lymphoma 2; BPA: Bisphenol A or 2,2-bis(4-hydroxy-phenol)propane; CML: Chronic Myeloid Leukemia; EDC: Endocrine Disruptor Compounds; ED: Endocrine Disruptor; ERK: Extracellular Signal-Regulated Kinase; FAS: Apoptosis-mediating Surface Antigen, Tumor necrosis factor receptor superfamily member 6; FLIP: FLICE Inhibitor Protein; TRAIL: TNF Related Apoptosis Inducing Ligand; RA: Retinoic Acid; RB: Retinoblastoma.

Competing interests

The authors declare that they have no competing interests.

Authors' contributions

PB, LM, AD, MM, AN, IL, GF, RM, VC, MC, FDB, FM, CDA, VDC, MM, AB, GDP, ND, M, LD, MTV, MC, RB, EN, VS, GDM and AM contributing in performing the experiments shown and in the conceptual understanding of the results. PB and LA critically discussed the experimental data and wrote the manuscript.

Acknowledgements

In memory of Ettore M. Schiavone. The work in the author's laboratories has been supported by: AIRC (LA), HEALTH-F2-2007-200620, HEALTH-F4-2007-200767, HEALTH-F4-2009-221952, la Regione Campania L5, annualità 2005, Fondazione Luigi Califano. Dr A. Bolli has been supported by a grant from the National Institute of Biostructures and Biosystems (INBB).

References

- Colborn T, vom Saal FS, Soto AM: **Developmental effects of endocrine-disrupting chemicals in wildlife and humans.** *Environ Health Perspect* 1993, **101**:378-384.
- Vandael L: **Endocrine disruption agents: environment, health, public policies, and the precautionary principle.** *Bull Acad Natl Med* 2000, **184**:1477-1486. discussion 14871490
- Vasseur P, Cossu-Leguille C: **Linking molecular interactions to consequent effects of persistent organic pollutants (POPs) upon populations.** *Chemosphere* 2006, **62**:1033-1042.
- Cheek AO, Kow K, Chen J, McLachlan JA: **Potential mechanisms of thyroid disruption in humans: interaction of organochlorine compounds with thyroid receptor, transthyretin, and thyroid-binding globulin.** *Environ Health Perspect* 1999, **107**:273-278.
- Welshons WV, Thayer KA, Judy BM, Taylor JA, Curran EM, vom Saal FS: **Large effects from small exposures. I. Mechanisms for endocrine-disrupting chemicals with estrogenic activity.** *Environ Health Perspect* 2003, **111**:994-1006.
- Kang JH, Kondo F, Katayama Y: **Human exposure to bisphenol A.** *Toxicology* 2006, **226**:79-89.
- Vandenberg LN, Hauser R, Marcus M, Olea N, Welshons WV: **Human exposure to bisphenol A (BPA).** *Reprod Toxicol* 2007, **24**:139-177.
- Durando M, Kass L, Piva J, Sonnenschein C, Soto AM, Luque EH, Munoz-de-Toro M: **Prenatal bisphenol A exposure induces preneoplastic lesions in the mammary gland in Wistar rats.** *Environ Health Perspect* 2007, **115**:80-86.
- Howdeshell KL, Hotchkiss AK, Thayer KA, Vandenberg JG, vom Saal FS: **Exposure to bisphenol A advances puberty.** *Nature* 1999, **401**:763-764.
- Howdeshell KL, Wilson VS, Furr J, Lambright CR, Rider CV, Blystone CR, Hotchkiss AK, Gray LE Jr, et al: **A mixture of five phthalate esters inhibits fetal testicular testosterone production in the sprague-dawley rat in a cumulative, dose-additive manner.** *Toxicol Sci* 2008, **105**:153-165.
- Kubo K, Arai O, Ogata R, Omura M, Hori T, Aou S, et al: **Exposure to bisphenol A during the fetal and suckling periods disrupts sexual differentiation of the locus coeruleus and of behavior in the rat.** *Neurosci Lett* 2001, **304**:73-76.
- Kubo K, Arai O, Omura M, Watanabe R, Ogata R, Aou S: **Low dose effects of bisphenol A on sexual differentiation of the brain and behavior in rats.** *Neurosci Res* 2003, **45**:345-356.
- Richter CA, Birnbaum LS, Farabolini F, Newbold RR, Rubin BS, Talsness CE, Vandenberg JG, Walsler-Kuntz DR, vom Saal FS: **In vivo effects of bisphenol A in laboratory rodent studies.** *Reprod Toxicol* 2007, **24**:199-224.
- Rubin BS, Lenkowski JR, Schaeberle CM, Vandenberg LN, Ronsheim PM, Soto AM: **Evidence of altered brain sexual differentiation in mice exposed perinatally to low, environmentally relevant levels of bisphenol A.** *Endocrinology* 2006, **147**:3681-3691.
- Schonfelder G, Flick B, Mayr E, Talsness C, Paul M, Chahoud I: **In utero exposure to low doses of bisphenol A lead to long-term deleterious effects in the vagina.** *Neoplasia* 2002, **4**:98-102.
- Timms BG, Howdeshell KL, Barton L, Bradley S, Richter CA, vom Saal FS, et al: **Estrogenic chemicals in plastic and oral contraceptives disrupt development of the fetal mouse prostate and urethra.** *Proc Natl Acad Sci USA* 2005, **102**:7014-7019.
- Terasaka H, Kadoma Y, Sakagami H, Fujisawa S: **Cytotoxicity and apoptosis-inducing activity of bisphenol A and hydroquinone in HL-60 cells.** *Anticancer Res* 2005, **25**:2241-2247.
- Terasaka H, Morshed SR, Hashimoto K, Sakagami H, Fujisawa S: **Hydroquinone-induced apoptosis in HL-60 cells.** *Anticancer Res* 2005, **25**:161-170.
- Scognamiglio A, Nebbioso A, Manzo F, Valente S, Mai A, Altucci L: **HDAC-class II specific inhibition involves HDAC proteasome-dependent degradation mediated by RANBP2.** *Biochim Biophys Acta* 2008, **1783**:2030-2038.
- Altucci L, Rossin A, Raffelsberger W, Reitmair A, Chomienne C, Gronemeyer H: **Retinoic acid-induced apoptosis in leukemia cells is mediated by paracrine action of tumor-selective death ligand TRAIL.** *Nat Med* 2001, **7**:680-686.
- Nebbioso A, Clarke N, Voltz E, Germain E, Ambrosino C, Bontempo P, Alvarez R, Schiavone EM, Ferrara F, Bresciani F, Weisz A, de Lera AR, Gronemeyer H, Altucci L: **Tumor-selective action of HDAC inhibitors involves TRAIL induction in acute myeloid leukemia cells.** *Nat Med* 2005, **11**:77-84.
- Mai A, Valente S, Nebbioso A, Simeoni S, Ragno R, Massa S, Brosch G, De Bellis F, Manzo F, Altucci L: **New pyrrole-based histone deacetylase inhibitors: Binding mode, enzyme- and cell-based investigations.** *Int J Biochem Cell Biol* 2009, **41**:235-247.
- Mai A, Cheng D, Bedford MT, Valente S, Nebbioso A, Perrone A, Brosch G, Sbardella G, De Bellis F, Miceli M, Altucci L: **epigenetic multiple ligands: mixed histone/protein methyltransferase, acetyltransferase, and class III deacetylase (sirtuin) inhibitors.** *J Med Chem* 2008, **51**:2279-2290.



Contents lists available at ScienceDirect

Bioorganic & Medicinal Chemistry

journal homepage: www.elsevier.com/locate/bmc

Epigenetic profiling of the antitumor natural product psammaplin A and its analogues

José García^a, Gianluigi Franci^{b,f}, Raquel Pereira^a, Rosaria Benedetti^{b,c,e}, Angela Nebbioso^b, Fátima Rodríguez-Barríos^a, Hinrich Gronemeyer^d, Lucia Altucci^{b,f,*}, Angel R. de Lera^{a,*}

^a Departamento de Química Orgánica, Universidad de Vigo, 36310 Vigo, Spain

^b Dipartimento di Patologia generale, Seconda Università di Napoli, Vico L. De Creschio 7, 80138 Napoli, Italy

^c Università di Napoli Federico II, Dipartimento di Chimica Organica e Biochimica, Italy

^d Department of Cancer Biology - Institut de Génétique et de Biologie Moléculaire et Cellulaire (IGBMC)/CNRS/INSERM/ULP, BP 163, 67404 Illkirch Cedex, C. U. de Strasbourg, France

^e Università di Napoli Federico II, Dipartimento di Fisica, 6, CNR-IGB, Via P. Castellino, 80100, Napoli, Italy

^f CNR-IGB, Via Pietro Castellino 80100 Napoli, Italy

ARTICLE INFO

Article history:

Received 30 September 2010

Accepted 8 December 2010

Available online 15 December 2010

Keywords:

Psammaplin A

Epigenetics

HDAC

DNMT

Total synthesis

Natural products

ABSTRACT

A collection of analogues of the dimeric natural product psammaplin A that differ in the substitution on the (halo)tyrosine aryl ring, the oxime and the diamine connection has been synthesized. The effects on cell cycle, induction of differentiation and apoptosis of the natural-product inspired series were measured on the human leukaemia U937 cell line. Epigenetic profiling included induction of p21^{WAF1}, effects on global H3 histone and tubulin acetylation levels as well as in vitro enzymatic assays using HDAC1, DNMT1, DNMT3A, SIRT1 and a peptide domain with p300/CBP HAT activity. Whereas the derivatives of psammaplin A with modifications in the length of the connecting chain, the oxime bond and the disulfide unit showed lower potency, the analogues with changes on the bromotyrosine ring exhibited activities comparable to those of the parent compound in the inhibition of HDAC1 and in the induction of apoptosis. The lack of HDAC1 activity of analogues modified on the disulfide bond suggests that its cleavage must occur in cells to produce the monomeric Zn²⁺-chelating thiol. This assumption is consistent with the molecular modelling of the complex of psammaplin A thiol with h-HDAC8. Only a weak inhibition of DNMT1, DNMT3A and residual activities with SIRT1 and a p300/CBP HAT peptide were measured for these compounds.

© 2010 Elsevier Ltd. All rights reserved.

1. Introduction

Psammaplin A (1, PsA, Scheme 1) is a symmetrical disulfide dimer derived from the condensation of modified tyrosine and cysteine units¹ (for a proposal of its biogenesis, see 2,3). Although it was first isolated in 1987 from an unidentified sponge⁴ and from *Psammaplysilla* sp.,^{5,6} PsA is found, together with biogenetically-related congeners, in several Verongidas^{2,3,6–10} and in some associations of these species.^{11,12}

Antibacterial and antitumor activities have been reported for PsA. The in vitro antibacterial activity of PsA against both *Staphylococcus aureus* (SA) and methicillin-resistant *Staphylococcus aureus* (MRSA) was considered the result of the inhibition of DNA gyrase¹³ and induced arrest of bacterial DNA synthesis. PsA also inhibits topoisomerase II (topo II),¹⁴ farnesyl protein transferase,⁸ leucine aminopeptidase,⁸ mycothiol-S-conjugate amidase,¹⁵ chitinase,¹⁰ Pol α -primase,¹⁶ PPAR γ ^{17–20} and mammalian aminopeptidase N

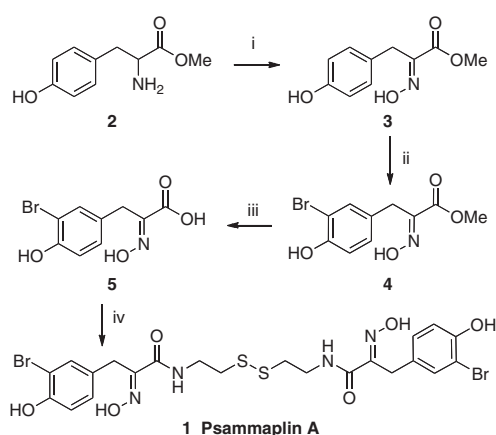
(APN).²¹ Targeting multiple proteins that impact on DNA topology, DNA replication, transcription, apoptosis, tumor invasion, and angiogenesis likely contributes to the significant cytotoxicity displayed by PsA in human lung (A549), ovarian (SKOV-3), skin (SK-MEL-2), CNS (XF498), and colon (HCT15) cancer cell lines.¹²

PsA was also reported to inhibit in vitro the chromatin-modifying enzymes histone deacetylase (HDAC) and DNA methyl transferase (DNMT).³ HDAC and DNMT are epigenetic enzymes that catalyze the covalent modifications of histone proteins and DNA in chromatin,²² and therefore they are considered prime new targets²³ for the treatment and prevention of cancer^{24–34} and other diseases.³⁵ The modification of chromatin is thus an addition to the list of potential mechanisms involved in the anticancer actions of the natural product PsA.

Histone acetylation is a dynamic process in which a cellular steady state is maintained by the opposing activities of histone acetyltransferases (HATs) and deacetylase enzymes (HDAC) acting at the ϵ -amino groups of evolutionally conserved lysine residues located at the histone N-termini. HATs transfer the acetyl moiety from acetyl CoA to the histone lysine residues whereas HDACs catalyze their removal. Individual HATs and HDACs display distinct

* Corresponding authors.

E-mail addresses: lucia.altucci@unina2.it (L. Altucci), qolera@uvigo.es (Angel R. de Lera).



Scheme 1. Reagents and conditions: (i) Na_2WO_4 , H_2O_2 , 25 °C, 3 h (63%); (ii) NBS, CH_3CN , 25 °C, 2 h (82%); (iii) LiOH, $\text{THF-H}_2\text{O}$, 23 °C, 12 h (99%); (iv) DCC, *N*-hydroxyphthalimide, Et_3N , cystamine, 1,4-dioxane, MeOH, 25 °C, 12 h (60%).

specificities for certain individual lysine residues and particular histones. Although the factors responsible for the specificity are poorly understood they might reflect different biological functions of the various enzymes. Regardless of the details, it is widely accepted that histone acetylation is essential to establish a transcriptionally competent state of chromatin²² and consequently contributes to the gene activation/gene repression transcriptional status of cells. Two histone deacetylase inhibitors (HDACis), suberoylanilide hydroxamic acid (SAHA, vorinostat, Zolinza[®]), and FK228 (romidepsin, Istodax[®]) are used as therapy for cutaneous T-cell lymphoma,³⁶ and several others are currently undergoing clinical trials as potential targeted cancer chemotherapeutic agents.^{37–41}

In eukaryotes DNMTs catalyze the addition of methyl groups from *S*-adenosyl-*L*-methionine (SAM) to the C5 position of cytosine bases within the CpG-rich islands in DNA. Methylation of DNA is an epigenetic mark associated to a repressed chromatin state which inhibits gene transcription.^{42,43} Several tumour suppressor genes are hypermethylated in tumours, which suggest a link between aberrant DNA methylation and cancer.^{44–47} DNA methyl transferase inhibitors (DNMTis)⁴⁸ structurally related to cytidine (5-azacytidine, Vidaza[®]) and 5-aza-deoxycytidine, Dacogen[®]) are already in the clinic for the treatment of myelodysplastic syndrome.⁴⁹

Since histone acetylation and DNA methylation play a key role in the pathophysiology of cells, dual inhibitors of HDAC or DNMT are therapeutically more appealing than combination of these drugs.^{50,51} We thus became intrigued by the reports on the potent activity of psammaplin A (**1**) in the inhibition of these two epigenetic enzymes (HDAC: $\text{IC}_{50} = 4.2$ nM; DNMT: $\text{IC}_{50} = 18.6$ nM using in vitro cell-free enzyme assays)³ as well as by the in vitro and in vivo inhibition of tumour growth induced by this natural product.²⁰ Despite the reports indicating some drawbacks for the development of **1** as a drug due to its poor physiological stability,^{15,21,52} we undertook the synthesis of a family of analogues with the aim to discover more potent and selective derivatives of **1** as well as to shed light into the mechanism of epigenetic inhibition by **1**. Apart from the work of Nicolaou focused on antibacterial activities, no structure–activity relationship studies of the anticancer activities of PsA analogues have been reported, which are necessary for an eventual lead optimization project within this class of modified tetrapeptides.

2. Chemistry. Synthesis of psammaplin A and derivatives

All previous synthetic approaches to **1** have focused on the final construction of the dimeric disulfide structure by condensation of

the corresponding carboxylic acid with the symmetrical diamine cystamine. Both Hoshino et al.⁵³ and Nicolaou et al.^{54,55} installed the oxime function after the synthesis of the corresponding pyruvic acid derived from *L*-tyrosine, in a sequence that afforded **1** in moderate overall yields. Nicolaou then screened in antibacterial assays a 3828-membered library of heterodimeric psammaplin A analogues¹⁵ obtained from symmetrical precursors by combinatorial scrambling via catalytically-induced disulfide exchange reactions. A recently described three-step (43% overall yield) synthesis of PsA **1** starts from the considerably more expensive and less versatile 4-hydroxyphenylpyruvic acid.⁵⁶

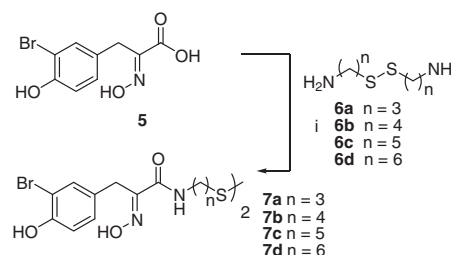
We modified the above synthesis of **1** by performing the bromination of the phenol ring on the corresponding oxime **3** (Scheme 1).⁵⁷ As shown on Scheme 1, the amino group of *L*-tyrosine **2** was oxidized to the hydroxyimino ester **3** in 60% yield using Na_2WO_4 and H_2O_2 in ethanol.⁵⁸ A monobrominated product **4** was obtained by treatment of **3** with one equivalent of NBS in CH_3CN at 25 °C,^{58,59} with no evidence of formation of the dibromo derivative or the dibrominated spirocyclic isoxazoline.⁵⁷ After saponification of **4** the carboxylic acid **5** was coupled with cystamine using Hoshino's conditions.⁵³ The overall yield for the synthetic sequence is 29%, with a slight improvement over the two routes previously described from *L*-tyrosine **2**. The synthetic scheme is advantageous for the preparation of diverse PsA analogues starting from commercial tyrosine derivatives.

Using the methodology depicted on Scheme 1, the synthesis of PsA homologues containing from three to six methylene units was completed, albeit in low yields (Scheme 2), using the non-commercial diamines **6a–d**, which were synthesized following a general methodology.⁶⁰

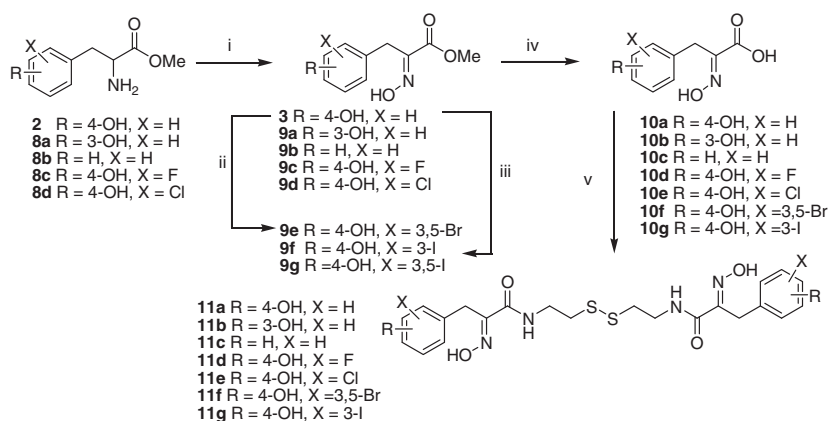
Similarly, PsA analogues that preserve the native connecting cystamine unit but differ in the substituents at the aryl ring (Scheme 3) were synthesized using either commercially available tyrosine derivatives or the synthetic halogenated analogues (with bromine or iodine at C3) after oxidation of the amine to the oxime (Scheme 3). Some compounds of the series (**11a**, **11c**, **11d** and **11e**) have previously been described by Nicolaou on his search for new antibacterial agents.⁵⁵ Bromopsammaplin A **11f** is also a natural product isolated from an association of the sponges *Jaspis wondensis* and *Poecillastra wondensis*.¹²

Condensation of acid **5** with amines **12** and **14a–c** (Scheme 4) provided analogues **13** and **15a–c** which were designed to further our understanding of the mechanism underlying the biological activity of the parent PsA as HDAC inhibitor. The dimer **13** contains an ethylene group replacing the disulfide bond functionality. Products **15b,c** are monomers that have, respectively, methyl ether and methyl sulfide as end groups. The primary alcohol **16** was obtained by acidic (7:2:1 $\text{THF}/\text{HCO}_2\text{H}/\text{H}_2\text{O}$) deprotection of silyl ether **15a**.

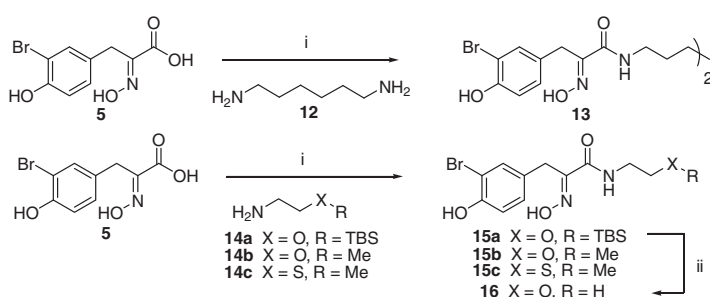
The derivative lacking the oxime was also of interest to reveal whether this functional group is critical for the epigenetic activity of **1**. Compound **20** was prepared as described on Scheme 5. The bromination of methyl 3-(4-hydroxyphenyl)propanoate using the



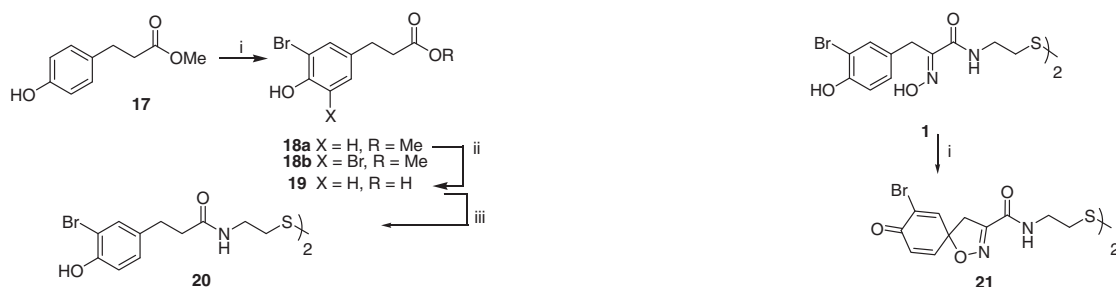
Scheme 2. Reagents and conditions: (i) DCC, *N*-hydroxyphthalimide, Et_3N , diamine **6**, 1,4-dioxane, MeOH, 25 °C, 12 h (**7a**, 16%; **7b**, 21%; **7c**, 34%; **7d**, 14%).



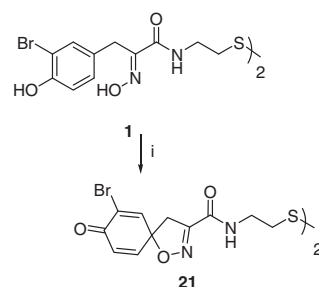
Scheme 3. Reagents and conditions: (i) Na_2WO_4 , H_2O_2 , 25 °C, 3 h (**9a**, 57%; **9b**, 50%; **9c**, 64%; **9d**, 80%); (ii) NBS, CH_3CN , 25 °C, 5 h (**9e**, 80%); (iii) I_2 , Ag_2SO_4 , MeOH, 25 °C, 15 min (**9f**, 51%; **9g**, 23%); (iv) LiOH, $\text{THF-H}_2\text{O}$, 23 °C, 12 h (**10a**, 99%; **10b**, 99%; **10c**, 99%; **10d**, 97%; **10e**, 98%; **10f**, 99%; **10g**, 99%); (v) DCC, *N*-hydroxyphthalimide, Et_3N , cystamine, 1,4-dioxane, MeOH, 25 °C, 12 h (**11a**, 46%; **11b**, 54%; **11c**, 15%; **11d**, 57%; **11e**, 57%; **11f**, 42%; **11g**, 52%).



Scheme 4. Reagents and conditions: (i) DCC, *N*-hydroxyphthalimide, Et_3N , **12** or **14a-c**, 1,4-dioxane, MeOH, 25 °C, 14 h (**13**, 70%; **15a**, 83%; **15b**, 20%; **15c**, 18%); (ii) 7:2:1 THF/ $\text{HCO}_2\text{H}/\text{H}_2\text{O}$, 25 °C, 14 h (76%).



Scheme 5. Reagents and conditions: (i) NBS, DMF, 25 °C, 5 h (**18a**, 56%; **18b**, 17%); (ii) LiOH, $\text{THF-H}_2\text{O}$, 23 °C, 12 h (99%); (iii) DCC, *N*-hydroxyphthalimide, Et_3N , cystamine, 1,4-dioxane, MeOH, 25 °C, 14 h (40%).



Scheme 6. Reagents and conditions: (i) MTA, CH_3CN , 25 °C, 15 h (5%).

conditions described for oxime **4** (NBS in CH_3CN) yielded a mixture of mono- and dibromo derivatives, **18a** and **18b**, respectively, in a 3:1 ratio. Hydrolysis of the former followed by the coupling of **19** with cystamine led to the desired disulfide **20** in moderate yield (Scheme 5).

Lastly the spirocyclic hexadienyl-isoxazoline **21**, a potential metabolite of PsA^1 could only be obtained, albeit in very low yield (5%), by the oxidative-induced cyclization⁶¹ of PsA^1 with manganese(III) tris(acetylacetonate) (MTA)⁶² (Scheme 6) after many other methods failed.

3. Biological characterization

Firstly, we focused on the reported inhibition of HDAC by PsA and the synthetic analogues, as well as on their effects on cell cycle, induction of differentiation and apoptosis on the U937 human

acute myeloid leukemia cell line. In vitro tests of the compounds at 5 μM on human recombinant HDAC1, using SAHA as a positive control, confirmed the enzymatic inhibition of PsA^1 (Fig. 1A). In addition, some analogues (**11a-e**, **11g**) reduced the activity of HDAC1 more efficiently than **1**. The other compounds of the series (**7a-d**, **11f**, **13**, **15b-c**, **16**, **20** and **21**) did not noticeably affect HDAC1 activity. Compounds with longer chain connecting the disulfide to the hydroxyimino amide (**7a-d**) lack significant inhibitory activity. A similar result was observed for compounds having the disulfide replaced by methylene units (**13**) and for the monomers with either methyl ether (-OMe), methyl thioether (-SMe) or alcohol (-OH) functionalities (**15b**, **15c** and **16**, respectively). In contrast, the inhibitory activity is maintained and even increased with compounds that preserve the general modified tetrapeptide scaffold of PsA regardless of the nature and pattern of the substituents at the aryl ring (**11a-f**). The more drastic change of the overall aryl ring structure imparted by the spirocycle together

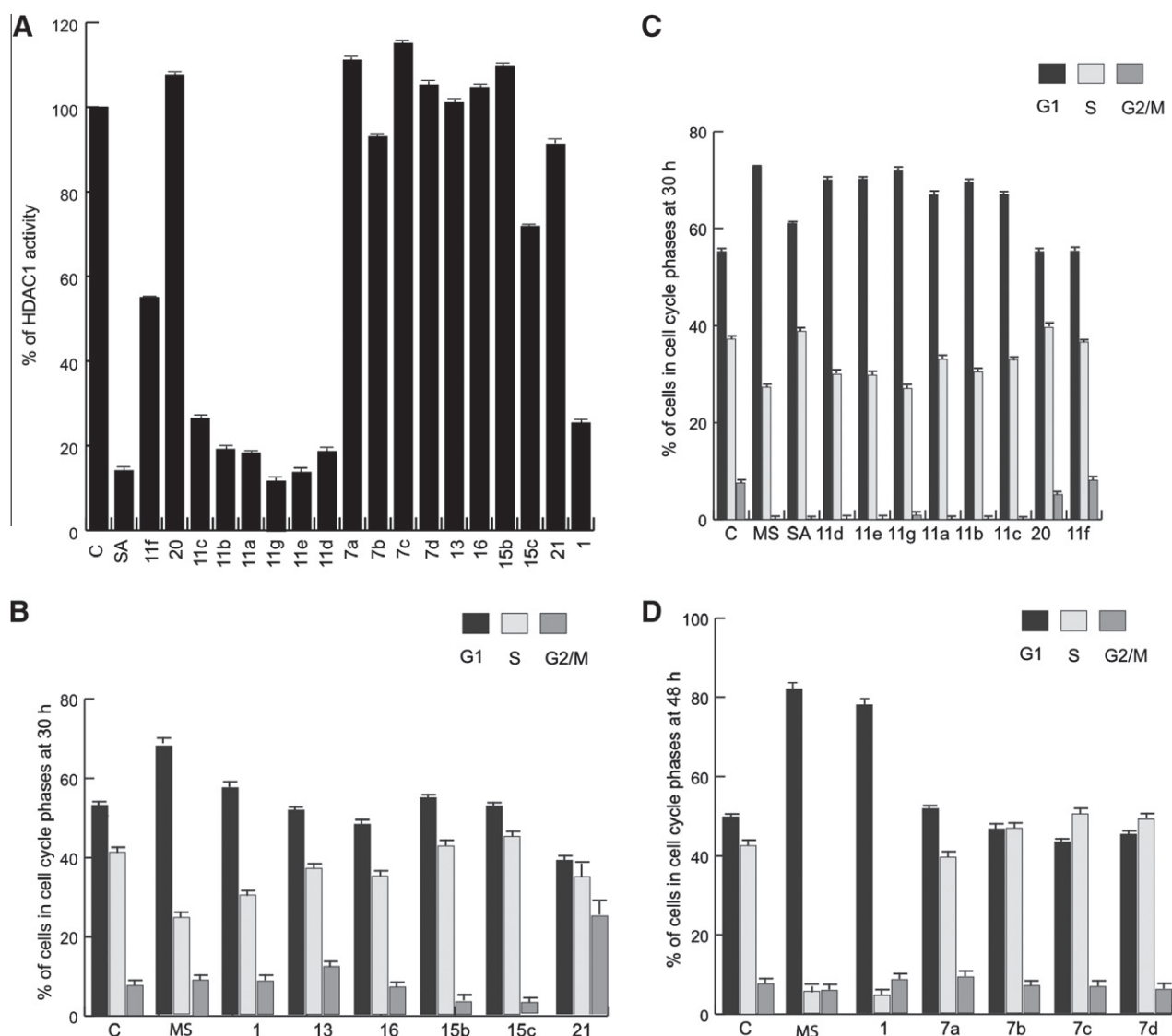


Figure 1. (A) HDAC1 fluorescent assay with the indicated compounds at 5 μ M. The inhibition is reported as percentage of activity relative to the control (100%). (B–D) Cell cycle analysis and apoptosis in U937 cells treated with the indicated compounds at 5 μ M for 30 h. The data represent the media of independent duplicates.

with the reduction of flexibility and the lack of free oxime in derivative **21** led to substantial loss of HDAC inhibitory activity.

Cell-based assays were performed on the U937 myeloid leukemia cells to determine the anti-proliferative potential and the ability of the compounds to revert myeloid tumor cells to differentiated granulocytes. Cell cycle progression, differentiation and amount of cells that undergo apoptosis following treatment with PsA **1** and analogues (5 μ M) for 30, 40, and 48 h were determined (Figs. 1B and 2). Compared to the vehicle-treated cells and relative to the positive control represented by the known HDACs MS275 (HDAC1,2,3-selective) and SAHA (also HDAC6 inhibitor),^{63,64} only PsA **1** and some analogues induced cell cycle arrest in G1 (Fig. 1, panels B–D). In particular after 30 h PsA induced a time-dependent accumulation of U937 cells in the G1 phase (60%), and analogues **11a–g** and **20** showed even greater arrest (80%), with values comparable to MS-275 (Fig. 1C). A clear correlation between the in vitro HDAC1 inhibition and the in vivo efficacy to induce cell cycle arrest was noticed for the most active compounds. Compound **21**, on the other hand, appears to block cell cycle at G2/M. The remaining analogues gave no detectable activities on cell cycle progression even after longer (48 h) treatment regimes (Fig. 1B and D).

The percentage of apoptotic cells (measured as caspase 3 activation by FACS analysis) increased when U937 cells were treated with **1** and series **11a–g** for 30 h (Fig. 2A). After 30 h induction with compounds **11a–e** and **11g** the percentage of apoptotic cells varied between 30% and 40%. Other compounds, including bromopsammaplin A (**11f**), and the derivative lacking the oxime function **20**, exhibited only minor effects even at longer incubation times (40 h). The results confirmed the in vitro findings since the most potent inducers of differentiation and apoptosis in U937 cells are the **11a–g** series of ring-modified PsA analogues (with the exception of bromopsammaplin A **11f**). Modifications in the chain length and the disulfide led to lower values of apoptosis, in agreement with the enzymatic assays. Interestingly, spiro derivative **21** showed comparable induction of apoptosis to parent **1**.

The differentiation of myeloid precursors to granulocytes was determined by measuring the presence on the cell membrane of the granulocytic differentiation marker CD11c antigen, which is highly expressed only on mature granulocytes, monocytes and certain lymphocytes, but not significantly on myeloid committed precursor cells. After treating the U937 cells with the PsA analogues at 5 μ M for 30 and 40 h, low differentiation levels

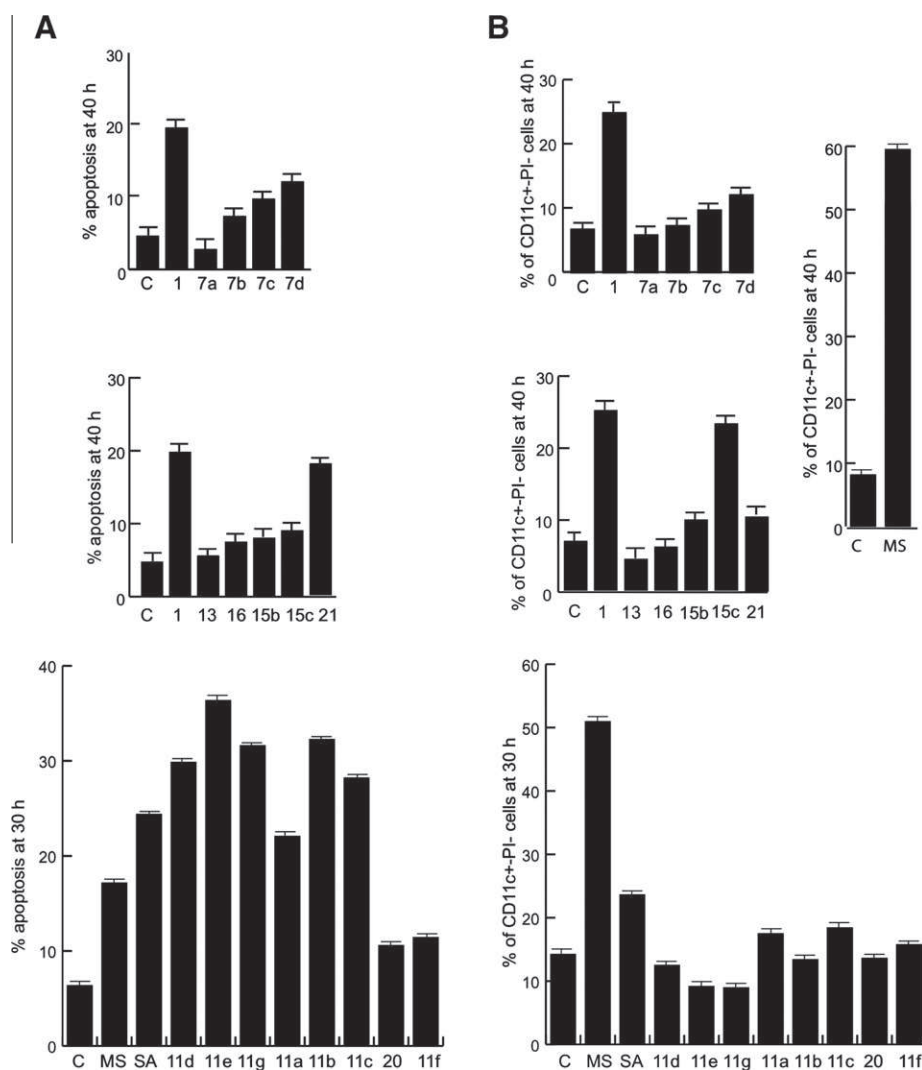


Figure 2. (A) Induction of apoptosis after treatment of U937 cells with the indicated compounds at 5 μ M, for 30 h (for the series **11a–11g**) and 40 h. (B) Differentiation analysis in U937 cells after 30 h treatment with the indicated compounds at 5 μ M. The percent value of CD11c positive/propidium iodide (PI) negative cells is represented. The data shown is the media of independent quadruplicates.

were measured (with the exception of parent **1** and methyl sulfide **15c**) relative to control (Fig. 2B) and to the class I-selective HDACi MS-275.

We next determined the expression levels of p21^{WAF1}, which is involved in the mechanism of tumor suppression, as well as the global acetylation status of histone (histone H3) and non-histone proteins (tubulin), that are substrates of HDACs family members. The up-regulation of p21^{WAF1} and the increase of tubulin acetylation levels were evaluated by Western blot analyses on total extracts after treating the U937 cells for 24 h with the compounds at 5 μ M (Fig. 3A–C). Compounds **7a–d**, **13**, **15b**, **16** and **21** failed to increase both p21^{WAF1} and tubulin acetylation expression levels. Methyl sulfide **15c** increased weakly these levels in line with its noticeable effect on the induction of differentiation. While the **11a–g** series did not show a significant effect on tubulin acetylation, some members (**11b–e**) up-regulated p21^{WAF1} to levels even higher than those of SAHA. The effect of the analogues on the level of histone acetylation was also analyzed by Western blot (Fig. 3D). After treating U937 cells for 24 h all compounds of the series **11a–g** displayed the ability to increase the level of acetylated histone H3, present in the histonic extract, as shown using the specific antibody.

In order to determine if the most potent analogues are endowed with additional epigenetic modulation activities, the series **11a–g** and **20** were also used in in vitro human SIRT1 fluorescent assay and in a radioactive assay on a peptide fragment having p300/CBP histone acetyl transferase (HAT) enzyme activity. As shown in Figure 4B, very weak SIRT1 inhibition was noted (ca. 30% relative to the control) for the majority of compounds at 50 μ M, far lower than the activity of the SIRT1 inhibitor suramin at the same concentration. In addition, none of the analogues displayed modulation of a peptide fragment of CBP containing the enzymatically active HAT domain (Fig. 4A) relative to the control and to the effects of the known inhibitor anacardic acid (AA) at the same concentration,^{65,66} thus confirming the specificity of the HDAC among other epigenetic inhibitory activities.

DNMT inhibition has also been reported for PsA.³ To verify the effective physical interaction between PsA and its analogues and DNA methyl transferase enzymes, two in vitro radioactive assays were performed using DNMT1 and DNMT3A (Fig. 4C and D). DNMT1 was immunoprecipitated from K562 cells and used in radioactive assay that employs [³H]-adenosyl-L-methionine as methyl donor and Poly dI-dC as methyl acceptor. The same conditions have been used for the DNMT3A radioactive assay, but the

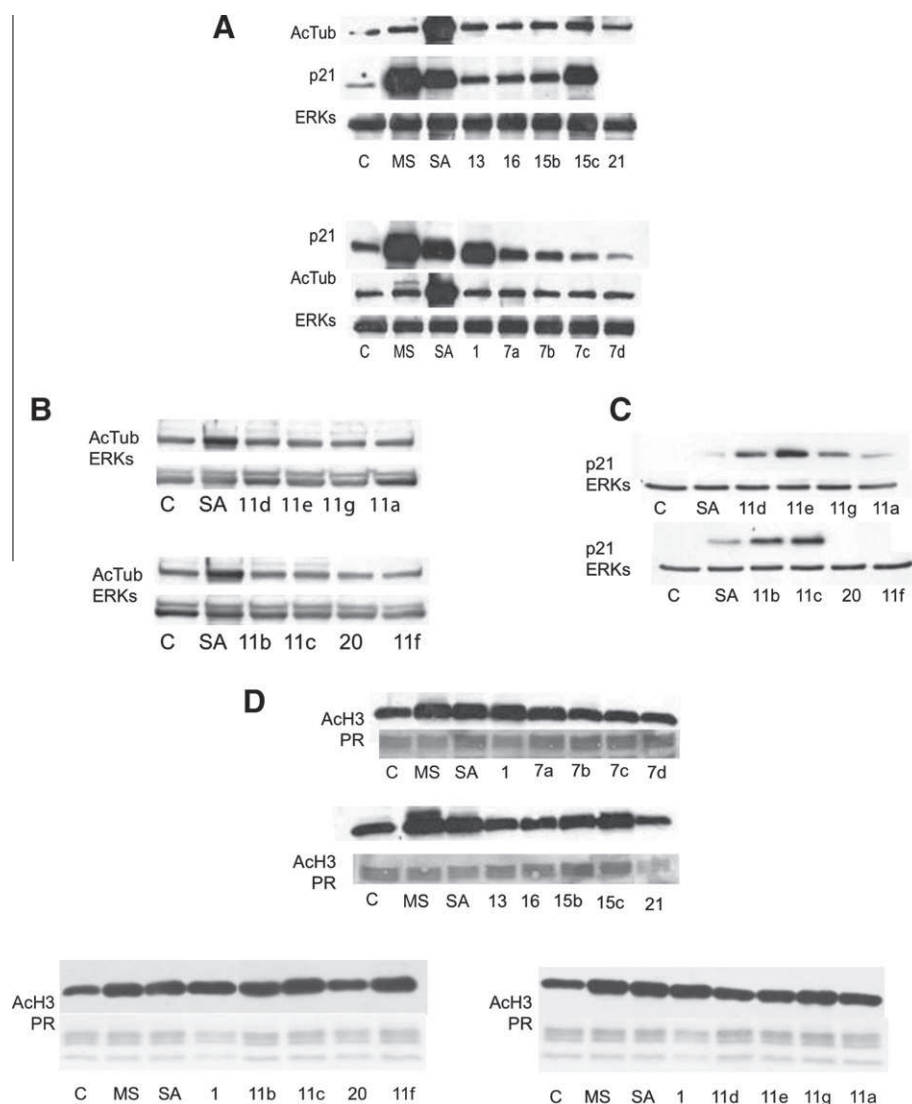


Figure 3. (A–C) Western blot analyses of p21^{WAF1/CIP1} expression and α -tubulin acetylation in U937 cells after treatment with the indicated compounds at 5 μ M for 24 h. ERK1 expression is shown as loading control. (D) Western blot analyses of histone H3 acetylation carried out in U937 cells, after 24 h induction with the compounds at 5 μ M.

recombinant enzyme was produced in *Escherichia coli* BL21, as GST fused protein. In neither assay compounds **11a–g** and **20** showed significant inhibition at 50 μ M (see Fig. 4C), in contrast to RG108⁶⁷ and SGI1027⁶⁸ at the same concentration for the DNMT1 assay.

Taken together, the enzymatic profiling suggests that the epigenetic activities of PsA are mainly restricted to the inhibition of the HDAC family in this context. Moreover, the HDAC activity of the series is likely linked to the formation of the monomeric thiol that originates from $-S \cdots S-$ bond cleavage (Scheme 7, vide infra), a known potent metal chelator. The Zn^{2+} -dependent histone deacetylase subfamily is composed of Class I HDACs (HDAC 1–3, 8 and 11) and Class II HDACs (HDAC 4–7, 9 and 10). In contrast, Class III (sirtuins), with seven members (SIRT1–7), require NAD^+ as a cofactor and release *O*-acetyl-ADP ribose and nicotinamide as a consequence of acetyl transfer from the acetylated lysine.⁶⁹

Metalloproteinase-targeted HDAC inhibitors are typically substrate mimics of the linear acetyl-lysine side chain with a Zn^{2+} -chelating ‘warhead’ group that replaces the scissile acetamide, a connector chain and a ‘cap’ at the other end that extend beyond the enzyme substrate-binding channel. These features are exhibited by the thiol derived from PsA (Scheme 7), in which

the active site binding/inactivating group is connected via a hydroxyimino amide linker to the HDAC recognition aryl group.

In order to address the nature of the interaction between the inhibitor and HDAC, the ab initio calculated structure of thiol **22** was docked into the active site of the human HDAC8–trichostatin A (TSA) crystal structure⁷⁰ after removal of the TSA ligand. The catalytic domain of about 390 amino acids responsible for the deacetylation is highly conserved among the metal-dependent HDACs, in particular the residues lining the ligand-binding pocket, but some differences can be exploited for the designed of selective Class I/Class II HDAC inhibitors.⁷¹

The highest scores using automated docking method for the interaction of the ligand with the Zn^{2+} ion in the active site, validated by the GRID maps, agree in having the thiol chelated to the metal, whereas the linker domain occupies the channel and the *o*-bromophenol is stabilized through interaction with Tyr100 and Phe152 at the rim of the active site entrance (Fig. 5 and Figs. S1–S3). This positioning facilitates the formation of a hydrogen bond between the oxime group and Asp101, which remains at a constant distance along the energy minimization and the simulation of the dynamic behaviour using unrestrained MD (Fig. S3). The Zn^{2+} ion is kept firmly coordinated to the four ligands (Asp178, Asp267, His180 and the thiol group of the inhibitor),

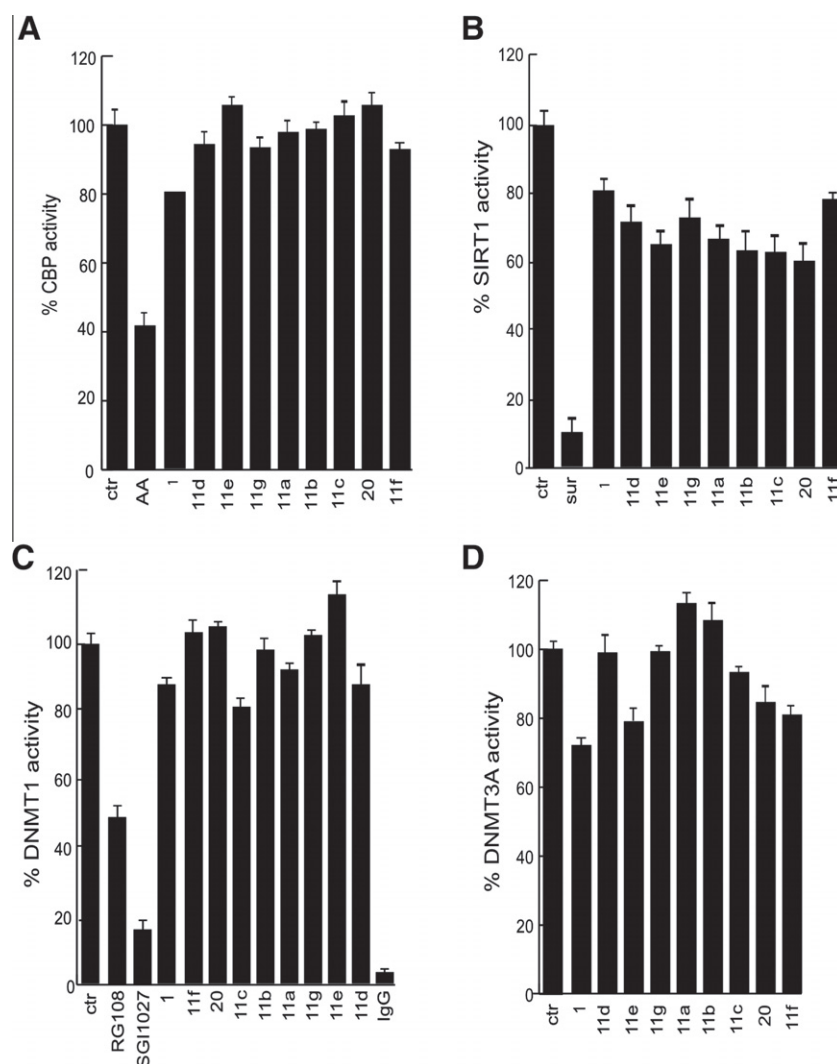
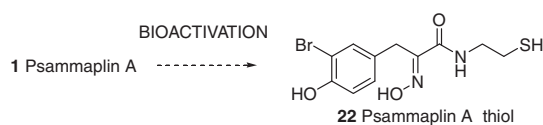


Figure 4. (A) CBP radioactive assay performed with 1 μ g of recombinant CBP enzyme peptide fragment and the psammaplin A analogues at 50 μ M. (B) SIRT1 fluorescence assay to measure the lysine deacetylase activity of the compounds at 50 μ M on human recombinant SIRT1 enzyme (1 U). (C) DNMT1 radioactive assay with synthetic poly dI-dC as methyl acceptor (0.1 μ g) and [3 H]-adenosyl-L-methionine (1 μ Ci) as methyl donor. DNMT1 was immunoprecipitated from K562 cells and the compounds **11a–g** were used at 50 μ M. (D) DNMT1 radioactive assay to measure the inhibition of recombinant DNMT3a (1 μ g, produced in *E. coli* BL21, as GST fused protein) by the compounds at 50 μ M. In each panel the inhibition/activation of the enzyme is reported as percentage of activity relative to the control.



Scheme 7. Bioactivation of PsA **1** to thiol **22** by the reductive environment of the cells.

and the electrostatic term (-59.2191 ± 1.7841 kcal/mol) makes an important contribution to the overall energy. Favourable van der Waals interactions of the ligand with Phe152 and Phe208 residues also account for a fraction of the intermolecular energy component (Fig. S2).

4. Discussion

Psammaplin A **1** is the prototype of a collection of metabolites isolated from sponges¹ that are biosynthesized by linear connections of (bromo)tyrosines and modified cysteines.¹² Their biological activities, common to most of the bromotyrosine/cysteine constructs, range from antimicrobial⁵⁴ to anticancer.^{1,6} The inhibi-

tion of several enzymes that impact different stages on the onset and progression of cancer such as topoisomerase II (growth),¹⁴ the zinc-dependent metalloproteinase aminopeptidase N (APN, tumor cell invasion or angiogenesis),²¹ HDAC and DNMT (chromatin remodeling),³ among others, likely conspire to account for the reported anticancer activities of PsA in several cancer cell lines and in the A549 lung xenograft mouse model.^{3,12} PsA was reported to activate Wnt signalling in a cell-based assay but the effect is likely due to HDAC inhibition rather than to an specific Wnt signalling pathway.⁷²

More recent molecular and cellular studies⁷³ confirmed the potent inhibitory activity of PsA in enzymatic (HDAC inhibition) and in anti-proliferation assays, and also the selective induction of histone hyperacetylation. The anti-proliferative effects were linked to the overexpression of genes related to cell cycle arrest and apoptosis (p53-independent p21^{WAF1} expression).⁷⁴

A series of PsA analogues modified at the aryl ring, with varying lengths of the amino thiol connecting unit, and some exchanges/deletions of functional groups have been prepared. These analogues have been characterized with regard to their enzymatic inhibitory potential and for their effects on cell cycle, differentia-

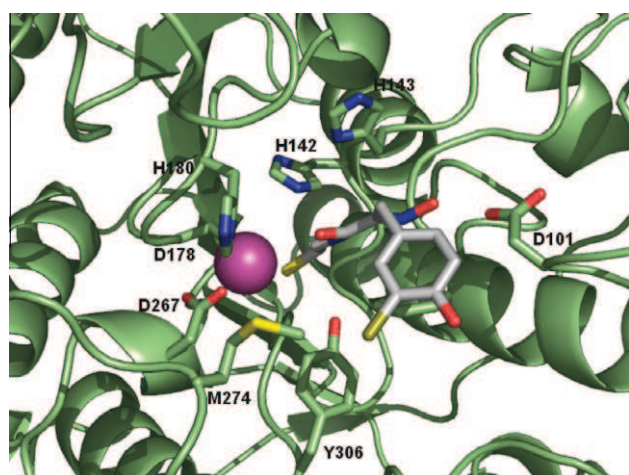


Figure 5. Proposed docking pose of biocleaved psammaplin A (thiol **22**) with HDAC8. The α trace of the enzyme is displayed as a ribbon, colored in green. The side chains of His142, His143, Asp178, Asp267, His180, Met274, Tyr306 are shown as sticks, with carbon atoms colored in green. The Zn^{2+} ion at the catalytic site is shown as a magenta sphere. The inhibitor is displayed also as sticks, but with carbon atoms colored in gray and the bromine atom colored in brown.

tion and apoptosis on the U937 acute myeloid leukemia cell line. For **1** and the most potent analogues, functional assays have also been carried out on the same cell line.

Enzymatic HDAC1 inhibition data for the series of analogues having chain lengths spanning from two to six methylene units (**7a–d**) established that the derivative of natural cystamine (the decarboxylated cysteine) present in psammaplin A was the most potent, and also that both the oxime and the disulfide functionalities were required for the HDAC inhibition activity, since analogues **13**, **15b–c**, **16** and **20** proved to be inactive (Fig. 1A). We then addressed the modifications of the aryl ring with analogues that preserve the same connecting diamine unit of the parent natural product. The substitution at the ring is well tolerated, and a general improvement in potency relative to PsA was noted when the ring was mono- (**11a–b**) or disubstituted (**11d,e,g**). The unsubstituted compound (the phenylalanine-derived **11c**) and the tri-substituted bromopsammaplin A **11f** were less active than **1**. Conversely the series of halogenated analogues **11d,e,g** exhibited greater potency than PsA and followed the order $Br < F < Cl < I$. The activities of the spiro derivative **21** are most intriguing, since it is the only compound showing a G2/M block (Fig. 1B) and strong induction of apoptosis (Fig. 2B), which appears not to be correlated with HDAC inhibition. A promising pro-differentiation profile is also noted for the methylsulfide **15c** (Fig. 2B), which merit further investigation.

It has previously been reported that human endometrial Ishikawa cancer cells treated with PsA showed accumulation of cells in the G1 phase and a significant decrease in the number of cells in the S phase,⁷⁴ a result in keeping with the effect of known HDAC inhibitors.⁷⁵ Our data confirm the time-dependent accumulation of cells in G1 upon treatment of human leukaemia U937 cells with PsA and analogues. Moreover, **1** and the **11a–g** series of related compounds induced apoptosis of U937 cells (Fig. 2B), an effect likely associated to their more selective inhibition of class I HDACs. The majority of these compounds (with the exception of **15c**) failed to induce tubulin acetylation (Fig. 3), which is a target of HDAC6 enzymes, and this finding is in agreement with previous reports for PsA in HeLa cells.⁷³ Although the result might suggest that psammaplin A show selectivity for histone proteins in preference to tubulin, it cannot be considered as a selective class I HDAC inhibitor, since it also inhibits HDAC4, a class II HDAC, in enzymatic assays (results not shown). Important differences between class I

and class II metallo-HDACs are noticeable in their size (with class II being from two to three times larger), their cellular localization, the conservation of sequence motifs in the catalytic domains, the identity of the protein–protein interaction complexes and the tissue distribution.⁷⁶

Western blot analysis of U937-treated cells confirmed the accumulation of acetylated histones using antibodies against acetylated H3 (Fig. 3D), in agreement with similar findings for PsA in endometrial cancer Ishikawa cells.⁷⁴ PsA and several analogues up-regulated cyclin-dependent kinase inhibitor p21^{WAF1} (Fig. 3), which is one of the genes induced by HDAC inhibitors,⁷⁶ and this effect might be related to the suppression of cell proliferation and induction of apoptosis.

PsA and its 5-bromo derivative have been reported to inhibit the bacterial methyltransferase SssI. However, cultured HCT116 human colon carcinoma cells treated with 1 μ M PsA did not reduce global genomic DNA methylation (the level of which was determined using a mass spectrometry assay) and failed to induce the hypomethylation or reactivation of cancer-testis antigen genes, known as methylation silenced genes.⁵⁶ Here, two different assays were performed on DNMT1 and DNMT3A (see Fig. 4C and D) to evaluate the inhibition of DNMT enzymes by PsA and derivatives (**11a–g**). Differently from expected, these compounds at 50 μ M failed to inhibit DNMT1 and DNMT3A, thus indicating their inability to alter DNMT in vitro. Therefore, the action of these compounds on cell cycle progression and induction of apoptosis can be better correlated with the HDAC inhibitory activities. It is likely that the absence of hypomethylation is not due to the low affinity of PsA (and its analogues) for DNMT, but instead to the inefficient transport of these compounds through the nuclear membrane. Inefficient transportation of the compound into the nucleus or poor cell membrane penetration might also explain the much greater concentration of **1** (1800 times) required to obtain similar potencies in cell-based assays relative to the HDAC enzymatic inhibition assay.⁵²

Lastly, no significant inhibition of SIRT1 and p300/CBP HAT enzymes was seen for the PsA-related series of analogues (Fig. 4A and B).

Other natural products of the depsipeptide class that act as inhibitors of HDAC also contain disulfide bonds, namely FK228 **23**, spiruchostatins **25** and FR901375 **26** (Fig. 6).^{39,71} FK228 (romi-

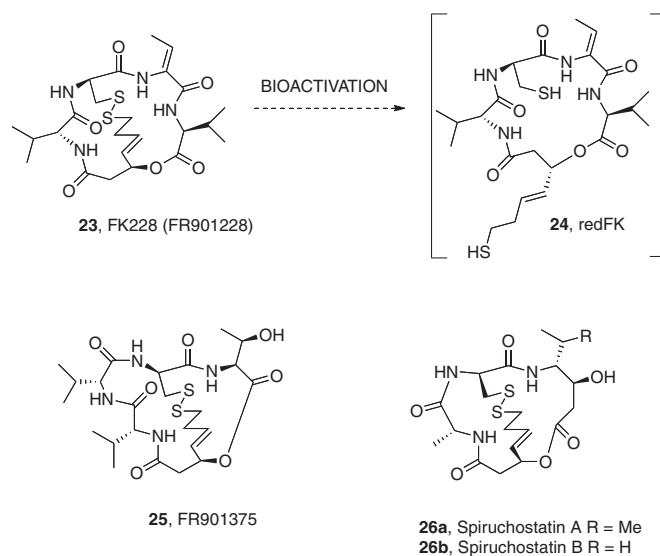


Figure 6. Natural depsipeptides **23–26** containing disulfide bonds are HDAC inhibitors. The structure of previously characterized active reduced form of FK228 (**24**, redFK) is shown by analogy with the reduced form of psammaplin A, **22**.

depsin, Istodax[®]) currently approved for T cell lymphoma is undergoing phase II clinical trials for the treatment of non-Hodgkin's lymphoma, acute myelogenous leukemia, and pancreatic cancer (www.clinicaltrials.gov). It has been shown that the disulfide bond of FK228 becomes cleaved in the cells by the reducing activity of glutathione to afford redFK **24**, and the thiol then interacts with the Zn²⁺ ion in the active site of HDAC.⁷⁷ Moreover, mass spectrometry analysis of blood samples identified the thiol and glutathione conjugates of FK228.⁷⁸ Upon bio-reduction decapeptides **25** and **26** must also release the Zn²⁺-binding butenylthiol.⁷⁹ From an structural point of view both redFK **25** and PsA thiol **22** have Zn²⁺ ion connecting chains that are shorter than those of common hydroxamic acid-based inhibitors (TSA, SAHA...). Thiol chelating groups connected via a 5 atom saturated chain to cyclic tetrapeptides have also shown potent HDAC inhibitory activities.^{80,81}

In agreement with these precedents, the dimer analogue lacking the disulfide bond (**13**) was inactive, which substantiates the proposal that PsA and analogues undergo thiolate exchange reaction with glutathione by –S–S– bond cleavage.⁸² Interestingly, Wang et al. have shown that glutathione-depleted cells were not sensitive to PsA, implying that the reducing environment of the cells triggered the conversion of the disulfide of **1** to the corresponding thiol,⁷⁹ which would be the species responsible for the HDAC inhibitory activity of psammaplin A after uptake into the cells.

Based on the reported crystal structure, the HDAC8·Zn²⁺·thiol **22** complex was constructed with the thiol group chelating the metal ion, and then refined using energy minimization. The dynamic behaviour of the complex using unrestrained molecular dynamics confirmed the feasibility of the proposed binding orientation and the mutual adaptation between HDAC8 and the ligand. The linker occupies the narrow channel whereas the bromophenol interacts with Tyr100 and Phe152 at the rim of the active site entrance, a pose that facilitates the formation of a robust hydrogen bond between the oxime group and Asp101 (Fig. 5).

Our results using alcohol **16**, ether **15b** and most importantly dimer **13** confirm the earlier findings with FK228⁷⁸ and suggest that psammaplin A **1** acts as a stable pro-drug⁸³ that is activated upon uptake by the reductive environment of the cells to afford thiol **22**, which then chelates the Zn²⁺ ion in the active site of the HDAC metalloenzymes.

5. Conclusion

PsA **1**, a natural product with a disulfide bond derived from the condensation of modified cystamine and tyrosine moieties, has been reported to display dual HDAC and DNMT epigenetic inhibitory activities. The intriguing ability to target simultaneously more than one member of the epigenetic machinery (epigenetic multiple ligands),⁸⁴ prompted us to synthesize a series of PsA analogues in an effort to determine the structural determinants for their epigenetic profile. We have analyzed the effects of the natural-product inspired collection on the human leukaemia U937 cell cycle, measuring induction of apoptosis and differentiation, induction of p21^{WAF1} and tubulin acetylation levels and total histone H3, and also examined their HDAC1 enzyme-based inhibition profile. From the results it is concluded that Nature has optimized the design of the PsA scaffold to fulfil this epigenetic role, since only closely related synthetic derivatives (with modifications at the bromotyrosine ring) exhibited comparable or greater potency than the natural product. Modifications of the connecting chain, oxime bond and disulfide unit afforded either inactive or considerable less potent analogues. Exploring the possibility that PsA and derivatives might display additional epigenetic activities we have also tested them as inhibitors of DNMT1, DNMT3A, SIRT1 and a peptide containing the p300/CBP HAT domain, but the values measured were

very low. Since epigenetic signalling by PsA appears to be restricted to inhibition of metalloproteinase HDACs, a model for the interaction of HDAC8 with the thiol derived from PsA **1** (by a presumed in vivo disulfide cleavage) was computed. The thiol binds the Zn²⁺ ion in the active site and the complex is additionally stabilized by a hydrogen bond interaction between the oxime group and the Asp101 residue located at the active site entrance. As with FK228, this bioactivation mechanism illustrates the ingenious solution adopted by Nature to protect the reactive zinc-binding thiol as a disulfide pro-drug with higher bioavailability. The increased levels of disulfide reductants (i.e., glutathione, thioredoxin and thioredoxin reductase) found in many cancer cells render such cells particularly susceptible to the action of PsA **1**.

Despite the failure to greatly improve the epigenetic inhibitory profile of PsA through the modifications reported, more significant skeletal alterations of the PsA structure might provide more potent derivatives, thus lending further support to the important role of natural products as inspiration⁸⁵ for the development of designed multiple ligands^{50,51} as new anticancer drugs.^{86,87}

6. Experimental section

6.1. General

Solvents were dried according to published methods and distilled before use. HPLC grade solvents were used for the HPLC purification. All other reagents were commercial compounds of the highest purity available. All reactions were carried out under argon atmosphere, and those not involving aqueous reagents were carried out in oven-dried glassware. Analytical thin layer chromatography (TLC) was performed on aluminium plates with Merck Kieselgel 60F254 and visualized by UV irradiation (254 nm) or by staining with a solution of phosphomolibdic acid. Flash column chromatography was carried out using Merck Kieselgel 60 (230–400 mesh) under pressure. Infrared spectra were obtained on JASCO FTIR 4200 spectrophotometer, from a thin film deposited onto a NaCl glass. ¹H NMR spectra were recorded in CDCl₃, CD₃OD, DMSO-*d*₆ and (CD₃)₂CO at ambient temperature on a Bruker AMX-400 spectrometer at 400 MHz with residual protic solvent as the internal reference (CDCl₃, δ_H = 7.26 ppm; (CD₃)₂CO, δ_H = 2.05 ppm; CD₃OD, δ_H = 3.31 ppm; DMSO-*d*₆, δ_H = 2.50 ppm); chemical shifts (δ) are given in parts per million (ppm), and coupling constants (*J*) are given in Hertz (Hz). The proton spectra are reported as follows: δ (multiplicity, coupling constant *J*, number of protons, assignment). ¹³C NMR spectra were recorded in CDCl₃, CD₃OD, DMSO-*d*₆ and (CD₃)₂CO at ambient temperature on the same spectrometer at 100 MHz, with the central peak of CDCl₃ (δ_C = 77.0 ppm), CD₃OD (δ_C = 49.0 ppm), DMSO-*d*₆ (δ_C = 39.4 ppm) or (CD₃)₂CO (δ_C = 30.8 ppm) as the internal reference. The DEPT135 sequence was used to aid in the assignment of signals on the ¹³C NMR spectra. Melting points were determined on a Stuart SMP10 apparatus. Elemental analyses were determined on a Carlo Erba EA 1108 analyzer. MS experiments were performed on an APEX III FT-ICR MS (Bruker Daltonics, Billerica, MA), equipped with a 7T actively shielded magnet. Ions were generated using an Apollo API electrospray ionization (ESI) source (Bruker Daltonics, Billerica, MA), with a voltage between 1800 and 2200 V (to optimize ionisation efficiency) applied to the needle, and a counter voltage of 450 V applied to the capillary. Samples were prepared by adding a spray solution of 70:29.9:0.1 (v/v/v) methanol/water/formic acid to a solution of the sample at a v/v ratio of 1–5% to give the best signal-to-noise ratio. Data acquisition and data processing were performed using the XMASS software, version 6.1.2 (Bruker Daltonics). FAB experiments were performed on a VG AutoSpec instrument, using 3-nitrobenzylalcohol or glycerol as matrix.

6.2. General procedure for the oxidation of amines with Na₂WO₄

To a solution of amine (18.0 mmol) in EtOH (40 mL) at 0 °C were added Na₂WO₄·2H₂O (18 mmol), 30% H₂O₂ (16 mL) and H₂O (30 mL). The resulting mixture was stirred for 4 h at room temperature and the reaction was quenched with aqueous saturated NH₄Cl and extracted with EtOAc (3×). The combined organic extracts were washed with brine, dried over Na₂SO₄ and evaporated. The residue was purified by column chromatography on silica gel as indicated.

6.3. General procedure for the hydrolysis of esters

Lithium hydroxide (15 mmol) was added to a solution of ester (1 mmol) in a 1:1 THF/H₂O (16 mL) mixture. The solution was stirred at room temperature for 2 h, neutralized with 10% HCl and extracted with EtOAc (4×). The combined organic layers were washed with brine, dried over Na₂SO₄, filtered and the solvent was evaporated in vacuo. Crystallization of the residue provided the desired acid as indicated.

6.4. General procedure for the amidation of tyrosine acid derivatives with amines

N-Hydroxyphthalimide (1 mmol) and DCC (1 mmol) were added to a solution of the carboxylic acid (1 mmol) in dioxane (2.5 mL). After the mixture had been stirred for 2 h at room temperature, a solution of the amine (0.5 mmol), Et₃N (2 mmol) and MeOH (1 mL) was added. The resulting mixture was stirred for 12 h at room temperature and the reaction was quenched with H₂O and extracted with EtOAc (3×). The combined organic extracts were washed with brine, dried over Na₂SO₄ and evaporated. The residue was dissolved in THF, filtered off and the solvent was evaporated in vacuo. The resulting residue was then purified by column chromatography on silica gel as indicated.

6.4.1. (*E*)-Methyl 2-(hydroxyimino)-3-(4-hydroxyphenyl)propanoate (**3**)⁸⁸

Following the general procedure for the oxidation of amines with Na₂WO₄·2H₂O, *L*-tyrosine methyl ester **2** (3.45 g, 17.68 mmol) gave, after purification by column chromatography (SiO₂, 50:50 hexane/EtOAc), 2.24 g (60%) of oxime **3** as a white powder. ¹H NMR (CD₃COCD₃, 400.13 MHz): δ 11.35 (s, 1H, OH), 8.11 (s, 1H, OH), 7.11 (d, *J* = 8.5 Hz, 2H, ArH), 6.73 (d, *J* = 8.5 Hz, 2H, ArH), 3.84 (s, 2H, 2H₃), 3.72 (s, 3H, CO₂CH₃) ppm.

6.4.2. (*E*)-Methyl 3-(3-bromo-4-hydroxyphenyl)-2-(hydroxyimino)propanoate (**4**)⁶¹

A solution of NBS (0.49 g, 2.75 mmol) in CH₃CN (6 mL) was added dropwise over 15 min to the solution of the oxime **3** (0.58 g, 2.75 mmol) in CH₃CN (6 mL). The reaction mixture was stirred at room temperature for 5 h, after which time the solvent was evaporated and the residue was treated with water and extracted with EtOAc (3×). The combined organic extracts were dried over Na₂SO₄, filtered, evaporated and the residue was purified by column chromatography (SiO₂, 50:50 hexane/EtOAc) to afford oxime **4** (0.65 g, 82%) as a yellow powder. ¹H NMR (CD₃COCD₃, 400.13 MHz): δ 11.49 (s, 1H, OH), 8.62 (s, 1H, OH), 7.44 (d, *J* = 1.6 Hz, 1H, H_{2'}), 7.13 (dd, *J* = 8.3, 1.6 Hz, 1H, H_{6'}), 6.90 (d, *J* = 8.3 Hz, 1H, H_{5'}), 3.85 (s, 2H, 2H₃), 3.74 (s, 3H, CO₂CH₃) ppm.

6.4.3. (*E*)-3-(3-Bromo-4-hydroxyphenyl)-2-(hydroxyimino)propanoic Acid (**5**)

In accordance with the general procedure for the hydrolysis of esters, ester **4** (0.61 g, 2.11 mmol) gave, after purification by column chromatography (SiO₂, 90:10 EtOAc/MeOH), 0.58 g (99%) of

acid **5** as a white powder, mp: 147–148 °C (hexane/CHCl₃) (lit. 147–148 °C, dec.).⁸⁹ ¹H NMR (CD₃COCD₃, 400.13 MHz): δ 7.45 (s, 1H, H_{2'}), 7.14 (d, *J* = 7.9 Hz, 1H, ArH), 6.90 (d, *J* = 7.9 Hz, 1H, ArH), 3.84 (s, 2H, 2H₃) ppm.

6.4.4. (2*E*,2'*E*)-*N,N'*-[2,2'-Disulfanediy]bis(ethane-2,1-diyl)]bis[3-(3-bromo-4-hydroxyphenyl)-2-(hydroxyimino)propanamide] (psammaplin A, **1**)⁵⁶

Following the general procedure for the amidation of tyrosine acid derivatives with amines, acid **5** (0.16 g, 0.59 mmol) afforded, after purification by column chromatography (SiO₂, gradient from 25:75 hexane/EtOAc to 95:5 CH₂Cl₂/MeOH), psammaplin A **1** (0.12 g, 60%) as a white foam. ¹H NMR (CD₃OD, 400.13 MHz) (data for monomer): δ 7.36 (s, 1H, H_{2'}), 7.07 (d, *J* = 8.3 Hz, 1H, ArH), 6.76 (d, *J* = 8.3 Hz, 1H, ArH), 3.79 (s, 2H, 2H₃), 3.52 (t, *J* = 6.7 Hz, 2H, 2H_{1''}), 2.81 (t, *J* = 6.7 Hz, 2H, 2H_{2''}), 2.15 (br, 2H, OH) ppm.

6.5. Molecular modeling of psammaplin A

6.5.1. Quantum mechanics calculations

The geometry of the thiol derived from psammaplin A was optimized using the ab initio quantum chemistry program Gaussian 03⁹⁰ and the HF/3-21G* basis set. A set of atom-centred RHF 6-31G*//3-21G* charges was then obtained by using the RESP methodology⁹¹ as implemented in the AMBER suite of programs (<http://amber.scripps.edu/>). Covalent and nonbonded parameters for the inhibitor atoms were assigned, by analogy or through interpolation, from those already present in the AMBER force field⁹² (parm99) or consistently derived, as explained in more detail elsewhere.⁹³

6.5.2. Molecular docking

The genetic algorithm⁹⁴ implemented in AutoDock⁹⁵ and the h-HDAC8 (PDB code 1t64)⁷⁰ as the target protein upon removal of trichostatin A was used to generate different HDAC-Zn²⁺-bound psammaplin A thiol conformers by randomly changing torsion angles and overall orientation of the molecule. A volume for exploration was defined in the shape of a three-dimensional cubic grid with a spacing of 0.3 Å that enclosed the residues that are known to make up the inhibitors binding pocket. At each grid point, the receptor's atomic affinity potentials for carbon, oxygen, nitrogen, sulfur, bromine and hydrogen atoms present in the ligand were precalculated for rapid intra- and intermolecular energy evaluation of the docking solution.

To obtain additional validation of the proposed binding mode for the ligands, the program GRID (<http://www.moldiscovery.com/>)⁹⁶ was also used to search for sites on the enzyme that could be complementary to the functional groups present in this inhibitor. For the GRID calculations, a 18 × 21 × 21 Å lattice of points spaced at 0.5 Å was established at the binding site. The probes used were C1 = (aromatic carbon), N1 (neutral flat NH, eg amide), N:# (sp nitrogen with lone pair), O (sp² carbonyl oxygen) and Br (bromine). The dielectric constants chosen were 4.0 for the macromolecule and 80.0 for the bulk water.

6.5.3. Molecular dynamics simulations

Ternary complexes (HDAC8-Zn²⁺-psammaplin A thiol) representative of the most populated solutions were then refined using the second generation AMBER force field and 3000 steps of steepest descent energy minimization and 6000 steps of conjugate gradient of only the side chain of the protein and those atoms of the bound ligand. This procedure allowed readjustment of covalent bonds and van der Waals contacts without changing the overall conformation of the complex. The HDAC-psammaplin A thiol complex was then neutralized by addition of eight sodium ions⁹⁷ that were placed in electrostatically favored positions and immersed

in rectangular boxes each containing about 450 TIP3P water molecules⁹⁸ that extended 1 Å away from any solute atom. The cutoff distance for the non-bonded interactions was 9 Å, and periodic boundary conditions were applied. Electrostatic interactions were represented using the smooth particle mesh Ewald method with a grid spacing of ~1 Å. Unrestrained molecular dynamics (MD) simulations at 300 K and 1 atm were then run for 6 ns using the SANDER module in AMBER 8.⁹⁹ The coupling constants for the temperature and pressure baths were 1.0 and 0.2 ps, respectively. SHAKE¹⁰⁰ was applied to all bonds involving hydrogens, and an integration step of 2 fs was used throughout. The nonbonded pair list was updated every 10 steps. The simulation protocol involving a series of progressive energy minimizations followed by a 20 ps heating phase and a 70 ps equilibration period before data collection. System coordinates were saved every 2 ps for further analysis.

6.5.4. Analysis of the molecular dynamics trajectories

Three-dimensional structures and trajectories were visually inspected using the computer graphics program InsightII. The root-mean-square (rms) deviations from both the initial structures and the average structures, the inter-atomic distances, and the snapshot geometries were obtained using the PTRAJ module in AMBER. Intermolecular van der Waals energies for individual residues were calculated with the ANAL module, whereas the solvent-corrected residue-based electrostatic interaction energies were calculated with DelPhi, following the procedure described.⁹³

All calculations were performed on the SGI R14000 Origin 3800 at CIEMAT (Madrid), on the SGI 1.5 GHz Itanium2 at CESGA (Santiago de Compostela) and locally on SGI R12000 Octane workstations.

6.6. Biological assays

6.6.1. Cell culture

Human leukaemia cell lines U937, K562 and HL60 were propagated in RPMI medium supplemented with 10% FBS (Foetal bovine serum; Hyclone) and antibiotics (100 U/mL penicillin, 100 µg/mL streptomycin and 250 ng/mL amphotericin-B). Cells were kept at the constant concentration of 200,000 cells per mL of culture medium.

6.6.2. Ligands and materials

SAHA (Merck) and MS-275 (a kind gift of Bayer-Schering AG) were dissolved in DMSO and used at 5×10^{-6} M. All other compounds described were dissolved in DMSO (Sigma-Aldrich) and used at 5 and 50 µM.

6.6.3. Cell cycle analysis

2.5×10^5 cells were collected and resuspended in 500 µL of hypotonic buffer (0.1% Triton X-100, 0.1% sodium citrate, 50 µg/mL propidium iodide, RNase A). Cells were incubated in the dark for 30 min. Samples were acquired on a FACS-Calibur flow cytometer using the Cell Quest software (Becton Dickinson) and analysed with standard procedures using the Cell Quest software (Becton Dickinson) and the ModFit LT version 3 Software (Verity) as previously reported.^{101,102} Apoptosis was revealed by monitoring nuclear fragmentation (the so-called 'sub-G1 DNA peak') by FACS and analysed by Cell Quest technology.

6.7. Caspase 3 activation assay

Caspase activity was detected in living U937 cells using the BIO-MOL and B-BRIDGE Kits supplied with cell-permeable fluorescent substrates. The fluorescent substrate for caspase 3 was FAM-DEVD-FMK. ca. 1×10^6 cells were washed twice in cold PBS and incubated for 1 h in ice with the corresponding substrates as rec-

ommended by the suppliers. The cells were analysed after washing using the CellQuest software applied to a FACScalibur (BD). Experiments were performed in duplicate and values were expressed as mean \pm SD.

6.7.1. Granulocyte differentiation

Granulocyte differentiation was carried out as previously described.¹⁰³ Briefly, U937 cells were harvested and resuspended in 10 µL phycoerythrin-conjugated CD11c (CD11c-PE). Control samples were incubated with 10 µL PE conjugated mouse IgG1 for 30 min at 4 °C in the dark, washed in PBS and resuspended in 500 µL PBS containing propidium iodide (0.25 µg/mL). Samples were analyzed by FACS with Cell Quest technology (Becton Dickinson). Propidium iodide (PI) positive cells have been excluded from the analysis.

6.7.2. Western blot analyses

Western blot analyses were performed according to standard procedures following suggestions of antibody suppliers. For the determination of p21^{WAF1/CIP1} 50 µg of total protein extracts were separated on a 15% polyacrylamide gels and blotted. Western blots were shown for p21 (Transduction Laboratories, dilution 1:500) and total ERKs (Santa Cruz) were used to normalize for equal loading. For α -Tubulin acetylation 25 µg of total protein extracts were separated on a 10% polyacrylamide gels and blotted. Western blots where shown for acetylated α -tubulin (Sigma, dilution 1:500) and total ERKs (Santa Cruz) or total tubulin (Sigma) were used to normalise for equal loading.

6.8. Histone extraction protocol

Cells were harvested and washed twice with ice-cold PBS and lysed in Triton Extraction Buffer (TEB: PBS containing 0.5% Triton X 100 (v/v), 2 mM phenyl methyl sulfonyl fluoride (PMSF), 0.02% (w/v) NaN₃) at a cellular density of 10^7 cells per mL for 10 min on ice, with gentle stirring. After a brief centrifugation at 2000 rpm at 4 °C, the supernatant was removed and the pellet was washed in half the volume of TEB and centrifuged as before. The pellet was resuspended in 0.2 M HCl at a cell density of 4×10^7 cells per mL and acid extraction was left to proceed overnight at 4 °C on a rolling table. Next, the samples were centrifuged at 2000 rpm for 10 min at 4 °C, the supernatant was removed and protein content was determined using the Bradford assay.

6.9. Determination of histone H3 specific acetylations

For the histone H3 acetylation in U937 cells, 10 µg of histone extract was separated on 15% polyacrylamide gels and blotted. Western blots were shown for pan-acetylated histone H3 (Upstate).

6.10. Fluorimetric human recombinant HDAC1 assays

GST-HDAC1 has been cloned into the pAcG2T baculovirus transfer vector (BD) and purified by using glutathione beads. The BD BaculoGold transfection system (BD) has been used in Sf9 insect cells for expression following supplier's instructions. The HDAC assay has been carried out as follows: the HDAC Fluorescent Activity Assay is based on the Fluor de Lys Substrate and Developer combination (BioMol) and has been carried out according to supplier's instructions. Briefly, the Fluor de Lys Substrate, which comprises an acetylated lysine side chain, has been incubated with the purified recombinant HDAC enzymes in presence or absence of the inhibitors, for 0.5 h at 37 °C. When a different incubation time has been used, it is specified into the text. Deacetylation of the substrate sensitizes the substrate so that, in the second step, treatment

with the Developer for 30 min produces a fluorophore. The fluorophore is excited with a 360 nm light and the emitted light (460 nm) has been quantified with a TECAN Inphinite M200 station.

6.11. Human recombinant Sirt1 assay

Recombinant human Sirt1 was prepared in *E. coli* BL21 and purified by affinity chromatography. The enzymatic reaction consisted of 1 µg of Sirt1 incubated with the acetylated p53 peptide (AA 379–382), 1 mM dithiothreitol, and a range of inhibitor concentrations, as described. Reactions were carried out at 37 °C for 60 min. Assays were performed in the presence of 200 µM NAD⁺ for each inhibitor. Fluorescence was measured with a fluorimetric reader (TECAN Inphinite M200 fluorescence plate reader) with excitation set at 360 nm and emission detection set at 450 nm. Results are expressed as the mean and standard deviation of four independent experiments as percentage of activity considering the untreated control as 100.

6.12. Human recombinant CBP assay

The recombinant CBP was prepared in *E. coli* BL21 and purified by affinity chromatography. Recombinant CBP fraction corresponded to amino acids 1098–1877. CBP was incubated in HAT buffer with 10 µg of histone H4 peptide (corresponding to amino acids 2–24) and 20 µM Acetyl CoA containing 0.5 µCi/mL [³H]-Acetyl CoA in the presence of inhibitors. After 2 h at 37 °C, 5 µL of samples were spotted onto Whatman P81 paper (in triplicate). The paper squares were washed three times in 5% TCA and once in 100% acetone and then placed into scintillation vials containing scintillation fluid to allow the DPM reading. The DPM of enzyme samples was compared to DPM of negative control. Data have been expressed as percentage of activity considering the control without treatment as 100.

6.13. Human recombinant DNMT3A radioactive assay

DNMT3A was produced in *E. coli* BL21 according to standard procedures. The methyltransferase radioactive assay was performed in a volume of 25 µL/point, using [³H]-adenosyl-L-methionine (1 µCi) as methyl donor and Poly dI-dC (0.1 γ) as methyl acceptor, while 30–50 ng of recombinant DNMT3A protein was used, depending on enzyme activity, stability and purity. The compounds were tested at 50 µM. After 2 h incubation at 37 °C, 5 µL of samples were spotted onto Whatman DE81 paper (in triplicate). The paper squares were washed three times in 5% Na₂HPO₄ and once in sterile water and then placed into scintillation vials containing 5 mL of scintillation fluid to allow the DPM reading. The DPM of enzyme samples was compared to the DPM of negative control. Data were expressed as a percentage of activity relative to control.

6.14. Immunoprecipitation of DNMT1 and radioactive assay

The K562 cells were cultured in the experimental conditions reported and lysed in TAP buffer pH 7–7.5 (50 mM Tris pH 7.0, 180 mM NaCl, 0.15% v/v NP40, 10% v/v glycerol, 1.5 mM MgCl₂, 1 mM Na₂MoO₄, 0.5 mM NaF, 1 mM DTT, 0.2 mM PMSF, 0.1 mM protease inhibitor cocktail) for 10 min in ice and centrifuged at 130,000 rpm for 30 min. 650 µg of extracts were diluted in TAP buffer up to 1 mL and pre-cleared by incubating with 20 µL A/G plus agarose (Santa Cruz) for 30 min to 1 h on a rocking table at 4 °C. Supernatant was transferred to a new tube and 3–5 µg of antibody against DNMT1 (Abcam) was added. IP was allowed to proceed overnight at 4 °C on a rocking table. As a negative control

the same amount of protein extracts were immunoprecipitated with purified IgG rabbit (Santa Cruz). The following day, 50 µL A/G plus agarose were added and incubation was continued for 2 h. The beads were recovered by brief centrifugation and washed with cold TAP buffer several times. After the last washing 20 µL of 2X concentrated electrophoresis sample buffer (217 mM Tris–HCl pH 8.0, 5.3% SDS, 17.4% glycerol, 8.7% β-mercaptoethanol, 0.026% bromophenol blue) was added and the sample was boiled for 5 min. A fraction of supernatants was loaded onto an SDS–PAGE gel in order to check the immunoprecipitation product. 10 µL of resin binding DNMT1 were used in DNMT radioactive assay (see above) to test the inhibitory potency of the PsA derivatives.

Acknowledgments

This work was supported by the EU (Epi tron LSHC-CT2005-518417; JG, RP, GLF and AN contracts; and ATLAS Contract 221952), the Spanish MICINN (SAF-07-63880-FEDER), Xunta de Galicia (INBIOMED), and the Italian Associazione Italiana per la ricerca contro il cancro.

Supplementary data

Supplementary data associated with this article can be found, in the online version, at doi:10.1016/j.bmc.2010.12.026.

References and notes

- Peng, J.; Li, J.; Hamann, M. T. *Alkaloids: Chem. Biol.* **2005**, *61*, 59.
- Jiménez, C.; Crews, P. *Tetrahedron* **1991**, *47*, 2097.
- Piña, I. C.; Gautschi, J. T.; Wang, G. Y. S.; Sanders, M. L.; Schmitz, F. J.; France, D.; Cornell-Kennon, S.; Sambucetti, L. C.; Remiszewski, S. W.; Perez, L. B.; Bair, K. W.; Crews, P. *J. Org. Chem.* **2003**, *68*, 3866.
- Arabshahi, L.; Schmitz, F. J. *J. Org. Chem.* **1987**, *52*, 3584.
- Rodríguez, A. D.; Akee, R. K.; Scheuer, P. J. *Tetrahedron Lett.* **1987**, *28*, 4989.
- Quiñoa, E.; Crews, P. *Tetrahedron Lett.* **1987**, *28*, 3229.
- Suzuki, A.; Matsunaga, K.; Shin, H.; Tabudrav, J.; Shizuri, Y.; Ohizumi, Y. *J. Pharmacol. Exp. Ther.* **2000**, *292*, 725.
- Shin, J.; Lee, H. S.; Seo, Y.; Rho, J. R.; Cho, K. W.; Paul, V. J. *Tetrahedron* **2000**, *56*, 9071.
- Pham, N. B.; Butler, M. S.; Quinn, R. J. *J. Nat. Prod.* **2000**, *63*, 393.
- Tabudravu, J. N.; Eijnsink, V. G. H.; Gooday, G. W.; Jaspars, M.; Komander, D.; Legg, M.; Synstad, B.; Van Aalten, D. M. F. *Bioorg. Med. Chem.* **2002**, *10*, 1123.
- Jung, J. H.; Sim, C. J.; Lee, C.-O. *J. Nat. Prod.* **1995**, *58*, 1722.
- Park, Y.; Liu, Y.; Hong, J.; Lee, C. O.; Cho, H.; Kim, D. K.; Im, K. S.; Jung, J. H. *J. Nat. Prod.* **2003**, *66*, 1495.
- Kim, D.; Lee, I. S.; Jung, J. H.; Yang, S. I. *Arch. Pharm. Res.* **1999**, *22*, 25.
- Kim, D.; Lee, I. S.; Jung, J. H.; Lee, C. O.; Choi, S. U. *Anticancer Res.* **1999**, *19*, 4085.
- Nicholas, G. M.; Eckman, L. L.; Ray, S.; Hughes, R. O.; Pfefferkorn, J. A.; Barluenga, S.; Nicolaou, K. C.; Bewley, C. A. *Bioorg. Med. Chem. Lett.* **2002**, *12*, 2487.
- Jiang, Y.; Ahn, E. Y.; Ryu, S. H.; Kim, D. K.; Park, J. S.; Yoon, H. J.; You, S.; Lee, B. J.; Lee, D. S.; Jung, J. H. *BMC Cancer* **2004**, *4*, 70.
- Fajas, L.; Egler, V.; Reiter, R.; Hansen, D.; Kristiansen, K.; Debril, M.-B.; Miard, S.; Auwerx, J. *Dev. Cell* **2002**, *3*, 903.
- Fajas, L.; Egler, V.; Reiter, R.; Miard, S.; Lefebvre, A.-M.; Auwerx, J. *Oncogene* **2003**, *22*, 4186.
- Fu, M.; Rao, M.; Bouras, T.; Wang, C.; Wu, K.; Zhang, X.; Li, Z.; Yao, T.-P.; Pestell, R. G. *J. Biol. Chem.* **2005**, *280*, 16934.
- Mora, F. D.; Jones, D. K.; Desai, P. V.; Patny, A.; Avery, M. A.; Feller, D. R.; Smillie, T.; Zhou, Y. D.; Nagle, D. G. *J. Nat. Prod.* **2006**, *69*, 547.
- Shim, J. S.; Lee, H.-S.; Shin, J.; Kwon, H. J. *Cancer Lett.* **2004**, *203*, 163.
- Allis, C. D.; Jenuwein, T.; Reinberg, D.; Caparros, M.-L. *Epigenetics*; Cold Spring Harbor Laboratory Press: Cold Spring Harbor (NY), 2007.
- Sippel, W.; Jung, M. In *Epigenetic Targets in Drug Discovery: Methods and Principles of Medicinal Chemistry*; Mannhold, R., Kubinyi, H., Folkers, G., Eds.; Wiley: Weinheim, 2009; Vol. 42.
- Archer, S. Y.; Hodin, R. A. *Curr. Opin. Gene Dev.* **1999**, *9*, 171.
- Marks, P. A.; Rifkin, R. A.; Richon, V. M.; Breslow, R.; Miller, T.; Kelly, W. K. *Nat. Rev. Cancer* **2001**, *1*, 194.
- Rosato, R. R.; Grant, S. *Cancer Biol. Ther.* **2003**, *2*, 30.
- Blanchard, F.; Chipoy, C. *Drug Discovery Today* **2005**, *10*, 197.
- Bolden, J. E.; Peart, M. J.; Johnstone, R. W. *Nat. Rev. Drug Disc.* **2006**, *5*, 769.
- Lin, H. Y.; Chen, C. S.; Lin, S. P.; Weng, J. R.; Chen, C. S. *Med. Res. Rev.* **2006**, *26*, 397.
- Mei, S.; Ho, A. D.; Mahlknecht, U. *Int. J. Oncol.* **2004**, *25*, 1509.

31. Minucci, S.; Pelicci, P. G. *Nat. Rev. Cancer* **2006**, *6*, 38.
32. Fouladi, M. *Cancer Invest.* **2006**, *24*, 521.
33. Botrugno, O. A.; Santoro, F.; Minucci, S. *Cancer Lett.* **2009**, *280*, 134.
34. Mai, A.; Altucci, L. *Int. J. Biochem. Cell Biol.* **2009**, *41*, 199.
35. Kazantsev, A. G.; Thompson, L. M. *Nat. Rev. Drug Disc.* **2008**, *7*, 854.
36. Marks, P. A.; Dokmanovic, M. *Expert Opin. Invest. Drugs* **2005**, *14*, 1497.
37. Drummond, D. C.; Noble, C. O.; Kirpotin, D. B.; Guo, Z.; Scott, G. K.; Benz, C. C. *Ann. Rev. Pharmacol. Toxicol.* **2005**, *45*, 495.
38. Rodriguez, M.; Aquino, M.; Bruno, I.; De Martino, G.; Taddei, M.; Gomez-Paloma, L. *Curr. Med. Chem.* **2006**, *13*, 1119.
39. Paris, M.; Porcelloni, M.; Binaschi, M.; Fattori, D. *J. Med. Chem.* **2008**, *51*, 1505.
40. Smith, K. T.; Workman, J. L. *Int. J. Biochem. Cell Biol.* **2009**, *41*, 21.
41. Witt, O.; Lindemann, R. *Cancer Lett.* **2009**, *280*, 123.
42. Klose, R. J.; Bird, A. P. *Trends Biochem. Sci.* **2006**, *31*, 89.
43. Ooi, S. K. T.; Bestor, T. H. *Cell* **2008**, *133*, 1145.
44. Baylin, S.; Bestor, T. H. *Cancer Cell* **2002**, *1*, 299.
45. Esteller, M. *Oncogene* **2002**, *21*, 5427.
46. Das, P. M.; Singal, R. *J. Clin. Oncol.* **2004**, *22*, 4632.
47. Baylin, S. B. *Nat. Clin. Pract. Oncol.* **2005**, *2*, 54.
48. Brueckner, B.; Lyko, F. *Trends Pharm. Sci.* **2004**, *25*, 551.
49. Kaminskis, E.; Farrell, A.; Abraham, S.; Baird, A.; Hsieh, L.-S.; Lee, S.-L.; Leighton, J. K.; Patel, H.; Rahmal, A.; Sridhara, R.; Wang, Y.-C.; Pazdur, R. *Clin. Cancer Res.* **2005**, *11*, 3604.
50. Morphy, R.; Kay, C.; Rankovic, Z. *Drug Discovery Today* **2004**, *9*, 641.
51. Morphy, R.; Rankovic, Z. *J. Med. Chem.* **2005**, *48*, 6523.
52. Remiszewski, S. W. *Curr. Med. Chem.* **2003**, *10*, 2393.
53. Hoshino, O.; Murakata, M.; Yamada, K. *Bioorg. Med. Chem. Lett.* **1992**, *2*, 1561.
54. Nicolaou, K. C.; Hughes, R.; Pfefferkorn, J. A.; Barluenga, S. *Chem. Eur. J.* **2001**, *7*, 4296.
55. Nicolaou, K. C.; Hughes, R.; Pfefferkorn, J. A.; Barluenga, S.; Roecker, A. J. *Chem. Eur. J.* **2001**, *7*, 4280.
56. Godert, A. M.; Angelino, N.; Woloszynska-Read, A.; Morey, S. R.; James, S. R.; Karpf, A. R.; Sufirin, J. R. *Bioorg. Med. Chem. Lett.* **2006**, *16*, 3330.
57. Boehlow, T. R.; Spilling, C. D. *Nat. Prod. Lett.* **1995**, *7*, 1.
58. Boehlow, T. R.; Harburn, J. J.; Spilling, C. D. *J. Org. Chem.* **2001**, *66*, 3111.
59. Carreño, M. C. R.; J.L.G.; Sanz, G.; Toledo, M. A.; Urbano, A. *Synlett* **1997**, 1241.
60. Pfammatter, M. J.; Siljegovic, V.; Darbre, T.; Keese, R. *Helv. Chim. Acta* **2001**, *84*, 678.
61. Nishiyama, S.; Yamamura, S. *Tetrahedron Lett.* **1982**, *23*, 1281.
62. Forrester, A. R. T.; R.H.; Woo, S. O. *J. Chem. Soc., Perkin Trans. 1* **1975**, 2340.
63. Khan, N.; Jeffers, M.; Kumar, S.; Hackett, C.; Boldog, F.; Khramtsov, N.; Qian, X.; Mills, E.; Berghs, S. C.; Carey, N.; Finn, P. W.; Collins, L. S.; Tumber, A.; Ritchie, J. W.; Jensen, P. B.; Lichenstein, H. S.; Sehested, M. *Biochem. J.* **2008**, *409*, 581.
64. Bradner, J. E.; Mak, R.; Tanguturi, S. K.; Mazitschek, R.; Haggarty, S. J.; Ross, K.; Chang, C. Y.; Bosco, J.; West, N.; Morse, E.; Lin, K.; Shen, J. P.; Kwiatkowski, N. P.; Gheldof, N.; Dekker, J.; DeAngelo, D. J.; Carr, S. A.; Schreiber, S. L.; Golub, T. R.; Ebert, B. L. *Proc. Natl. Acad. Sci. U.S.A.* **2010**, *107*, 12617.
65. Balasubramanyam, K.; Swaminathan, V.; Ranganathan, A.; Kundu, T. K. *J. Biol. Chem.* **2003**, *278*, 19134.
66. (a) Souto, J. A.; Conte, M.; Alvarez, R.; Nebbioso, A.; Carafa, V.; Altucci, L.; de Lera, A. R. *ChemMedChem* **2008**, *3*, 1435; (b) Souto, J. A.; Bebedetti, R.; Otto, K.; Miceli, M.; Alvarez, R.; Altucci, L.; de Lera, A. R. *ChemMedChem* **2010**, *5*, 1530; (c) Souto, J. A.; Vaz, E.; Lepore, I.; Pöppler, A.-C.; Franci, J. L.; Alvarez, R.; Altucci, L.; de Lera, A. R. *J. Med. Chem.* **2010**, *53*, 4654.
67. Siedlecki, P.; Boy, R. G.; Musch, T.; Brueckner, B.; Suhai, S.; Lyko, F.; Zielenkiewicz, P. *J. Med. Chem.* **2006**, *49*, 678.
68. Datta, J.; Ghoshal, K.; Denny, W. A.; Gamage, S. A.; Brooke, D. G.; Phiasivongsa, P.; Redkar, S.; Jacob, S. T. *Cancer Res.* **2009**, *69*, 4277.
69. Biel, M.; Wascholowski, V.; Giannis, A. *Angew. Chem., Int. Ed.* **2005**, *44*, 3186.
70. Somoza, J. R.; Skene, R. J.; Katz, B. A.; Mol, C.; Ho, J. D.; Jennings, A. J.; Luong, C.; Arvai, A.; Buggy, J. J.; Chi, E.; Tang, J.; Sang, B. C.; Verner, E.; Wynands, R.; Leahy, E. M.; Dougan, D. R.; Snell, G.; Navre, M.; Knuth, M. W.; Swanson, R. V.; McRee, D. E.; Tari, L. W. *Structure* **2004**, *12*, 1325.
71. Bieliauskas, A. V.; Pflum, M. K. H. *Chem. Soc. Rev.* **2008**, *37*, 1402.
72. McCulloch, M. W. B.; Coombs, G. S.; Banerjee, N.; Bugni, T. S.; Cannon, K. M.; Harper, M. K.; Veltri, C. A.; Virshup, D. M.; Ireland, C. M. *Bioorg. Med. Chem.* **2009**, *17*, 2189.
73. Kim, D. H. S. J.; Kwon, H. J. *Exp. Mol. Med.* **2007**, *39*, 47.
74. Ahn, M. Y.; Jung, J. H.; Na, Y. J.; Kim, H. S. *Gynecol. Oncol.* **2008**, *108*, 27.
75. Richon, V. M.; Sandhoff, T. W.; Rifkind, R. A.; Marks, P. A. *Proc. Natl. Acad. Sci. U.S.A.* **2000**, *97*, 10014.
76. Mai, A.; Massa, S.; Rotili, D.; Cerbara, I.; Valente, S.; Pezzi, R.; Simeoni, S.; Ragna, R. *Med. Res. Rev.* **2005**, *25*, 261.
77. Furumai, R.; Matsuyama, A.; Kobashi, N.; Lee, K. H.; Nishiyama, M.; Nakajima, H.; Tanaka, A.; Komatsu, Y.; Nishino, N.; Yoshida, M.; Horinouchi, S. *Cancer Res.* **2002**, *62*, 4916.
78. Xiao, J. J.; Byrd, J.; Marcucci, G.; Grever, M.; Can, K. K. *Rapid Commun. Mass Spectrom.* **2003**, *17*, 757.
79. Wang, D.; Helquist, P.; Wiest, O. *J. Org. Chem.* **2008**, *72*, 5446.
80. Nishino, N.; Jose, B.; Okamura, S.; Ebisusaki, S.; Kato, T.; Sumida, Y.; Yoshida, M. *Org. Lett.* **2003**, *5*, 5079.
81. Nishino, N.; Shivashimpi, G. M.; Soni, P. B.; Bhuiyan, M. P. I.; Kato, T.; Maeda, S.; Nishino, T. G.; Yoshida, M. *Bioorg. Med. Chem.* **2008**, *16*, 437.
82. Bach, R. D.; Dmitrenko, O.; Thorpe, C. J. *Org. Chem.* **2008**, *73*, 12.
83. Rautio, J.; Kumpulainen, H.; Heimbach, T.; Oliyai, R.; Oh, D.; Järvinen, T.; Savolainen, J. *Nat. Rev. Drug Disc.* **2008**, *7*, 255.
84. Mai, A.; Cheng, D.; Bedford, M. T.; Valente, S.; Nebbioso, A.; Perrone, A.; Brosch, G.; Sbardella, G.; De Bellis, F.; Miceli, M.; Altucci, L. *J. Med. Chem.* **2008**, *51*, 2279.
85. Li, J. W. H.; Vederas, J. C. *Science* **2009**, *325*, 161.
86. Newman, D. J. *J. Med. Chem.* **2008**, *51*, 2589.
87. Molinski, T. F.; Dalisay, D. S.; Lievens, S. L.; Saludes, J. P. *Nat. Rev. Drug Disc.* **2009**, *8*, 69.
88. Kotoku, N.; Tsujita, H.; Hiramatsu, A.; Mori, C.; Koizumi, N.; Kobayashi, M. *Tetrahedron* **2005**, *61*, 7211.
89. Knapp, S.; Amorelli, B.; Darout, E.; Ventocilla, C. C.; Goldman, L. M.; Huhn, R. A.; Minnihan, E. C. *J. Carbohydr. Chem.* **2005**, *24*, 103.
90. Frisch, M. J.; G. W. T.; Schlegel, H. B.; Scuseria, G. E.; Robb, M. A.; Cheeseman, J. R.; Montgomery, Jr., J. A.; Vreven, T.; Kudin, K. N.; Burant, J. C.; Millam, J. M.; Iyengar, S. S.; Tomasi, J.; Barone, V.; Mennucci, B.; Cossi, M.; Scalmani, G.; Rega, N.; Petersson, G. A.; Nakatsuji, H.; Hada, M.; Ehara, M.; Toyota, K.; Fukuda, R.; Hasegawa, J.; Ishida, M.; Nakajima, T.; Honda, Y.; Kitao, O.; Nakai, H.; Klene, M.; Li, X.; Knox, J. E.; Hratchian, H. P.; Cross, J. B.; Bakken, V.; Adamo, C.; Jaramillo, J.; Gomperts, R.; Stratmann, R. E.; Yazyev, O.; Austin, A. J.; Cammi, R.; Pomelli, C.; Ochterski, J. W.; Ayala, P. Y.; Morokuma, K.; Voth, G. A.; Salvador, P.; Dannenberg, J. J.; Zakrzewski, V. G.; Dapprich, S.; Daniels, A. D.; Strain, M. C.; Farkas, Malick, O.; D. K.; Rabuck, A. D.; Raghavachari, K.; Foresman, J. B.; Ortiz, J. V.; Cui, Q.; Baboul, A. G.; Clifford, S.; Cioslowski, J.; Stefanov, B. B.; Liu, G.; Liashenko, A.; Piskorz, P.; Komaromi, I.; Martin, R. L.; Fox, D. J.; Keith, T.; Al-Laham, M. A.; Peng, C. Y.; Nanayakkara, A.; Challacombe, M.; Gill, P. M. W.; Johnson, B.; Chen, W.; Wong, M. W.; Gonzalez, C.; Pople, J. A. *Gaussian, Pittsburg*: 2004.
91. Bayly, C. I.; Cieplak, P.; Cornell, W. D.; Kollman, P. A. *J. Phys. Chem.* **1993**, *97*, 10269.
92. Cornell, W. D.; Cieplak, P.; Bayly, C. I.; Gould, I. R.; Merz, K. M.; Ferguson, D. M.; Spellmeyer, D. C.; Fox, T.; Caldwell, J. W.; Kollman, P. A. *J. Am. Chem. Soc.* **1995**, *117*, 5179.
93. Rodríguez-Barríos, F.; Pérez, C.; Lobatón, E.; Velázquez, S.; Chamorro, C.; San-Félix, A.; Pérez-Pérez, M. J.; Camarasa, M. J.; Pelemans, H.; Balzarini, J.; Gago, F. *J. Med. Chem.* **2001**, *44*, 1853.
94. Morris, G. M.; Goodsell, D. S.; Halliday, R. S.; Huey, R.; Hart, W. E.; Belew, R. K.; Olson, A. J. *J. Comput. Chem.* **1998**, *19*, 1639.
95. Morris, G. M.; Goodsell, D. S.; Huey, R.; Hart, W. E.; Halliday, S.; Belew, R.; Olson, A. J.; AutoDock, 3.0 ed. La Jolla, CA, 1999.
96. Goodford, P. J. *J. Med. Chem.* **1985**, *28*, 849.
97. Åqvist, J. *J. Phys. Chem.* **1990**, *94*, 8021.
98. Jorgensen, W. L.; Chandrasekhar, J.; Madura, J. D. *J. Chem. Phys.* **1983**, *79*, 926.
99. <http://amber.scripps.edu/doc8>.
100. Ryckaert, J. P.; Cicotti, G.; Berendsen, H. J. C. *J. Comput. Phys.* **1977**, *23*, 327.
101. Nebbioso, A.; Clarke, N.; Voltz, E.; Germain, E.; Ambrosino, C.; Bontempo, P.; Alvarez, R.; Schiavone, E. M.; Ferrara, F.; Bresciani, F.; Weisz, A.; de Lera, A. R.; Gronemeyer, H.; Altucci, L. *Nat. Med.* **2005**, *11*, 77.
102. Scognamiglio, A.; Nebbioso, A.; Manzo, F.; Valente, S.; Mai, A.; Altucci, L. *Biochem. Biophys. Acta* **2008**, *1783*, 203.
103. Altucci, L.; Rossini, A.; Raffelsberger, W.; Reitmair, A.; Chomienne, C.; Gronemeyer, H. *Nat. Med.* **2001**, *7*, 680.